DE WET RAUTENBACH, C J

INTRODUCTION OF A HYBRID VERTICAL CO-ORDINATE TO AN ATMOSPHERIC GENERAL CIRCULATION MODEL

D.Phil UP 1999

Introduction of a hybrid vertical co-ordinate to an Atmospheric General Circulation Model

by

Cornelis Johannes de Wet Rautenbach

Submitted in partial fulfilment of the requirements

for the degree of

DOCTOR OF PHILOSOPHY

in the

Faculty of Science of the

University of Pretoria

July 1999

Introduction of a hybrid vertical co-ordinate to an Atmospheric General Circulation Model

Cornelis Johannes de Wet Rautenbach

Promotor:	Prof J van Heerden
Department / Faculty:	Department of Earth Science, Faculty of Science
University:	University of Pretoria
Degree:	Doctor of Philosophy

Summary

Both the R21 and T63 versions of the CSIRO-9 (MARK II) Atmospheric General Circulation Model (AGCM) utilise a sigma vertical co-ordinate ($\sigma=p/P_S$) which was introduced to compensate for the influence of uneven surface topography on atmospheric circulation patterns. In addition, climate model simulations may also be performed with pressure as a vertical co-ordinate. Trough the depth of the atmosphere, over high surface topography, the formulation of the sigma vertical co-ordinate system allows for numerical analyses to be carried out at higher geometric levels than equivalent pressure co-ordinate analyses, where the effect of topography is ignored. If compared with pressure co-ordinates, sigma co-ordinate simulations therefore usually provide better results at lower altitudes (near the Earth's surface), but often fail to perform well in the upper atmosphere where the influence of surface topography is in reality much less profound.

The *hybrid vertical co-ordinate system* (or η-system) addresses this problem by converging to a *sigma vertical co-ordinate system* (or σ-system) near the Earth's surface, while gradually changing to a *pressure vertical co-ordinate system* (or p-system) in the upper atmosphere.

The CSIRO-9 (MARK II) AGCM utilises the flux formulation of the atmospheric equations. In this study a η-system is introduced to the non-linear dynamics of the model. A 5-year seasonal cycle η-system control run has been performed. Climate parameters from this simulation are compared with output results from a different 5-year σ-system control run. Both model simulations were started with exactly equivalent initial conditions. Actual climate fields extracted from ECMWF analyses are finally used to compare and validate model output from both the σ- and η-systems.

The study reveals noticeable improvements by η-system simulations at stratospheric pressure-levels over high surface topography.

Instelling van ‘n hibriede vertikale koördinaat in ‘n Atmosferiese Algemene Sirkulasiemodel

Cornelis Johannes de Wet Rautenbach

Promotor:	Prof J van Heerden
Departement / Fakulteit:	Departement Aardwetenskappe, Fakulteit Natuurwetenskappe
Universiteit:	Universiteit van Pretoria
Graad:	Doctor in Philosophy

Samevatting

Beide die R21 en T63 weergawes van die CSIRO-9 (MERK II) Atmosferiese Algemene Sirkulasie Klimaatmodel (AASM) maak gebruik van ‘n sigma vertikale koördinaatstelsels ($\sigma = p/P_S$) wat ingestel is om te kompenseer vir die invloed van oneweredige oppervlaktopografie op atmosferiese sirkulasiepatrone. Klimaatmodel simulasies kan addisioneel ook uitgevoer word met druk as vertikale koördinaat. Deur die diepte van die atmosfeer, oor hoë topografiese gebiede, veroorsaak die formulasie van die sigma vertikale koördinaatstelsel dat numeriese analises op relatief hoër geometriese vlakke uitgevoer word as die ooreenstemmende druk koördinaat analises, waar die effek van die topografie geignoreer word. Indien vergelyk word met druk koördinate, lewer sigma koördinaatanalises dus beter resultate oor lae atmosferiese hoogtes (naby die oppervlak van die Aarde), maar dikwels ook onbevredigende resultate in die bolug waar die invloed van oppervlak topografie in die realiteit aansienlik kleiner is.

Die *hibriede vertikale koördinaatstelsel* (of η-stelsel) spreek hierdie probleem aan deur naby die oppervlak van die Aarde na ‘n *sigma vertikale koördinaatstelsel* (of σ-stelsel) te konvergeer, terwyl dit gelydelik verander na ‘n *druk vertikale koördinaatstelsel* (of p-stelsel) in die bolug.

Die CSIRO-9 (MARK II) AASM gebruik die vloedformulasie van die atmosferiese vergelykings. In hierdie studie word die η-stelsel geimplimenteer op die nie-liniêre dinamika van die model. ‘n Vyf-jaar seisoenale siklus η-stelsel kontrolelopie is uitgevoer. Klimaatparameters van hierdie simulasie word vergelyk met uitvoerresultate van ‘n addisionele vyf-jaar σ-stelsel kontrolelopie. Beide modelsimulasies is geinisieer met presies ekwivalente beginwaardes. Waargenome klimaatvelde verkry van ECMWF analises is ten einde gebruik om modeluitvoere van beide die σ- en η-stelsels te vergelyk en evalueer.

Die studie dui op merkbare verbeteringe deur η-stelsel simulasies in troposferiese drukvlakke oor hoë oppervlak topografie.

ACKNOWLEDGEMENTS

The author wishes to express his appreciation to the following persons and organisations for their assistance and contribution to make this dissertation possible:

- *Mr Barrie Hunt* (Program leader, Climate Modelling) from the CSIRO (Atmospheric Research), Australia, for his encouragement. I wish to thank him for supporting this research and providing the necessary office space and computer facilities during the 4 months I spent at the CSIRO.

- *Dr Hal Gordon* (Specialist Scientist) from the CSIRO (Atmospheric Research), Australia, for his supervision while performing the research at the CSIRO, as well as his guidance afterwards. His contribution to this dissertation is gratefully acknowledged.

- *Prof J van Heerden* for his support and advice.

- *The Foundation for Research Development* (FRD) and *Mr John Jordaan* of the *CORDATA / South African Weather Bureau Educational Trust* for the financial support which enabled me to visit the CSIRO (Atmospheric Research), Australia.

- The *CORDATA / South African Weather Bureau Educational Trust* for providing a CRAY (EL94) super computer which enable me to implement and run the CSIRO-9 model locally in South Africa.

- My wife Marinda for her encouragement and support during the course of this study.

TABLE OF CONTENTS

LIST OF SYMBOLS

a	:	Radius of the earth (6370 km).
a_{on}	:	Coefficients in the hybrid co-ordinate condition matrix.
A	:	Any atmospheric variable at point C in space.
A	:	Indicator for horizontal global integral.
A_O	:	P_{OO}- weighted *pressure component* in the η-system.
$\underline{\underline{A}}$	:	Matrix that directly relates geopotential to temperature.
$\hat{A}_m$	:	Non-linear terms in the spectral equations.
b_n	:	Coefficients in the hybrid co-ordinate condition matrix.
B	:	Part of the *sigma component* in the η-system.
$\hat{B}_m$	:	Non-linear terms in the spectral equations.
c_p	:	Specific heat at constant pressure.
C	:	Any point in a co-ordinate space.
$\hat{C}$	:	Non-linear terms from the momentum equation.
D	:	Horizontal divergence ($\underline{\nabla} \cdot \underline{V}$).
$\hat{D}$	:	μ-weighted horizontal divergence ($\underline{\nabla} \cdot \hat{\underline{V}}$).
E	:	Kinetic energy per unit mass.
E_O	:	Global mean kinetic energy - different at each model level.
E'	:	Energy perturbation from E_O.
$\hat{E}_m$	:	Non-linear terms in the spectral equations.
$\hat{E}$	:	Non-linear terms from the momentum equation.
$\hat{E}$	:	μ-weighted kinetic energy (μE).
f	:	Function close to unity in the η-system ($f=\eta\mu/p$).
f	:	Coriolis parameter.
$\underline{F}$	:	Frictional forces.
$\hat{F}_m$	:	Non-linear terms in the spectral equations.
$\hat{G}_m$	:	Non-linear terms in the spectral equations.
$\hat{H}_m$	:	Non-linear terms in the spectral equations.

$\underline{i}$	:	Unit vector in the eastward direction.
$\underline{j}$	:	Unit vector in the northward direction.
j	:	Indicator for any full level of the model in a summation.
J	:	Wave number for truncation in the spectral analysis.
k	:	Indicator (k = 1 to 10) for the model's full levels.
$\underline{k}$	:	Unit vector in the vertical direction.
K	:	Constant value: R/c_p.
m	:	Related to the number of conditions when defining the η-system.
m	:	Meridional wave number in the spectral analysis.
n	:	Indicator in the polynomial expression for A_O and B.
n	:	Wave number in the spectral analyses (zonal = n-m).
p	:	Pressure (hPa).
P_{OO}	:	Global mean of the sea-level pressure (1013.2 hPa).
P_S	:	Surface-pressure (hPa).
PL_S	:	Surface-pressure over the lowest model orography (hPa) (sea-level pressure = 1013.2 hPa).
PH_S	:	Surface-pressure over the highest model orography = 500 hPa).
P_n^m	:	Legendre polynomials.
Q	:	Heat ($\hat{Q}$: μ-weighted heat).
r	:	Distance from centre of earth to position at point in space (m).
R	:	Specific gas constant for dry air (287 J kg^{-1} K^{-1}).
t	:	Time variable in the hybrid co-ordinate system (s).
T	:	Temperature (K).
T_O	:	Global mean temperature - isothermal in the vertical (290 K).
T′	:	Temperature perturbation from T_O (K)
$\hat{T}$	:	μ-weighted temperature perturbation.
u	:	Zonal wind velocity (ms^{-1}).
U	:	u cos(φ).
v	:	Meridional wind velocity (ms^{-1}).

V	:	Indicator for vertical integral or v cos(φ).
$\underline{V}$	:	Horizontal wind velocity vector (ms^{-1}).
$\hat{\underline{V}}$	:	μ-weighted horizontal wind velocity ($\mu\underline{V}$)
x,y,z	:	Eastward, northward and upward distances in the rotating co-ordinate system.
X,Y,Z	:	Eastward, northward and upward distances in the pressure co-ordinate system.
$X^{"},Y^{"},Z^{"}$	:	Eastward, northward and upward distances in the inertial co-ordinate system.
Y_n^m	:	Spherical harmonic in the spectral analysis.
α	:	Ratio of pressure thickness between highest and lowest orography.
α_0 , α_1	:	Constants in the co-ordinate condition matrix.
χ	:	Velocity potential.
δ_1, δ_2	:	$\delta_1 = \underline{k}\cdot(\underline{V}\times\underline{\nabla})P_s$ and $\delta_2 = \underline{V}\cdot\underline{\nabla}P_s$
ξ	:	Vertical component of vorticity ($\nabla^2\psi$).
$\hat{\xi}$	:	Vorticity from the μ-weighted horizontal wind velocity($\hat{\xi} = \underline{k}\cdot\underline{\nabla}\times\mu\underline{V}$)
ρ	:	Density of air.
$\dot{\sigma}$	:	Vertical velocity in the sigma co-ordinate system (dσ/dt).
σ	:	Vertical co-ordinate in the sigma co-ordinate system.
τ	:	Time variable in the pressure co-ordinate system (s).
χ	:	Velocity potential.
ϕ	:	Geopotential height from the surface of the earth.
ϕ_O	:	Global mean geopotential height - different at each model level.
ϕ'	:	Perturbation from ϕ_O.
ϕ_S	:	Geopotential height of the smoothed orography ($\Phi = \phi_S+\phi$)
ϕ_{SO}	:	The mean value of ϕ_S.
ϕ'_S	:	Perturbation from ϕ_{SO}.
$\hat{\phi}$	:	Function in the hybrid co-ordinate system. (not equal to $\mu\phi'$)

Φ	:	Geopotential.
η	:	Vertical co-ordinate in the η-system.
$\dot{\eta}$	:	Vertical velocity in the η-system ($d\eta/dt$).
λ,φ	:	Longitude / latitude in the spherical co-ordinate system.
μ	:	Pressure derivative in the η-system ($\partial\eta / \partial p$).
ν,κ	:	Any function.
ψ	:	Stream function.
ω	:	Vertical velocity in the isobaric co-ordinate system (dp/dt).
$\hat{\omega}$	:	Vertical velocity diagnostic ($\mu\dot{\eta}$)

LIST OF FIGURES

LIST OF TABLES

LIST OF ABBREVIATIONS

AGCM	:	Atmospheric General Circulation Model.
CSIRO	:	Commonwealth Scientific and Industrial Research Organisation (Australia).
DAR	:	Division of Atmospheric Research.
DJF	:	December, January, February
ECMWF	:	European Centre for Medium-Range Weather Forcasting (U.K.).
GCM	:	General Circulation Model
JJA	:	June, July, August
LHS	:	Left hand side
RHS	:	Right hand side
SST	:	Sea Surface Temperature
TOGA	:	Tropical Ocean Global Atmosphere.
UP	:	University of Pretoria.
N	:	North
S	:	South
E	:	East
W	:	West

CHAPTER 1

INTRODUCTION

1.1 BACKGROUND

The synoptic general circulation of the atmosphere is governed by a number of forces that collectively originate from factors like the rotation of the earth, gravity and horizontal pressure gradients. Through large scale atmospheric flow, the forces modulate the exchange of energy between the equatorial and polar regions. Prevailing horizontal atmospheric features arising from these circulation patterns vary from persistent zonal high-pressure regions over the sub-tropics and poles to complex zonal low-pressure belts, accompanied with fast moving frontal systems, over the mid-latitudes. In the vertical, well defined Hadley and Ferrel secondary circulation cells dominates the meridional atmospheric flow, while Walker cells contribute significantly to the zonal shift and location of high- and low-pressure systems. The seasonal north-south displacement of synoptic systems results in a strong seasonal variability in weather conditions over most regions of the Earth. The variation in space and time of synoptic (and smaller scale) atmospheric circulation patterns can however be considered as non-linear or chaotic.

In an effort to improve our understanding of the many factors that contribute to atmospheric circulation patterns, scientists expressed the flow in the atmosphere in terms of a number of mathematical equations known as the *primitive equations* (the Eulerian hydrodynamic equations modified by the assumption of hydrostatic equilibrium). Like the atmosphere, the primitive equations are *non-linear* and therefore have no known analytical solutions. The only recourse for solving these equations is by the use of *numerical approximations*. In numerical models, the future state of atmospheric flow patterns may be predicted to a certain degree of accuracy by integrating the numerical formulation of the primitive equations forward with respect to time. A simulated prediction is started with defined atmospheric initial conditions (usually observed values at the initial state). Correct boundary values are also essential. However, an important requirement, which also applies to the numerical approximations, is that total *momentum, mass* and *energy* must be conserved.

The first attempt to utilise numerical methods for predicting weather was made by the British scientist Lewis Fry Richardson (1882-1953). Richardson showed that the primitive equations could be approximated in numerical terms by using *finite difference* methods. By considering a discrete field of observed grid point values as initial input, he extrapolated the numerically computed tendencies of various meteorological variables ahead with small increments in time. All the

computation was performed by hand. Unfortunately, Richardson's results were out by several orders of magnitude, which might be attributed to inadequate upper air data. He was also unaware of the development of linear instability in numerical solutions caused by truncation errors. Besides, the first basis for modern numerical modelling was hereby established.

Richardson, however, was a genius to have written:

" *Big whirls have little whirls that feed upon their velocity*
and little whirls have lesser whirls and so on to viscosity "

(Hess, 1959)

A consequence of using numerical methods to integrate the primitive equations is that extremely large numbers of calculations are required per model time step. With the arrival of the first electronic computer during the late 1940s, computing power became available to assist in the numerical integration of the primitive equations. The development of the first numerical weather prediction models soon followed. Through the advent of numerical modelling, as well as the rapidly improved capacity of super computers during the past five decades, climate- and weather prediction models have collectively led to surprisingly realistic simulations of all the major observed features of the atmosphere.

Apart from predicting the day to day weather, computerised numerical models of the atmospheric circulation have been used for many purposes such as estimating the possible impact of rising levels in atmospheric chemicals (carbon dioxide, methane etc.) on the Earth's climate. In addition, the effect of thermal boundary forcing, originating from sea-surface temperature (SST) and atmospheric albedo anomalies, on the inter- and intra-seasonal climate variability has become an increasingly important meteorological research field.

1.2 THE SPECTRAL METHOD

The numerical integration of the primitive equations requires a vast number of computations. The primitive equations may be integrated using *finite difference methods* by means of computations at a discrete set of grid points covering the globe and for a number of pressure levels in the vertical. Even with the appearance of high speed vector processors, which are capable of processing multiple arrays of data simultaneously, such computer models are extremely time consuming to run. Meteorologists were therefore encouraged to search for more effective numerical methods to perform atmospheric flow simulations.

The formulation of the *spectral method* can be traced back to the work of Isadore Silberman (1954). The dependant atmospheric variables were expressed as the finite sum of orthogonal surface spherical harmonics (associated Legendre functions) and coefficients. Subsequent research on the spectral method was

conducted by Platzman (1960), Baer (1964), Robert (1966), Bourke (1974) and Kasahara (1978). The major advantages (Ellsaesser, 1966) of the spectral method relative to finite difference methods are:

- The spectral representations of the atmospheric equations do not include any approximations. Truncation errors generated by finite different methods are therefore completely eliminated.

- Computer coding is simplified and the ease of modelling atmospheric flow patterns over the entire globe makes computations during the spectral analysis of the atmosphere far less time consuming.

The spectral method became well established and is applied in many modern global general circulation models, including climate and weather prediction models.

1.3 THE CSIRO-9 GENERAL CIRCULATION CLIMATE MODEL

The 9-level R21 spectral CSIRO-9 (Mark II) Atmospheric General Circulation Model (AGCM) used in this study was developed by the CSIRO (Atmospheric Research), Melbourne, Australia (McGregor et al. 1993). The original CSIRO AGCM contained two levels in the vertical, and was developed by the Australian Numerical Meteorology Research Centre (Gordon 1983; Gordon and Hunt 1987; Hunt and Gordon 1988, 1989). The CSIRO (Atmospheric Research) subsequently developed a more advanced version of the model utilising 4 levels in the vertical (Gordon and Hunt 1991; Hunt and Gordon 1991; Smith and Gordon 1992; Hunt et al. 1994; Smith 1995). Further research led to the development of the present CSIRO-9 (Mark II) AGCM.

The CSIRO-9 (Mark II) AGCM is a 9-level climate model with a R21 (rhomboidal truncation at wave number 21) spectral resolution. A T63 (triangular truncation at wave number 63) version of the model is also available. The model integrates the primitive equations forward in time over a horizontal equally spaced grid of 64 from east to west and 56 unevenly spaced Gaussian latitudes from north to south (28 latitudes per hemisphere). The model utilises a sigma vertical co-ordinate system (σ-system) in the vertical - which is converted to a hybrid vertical co-ordinate system (η-system) in this study.

Many unique parameterisation schemes for atmospheric processes (atmospheric physics) are included in the model's code. This study, however, concentrates on the primitive equations and emphasis is placed on the model dynamics. The CSIRO-9 (Mark II) AGCM integrates the "flux" formulation of the primitive equations (Gordon 1981) forward in time. Unlike the "advective" formulation (Bourke 1974), this formulation ensures that both energy and mass are conserved during the model integration. This is a fundamental requirement when

modelling the climatic system of the earth. The main prognostic variables are surface-pressure (P_S), surface-pressure weighted divergence, surface-pressure weighted vorticity, temperature and moisture. Apart from the moisture, which is a grid variable formulated in terms of a semi-Lagrangian moisture transport scheme (McGregor 1993), the remaining variables are all spectrally analysed. The main prognostic variables are calculated at full σ (or η) model levels in the vertical, while the diagnostics of vertical velocity and geopotential height are derived at half-levels.

Time integration is performed by using a semi-implicit Leapfrog scheme where linearised fast moving gravity wave generating terms are used to link the divergence, thermodynamic and surface-pressure equations (Hoskins and Simmons 1975; Simmons and Hoskins 1978). This means that the time step is no longer restricted by gravity wave generated terms, and that longer time steps can be used. A time step of 30 minutes is used during model simulations in this study.

1.4 PRELIMINARY RESEARCH

The CSIRO-4 AGCM was brought to South Africa during the early 1990s after J.Lindesay (University of the Witwatersrand) visited the CSIRO (Division of Atmospheric Research) to do research on regional Southern African SST/atmosphere interactions (Mason *et al.* 1994). Subsequently researchers at the CSIRO encouraged meteorologists from the University of Pretoria (UP) to use the CSIRO-9 (Mark II) AGCM for further climate experiments (Hunt 1993, personal communication). Initially the CSIRO-4 AGCM was obtained through a licence agreement by the University of Pretoria, and was locally installed on a CONVEX C-120 super computer. A number of model simulations were performed which included a 20 year control run as well as selected Indian and Pacific Ocean SST/atmosphere interaction experimental runs (Truter and Rautenbach 1994, van Heerden *et al.* 1995, Jury *et al.* 1996, van Heerden and Rautenbach 1997).

With the prospect of implementing the CSIRO-9 (Mark II) AGCM locally, the author visited the CSIRO (Atmospheric Research) in 1995. During the visit the following research objectives were completed:

- Continuous model simulations to investigate the effect of Indian Ocean thermal boundary forcing on the rainfall and general circulation over Southern Africa were done using the more advanced CSIRO-9 (Mark II) AGCM (Van Heerden and Rautenbach 1997).

- With the assistance from CSIRO researchers the CSIRO-9 (Mark II) AGCM was installed on a CRAY-EL94 super computer located at the South African Weather Bureau (Rautenbach and van Heerden 1995). A number of global

SST/atmosphere interaction AGCM experimental runs were performed (Rautenbach and van Heerden 1996, Rautenbach 1997).

- At the CSIRO (DAR) in Australia the vertical co-ordinate of the CSIRO-9 (Mark II) AGCM was converted from the conventional σ-system to a η-system. The η-system was introduced to the non-linear dynamics of the AGCM.

The work performed in modifying the vertical co-ordinate system of the CSIRO-9 (Mark II) AGCM at the CSIRO is discussed in detail and forms a major part of this thesis.

1.5 OBJECTIVES OF THE RESEARCH

The objectives of the research detailed in this thesis are:

The *primary* objective is to improve the CSIRO-9 (Mark II) AGCM simulated climate output at upper atmospheric levels.

This was accomplished by modifying the conventional vertical co-ordinate system (σ-system) of the model. The study does not include changes to the model physics and therefore only specifies modifications to the model dynamics. Model output fields from the modified vertical co-ordinate system (η-system) are validated by comparing σ- and η-system results with European Centre for Medium-Range Weather Forcasting (ECMWF) analyses.

The second objective of this study is to better understand the structure and formulation of the non-linear dynamics of the CSIRO-9 (Mark II) AGCM.

This was attained by a thorough study of the formulation of the primitive equations prior to modifying the equations from a σ-system to a η-system.

In order to address these objectives, and to build a local modelling facility, it was essential to become familiar with the flow structure of the code of the CSIRO-9 (Mark II) AGCM. The code, which reads input data (initial fields etc.) and generates output data, were studied and some minor changes were introduced to make the output fields more manageable for locally developed graphical routines. The model was successfully installed on a CRAY EL94 super computer and numerous model runs, including seasonal forecasting experiments, have been completed.

1.6 ORGANISATION OF THE REPORT

General vertical co-ordinate systems commonly used in atmospheric models, as well as their advantages and disadvantages, are outlined in *Chapter 2*. Here the proposed η-system is defined and constant η-values are allocated to each model half-level in the vertical.

The transformation of the standard *momentum*, *continuity*, *thermodynamic* and *moisture* equations from a p- to η-system is presented in *Appendix A*.

Chapter 3 deals with the compilation of the atmospheric equations for the η-system. The *flux* formulation of these equations is derived in *Chapter 3*. This includes the *flux* formulation of the *momentum*, *vorticity*, *divergence* and *thermodynamic* equations as well as the *surface-pressure tendency* equation. These equations are linearised to obtain linear components for the gravity wave generating terms, which serve to link the *divergence*, *thermodynamic* and *surface-pressure tendency* equations during the semi-implicit time integration (*Chapter 5*)

Energy conservation is an essential requirement for climate model simulations. In *Chapter 4* equations for the *kinetic* and *internal* energies are derived, which are added to eventually yield an equation for the *total energy*. Global vertical integration of *the total energy* equation provides valuable information concerning energy conservation, and specific energy conservation requirements are accordingly defined. These requirements are vital when setting up the vertical finite difference (discrete) forms of the atmospheric equations.

Numerical solutions and the semi-implicit time integration are briefly outlined in *Chapter 5*. The *vorticity* and *divergence* equations are expressed in terms of the *stream function* and *velocity potential*, which make these equations more suitable for spectral representations. The atmospheric equations (*vorticity*, *divergence*, *thermodynamic* and *surface-pressure tendency*) are expressed in terms of spherical harmonics in the spherical co-ordinate reference frame. During model simulations, the μ-weighted (μ is defined in equation **2.1**) *vorticity*, *divergence*, *temperature*, *stream function*, *velocity potential* and horizontal *wind* components as well as the *surface-pressure* variables are spectrally carried. A spectral to grid transform of these variables allows for the calculation of non-linear terms. By using the inverse transform, the spectral atmospheric equations are constructed. The *moisture* and *vorticity* spectral prognoses are calculated by the application of a direct leapfrog method. Spectral prognoses of the *divergence*, *thermodynamic* and *surface-pressure* equations are time integrated by using a "semi-implicit" leapfrog method. In order to achieve longer time steps, these equations are coupled (linked) by means of the linear components from the gravity wave generating terms.

Two five-year seasonal cycle control runs were performed using both the η- and σ-systems respectively. In *Chapter 6* five-year ensemble means of zonal and meridional *wind*, *temperature* and *mean-sea level pressure* (MSLP) are compared with observed climate data fields. Two seasons namely summer (December, January, February) and winter (June, July, August) climate fields are validated. Model simulations using the η-system indicate significant improvements in the upper atmosphere (relative to the σ-system), especially in the vicinity of high orograpy in the summer hemisphere. Some conclusions are made.

Appendix A summarises the transformation of the *momentum*, *continuity, thermodynamic* and *moisture* equations from the p- to a η-system.

Appendix B contains the FORTRAN code developed to solve the hybrid co-ordinate condition matrix constructed in *Chapter 2* to obtain constant η-values for each model half-level.

In *Appendix C* a function and matrix relation, which directly relates the geopotential with temperature, is presented. This is derived from the *hydrostatic* approximation.

CHAPTER 2

THE HYBRID VERTICAL CO-ORDINATE SYSTEM

2.1 INTRODUCTION TO CO-ORDINATE SYSTEMS

A variety of co-ordinate systems have been applied on the primitive equations (Burger and Riphagen, 1990; Kasahara, 1974; Spiegel, 1974). Some co-ordinate systems have obvious advantages, and may contribute to the simplification of mathematical terms in the primitive equations.

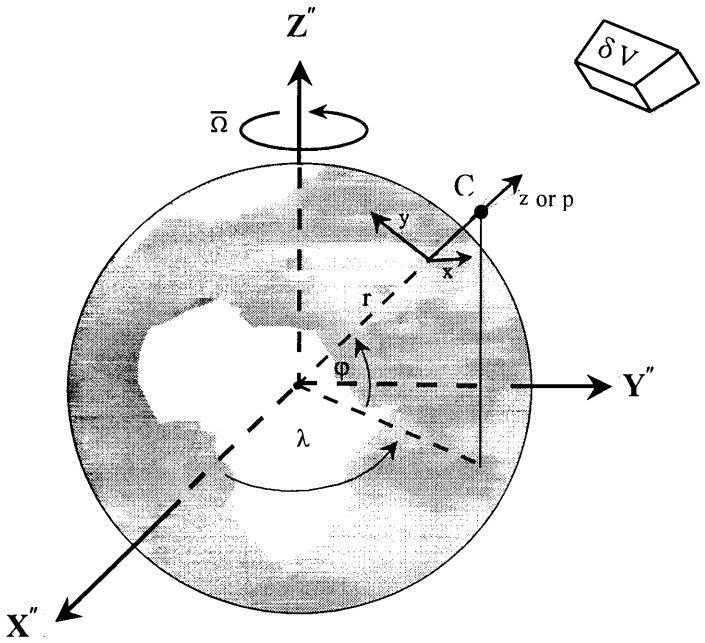

Figure 1. The position of any point C in space relative to the *inertial (X″,Y″,Z″), rotating* (x,y,z), *pressure* or *isobaric* (x,y,p) and *spherical* (λ,φ,r) co-ordinate systems. An atmospheric particle located at point C is, in meteorology, usually considered a small parcel of air with volume δV.

Atmospheric variables are often expressed in terms of a rigid orthogonal co-ordinate system (X″, Y″, Z″) referred to as the *inertial reference frame* (Holton, 1992) with the origin at the centre of the Earth and Z″-axis along the rotation axis of the earth (figure 1). At any time, the position of an atmospheric particle (parcel), or the physical state of an atmospheric variable, at any point C (figure 1) is viewed from space in the fixed (X″, Y″, Z″) co-ordinate system. In order to include the forces experienced by atmospheric particles (parcels) subjected to the rotation of the Earth, transformations to a *rotating co-ordinate system* (x, y, z)

had been introduced. Changes in the z (or p as defined in section 2.2) direction denote vertical changes in the position of point C above sea-level, while x and y denote changes from west to east and south to north (figure 1). Since the shape of the Earth may be approximated as a smooth sphere, it is also generally recommended to express the atmospheric variables, on a rotating earth, in terms of a *spherical co-ordinate system* (λ, φ, r) which is fixed to the rotating earth. Here λ is longitude and φ is latitude. The constant radius of the Earth is indicated by a, where $r = a + z$ denotes the direct distance from the centre of the Earth to point C. When considering infinitesimal displacements, Holton (1992) suggested that

$$\delta x = r\cos(\varphi)\delta\lambda$$
$$\delta y = r\delta\varphi$$

where (δx) and (δx) are measured along the curve of the Earth's surface.

2.2 THE PRESSURE VERTICAL CO-ORDINATE

The rotating (x, y, z)- and spherical (λ, φ, r) co-ordinate systems provide standard co-ordinate systems to mathematically express the flow patterns of atmospheric particles (parcels), as well as the physical changes of atmospheric variables, on the Earth. However, the nature of these changes does not necessarily rely upon the spherical shape of the earth only. Changes in atmospheric variables also depend on horizontal and vertical variations in the pressure, density and temperature fields above the surface of the Earth.

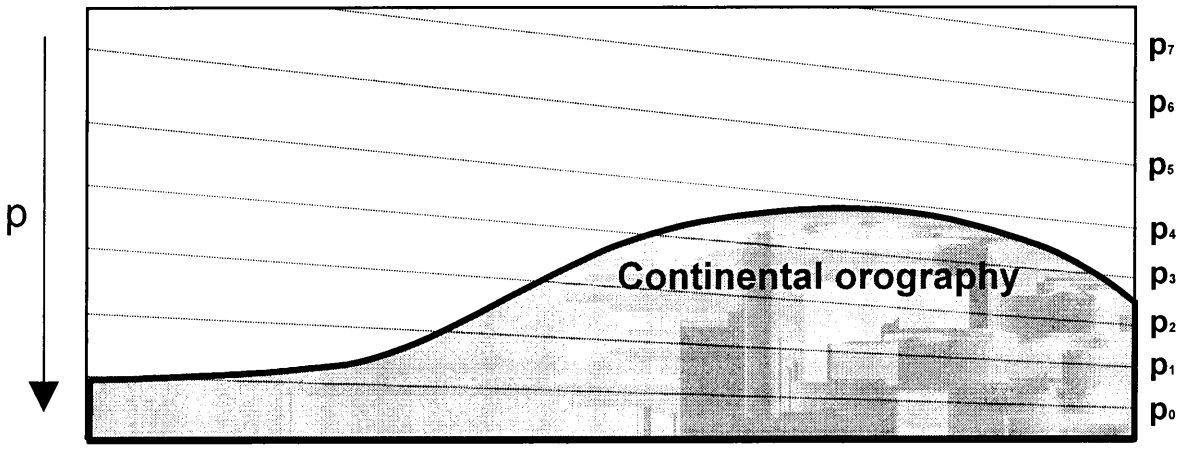

Figure 2(a): The vertical structure of a typical *pressure vertical co-ordinate system* (or p-system). The dotted lines represent constant pressure-levels ($\mathbf{p_0}$ to $\mathbf{p_7}$). Note that $\mathbf{p_7 < p_0}$.

Pressure as an independent vertical co-ordinate, was introduced for the first time during the late 1940's (Eliassen, 1949; Godart, 1984). A major advantage of the pressure (isobaric) co-ordinate system (p-system), is that density of the air no longer appears explicitly in the pressure gradient force terms. A second advantage is that the continuity equation in the p-system has no time derivatives and reduces to a pure diagnostic equation (Holton, 1992).

An important disadvantage, however, is that the lower boundary of the atmosphere (continental orography) does not represent a co-ordinate surface. The constant pressure-levels in the vertical therefore often intersect the surface of the earth over regions with high orography (figure 2a). The intersection may even occur over the oceans, especially over regions of low surface-pressure.

2.3 THE SIGMA VERTICAL CO-ORDINATE

The orography of the Earth's surface has a profound affect on the general circulation of the atmosphere. For example, vertical forcing due to the underlying orography (Chouinard, 1986) significantly influences the amplitudes of mid-latitude planetary waves. Vertically propagating gravity waves, which originate from air flowing over rough terrain, transport momentum from the surface of the earth to the upper atmosphere where, in turn, momentum flux divergence occurs. These atmospheric disturbances decelerate the synoptic-scale winds in such a way that planetary wave amplitudes are enhanced.

Tennant and van Heerden (1994) showed that orography contributes significantly to the development of cut-off low-pressure systems in the upper atmosphere over the South African interior. These systems occasionally develop as a result of mid-latitude planetary wave disturbances (anti-cyclonic disruption) in the upper atmosphere (Van Heerden and Hurry, 1987; Taljaart, 1985). Cut-off low-pressure systems are often responsible for extreme rainfall and extensive flooding over the country (Triegaardt *et.al.*, 1988).

Long experience in numerical modelling emphasises the necessity for the inclusion of orography as a co-ordinate surface in atmospheric models. This is achieved by the introduction of a terrain following, or sigma vertical co-ordinate system (σ-system), proposed by Phillips (1957). The σ-system is nothing less than a modified version of the p-system, where $p=\sigma P_S$ (figure 2b) and σ representing the independent vertical co-ordinate.

The lowest sigma-level ($\sigma = 1$) follows the continental orography, which is also as required, a co-ordinate surface. This is a major advantage of the σ-system. Another positive aspect is that the vertical velocity ($\dot{\sigma} = d\sigma / dt$) becomes zero at the top and bottom of the atmosphere.

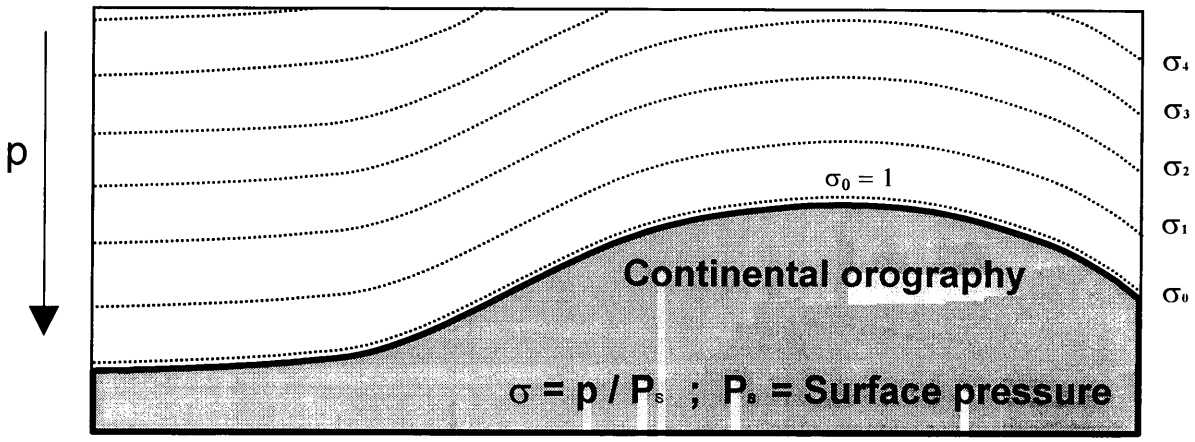

Figure 2(b): The vertical structure of a typical *sigma vertical co-ordinate system* (or σ-system). The dotted lines represent constant sigma (σ) levels. **σ = 0** where **p= 0** and **σ = 1** where **p=Ps**.

The absence of a sufficient number of constant pressure levels in the upper atmosphere is a certain limitation in the σ-system. The top σ-level (σ = 0 which means that p=0) represents the only constant pressure level. In the σ-system, large errors may be generated over steep mountains when calculating the difference between the relatively large terms $\sigma\underline{\nabla}\ln(P_S)\partial\Phi/\partial\sigma - \underline{\nabla}\Phi$ (Kasahara, 1966; Nakamura, 1978) in the momentum equation. The result is obtained as a small residual of these two terms, which may generate relative large errors over regions where the constant σ-surfaces have steep slopes.

2.4 THE HYBRID VERTICAL CO-ORDINATE

Both the p- and σ-systems have selective advantages. The p-system provides a suitable framework for describing the actual change of the atmosphere at stratospheric levels, while the σ-system incorporates the contribution of orography on the atmospheric circulation by including the lowest atmospheric level as a constant sigma co-ordinate surface. Proposing a hybrid vertical co-ordinate system (η-system) combines both these advantageous features. Sangster (1960) introduced one of the first hybrid co-ordinate systems, where the 500 hPa pressure-level was defined as a fixed level of transition from a σ- to p-system. All levels above 500 hPa were therefore isobaric.

In this thesis a η-system is introduced where the Earth's surface forms the first co-ordinate surface (identical to the σ-system), while the remaining co-ordinate surfaces gradually revert with altitude to isobaric-levels (as found in the p-system) (Simmons and Burridge, 1981; Mechoso *et al.,* 1982; Simmons and Strüfing 1981,1983, Hack *et al.* 1993). This system is introduced to the non-linear dynamics of the CSIRO-9 (Mark II) AGCM.

In the η-system (figure 2c) the pressure (p) at each half-level (any full-level $\eta_k = 0.5(\eta_{k+0.5} + \eta_{k-0.5})$, k=1 to 9, (figure 3)) of the model is defined as:

$$p = A_O + P_S B \qquad \text{where} \qquad \mu = \frac{\partial p}{\partial \eta} = \frac{\partial A_O}{\partial \eta} + P_S \frac{\partial B}{\partial \eta} \qquad \textbf{(2.1)}$$

P_S denotes the surface pressure. A_0 (a mean sea-level pressure (P_{OO}) weighted quantity) and B are constant values, which are pre-defined for each model half-level (figure 3). Note that $P_S = P_S(x,y,t)$, $A_O = A_O(\eta)$ and $B = B(\eta)$.

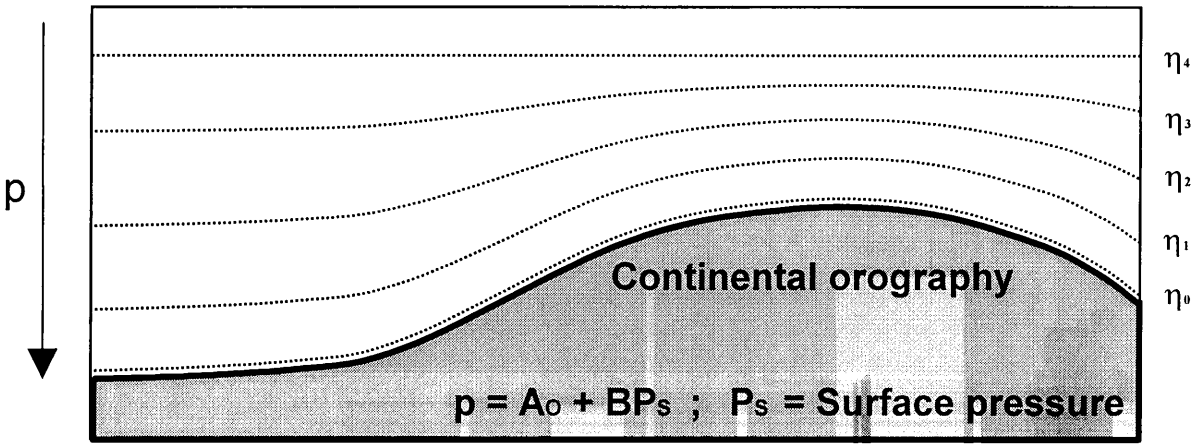

Figure 2(c): The vertical structure of a typical *hybrid vertical co-ordinate system* (or η-system). The dotted lines represent constant hybrid (η) levels. Prescribed pre-defined conditions are required to determine the value of constants **A_o** and **B** at each vertical half- level of the CSIRO-9 (Mark II) AGCM.

$A_0 = 0$ in equation **(2.1)** implies that $p = P_S B$, which is analogue to the relation defining the σ-system ($B = \sigma = p/P_S$). In addition, if $B = 0$ it means that the model half-levels are isobaric (as found in the p-system) since $p = A_0 =$ constant for each model half-level.

Since both the σ- and p- systems are included in equation **(2.1)** the first term (A_O) will subsequently be refered to as the **p-*component*** and the second term ($P_S B$) as the **σ-*component*** of the η-system.

In figure 3 the vertical structure of the co-ordinate surfaces of the proposed η-system, over a flat surface, is displayed. Values for the hybrid half-levels were derived from a generalised cubic polynomial formula, symmetric about η_5=0.5. The formula (programmed in Appendix B) first proposed by Smagorinsky *et, al.* (1965), was modified by John L. McGregor CSIRO (Atmospheric Research) (personal communication) to provide a smoothly varying set of levels in the

vertical suitable for use in the vertical advection part of the semi-Lagrangian moisture advection code used in the CSIRO-9 (Mark II) AGCM. The co-ordinate variable (η) varies from a maximum of η=1 at the surface of the Earth to a minimum of η=0 at the top layer of the model.

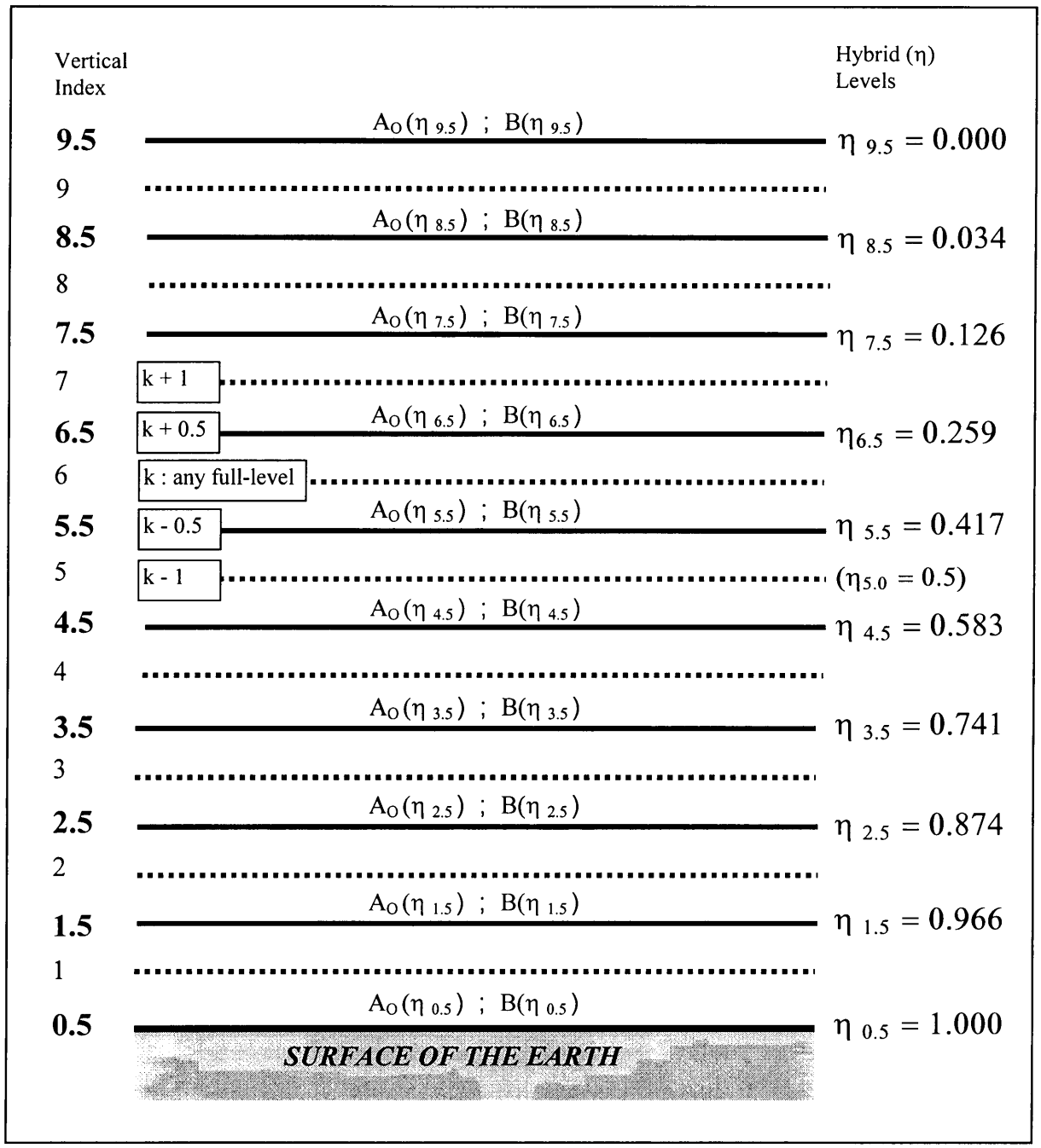

Figure 3: The vertical layers (η) of the CSIRO-9 (Mark II) AGCM, over a flat surface, expressed in terms of a generalised cubic polynomial formula, symmetric about η_5 = 0.5. Half-levels are depicted by solid lines.

2.5 PRE-DEFINED HYBRID CO-ORDINATE CONDITIONS

In this section, $A_0(\eta)$ and $B(\eta)$ are expressed as pre-defined smoothly varying functions of η (Simmons and Strüfing, 1981). The functions $A_0(\eta)$ and $B(\eta)$, contained in the p- and σ–*components* in equation **(2.1)**, may be presented by polynomial expressions (Washington, 1965) of the form:

$$A_O(\eta) = \sum_{n=1}^{m} a_{on}\eta^n \qquad \text{and} \qquad B(\eta) = \sum_{n=1}^{m} b_n\eta^n \qquad \textbf{(2.2)}$$

where m is the number of unknown values (a_{on}, b_n, $n = 1$ to m) to be solved in each polynomial expression. Substitution of the two relations from **(2.2)** into equation **(2.1)** gives

$$p = \sum_{n=1}^{m} a_{on}\eta^n + P_S\sum_{n=1}^{m} b_n\eta^n \qquad \textbf{(2.3)}$$

A number of pre-defined conditions, expressed in terms of **(2.2)** and **(2.3)**, are required to ultimately determine the values of $A_0(\eta)$ and $B(\eta)$ at each one of the hybrid half-levels depicted in figure 3. The vertical altitude of the hybrid half-levels is subsequently expressed in terms of atmospheric pressures or vertical pressure thicknesses. Let $\mathbf{P_{oo}}$**=1013.2 hPa** be the global *mean sea-level pressure* (MSLP). The altitude of Mount Everest (the highest mountain on Earth) is 8 840 meter (29 140 feet), which lies just below the 300 hPa level (Read and Watson, 1970). However, the topography used in the model is spectrally truncated at wave number R21, and is thus unable to resolve individual features such as Mount Everest. In fact the model topography over the Himalayas yields minimum surface pressures of about **500 hPa**. Thus to achieve suitable conditions for a set of well-behaved hybrid half-levels over any terrain, surface-pressures at the following two extreme orographic limits are defined:

i) ***Lowest orography*** : Surface-pressure (PL_S) = Sea-level pressure (P_{oo}) = 1013.2 hPa

ii) ***Highest orography*** : Surface-pressure (PH_S) = 500 hPa

Conditions C1 and C2:

A terrain-following co-ordinate, equivalent to the σ-system, is required for the first hybrid half-level (Earth's surface) where $\eta_{0.5} = 1$. As a first condition, the *p-component* in equation **(2.1)** therefore needs to be zero. From equations **(2.2)** and **(2.3)** it then follows that

$$A_O(\eta_{0.5}) = \sum_{n=1}^{m} a_{on}\eta_{0.5}{}^{n} = 0 \qquad \textbf{C1}$$

The remaining *σ-component* in equation **(2.1)** only meets the requirements set for the σ-system at the surface of the Earth if $B(\eta) = \sigma = 1$. Therefore, as second condition equations **(2.2)** yield

$$B\ (\eta_{0.5}) = \sum_{n=1}^{m} b_n\eta_{0.5}{}^{n} = 1 \qquad \textbf{C2}$$

Conditions C3, C4, C5 and C6:

A basic requirement for defining the η-system is that the top three half-levels should be constant pressure-levels. From equation **(2.3)** it follows that $p = 0$ when $\eta = 0$ implying that the top hybrid half-level $\eta_{9.5} = 0$ is already isobaric. Since constant pressures are specified for the next two lower half-levels, the *σ-component* in equation **(2.1)** for half-levels $\eta_{8.5} = 0.034$ and $\eta_{7.5} = 0.126$ must be zero. But $P_S \neq 0$, requiring that $B(\eta) = 0$ for both levels. Equation **(2.2)** yields

$$B\ (\eta_{8.5}) = \sum_{n=1}^{m} b_n\eta_{8.5}{}^{n} = 0 \qquad \textbf{C3}$$

$$B\ (\eta_{7.5}) = \sum_{n=1}^{m} b_n\eta_{7.5}{}^{n} = 0 \qquad \textbf{C4}$$

The *p-component* in equation **(2.1)** needs to be constant at hybrid half-levels $\eta_{8.5} = 0.034$ and $\eta_{7.5} = 0.126$. Atmospheric pressures at these half-levels are $0.034 \times P_{oo}$ =34 hPa for half-level $\eta_{8.5}$ and $0.126 \times P_{oo}$ =127 hPa for half-level $\eta_{7.5}$. Since $B(\eta) = 0$ from ***C3*** and ***C4*** equation **(2.3)** yields

$$A_O(\eta_{8.5}) = \sum_{n=1}^{m} a_{on}\eta_{8.5}{}^{n} = \eta_{8.5}P_{oo} \qquad \textbf{C5}$$

$$A_O(\eta_{7.5}) = \sum_{n=1}^{m} a_{on}\eta_{7.5}{}^{n} = \eta_{7.5}P_{oo} \qquad \textbf{C6}$$

Conditions C7 and C8:

Note that setting the pressures of the top two half-levels in ***C5*** and ***C6*** effectively reduces the atmospheric depth over which the remaining co-ordinate conditions can be imposed (reduced depth is unshaded in figure 4). Over the *lowest and*

highest orography, the reduced depths, which are expressed in terms of pressure thicknesses (figure 4), are:

ΔPL = P_{oo} - 127 hPa = 1013.2 hPa - 127 hPa = 886 hPa
ΔPH = 500 hPa - 127 hPa = 373 hPa

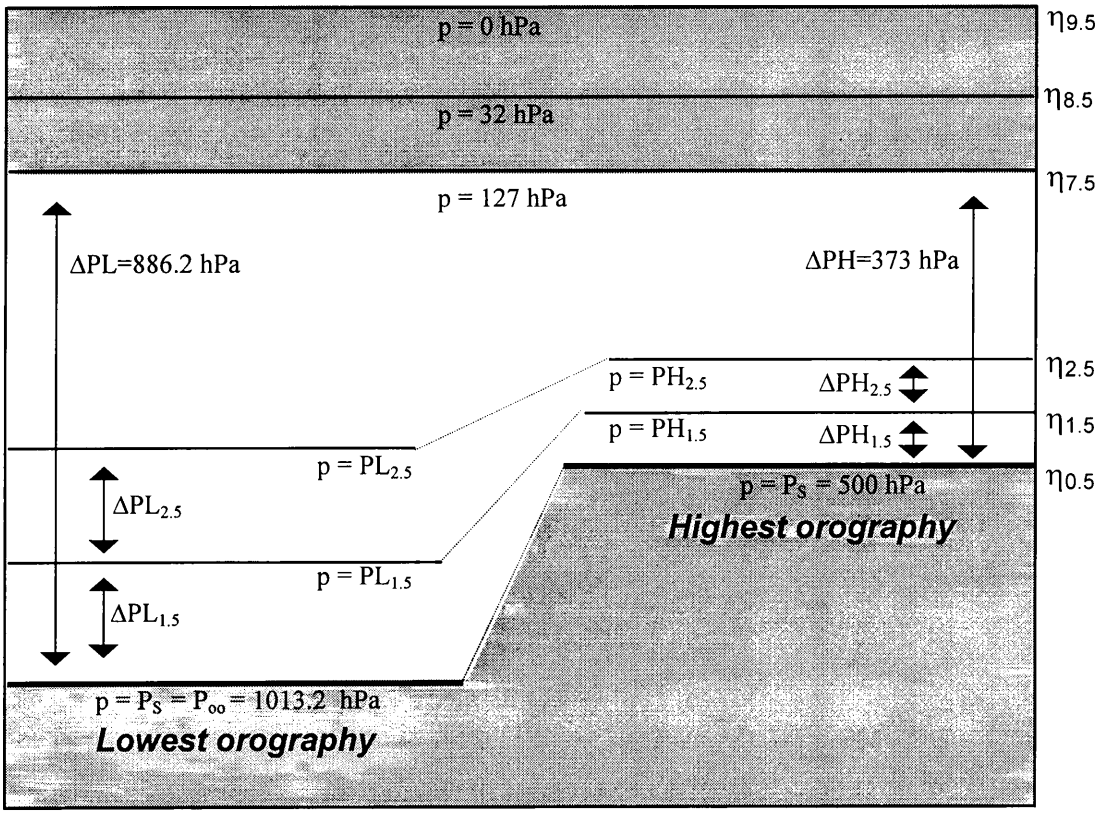

Figure 4: The three top (shaded) and three bottom hybrid half-levels prescribed in conditions ***C1*** to ***C8***. The unshaded area depicts the reduced atmospheric depth available for prescribing the lower six hybrid half-levels (surface level excluded).

The magnitude of the ratio between the reduced atmospheric depth over *the highest* and *lowest orography* (figure 4), which also represents the *maximum* ratio above any two surface locations, is given α_{max} where

$$\alpha_{\max} = \frac{\Delta PH}{\Delta PL} = \frac{373}{886} = 0.42$$

In this analysis, a constraint on the pressure thickness of the lowest two model levels over the highest orography is to be determined. This constraint is set to be such that the pressure thickness below half-levels $\eta_{1.5}$ and $\eta_{2.5}$ over the *highest orography* ($\Delta PH_{1.5}$ and $\Delta PH_{2.5}$ in figure 4) should be a factor α_{max} of the pressure thickness below the same two hybrid half-levels over the *lowest*

orography ($\Delta PL_{1.5}$ and $\Delta PL_{2.5}$ in figure 4). In practice, a value of $\alpha = (0.5)\alpha_{max} = 0.21$ was found to give acceptable layer thicknesses over the highest topography in the CSIRO-9 AGCM. Before applying the α–ratio, the pressures at half-levels $\eta_{1.5}$ and $\eta_{2.5}$ over the *lowest orography* ($PL_{1.5}$ and $PL_{2.5}$) and over the *highest orography* ($PH_{1.5}$ and $PH_{2.5}$) are expressed in terms of equation **(2.3)**:

$$PL_{1.5} = \sum_{n=1}^{m} a_{on}\eta_{1.5}{}^{n} + P_{oo}\sum_{n=1}^{m} b_n\eta_{1.5}{}^{n} \qquad (\text{with } P_S = P_{oo}) \qquad \textbf{(2.4)}$$

$$PH_{1.5} = \sum_{n=1}^{m} a_{on}\eta_{1.5}{}^{n} + 500\sum_{n=1}^{m} b_n\eta_{1.5}{}^{n} \qquad (\text{with } P_S = 500 \text{ hPa}) \qquad \textbf{(2.5)}$$

$$PL_{2.5} = \sum_{n=1}^{m} a_{on}\eta_{2.5}{}^{n} + P_{oo}\sum_{n=1}^{m} b_n\eta_{2.5}{}^{n} \qquad (\text{with } P_S = P_{oo}) \qquad \textbf{(2.6)}$$

$$PH_{2.5} = \sum_{n=1}^{m} a_{on}\eta_{2.5}{}^{n} + 500\sum_{n=1}^{m} b_n\eta_{2.5}{}^{n} \qquad (\text{with } P_S = 500 \text{ hPa}) \qquad \textbf{(2.7)}$$

As decided earlier, the layer thickness condition for half-level $\eta_{1.5}$ yields

$$\Delta PH_{1.5} = \alpha\Delta PL_{1.5}$$
$$\therefore\ (500 - PH_{1.5}) = \alpha(P_{oo} - PL_{1.5})$$

Using equations **(2.4)** and **(2.5)** gives

$$(500) - (\sum_{n=1}^{m} a_{on}\eta_{1.5}{}^{n} + 500\sum_{n=1}^{m} b_n\eta_{1.5}{}^{n}) = (\alpha P_{oo}) - (\alpha\sum_{n=1}^{m} a_{on}\eta_{1.5}{}^{n} + \alpha P_{oo}\sum_{n=1}^{m} b_n\eta_{1.5}{}^{n})$$

$$(\alpha - 1)\sum_{n=1}^{m} a_{on}\eta_{1.5}{}^{n} + (\alpha P_{oo} - 500)\sum_{n=1}^{m} b_n\eta_{1.5}{}^{n} = (\alpha P_{oo} - 500) \qquad \boxed{C7}$$

The layer thickness condition for half-level $\eta_{2.5}$ is similarly expressed as

$$\Delta PH_{2.5} = \alpha\Delta PL_{2.5}$$
$$\therefore\ (PH_{1.5} - PH_{2.5}) = \alpha(PL_{1.5} - PL_{2.5})$$

Substitution from equations **(2.4)**, **(2.5)**, **(2.6)** and **(2.7)** yields

$$(\sum_{n=1}^{m} a_{on}\eta_{1.5}{}^{n} + 500\sum_{n=1}^{m} b_n\eta_{1.5}{}^{n}) - (\sum_{n=1}^{m} a_{on}\eta_{2.5}{}^{n} + 500\sum_{n=1}^{m} b_n\eta_{2.5}{}^{n})$$
$$= (\alpha\sum_{n=1}^{m} a_{on}\eta_{1.5}{}^{n} + \alpha P_{oo}\sum_{n=1}^{m} b_n\eta_{1.5}{}^{n}) - (\alpha\sum_{n=1}^{m} a_{on}\eta_{2.5}{}^{n} + \alpha P_{oo}\sum_{n=1}^{m} b_n\eta_{2.5}{}^{n})$$

and finally

$$(1-\alpha)\sum_{n=1}^{m} a_{on}(\eta_{1.5}{}^{n} - \eta_{2.5}{}^{n}) - (\alpha P_{oo} - 500)\sum_{n=1}^{m} b_{n}(\eta_{1.5}{}^{n} - \eta_{2.5}{}^{n}) = 0 \qquad \textbf{C8}$$

Two further conditions need to be imposed for *selected* hybrid half-levels in the middle atmosphere since the top and bottom three half-levels already have constraints. A constant pressure is imposed for the *lowest orography* ($P_S = P_{oo}$) for each one of the two hybrid half-levels $\eta_{4.5} = 0.583$ and $\eta_{6.5} = 0.259$. These pressures are (0.583 x P_{oo} = 590 hPa) at half-level $\eta_{4.5}$ and (0.259 x P_{oo} = 262 hPa) at half-level $\eta_{6.5}$. Note that these conditions are applied for pressures above the *lowest orography* only.

By replacing ($P_S = P_{oo}$) in equation **(2.3)** the following two conditions are prescribed for half-levels $\eta_{4.5}$ and $\eta_{6.5}$ respectively:

$$\sum_{n=1}^{m} a_{on}\eta_{4.5}{}^{n} + P_{00}\sum_{n=1}^{m} b_{n}\eta_{4.5}{}^{n} = \eta_{4.5}P_{oo} \qquad \textbf{C9}$$

$$\sum_{n=1}^{m} a_{on}\eta_{6.5}{}^{n} + P_{00}\sum_{n=1}^{m} b_{n}\eta_{6.5}{}^{n} = \eta_{6.5}P_{oo} \qquad \textbf{C10}$$

This finally yields a total of 10 pre-defined condition equations (***C1*** to ***C10***). Setting of **m = 5** in the polynomial expressions **(2.2)** will generate 10 unknowns (a_{o1} to a_{o5} and b_1 to b_5). These unknowns are solved through matrix analysis by expressing the 10 condition equations in the form of the so-called *co-ordinate condition matrix* (section 2.6). Substitution of the 10 solutions into **(2.2)** will allow for $A_O(\eta)$ and $B(\eta)$ to be solved at each hybrid half-level. These prescribed values of $A_O(\eta)$ and $B(\eta)$ form the basis of the η-system, and are applied in the numerical integration of the η-formulation of the primitive equations.

The *Fortran* code developed to solve the functions $A_O(\eta)$ and $B(\eta)$ at each hybrid half-level is attached to this document as Appendix B.

2.6 SELECTIVE PRESSURE THICKNESS RATIOS

Output results of $A_O(\eta)$ and $B(\eta)$ from the *Fortran* code (Appendix B) determined for α = 0.21 are listed in Table 1. These results are considered acceptable since the *p-component* at the surface of the earth is zero, while the σ-*component* does not affect the three top half-levels, which are specified as constant pressure-levels. In-between a gradual change from a dominant σ-*component* to a dominant *p-component* is evident with increasing height.

$A_O(\eta_{0.5})$ = 0.0000	$B(\eta_{0.5})$ = 1.0000
$A_O(\eta_{1.5})$ = 19.4342	$B(\eta_{1.5})$ = 0.9465
$A_O(\eta_{2.5})$ = 71.5221	$B(\eta_{2.5})$ = 0.8032
$A_O(\eta_{3.5})$ = 150.3720	$B(\eta_{3.5})$ = 0.5923
$A_O(\eta_{4.5})$ = 235.5229	$B(\eta_{4.5})$ = 0.3505
$A_O(\eta_{5.5})$ = 276.0961	$B(\eta_{5.5})$ = 0.1445
$A_O(\eta_{6.5})$ = 231.8971	$B(\eta_{6.5})$ = 0.0304
$A_O(\eta_{7.5})$ = 127.8661	$B(\eta_{7.5})$ = 0.0000
$A_O(\eta_{8.5})$ = 34.7462	$B(\eta_{8.5})$ = 0.0000
$A_O(\eta_{9.5})$ = 0.0000	$B(\eta_{9.5})$ = 0.0000

Table 1. $A_O(\eta)$ and $B(\eta)$ values for each hybrid half-level with α = **0.21**.

Figure 5 depicts the vertical layer pressure thickness ($p_{k+0.5} - p_{k-0.5}$, k = 1 to 9) of nine hybrid half-levels (surface layer excluded) as determined for α=0.21. The vertical variation in layer pressure thickness is shown for selected cases where the surface pressure (P_S) is equal to 1013 hPa (*lowest orography* = MSLP), 800 hPa, 600 hPa and 500 hPa. Figure 5 indicates that all the layer pressure thicknesses of the nine hybrid half-levels, over all the selected orographies, continuously increase from the surface of the earth to a specific point in the upper atmosphere, whereafter a general decrease is noticeable into the stratosphere.

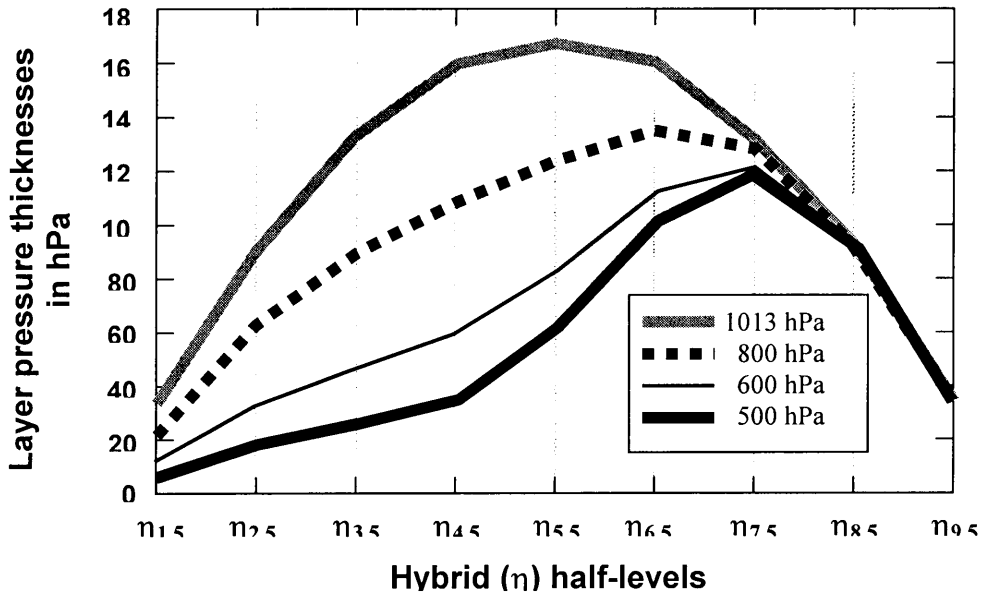

Figure 5: The vertical layer pressure thickness ($p_{k+0.5} - p_{k-0.5}$, k = 1 to 9) variation of nine hybrid half-levels as determined from α = **0.21**.

2.7 CO-ORDINATE CONDITION MATRIX

Known values are designated to variables $a_{o\eta}$ and b_n (for n=1 to 5) by solving the following matrix. $A_O(\eta)$ and $B(\eta)$, which are constant at each one of the 10 hybrid half-levels, may subsequently be calculated with the aid of equation **(2.2)**. The Fortran code used to solve the matrix is presented in APPENDIX B.

* Let $\alpha_0 = (1 - \alpha)$ and $\alpha_1 = (\alpha P_{oo} - 500)$.

$$
\begin{bmatrix}
\eta_{0.5}^{1} & \eta_{0.5}^{2} & \eta_{0.5}^{3} & \eta_{0.5}^{4} & \eta_{0.5}^{5} & 0 & 0 & 0 & 0 & 0 \\
0 & 0 & 0 & 0 & 0 & \eta_{0.5}^{1} & \eta_{0.5}^{2} & \eta_{0.5}^{3} & \eta_{0.5}^{4} & \eta_{0.5}^{5} \\
0 & 0 & 0 & 0 & 0 & \eta_{8.5}^{1} & \eta_{8.5}^{2} & \eta_{8.5}^{3} & \eta_{8.5}^{4} & \eta_{8.5}^{5} \\
0 & 0 & 0 & 0 & 0 & \eta_{7.5}^{1} & \eta_{7.5}^{2} & \eta_{7.5}^{3} & \eta_{7.5}^{4} & \eta_{7.5}^{5} \\
\eta_{8.5}^{1} & \eta_{8.5}^{2} & \eta_{8.5}^{3} & \eta_{8.5}^{4} & \eta_{8.5}^{5} & 0 & 0 & 0 & 0 & 0 \\
\eta_{7.5}^{1} & \eta_{7.5}^{2} & \eta_{7.5}^{3} & \eta_{7.5}^{4} & \eta_{7.5}^{5} & 0 & 0 & 0 & 0 & 0 \\
-\alpha_0\eta_{1.5}^{1} & -\alpha_0\eta_{1.5}^{2} & -\alpha_0\eta_{1.5}^{3} & -\alpha_0\eta_{1.5}^{4} & -\alpha_0\eta_{1.5}^{5} & \alpha_1\eta_{1.5}^{1} & \alpha_1\eta_{1.5}^{2} & \alpha_1\eta_{1.5}^{3} & \alpha_1\eta_{1.5}^{4} & \alpha_1\eta_{1.5}^{5} \\
\alpha_0\eta_{1.5}^{1} - \alpha_0\eta_{2.5}^{1} & \alpha_0\eta_{1.5}^{2} - \alpha_0\eta_{2.5}^{2} & \alpha_0\eta_{1.5}^{3} - \alpha_0\eta_{2.5}^{3} & \alpha_0\eta_{1.5}^{4} - \alpha_0\eta_{2.5}^{4} & \alpha_0\eta_{1.5}^{5} - \alpha_0\eta_{2.5}^{5} & -\alpha_1\eta_{1.5}^{1} + \alpha_1\eta_{2.5}^{1} & -\alpha_1\eta_{1.5}^{2} + \alpha_1\eta_{2.5}^{2} & -\alpha_1\eta_{1.5}^{3} + \alpha_1\eta_{2.5}^{3} & -\alpha_1\eta_{1.5}^{4} + \alpha_1\eta_{2.5}^{4} & -\alpha_1\eta_{1.5}^{5} + \alpha_1\eta_{2.5}^{5} \\
\eta_{4.5}^{1} & \eta_{4.5}^{2} & \eta_{4.5}^{3} & \eta_{4.5}^{4} & \eta_{4.5}^{5} & P_{oo}\eta_{4.5}^{1} & P_{oo}\eta_{4.5}^{2} & P_{oo}\eta_{4.5}^{3} & P_{oo}\eta_{4.5}^{4} & P_{oo}\eta_{4.5}^{5} \\
\eta_{6.5}^{1} & \eta_{6.5}^{2} & \eta_{6.5}^{3} & \eta_{6.5}^{4} & \eta_{6.5}^{5} & P_{oo}\eta_{6.5}^{1} & P_{oo}\eta_{6.5}^{2} & P_{oo}\eta_{6.5}^{3} & P_{oo}\eta_{6.5}^{4} & P_{oo}\eta_{6.5}^{5}
\end{bmatrix}
\begin{bmatrix} a_{01} \\ a_{02} \\ a_{03} \\ a_{04} \\ a_{05} \\ b_1 \\ b_2 \\ b_3 \\ b_4 \\ b_5 \end{bmatrix}
=
\begin{bmatrix} 0 \\ 1 \\ 0 \\ 0 \\ P_{oo}\eta_{8.5} \\ P_{oo}\eta_{7.5} \\ \alpha_1 \\ 0 \\ P_{oo}\eta_{4.5} \\ P_{oo}\eta_{6.5} \end{bmatrix}
$$

CHAPTER 3

THE FLUX FORMULATION OF THE SPECTRAL ATMOSPHERIC EQUATIONS IN A HYBRID VERTICAL CO-ORDINATE SYSTEM

3.1 INTRODUCTION

In order to achieve conservation of *momentum*, *mass* and *energy*, the *flux* formulation of the spectral atmospheric equations was introduced into an earlier version of the CSIRO-9 AGCM (Gordon 1981). This formulation is still used in the sigma vertical co-ordinate system (σ-system) models. In contrast with weather forcasting models, where the *advective* formulation of the atmospheric equations (Bourke *et al.*, 1977) are used, it is essential that *momentum*, *mass* and *energy* are conserved during climate model simulations. This is especially important where long time integrations (one year and more) are performed. The *flux* formulation results when the *continuity* equation is incorporated into the *momentum, thermodynamic* and *moisture* equations. Here the model variables in the σ-system are weighted by the surface-pressure (P_S).

In this chapter a hybrid vertical co-ordinate system (η-system) will be introduced to the flux formulation of the atmospheric equations of the CSIRO-9 (Mark II) AGCM. The P_S-weighting, as considered in the σ-system, will be replaced by a μ-weighting, where (μ) is defined in equation **(2.1)**:

$$\mu = \frac{\partial p}{\partial \eta} = \frac{\partial A_o}{\partial \eta} + P_s \frac{\partial B}{\partial \eta}$$

In APPENDIX A the *momentum, continuity* and *thermodynamic* equations are transformed from an isobaric vertical co-ordinate system (p-system) to the proposed η-system.

The μ-weighted *vertical component of vorticity* ($\hat{\xi}$) and *horizontal divergence* ($\hat{D}$) in the η-system are defined as

$\xi = \underline{k} \cdot \underline{\nabla} \times \underline{V}$: $\quad \hat{\xi} = \underline{k} \cdot \underline{\nabla} \times \hat{\underline{V}}$

$D = \underline{\nabla} \cdot \underline{V}$: $\quad \hat{D} = \underline{\nabla} \cdot \hat{\underline{V}}$ $\quad$ where $\hat{\underline{V}} = \mu \underline{V}$ and $\underline{V} = u\underline{i} + v\underline{j}$

Note that $\underline{\nabla}$ refers to $\underline{\nabla}_\eta$ in the η-system where $\underline{\nabla}_\eta = \frac{\partial}{\partial x}\underline{i} + \frac{\partial}{\partial y}\underline{j}$.

3.2 FLUX FORM OF THE MOMENTUM EQUATION

From APPENDIX A, equation **(A.8)**, the *momentum* equation in the η-system may be expressed as:

$$\frac{\partial \underline{V}}{\partial t} + (\underline{V}\cdot\underline{\nabla})\underline{V} + \dot{\eta}\frac{\partial \underline{V}}{\partial \eta} + \underline{\nabla}\Phi + \frac{RTB}{p}\underline{\nabla}P_s + f\underline{k}\times\underline{V} = \underline{F} \qquad \textbf{(3.1)}$$

From APPENDIX A, equation **(A.11)**, the *continuity* equation in the η-system may be expressed as:

$$\frac{\partial \mu}{\partial t} + \underline{\nabla}\cdot(\mu\underline{V}) + \frac{\partial}{\partial \eta}(\mu\dot{\eta}) = 0 \qquad \textbf{(3.2)}$$

The *flux* formulation of the *momentum* equation can be obtained by multiplying equation **(3.1)** by μ and equation **(3.2)** by $\underline{V}$ and then add the result.

$$\frac{\partial(\mu\underline{V})}{\partial t} + \underline{V}(\underline{\nabla}\cdot(\mu\underline{V})) + \mu(\underline{V}\cdot\underline{\nabla})\underline{V} + \frac{\partial(\mu\dot{\eta}\underline{V})}{\partial \eta} + \mu\underline{\nabla}\Phi + \frac{RT\mu B}{p}\underline{\nabla}P_s + \mu f\underline{k}\times\underline{V} = \mu\underline{F}$$

Replace the quantities $\hat{D} = \underline{\nabla}\cdot(\mu\underline{V})$, $\hat{\omega} = \mu\dot{\eta}$ and let $\hat{\underline{F}} = \mu\underline{F}$

$$\frac{\partial \hat{\underline{V}}}{\partial t} + \hat{D}\underline{V} + \mu(\underline{V}\cdot\underline{\nabla})\underline{V} + \frac{\partial(\hat{\omega}\underline{V})}{\partial \eta} + \mu\underline{\nabla}\Phi + \frac{RT\mu B}{p}\underline{\nabla}P_s + \mu f\underline{k}\times\underline{V} = \hat{\underline{F}} \qquad \textbf{(3.3)}$$

Considering the following vector identity (Spiegel, 1974), with the atmospheric flow ($\underline{V}$) along constant η–levels (quasi-horizontal flow)

$$(\underline{V}\cdot\underline{\nabla})\underline{V} = \underline{\nabla}(\frac{\underline{V}\cdot\underline{V}}{2}) + (\underline{\nabla}\times\underline{V})\times\underline{V} = \underline{\nabla}(\frac{V^2}{2}) + \xi\underline{k}\times\underline{V}$$

The *advection term* (third term on the left hand side (LHS) in equation **(3.3)**) may be expressed as:

$$\mu(\underline{V}\cdot\underline{\nabla})\underline{V} = \mu\left\{\underline{\nabla}(\frac{V^2}{2}) + \xi\underline{k}\times\underline{V}\right\} = \mu\underline{\nabla}E + (\mu\xi)\underline{k}\times\underline{V} \quad \text{where} \quad E = \left\{\frac{V^2}{2}\right\} \qquad \textbf{(3.4)}$$

The variable E denotes the *kinetic energy* per unit mass.

But $$\hat{\xi} = \underline{k} \cdot \underline{\nabla} \times (\mu \underline{V}) = \underline{k} \cdot (\nabla\mu \times \underline{V} + \mu \underline{\nabla} \times \underline{V}) = \underline{k} \cdot (\mu \underline{\nabla} \times \underline{V} - \underline{V} \times \underline{\nabla}\mu)$$

$$= \mu(\underline{k} \cdot \underline{\nabla} \times \underline{V}) - \underline{k} \cdot (\underline{V} \times \underline{\nabla}\mu) = \mu\xi - \underline{k} \cdot (\underline{V} \times \underline{\nabla}\mu)$$

$$= \mu\xi - \underline{k} \cdot (\underline{V} \times \underline{\nabla}\left\{\frac{\partial A_o}{\partial \eta} + \frac{\partial B}{\partial \eta} P_s\right\}) = \mu\xi - \left\{\frac{\partial B}{\partial \eta} \underline{k} \cdot (\underline{V} \times \underline{\nabla}) P_s\right\}$$

$$= \mu\xi - \left\{\frac{\partial B}{\partial \eta} \delta_1\right\} \qquad \text{where} \quad \boxed{\delta_1 = \underline{k} \cdot (\underline{V} \times \underline{\nabla}) P_s} \qquad \textbf{(3.5)}$$

and therefore

$$\mu\xi = \hat{\xi} + \left\{\frac{\partial B}{\partial \eta} \delta_1\right\}$$

When the above expression is replaced in equation **(3.4)**, the *advection term* becomes

$$\mu(\underline{V} \cdot \underline{\nabla})\underline{V} = \mu \underline{\nabla} E + \left\{\hat{\xi} + \frac{\partial B}{\partial \eta} \delta_1\right\} \underline{k} \times \underline{V}$$

Replace this term into the *flux* formulation of the *momentum* equation **(3.3)**

$$\frac{\partial \hat{\underline{V}}}{\partial t} + \hat{D}\underline{V} + \mu \underline{\nabla} E + \left\{\hat{\xi} + \frac{\partial B}{\partial \eta} \delta_1\right\} \underline{k} x \underline{V} + \frac{\partial(\hat{\omega}\underline{V})}{\partial \eta} + \mu \underline{\nabla}\Phi + \frac{RT\mu B}{p} \underline{\nabla} P_s + \mu f \underline{k} \times \underline{V} = \hat{\underline{F}}$$

which may also be expressed as

$$\boxed{\frac{\partial \hat{\underline{V}}}{\partial t} + \left\{\hat{\xi} + \frac{\partial B}{\partial \eta} \delta_1 + \mu f\right\} \underline{k} \times \underline{V} + \underline{C} = 0} \qquad \textbf{(3.6)}$$

with some additional non-linear terms

$$\underline{C} = \frac{\partial(\hat{\omega}\underline{V})}{\partial \eta} + \left\{\mu \underline{\nabla} E + \mu \underline{\nabla}\Phi + \frac{RT\mu B}{p} \underline{\nabla} P_s\right\} + \hat{D}\underline{V} - \hat{\underline{F}}$$

(a) **(b)** **(c)**

3.3 MEAN AND PERTURBATION COMPONENTS

Time integration of the CSIRO-9 (Mark II) AGCM is performed using a semi-implicit method in which the *linearised* gravity wave generating terms in the *momentum* and *thermodynamic* equations are time averaged resulting in the suppression of fast moving gravity waves. This allows longer time steps in climate models. In order to accomplish this the *non-linear* gravity wave generating terms have to be *linearised* about a basic state.

The process of linearisation requires the decomposition of the *temperature* (T), *geopotential* (Φ) and *kinetic energy* (E) variables in terms of mean and perturbation components:

3.3.1 TEMPERATURE (T):

The temperature (T) is replaced by $T_O + T'$, where T_O is a pre-set *global* mean value. It is defined to be *isothermal* in the vertical in order to maintain stability during model simulations (Gordon 1981). It is also set to be slightly greater than the global mean temperature of the lowest model level (290°K in this case). T' denotes the perturbation from T_O.

3.3.2 GEOPOTENTIAL (Φ):

The geopotential is written as $\Phi = gz = \phi + \phi_S$ where ϕ_S is the *surface (spectrally truncated topography)* contribution. These variables also present the *potential energy* in the atmospheric equations. Let

$$(\phi = \phi_O + \phi') \quad \text{and} \quad (\phi_S = \phi_{SO} + \phi'_S)$$

where ϕ_O is the mean geopotential which is a global constant at *each model level* and calculated from the global mean temperature (T_O) using the *hydrostatic approximation.* This process is detailed in Appendix C. ϕ_{SO} represents the global mean surface geopotential. ϕ' and ϕ'_S are perturbations from ϕ_O and ϕ_{SO} respectively.

3.3.3 KINETIC ENERGY (E):

Similarly, for the *kinetic energy* per unit mass $(E = V^2/2)$ let $E = E_O + E'$. E_O is pre-set to approximate global mean values for *each model level* and E' represents the perturbation from E_O.

3.4 LINEARISATION OF THE MOMENTUM EQUATION

The terms which require linearisation in the *momentum* equation are the non-linear terms (**a**), (**b**) and (**c**) of $\underline{C}$ in equation **(3.6)**.

The *kinetic energy per unit mass* of the *momentum* equation (term (**a**) from $\underline{C}$ in equation **(3.6)**) is linearised as follows:

$$\mu\underline{\nabla}E = \mu\underline{\nabla}(E_o + E') = \mu\underline{\nabla}E' = \underline{\nabla}(\mu E') - E'\underline{\nabla}\mu$$
$$= \underline{\nabla}(\mu E') - E'\underline{\nabla}\left\{\frac{\partial A_o}{\partial \eta} + P_s\frac{\partial B}{\partial \eta}\right\}$$
$$= \underline{\nabla}(\mu E') - E'\frac{\partial B}{\partial \eta}\underline{\nabla}P_s$$

The first term on the right hand side (RHS) is linear.

The first gravity wave generating term to be linearised is the *surface-pressure gradient* (term (**c**) from $\underline{C}$ in equation **(3.6)**). This is achieved by adding and subtracting an additional term containing the global mean temperature (section 3.3.1). The additional term is analogous to a term used by Gordon (1981) in the σ–system formulation.

$$\frac{RT\mu B}{p}\underline{\nabla}P_s = \frac{RT\mu B}{p}\underline{\nabla}P_s + RT_o\underline{\nabla}P_s - RT_o\underline{\nabla}P_s$$
$$= RT_o\underline{\nabla}P_s + R\left\{\frac{T\mu B}{p} - T_o\right\}\underline{\nabla}P_s$$
$$= RT_o\underline{\nabla}P_s + R(T^*)\underline{\nabla}P_s \qquad \text{where} \qquad T^* = \left\{\frac{T\mu B}{p} - T_o\right\}$$

The gravity wave generating component ($RT_o\underline{\nabla}P_s$) is linear (note that R and T_0 are constants) and will be treated semi-implicitly.

The second gravity wave generating term to be linearised is the *geopotential gradient* (term (**b**) from $\underline{C}$ in equation **(3.6)**).

$$\mu\underline{\nabla}\Phi = \mu\underline{\nabla}(\phi_o + \phi' + \phi_{so} + \phi'_s) = \mu\underline{\nabla}\phi' + \mu\underline{\nabla}\phi'_s$$
$$= \underline{\nabla}(\mu\phi') - \phi'\underline{\nabla}\mu + \underline{\nabla}(\mu\phi'_s) - \phi'_s\underline{\nabla}\mu$$

$$= \underline{\nabla}(\mu\phi') + \underline{\nabla}(\mu\phi'_s) - (\phi' + \phi'_s)\underline{\nabla}\mu$$

$$= \underline{\nabla}(\mu\phi') + \underline{\nabla}(\mu\phi'_s) - (\phi' + \phi'_s)\frac{\partial B}{\partial \eta}\underline{\nabla}P_s \qquad \textbf{(3.7)}$$

In the σ-version of the semi-implicit equations Gordon (1981) found that the linear part of the *geopotential gradient* term $(\underline{\nabla}P_s\phi')$ could be treated semi-implicitly by directly relating $(P_s\phi')$ to (P_sT') using the hydrostatic approximation. The relation $(\underline{P_s\phi'} = \underline{\underline{A}}\underline{P_sT'})$, for the σ-system, is derived in Appendix C.

In the η-system, however, it is not possible to relate the quantity $(\underline{\nabla}\mu\phi')$ directly to $\mu T'$ $(= \hat{T})$ via the hydrostatic approximation in order to compute an equivalent vector-matrix equation in the vertical. To overcome this, a quantity $(\hat{\phi})$ is defined such that $(\underline{\hat{\phi}} = \underline{\underline{A}}\underline{\hat{T}})$. This $\hat{\phi}$, introduced to equation **(3.7)** allows the term (**b**) from $\underline{C}$ in equation **(3.6)** to be treated semi-implicitly via the hydrostatic equation. (Note that $\hat{\phi} \neq \mu\phi'$ but similar in magnitude). Further details are given in Appendix C.

An additional linear gravity wave generating component $(\underline{\nabla}\hat{\phi}\ ;\ \hat{\phi} \neq \mu\phi')$, which is treated semi-implicitly, is introduced to the *geopotential gradient* term

$$\mu\underline{\nabla}\Phi = \underline{\nabla}(\mu\phi' + \mu\phi'_s) - (\phi' + \phi'_s)\frac{\partial B}{\partial \eta}\underline{\nabla}P_s + \underline{\nabla}\hat{\phi} - \underline{\nabla}\hat{\phi}$$

$$= \underline{\nabla}(\mu\phi' + \mu\phi'_s - \hat{\phi}) - (\phi' + \phi'_s)\frac{\partial B}{\partial \eta}\underline{\nabla}P_s + \underline{\nabla}\hat{\phi}$$

The substitution of the linearised results of terms (**a**), (**b**) and (**c**) in expression $\underline{C}$ of the *momentum* equation (equation **(3.6)**) yields

$$\underline{C} = \frac{\partial(\hat{\omega}\underline{V})}{\partial \eta} + \underline{\nabla}(\mu E') - E'\frac{\partial B}{\partial \eta}\underline{\nabla}P_s + \underline{\nabla}(\mu\phi' + \mu\phi'_s - \hat{\phi}) - \phi'\frac{\partial B}{\partial \eta}\underline{\nabla}P_s - \phi'_s\frac{\partial B}{\partial \eta}\underline{\nabla}P_s + \underline{\nabla}\hat{\phi}$$

$$+ RT_o\underline{\nabla}P_s + RT^*\underline{\nabla}P_s + \hat{D}\underline{V} - \underline{\hat{F}}$$

$$= \frac{\partial(\hat{\omega}\underline{V})}{\partial \eta} + \underline{\nabla}\left\{\mu E' + \mu\phi' + \mu\phi'_s - \hat{\phi}\right\} + \underline{\nabla}\hat{\phi} + RT_o\underline{\nabla}P_s + \left\{RT^* - (\phi' + \phi'_s + E')\frac{\partial B}{\partial \eta}\right\}\underline{\nabla}P_s$$

$$+ \hat{D}\underline{V} - \underline{\hat{F}}$$

$$= \frac{\partial(\hat{\omega}\underline{V})}{\partial\eta} + \underline{\nabla}\hat{E} + \underline{\nabla}\hat{\phi} + RT_O\underline{\nabla}P_s + \left\{RT^* - (\phi' + \phi'_s + E')\frac{\partial B}{\partial\eta}\right\}\underline{\nabla}P_s + \hat{D}\underline{V} - \underline{\hat{F}}$$

Note that $\hat{E} = (\mu E' + \mu\phi' + \mu\phi'_S - \hat{\phi}) = \mu(E' + \phi'_S) + (\mu\phi' - \hat{\phi})$. The term $(\mu\phi' - \hat{\phi})$ is very small by virtue of the fact that the components $\mu\phi'$ and $\hat{\phi}$ are of the same magnitude. Ignoring this term results in a expression of the same form as derived by Gordon (1981) for the σ-system formulation where $\hat{E} = P_S(E' + \phi'_S)$.

Considering

$$\underline{C} = \underline{\hat{C}} + \underline{\nabla}\hat{E} + \underline{\nabla}\hat{\phi} + RT_O\underline{\nabla}P_s$$

where

$$\underline{\hat{C}} = \frac{\partial(\hat{\omega}\underline{V})}{\partial\eta} + \left\{RT^* - (\phi' + \phi'_s + E')\frac{\partial B}{\partial\eta}\right\}\underline{\nabla}P_s + \hat{D}\underline{V} - \mu\underline{F}$$

the *linearised* form of the *flux momentum equation* **(3.6)** can be expressed as:

$$\frac{\partial\underline{\hat{V}}}{\partial t} + (\hat{\xi} + \frac{\partial B}{\partial\eta}\delta_1 + \mu f)\underline{k}\times\underline{V} = -\underline{\hat{C}} - \underline{\nabla}\hat{E} - RT_O\underline{\nabla}P_s - \underline{\nabla}\hat{\phi} \qquad \textbf{(3.8)}$$

In this expression the second term on (LHS) and first and second terms on the (RHS) are the terms still containing some non-linear components.

3.5 FLUX FORM OF THE VORTICITY EQUATION

To obtain the *flux* form of the *vorticity* equation apply the operator $(\underline{k}\cdot\underline{\nabla}\times)$ to equation **(3.8)**

$$\frac{\partial\hat{\xi}}{\partial t}+\underline{k}\cdot\underline{\nabla}\times\left\{(\hat{\xi}+\frac{\partial B}{\partial\eta}\delta_1+\mu f)\underline{k}\times\underline{V}\right\}=-\underline{k}\cdot\underline{\nabla}\times\hat{\underline{C}}$$

$$\boxed{\frac{\partial\hat{\xi}}{\partial t}=-\underline{\nabla}\cdot\left\{(\hat{\xi}+\frac{\partial B}{\partial\eta}\delta_1+\mu f)\underline{V}\right\}-\underline{k}\cdot\underline{\nabla}\times\hat{\underline{C}}} \qquad \textbf{(3.9)}$$

3.6 FLUX FORM OF THE DIVERGENCE EQUATION

To obtain the *flux* form of the *divergence* equation apply the divergence operator $(\underline{\nabla}\cdot)$ to equation **(3.8)**

$$\frac{\partial\hat{D}}{\partial t}+\underline{\nabla}\cdot\left\{(\hat{\xi}+\frac{\partial B}{\partial\eta}\delta_1+\mu f)\underline{k}\times\underline{V}\right\}=-\underline{\nabla}\cdot\hat{\underline{C}}-\underline{\nabla}\cdot(\underline{\nabla}\hat{E}+RT_O\underline{\nabla}P_S+\underline{\nabla}\hat{\phi})$$

$$\boxed{\frac{\partial\hat{D}}{\partial t}=\underline{k}\cdot\underline{\nabla}\times\left\{(\hat{\xi}+\frac{\partial B}{\partial\eta}\delta_1+\mu f)\underline{V}\right\}-\underline{\nabla}\cdot\hat{\underline{C}}-\nabla^2\hat{E}-RT_O\nabla^2P_S-\nabla^2\hat{\phi}} \qquad \textbf{(3.10)}$$

The last two terms on the RHS of equation **(3.10)** are the linear gravity wave generating terms which are treated semi-implicitly during time integration. Here the *divergence* equation **(3.10)** is linked to the *thermodynamic* equation **(3.18)** through $\hat{\phi}$, since $\hat{\phi}$ may be linked to $\hat{T}=\mu T'$ using the hydrostatic equation, as indicated in APPENDIX C.

3.7 LINEARISATION OF THE THERMODYNAMIC EQUATION

From APPENDIX A, equation **(A.12)**, the *thermodynamic* equation in the η-system may be expressed as:

$$\frac{\partial T}{\partial t} + \underline{V} \cdot \underline{\nabla} T + \dot{\eta} \frac{\partial T}{\partial \eta} = \frac{K T \omega}{p} + \frac{Q}{c_p} \qquad \textbf{(3.11)}$$

Q/c_p is the non-adiabatic heating term and $K = R/c_p$ is considered constant. Gordon (1981) found that the usual weighted temperature variable (μT) should be based on ($\hat{T} = \mu T'$) because of numerical stability requirements.

The *thermodynamic* equation requires some linearisation before converting to *flux* formulation.

Apply $T = T_O + T'$ (defined in section 3.3 to the *thermodynamic* equation **(3.11)**).

$$\frac{\partial (T_O + T')}{\partial t} + \underline{V} \cdot \underline{\nabla} (T_O + T') + \dot{\eta} \frac{\partial (T_O + T')}{\partial \eta} = \frac{K T \omega}{p} + \frac{Q}{c_p}$$

Note that T_O is a global mean. The first term on the right will be treated semi-implicitly and require linearisation. This was done in section 3.11 where an expression for the vertical velocity (ω) was derived. Applying to the *thermodynamic* equation yields

$$\frac{\partial (T')}{\partial t} + \underline{V} \cdot \underline{\nabla} (T') + \dot{\eta} \frac{\partial (T')}{\partial \eta} = \frac{K T \omega}{p} + \frac{Q}{c_p} \qquad \textbf{(3.12)}$$

3.8 FLUX FORM OF THE THERMODYNAMIC EQUATION

The *flux* formulation of the *thermodynamic* equation is derived by multiplying equation **(3.12)** by (μ) and equation **(3.2)** by (T') and then adding.

$$\frac{\partial (\mu T')}{\partial t} + \underline{\nabla} \cdot (\mu \underline{V} T') + \frac{\partial (\mu \dot{\eta} T')}{\partial \eta} = \frac{\mu K T \omega}{p} + \frac{\mu Q}{c_p}$$

substitution of ($\hat{T} = \mu T'$), ($\hat{\omega} = \mu \dot{\eta}$), $\underline{\hat{V}} = \mu \underline{V}$ and $\hat{Q} = \frac{\mu Q}{c_p}$

$$\frac{\partial \hat{\Gamma}}{\partial t} + \underline{\nabla} \cdot (\hat{\underline{V}} T') + \frac{\partial (\hat{\omega} T')}{\partial \eta} = \frac{\mu K T \omega}{p} + \hat{Q} \qquad \textbf{(3.13)}$$

(a)

The first term on the RHS of equation **(3.13)**, namely term (**a**), represents the gravity wave generating term in the *flux* formulation of the *thermodynamic* equation, and needs to be treated semi-implicitly. Term (**a**), however, first requires some modification, as discussed in the following sections.

3.9 SURFACE-PRESSURE TENDENCY EQUATION

The *continuity* equation (equation **(A.11)** in Appendix A) is used to derive a prognostic equation for surface-pressure (P_s).

$$\frac{\partial \mu}{\partial t} + \underline{\nabla} \cdot (\mu \underline{V}) + \frac{\partial}{\partial \eta}(\mu \dot{\eta}) = 0$$

Equation **(2.1)** gives $\mu = \frac{\partial p}{\partial \eta} = \frac{\partial A_O}{\partial \eta} + P_s \frac{\partial B}{\partial \eta}$ and since $A = A(\eta)$ and $B = B(\eta)$ this becomes $\frac{\partial \mu}{\partial t} = \frac{\partial B}{\partial \eta} \frac{\partial P_s}{\partial t}$. Also $\hat{D} = \underline{\nabla} \cdot (\mu \underline{V})$ and $\hat{\omega} = \mu \dot{\eta}$

The prognostic equation for surface pressure is obtained by integrating the *continuity* equation **(A.11)** between η=0 and η=1.

$$\int_0^1 \frac{\partial B}{\partial \eta} \frac{\partial P_s}{\partial t} d\eta + \int_0^1 \hat{D} d\eta + \int_0^1 \frac{\partial \hat{\omega}}{\partial \eta} d\eta = 0$$

but $$\int_0^1 \frac{\partial B}{\partial \eta} \frac{\partial P_s}{\partial t} d\eta = \frac{\partial P_s}{\partial t} \int_0^1 \frac{\partial B}{\partial \eta} d\eta = \frac{\partial P_s}{\partial t} (B_{[\eta=1]} - B_{[\eta=0]}) = \frac{\partial P_s}{\partial t} (1 - 0) = \frac{\partial P_s}{\partial t}$$

and $$\int_0^1 \frac{\partial \hat{\omega}}{\partial \eta} d\eta = \hat{\omega}_{[\eta=1]} - \hat{\omega}_{[\eta=0]} = 0$$

Define $[\nu]^{\eta} = \int_0^{\eta} \nu d\eta$ **(3.14)**

The prognostic equation for surface-pressure (or *surface-pressure tendency* equation) may then be expressed as

$$\boxed{\frac{\partial P_s}{\partial t} = -\int_0^1 \hat{D} d\eta = -[\hat{D}]^1} \qquad \textbf{(3.15)}$$

3.10 VERTICAL VELOCITY DIAGNOSTIC EQUATION

The *vertical velocity diagnostic* ($\hat{\omega} = \mu\dot{\eta}$) equation which is required for the *thermodynamic* equation **(3.13)**, as well as the *momentum* equation **(3.6)**, is obtained by integrating the *continuity* equation **(A.11)** between η=0 and any half-level η. A similar integration was applied in section 3.9.

$$\int_0^{\eta} \frac{\partial B}{\partial \eta}\frac{\partial P_s}{\partial t} d\eta + \int_0^{\eta} \hat{D} d\eta + \int_0^{\eta} \frac{\partial \hat{\omega}}{\partial \eta} d\eta = 0$$

but $$\int_0^{\eta} \frac{\partial B}{\partial \eta}\frac{\partial P_s}{\partial t} d\eta = \frac{\partial P_s}{\partial t}\int_0^{\eta} \frac{\partial B}{\partial \eta} d\eta = \frac{\partial P_s}{\partial t}(B_{[\eta]} - B_{[\eta=0]}) = \frac{\partial P_s}{\partial t}(B - 0) = B\frac{\partial P_s}{\partial t}$$

and $$\int_0^{\eta} \frac{\partial \hat{\omega}}{\partial \eta} d\eta = \hat{\omega}_{[\eta]} - \hat{\omega}_{[\eta=0]} = \hat{\omega}$$

thus

$$B\frac{\partial P_s}{\partial t} + \int_0^{\eta} \hat{D} d\eta + \hat{\omega} = 0$$

Use $[\nu]^{\eta} = \int_0^{\eta} \nu d\eta$ as defined in equation **(3.14)**

$$\hat{\omega} = -B\frac{\partial P_s}{\partial t} - [\hat{D}]^{\eta}$$

From the *surface-pressure tendency* equation *(*equation **(3.15)**) it follows that $\frac{\partial P_s}{\partial t} = -[\hat{D}]^1$.

This yields a *vertical velocity diagnostic* equation expressed in terms of the horizontal divergence at each model half-level. **It is important to remember that** $(\hat{\omega})$ **is a half-level quantity**.

$$\hat{\omega} = B[\hat{D}]^l - [\hat{D}]^\eta \qquad \textbf{(3.16)}$$

3.11 VERTICAL VELOCITY IN THE THERMODYNAMIC EQUATION

The *vertical velocity* (ω) is required in term (**a**) of the *flux* formulation of the *thermodynamic* equation **(3.13)**.

$$\omega = \frac{dp}{dt}$$

$$= \frac{\partial p}{\partial t} + \underline{V}\cdot\underline{\nabla}p + \dot{\eta}\frac{\partial p}{\partial \eta} \qquad \text{apply equation (2.1)}$$

$$= \frac{\partial}{\partial t}(A_O + P_S B) + \underline{V}\cdot\underline{\nabla}(A_O + P_S B) + \dot{\eta}\mu \qquad \text{but } \hat{\omega} = \dot{\eta}\mu \text{ and } A_O = A_O(\eta)$$

$$= B\frac{\partial P_s}{\partial t} + B\underline{V}\cdot\underline{\nabla}P_S + \hat{\omega} \qquad \text{equation (3.15) gives } \frac{\partial P_s}{\partial t} = -[\hat{D}]^l$$

$$= -B[\hat{D}]^l + B\underline{V}\cdot\underline{\nabla}P_S + \hat{\omega} \qquad \text{let } \delta_2 = \underline{V}\cdot\underline{\nabla}P_S \text{ and apply (3.16)}$$

$$= -B[\hat{D}]^l + B\delta_2 + \{B[\hat{D}]^l - [\hat{D}]^\eta\}$$

$$= B\delta_2 - [\hat{D}]^\eta \qquad \textbf{(3.17)}$$

Equation **(3.17)** provides a substitution for ω in equation **(3.13)**

By using the corresponded term from the σ-system (Gordon 1981) namely $\omega = \delta_2 - [\hat{D}]^{\sigma}$ as well as $T = T_o + T'$ it follows that:

$$\frac{KT\omega}{\sigma} = \frac{K(T_o + T')\omega}{\sigma} = \frac{KT_o\omega}{\sigma} + \frac{KT'\omega}{\sigma} = \frac{KT_O}{\sigma}(\delta_2 - [\hat{D}]^{\sigma}) + \frac{KT'\omega}{\sigma} = -\frac{KT_O}{\sigma}[\hat{D}]^{\sigma} + \frac{K}{\sigma}(T'\omega + T_O\delta_2)$$

The first term on the RHS is treated semi-implicitly during the time integration.

Term (**a**) in equation **(3.13)** is $\frac{KT\omega\mu}{p}$, and since $\eta \neq \frac{p}{\mu}$, it is impossible to obtain a similar expression for the η-system. A corresponding term $(-\frac{KT_o}{\eta}[\hat{D}]^{\eta})$, which will require semi-implicit treatment, is prescribed for equation **(3.13)**.

An additional term is added and subtracted from term (**a**) in equation **(3.13)**

$$\frac{KT\omega\mu}{p} = \{-\frac{KT_O}{\eta}[\hat{D}]^{\eta} + \frac{KT_O}{\eta}[\hat{D}]^{\eta}\} + \frac{KT\omega\mu}{p}$$

From section A.4 and equation **(3.17)** it follows that $K = \frac{R}{c_p}$ and $\omega = B\delta_2 - [\hat{D}]^{\eta}$

$$\frac{KT\omega\mu}{p} = \left\{-\frac{KT_O}{\eta}[\hat{D}]^{\eta} + \frac{KT_O}{\eta}[\hat{D}]^{\eta}\right\} + \frac{1}{c_p}\frac{RT\mu}{p}(B\delta_2 - [\hat{D}]^{\eta})$$

$$= -\frac{KT_O}{\eta}[\hat{D}]^{\eta} + \left\{\frac{KT_O}{\eta}[\hat{D}]^{\eta} + \frac{1}{c_p}\frac{RT\mu}{p}B\delta_2 - \frac{1}{c_p}\frac{RT\mu}{p}[\hat{D}]^{\eta}\right\}$$

In equation **(C.1)** the *hydrostatic approximation* is expressed as $\frac{\partial\phi}{\partial\eta} = -\frac{RT\mu}{p}$

$$\frac{KT\omega\mu}{p} = -\frac{KT_O}{\eta}[\hat{D}]^{\eta} + \left\{\frac{KT_O}{\eta}[\hat{D}]^{\eta} + \frac{1}{c_p}\frac{RT\mu}{p}B\delta_2 + \frac{1}{c_p}\frac{\partial\phi}{\partial\eta}[\hat{D}]^{\eta}\right\}$$

$$= -\frac{KT_O}{\eta}[\hat{D}]^{\eta} + \left\{\frac{KT_O}{\eta} + \frac{1}{c_p}\frac{\partial\phi}{\partial\eta}\right\}[\hat{D}]^{\eta} + \frac{1}{c_p}RT\frac{\mu B}{p}(\underline{V}\cdot\underline{\nabla}P_S)$$

where $\delta_2 = \underline{V}\cdot\underline{\nabla}P_S$. Substitution of this expression into the *flux* formulation *thermodynamic* equation **(3.13)** yields:

$$\frac{\partial \hat{T}}{\partial t} = -\underline{\nabla}\cdot(\hat{\underline{V}}T') + \left\{\frac{KT_O}{\eta}[\hat{D}]^{\eta} + \frac{1}{c_p}\frac{\partial \phi}{\partial \eta}[\hat{D}]^{\eta} + \frac{1}{c_p}RT\frac{\mu B}{p}(\underline{V}\cdot\underline{\nabla}P_S) + \hat{Q} - \frac{\partial(\hat{\omega}T')}{\partial \eta}\right\} - \frac{KT_O}{\eta}[\hat{D}]^{\eta} \qquad \textbf{(3.18)}$$

In equation **(3.18)** the last term on the RHS is linear and is treated semi-implicitly during the time integration. This is achieved by linking this term to $\hat{D}$ in the *divergence* equation **(3.10)**. The remaining terms on the RHS are generally non-linear and are treated explicitly using the grid transform method.

The implicitly evaluated terms are $RT_O\underline{\nabla}^2 P_S$ and $\underline{\nabla}^2\hat{\phi}$ in the *divergence* equation **(3.10)**, $\hat{D}$ in the *surface pressure tendency* equation **(3.15)** and $\frac{KT_O}{\eta}[\hat{D}]^{\eta}$ in the *thermodynamic* equation **(3.18)**.

3.12 FLUX FORM OF THE MOISTURE EQUATION

In APPENDIX A, equation **(A.13)** the *moisture* equation in the η-system is expressed as:

$$\frac{\partial q}{\partial t} + \underline{V}\cdot\underline{\nabla}_{\eta}q + \dot{\eta}\frac{\partial q}{\partial \eta} = S_q \qquad \textbf{(3.19)}$$

The *flux* formulation of the *moisture* equation is obtained by multiplying equation **(3.19)** by (μ) and equation **(3.2)** by (q). Adding then results in:

$$\frac{\partial(\mu q)}{\partial t} + \underline{\nabla}\cdot(\mu\underline{V}q) + \frac{\partial(\mu\dot{\eta}q)}{\partial \eta} = \mu S_q$$

substitution of $(\hat{q} = \mu q)$, $(\hat{\omega} = \mu\dot{\eta})$, $(\hat{S}_q = \mu S_q)$ and $(\hat{\underline{V}} = \mu\underline{V})$ yields the *flux* formulation of the *moisture* equation

$$\frac{\partial \hat{q}}{\partial t} + \underline{\nabla}\cdot(\hat{\underline{V}}q) + \frac{\partial(\hat{\omega}q)}{\partial \eta} = \hat{S}_q \qquad \textbf{(3.20)}$$

CHAPTER 4

ENERGY CONSERVATION

4.1 INTRODUCTION

Numerical climate model simulations require long time integrations (one year and more). It is therefore vital that the total energy in the atmospheric system is conserved, especially when constructing the vertical discrete formulation of the atmospheric equations (Burger and Riphagen 1999). In this chapter, it is demonstrated that the total energy (external kinetic and potential energy derived from the *momentum* equation, as well as internal energy in the *thermodynamic* equation) is conserved when the flux formulation of the atmospheric equations is integrated forward in time. It is also important to note that there are some specific requirements for energy conservation when formulating the vertical finite difference forms of the atmospheric equations. When formulating *the total energy* equation *adiabatic* and *frictionless* conditions are assumed.

Equation **(A.8)** in APPENDIX A is the *momentum* equation in the η-system. Frictionless conditions are assumed which means that $\underline{F} = 0$.

$$\frac{\partial \underline{V}}{\partial t} + (\underline{V} \cdot \underline{\nabla})\underline{V} + \dot{\eta}\frac{\partial \underline{V}}{\partial \eta} + \underline{\nabla}\phi + \frac{RTB}{p}\underline{\nabla}P_s + f\underline{k}x\underline{V} = 0 \qquad \textbf{(4.1)}$$

Using equation **(A.11)** (APPENDIX A) the *continuity* in the η-system may be expressed as:

$$\frac{\partial \mu}{\partial t} + \underline{\nabla} \cdot (\mu \underline{V}) + \frac{\partial}{\partial \eta}(\mu \dot{\eta}) = 0 \qquad \textbf{(4.2)}$$

Equation **(3.13)** is the *flux* formulation of the *thermodynamic* equation in the η-system. Adiabatic conditions are assumed which means that $\hat{Q} = 0$.

$$\frac{\partial \hat{T}}{\partial t} + \underline{\nabla} \cdot (\hat{\underline{V}}T') + \frac{\partial(\hat{\omega}T')}{\partial \eta} - \frac{\mu K T \omega}{p} = 0 \qquad \textbf{(4.3)}$$

4.2 FLUX FORM OF THE KINETIC ENERGY EQUATION

In equation **(3.4)** the *kinetic energy* per unit mass is expressed as $E = \left\{\frac{V^2}{2}\right\}$

A prognostic equation for kinetic energy (*kinetic energy* equation) is required. This is achieved by multiplying equation **(4.1)**, which is the standard (not *flux*) form of the *momentum* equation, by $\underline{V}$.

The *flux* formulation of the *kinetic energy* equation, however, is derived by multiplying equation **(4.1)** by $\mu\underline{V}$ and equation **(4.2)** by E and then adding the two equations. Note that $\underline{V}\cdot\underline{k}\times\underline{V} = -\underline{V}\cdot\underline{V}\times\underline{k} = -\underline{V}\times\underline{V}\cdot\underline{k} = 0$

$$\mu\underline{V}\cdot\frac{\partial\underline{V}}{\partial t}+\mu\underline{V}\cdot(\underline{V}\cdot\nabla)\underline{V}+\mu\dot{\eta}\underline{V}\cdot\frac{\partial\underline{V}}{\partial\eta}+\mu\underline{V}\cdot\nabla\phi+\frac{\mu RTB}{p}\underline{V}\cdot\nabla P_s+E\frac{\partial\mu}{\partial t}+E\nabla\cdot(\mu\underline{V})+E\frac{\partial}{\partial\eta}(\mu\dot{\eta})=$$

But $\frac{\partial V^2}{\partial t}=\frac{\partial(\underline{V}\cdot\underline{V})}{\partial t}=2(\underline{V}\cdot\frac{\partial\underline{V}}{\partial t})$, $\frac{\partial V^2}{\partial\eta}=\frac{\partial(\underline{V}\cdot\underline{V})}{\partial\eta}=2(\underline{V}\cdot\frac{\partial\underline{V}}{\partial\eta})$ and similar to

(3.4) $\underline{V}\cdot(\underline{V}\cdot\nabla)\underline{V}=\underline{V}\cdot\{\nabla E+\xi\underline{k}\times\underline{V}\}=\underline{V}\cdot\nabla E+\xi\underline{V}\cdot\underline{k}\times\underline{V}=\underline{V}\cdot\nabla E+0$

$$\mu\frac{\partial E}{\partial t}+(\mu\underline{V})\cdot\nabla E+(\mu\dot{\eta})\frac{\partial E}{\partial\eta}+\mu\underline{V}\cdot\nabla\phi+\frac{\mu RTB}{p}\underline{V}\cdot\nabla P_s+E\frac{\partial\mu}{\partial t}+E\nabla\cdot(\mu\underline{V})+E\frac{\partial}{\partial\eta}(\mu\dot{\eta})=0$$

Regrouping of terms and substitution of $\hat{\underline{V}}=\mu\underline{V}$, $\hat{\omega}=\mu\dot{\eta}$ and $\hat{E}=\mu E$, results in:

$$\mu\frac{\partial E}{\partial t}+E\frac{\partial\mu}{\partial t}+(\mu\underline{V})\cdot\nabla E+E\nabla\cdot(\mu\underline{V})+(\hat{\omega})\frac{\partial E}{\partial\eta}+E\frac{\partial(\hat{\omega})}{\partial\eta}+\hat{\underline{V}}\cdot\nabla\phi+\frac{\mu RTB}{p}\underline{V}\cdot\nabla P_s=0$$

$$\frac{\partial\hat{E}}{\partial t}+\nabla\cdot(\hat{\underline{V}}E)+\frac{\partial(\hat{\omega}E)}{\partial\eta}+\hat{\underline{V}}\cdot\nabla\phi+\frac{\mu RTB}{p}\underline{V}\cdot\nabla P_s=0$$

Substitution of $\hat{\underline{V}}\cdot\nabla\phi=\nabla\cdot(\hat{\underline{V}}\phi)-\phi\nabla\cdot\hat{\underline{V}}=\nabla\cdot(\hat{\underline{V}}\phi)-\phi\hat{D}$ yields the final composition of the *flux* formulation of the *kinetic energy* equation

$$\frac{\partial\hat{E}}{\partial t}+\nabla\cdot\hat{\underline{V}}E+\frac{\partial(\hat{\omega}E)}{\partial\eta}+\frac{RT\mu B}{p}\underline{V}\cdot\nabla P_s+\nabla\cdot\hat{\underline{V}}\phi-\phi\hat{D}=0 \qquad \textbf{(4.4)}$$

The second, third, fifth and sixth terms on the LHS of equation **(4.4)** are flux divergence terms involving kinetic- and potential energy, while the fourth term represents sources or sinks of *kinetic energy*.

4.3 FLUX FORM OF THE INTERNAL ENERGY EQUATION

A second energy equation introduced is a prognostic equation for *internal energy*. The *flux* formulation of the *internal energy* equation is formed by multiplying equation **(4.3)** by c_p and recalling that $K=R/c_p$ is considered as constant.

$$\frac{\partial c_p \hat{T}}{\partial t} + \underline{\nabla} \cdot (c_p \underline{\hat{V}} T') + \frac{\partial (c_p \hat{\omega} T')}{\partial \eta} - \frac{RT\mu\omega}{p} = 0 \qquad \textbf{(4.5)}$$

4.4 TOTAL ENERGY EQUATION

Adding equations **(4.4)** and **(4.5)** results in the *total energy* equation:

$$\frac{\partial (c_p \hat{T} + \hat{E})}{\partial t} + \underline{\nabla} \cdot \{\underline{\hat{V}}(c_p T' + E)\} + \frac{\partial \{\hat{\omega}(c_p T' + E)\}}{\partial \eta} + \underline{\nabla} \cdot (\underline{V}\phi) - \phi \hat{D} + \frac{RT\mu}{p}(B\underline{V} \cdot \underline{\nabla} P_S - \omega) = 0$$

(a) **(b)** **(c)** **(d)** **(e)** **(f)**

(4.6)

To identify features affecting the temporal change in the mean energy over the model atmosphere, the *total energy* equation **(4.6)** is integrated horizontally and vertically.

Over a closed surface, the *globally* (A) integrated flux divergence of any quantity (ν) is zero:

$\int_A \underline{\nabla} \cdot (\underline{\hat{V}}\nu) dA = 0$ which eliminates terms (**b**) and (**d**) when integrated.

Through the depth of the model atmosphere, the *vertically* (v) integrated flux divergence (with $\hat{\omega} = 0$ at $\eta = 0$ and 1) is zero:

$\int_v \frac{\partial (\hat{\omega}\nu)}{\partial \eta} d\eta = 0$ which eliminates term (**c**).

The global vertically integrated form of equation **(4.6)** is:

$$\int_A \int_V \left\{\frac{\partial(c_p\hat{T}+\hat{E})}{\partial t}\right\}d\eta dA = \int_A \int_V \left\{\phi\hat{D} - \frac{RT\mu}{p}(B\underline{V}\cdot\underline{\nabla}P_s - \omega)\right\}d\eta dA \qquad \textbf{(4.7)}$$

Consider the integral on the RHS, which includes term (**e**) and (**f**) in equation **(4.6)**

$$\phi\hat{D} - \frac{RT\mu}{p}(B\underline{V}\cdot\underline{\nabla}P_s - \omega)$$

The *hydrostatic approximation* **(C.1)** states that $\frac{\partial\phi}{\partial\eta} = -\frac{RT\mu}{p}$ which yields

$$\phi\hat{D} + \frac{\partial\phi}{\partial\eta}(B\underline{V}\cdot\underline{\nabla}P_s - \omega)$$

From equation **(3.17)** it follows that $\omega = B\delta_2 - [\hat{D}]^\eta = B(\underline{V}\cdot\underline{\nabla}P_s) - [\hat{D}]^\eta$

$$\phi\hat{D} + \frac{\partial\phi}{\partial\eta}\left\{B\underline{V}\cdot\underline{\nabla}P_s - (B\underline{V}\cdot\underline{\nabla}P_s - [\hat{D}]^\eta)\right\}$$

$$= \phi\hat{D} + \frac{\partial\phi}{\partial\eta}[\hat{D}]^\eta$$

Replace this result into equation **(4.7)**

$$\int_A \int_V \left\{\frac{\partial(c_p\hat{T}+\hat{E})}{\partial t}\right\}d\eta dA = \int_A \int_V \left\{\phi\hat{D} + \frac{\partial\phi}{\partial\eta}[\hat{D}]^\eta\right\}d\eta dA$$

$$= \int_A \int_0^1 \left\{\phi\hat{D} + \frac{\partial\phi}{\partial\eta}[\hat{D}]^\eta\right\}d\eta dA$$

$$= \int_A \left\{\int_0^1 \phi\hat{D}d\eta + \int_0^1 \frac{\partial\phi}{\partial\eta}[\hat{D}]^\eta d\eta\right\}dA$$

$$= \int_A \left\{\int_0^1 \phi\hat{D}d\eta + \left[\left|[\hat{D}]^\eta\phi\right|_0^1 - \int_0^1 \phi\frac{\partial}{\partial\eta}[\hat{D}]^\eta d\eta\right]\right\}dA$$

but from **(3.14)** follows $\frac{\partial}{\partial\eta}[\hat{D}]^\eta = \frac{\partial}{\partial\eta}\left\{\int_0^\eta \hat{D}d\eta\right\} = \hat{D}$ which yields

$$= \int_A \left\{ \int_0^1 \phi \hat{D} d\eta + \left| [\hat{D}]^\eta \phi \right|_0^1 - \int_0^1 \phi \hat{D} d\eta \right\} dA$$

$$= \int_A \left\{ \phi_S [\hat{D}]^1 \right\} dA \qquad \text{equation (3.15) gives } [\hat{D}]^1 = -\frac{\partial P_S}{\partial t}$$

$$= -\int_A \left\{ \phi_S \frac{\partial P_S}{\partial t} \right\} dA$$

To summarise

$$\int_A \int_V \left\{ \frac{\partial (c_p \hat{T} + \hat{E})}{\partial t} \right\} d\eta dA = -\int_A \left\{ \phi_S \frac{\partial P_S}{\partial t} \right\} dA \qquad \textbf{(4.8)}$$

The RHS provides the global integral of the *mountain torque* term. Equation **(4.8)** clearly indicates, as expected, that the globally vertically integrated- or mean *total energy* will only change in time as a result of changes induced by the flow interacting with the surface topography.

4.5 REQUIREMENTS FOR ENERGY CONSERVATION

There are, however, specific requirements for energy conservation when formulating the vertical finite difference forms of the terms in the *flux* formulation of the *momentum* and *thermodynamic* equations. These requirements must ensure that the energy condition in equation **(4.8)** is met.

Equation **(3.3)** gives the *flux* formulation of the *momentum* equation

$$\underset{\textbf{(a)}}{\frac{\partial \hat{\underline{V}}}{\partial t}} + \underset{\textbf{(b)}}{\hat{D}\underline{V}} + \underset{\textbf{(c)}}{\mu(\underline{V} \cdot \underline{\nabla})\underline{V}} + \underset{\textbf{(d)}}{\frac{\partial (\hat{\omega}\underline{V})}{\partial \eta}} + \underset{\textbf{(e)}}{\mu \underline{\nabla} \Phi} + \underset{\textbf{(f)}}{\frac{RT\mu B}{p} \underline{\nabla} P_S} + \underset{\textbf{(g)}}{\mu f \underline{k} x \underline{V}} = \underset{\textbf{(h)}}{\hat{\underline{F}}} \qquad \textbf{(4.9)}$$

and equation **(3.13)** the *flux* formulation of the *thermodynamic* equation

$$\underset{\textbf{(a)}}{\frac{\partial \hat{T}}{\partial t}} + \underset{\textbf{(b)}}{\underline{\nabla} \cdot (\hat{\underline{V}} T')} + \underset{\textbf{(c)}}{\frac{\partial (\hat{\omega} T')}{\partial \eta}} = \underset{\textbf{(d)}}{\frac{\mu K T \omega}{p}} + \underset{\textbf{(e)}}{\hat{Q}} \qquad \textbf{(4.10)}$$

When formulating the global vertical integrated form of *the total energy* **(4.8)**, all the terms involving the vertical and global integrated flux divergence became zero. It implies that term (**b**), (**c**) and (**d**) in equation **(4.9)** and term (**b**) and (**c**) in equation **(4.10)** are irrelevant when setting up requirements to meet the energy conditions. *Adiabatic* and *frictionless* conditions are assumed which means that friction terms (term (**h**) in equation **(4.9)**) and heating terms (term (**e**) in equation **(4.10)**) may also be ignored. When formulating up the *flux* formulation of the *kinetic energy* equation, multiplication by $\mu\underline{V}$ results in the elimination of the Coriolis term (**g**) in equation **(4.9)**. The only remaining relevant terms to deal with are:

i) $(\mu\underline{\nabla}\phi + \frac{RT\mu B}{p}\underline{\nabla}P_s)$ terms (**e**) and (**f**) from equation **(4.9)**

ii) $(\frac{\mu KT\omega}{p})$ term (**d**) from equation **(4.10)**

Before setting the necessary energy conservation requirements for these terms, the discrete notation used for the vertical integrals with regard to the vertical structure of the model (illustrated in figure 3) are defined:

The vertical integral from the top of the atmosphere (η=0) to any half-level, with regard to the vertical indexing illustrated in figure 3, is defined as

$$[\hat{D}]^{\eta_{k+0.5}} = \int_0^{\eta_{k+0.5}} \hat{D}d\eta = \sum_{j=9}^{k+1} \hat{D}_j \Delta\eta_j \quad \text{and} \quad [\hat{D}]^{\eta_{k-0.5}} = \int_0^{\eta_{k-0.5}} \hat{D}d\eta = \sum_{j=9}^{k} \hat{D}_j \Delta\eta_j$$

for a 9-level model as the CSIRO-9 Mark II AGCM **(4.11)**

4.5.1 Thermodynamic equation

The vertical velocity (ω) is required for the remaining term (**d**) in equation **(4.10)**. From equation **(3.17)** it follows that

$$\omega = B\delta_2 - [\hat{D}]^{\eta} = B(\underline{V}\cdot\underline{\nabla}P_s) - [\hat{D}]^{\eta}$$

From equation **(3.16)** it follows that

$$\omega = \hat{\omega} + B\left\{\underline{V}\cdot\underline{\nabla}P_s - [\hat{D}]^{1}\right\}$$

Equation **(3.16)** gives $\hat{\omega} = B[\hat{D}]^1 - [\hat{D}]^\eta$ where $(\hat{\omega})$ is a half-level quantity. Thus for full-levels $\hat{\omega}_k = 0.5(\hat{\omega}_{k+0.5} + \hat{\omega}_{k-0.5}) = 0.5(B_{k+0.5}[\hat{D}]^1 - [\hat{D}]^{\eta_{k+0.5}} + B_{k-0.5}[\hat{D}]^1 - [\hat{D}]^{\eta_{k-0.5}})$ and therefore

$$\begin{aligned}\omega_k &= 0.5(B_{k+0.5}[\hat{D}]^1 - [\hat{D}]^{\eta_{k+0.5}} + B_{k-0.5}[\hat{D}]^1 - [\hat{D}]^{\eta_{k-0.5}}) + B_k\{\underline{V}_k \cdot \underline{\nabla}P_S - [\hat{D}]^1\} \\ &= B_k \underline{V}_k \cdot \underline{\nabla}P_S - B_k[\hat{D}]^1 + 0.5(B_{k+0.5} + B_{k-0.5})[\hat{D}]^1 - 0.5([\hat{D}]^{\eta_{k+0.5}} + [\hat{D}]^{\eta_{k-0.5}}) \\ &= B_k \underline{V}_k \cdot \underline{\nabla}P_S - 0.5(B_{k+0.5} + B_{k-0.5})[\hat{D}]^1 + 0.5(B_{k+0.5} + B_{k-0.5})[\hat{D}]^1 - 0.5([\hat{D}]^{\eta_{k+0.5}} + [\hat{D}]^{\eta_{k-0.5}}) \\ &= B_k \underline{V}_k \cdot \underline{\nabla}P_S - 0.5([\hat{D}]^{\eta_{k+0.5}} + [\hat{D}]^{\eta_{k-0.5}}) \qquad \textbf{(4.12)}\end{aligned}$$

> ***E1***: (B_k) at any full-level (k) **must** be defined as $B_k = 0.5(B_{k+0.5} + B_{k-0.5})$ for cancellation of the products containing $[\hat{D}]^1$.

E1 represents the first energy conservation requirement.

Using figure 3 and the relations in **(4.11)**, the discrete notation of the integrals in the last part of equation **(4.12)** becomes

$$\begin{aligned}0.5([\hat{D}]^{\eta_{k+0.5}} + [\hat{D}]^{\eta_{k-0.5}}) &= 0.5\left\{\int_0^{\eta_{k+0.5}} \hat{D}d\eta + \int_0^{\eta_{k-0.5}} \hat{D}d\eta\right\} = 0.5\left\{\sum_{j=9}^{k+1} \hat{D}_j \Delta\eta_j + \sum_{j=9}^{k} \hat{D}_j \Delta\eta_j\right\} \\ &= 0.5\left\{2\sum_{j=9}^{k+1} \hat{D}_j \Delta\eta_j + \hat{D}_k \Delta\eta_k\right\} = \int_0^{\eta_{k+0.5}} \hat{D}d\eta + 0.5\hat{D}_k \Delta\eta_k \\ &= [\hat{D}]^{\eta_{k+0.5}} + 0.5\hat{D}_k \Delta\eta_k\end{aligned}$$

and

$$\begin{aligned}[\hat{D}]^{\eta_k} &= \int_0^{\eta_k} \hat{D}d\eta = \sum_{j=9}^{k+1} \hat{D}_j \Delta\eta_j + 0.5\hat{D}_k \Delta\eta_k = \int_0^{\eta_{k+0.5}} \hat{D}d\eta + 0.5\hat{D}_k \Delta\eta_k \\ &= [\hat{D}]^{\eta_{k+0.5}} + 0.5\hat{D}_k \Delta\eta_k\end{aligned}$$

> ***E2***: As a result $[\hat{D}]^{\eta_k} = 0.5([\hat{D}]^{\eta_{k+0.5}} + [\hat{D}]^{\eta_{k-0.5}})$ which means that the discrete formulation is internally consistent.

Term (**d**) in equation **(4.10)** also contains the quantities p and μ. From equation **(2.1)** it follows that $p = A_O + P_S B$ and $\mu = \frac{\partial A_O}{\partial \eta} + P_S \frac{\partial B}{\partial \eta}$. Here A_0 and B are known constants at each half-level.

E3: Since A_0 and B are co-ordinate constants calculated on equal half-levels, and $B_k = 0.5(B_{k+0.5} + B_{k-0.5})$ from condition ***E1***, it is required that A_{0k} at any full-level (k) **must** be defined as $A_{Ok} = 0.5(A_{Ok+0.5} + A_{Ok-0.5})$.

Therefore

$$p_k = A_{Ok} + P_S B_k = 0.5(B_{k+0.5} + B_{k-0.5}) + P_S\, 0.5(A_{Ok+0.5} + A_{Ok-0.5}) \qquad \textbf{(4.13)}$$

E4: For consistency the derivatives $\frac{\partial A_O}{\partial \eta}$ and $\frac{\partial B}{\partial \eta}$ at any full-level (k) **must** also be computed from half-level values of A_O and B.

Therefore

$$\mu_k = \left\{\frac{\partial A_O}{\partial \eta}\right\}_k + P_S \left\{\frac{\partial B}{\partial \eta}\right\}_k = \left\{\frac{(A_{Ok-0.5} - A_{Ok+0.5})}{\Delta \eta_k} + P_S \frac{(B_{k-0.5} - B_{k+0.5})}{\Delta \eta_k}\right\} \qquad \textbf{(4.14)}$$

By replacing ω from equation **(4.12)** and the notations in equations **(4.13)** and **(4.14)**, the term (**d**) in equation **(4.10)** at any full-level (k) becomes

$$0.5(B_{k+0.5} + B_{k-0.5}) \frac{\mu_k K T_k}{p_k} \underline{V}_k \cdot \underline{\nabla} P_S - 0.5([\hat{D}]^{\eta_{k+0.5}} + [\hat{D}]^{\eta_{k-0.5}}) \frac{\mu_k K T_k}{p_k} \qquad \textbf{(4.15)}$$

(**a**) (**b**)

where $\frac{\mu_k}{p_k} = \left\{ \frac{\frac{(A_{Ok-0.5} - A_{Ok+0.5})}{\Delta \eta_k} + P_S \frac{(B_{k-0.5} - B_{k+0.5})}{\Delta \eta_k}}{0.5(B_{k+0.5} + B_{k-0.5}) + P_S\, 0.5(A_{Ok+0.5} + A_{Ok-0.5})} \right\}$

In section 4.5.2 it will be shown that term (**a**) in equation **(4.15)** will cancel with an identical term in the *momentum* equation. The only remaining term in the *thermodynamic* equation then becomes term (**b**) in equation **(4.15)**. When applying the hydrostatic approximation (equation **(C.1)**), which are also used in the formal derivation of the *total energy* equation, (**b**) in equation **(4.15)** becomes:

$$0.5([\hat{D}]^{\eta_{k+0.5}} + [\hat{D}]^{\eta_{k-0.5}})\frac{\mu_k K T_k}{p_k} = [\hat{D}]^{\eta_k}\frac{\mu_k K T_k}{p_k} \qquad \text{but } K = \frac{R}{c_p}$$

$$= [\hat{D}]^{\eta_k}\frac{\mu_k R T_k}{p_k c_p} \qquad \text{apply } \frac{\partial\phi}{\partial\eta} = -\frac{RT\mu}{p}$$

$$= -[\hat{D}]^{\eta_k}\frac{1}{c_p}\left\{\frac{\partial\phi}{\partial\eta}\right\}_k \qquad \textbf{(4.16)}$$

4.5.2 Momentum equation

The remaining terms (**e**) and (**f**) of equation **(4.9)** are $\mu\underline{\nabla}\phi$ and $\frac{RT\mu B}{p}\underline{\nabla}P_S$ which, in discrete notation, becomes

$$\mu_k\underline{\nabla}\phi_k + B_k\frac{\mu_k RT_k}{p_k}\underline{\nabla}P_S = \mu_k\underline{\nabla}\phi_k + 0.5(B_{k+0.5} + B_{k-0.5})\frac{\mu_k RT_k}{p_k}\underline{\nabla}P_S \qquad \textbf{(4.17)}$$

(**a**) (**b**)

The *flux* formulation of the *total energy* equation is derived by multiplying the *momentum* equation (in *flux* form) by $\underline{V}$ and the *flux* formulation of the *thermodynamic* equation by c_p. When multiplying term (**b**) in equation **(4.17)** by $\underline{V}_k$ and term (**a**) in equation **(4.15)** by (c_p), both terms will become identical:

$$0.5(B_{k+0.5} + B_{k-0.5})\frac{\mu_k RT_k}{p_k}\underline{V}_k \cdot \underline{\nabla}P_S$$

These two identical terms, are of opposite sign in equations **(4.9)** and **(4.10)**, and cancel when the *momentum* and *thermodynamic* equations are added to form the *total energy* equation.

E5: This, however, only holds if the same T_k applies.

4.5.3 Discrete requirements for geopotential

At this point, the only remaining terms relevant for energy conservation are:

i) $\left(-[\hat{D}]^{\eta_k}\frac{1}{c_p}\left\{\frac{\partial\phi}{\partial\eta}\right\}_k\right)$ from equation **(4.16)**

ii) $(\mu_k \underline{\nabla}\phi_k)$ term (**a**) from equation **(4.17)**

Note that $\mu_k \underline{\nabla}\phi_k = \underline{\nabla}(\mu_k\phi_k) - \phi_k \underline{\nabla}\mu_k$. The latter form is used in the model, and is consistent with the formal derivation of the prognostic of *total energy*. The ϕ_k term used in $\underline{\nabla}(\mu_k\phi_k)$ must be derived in an identical manner to that used for the term $-\phi_k \underline{\nabla}\mu$.

Similar to the results emanating from the derivation of the *total energy* equation **(4.8)** some requirements for the vertical finite difference formulation of ϕ_k, when considering $(\partial\phi/\partial\eta)_k$, are defined. Following the derivation of equation **(4.8)** (through the global vertical integration of the *total energy* equation **(4.6)**) for energy conservation it is required that

$$\int_0^1 \left\{\phi\hat{D} + \frac{\partial\phi}{\partial\eta}[\hat{D}]^{\eta}\right\}d\eta = \phi_S[\hat{D}]^1$$

which yields the *mountain torque* term since $[\hat{D}]^1 = -\frac{\partial P_S}{\partial t}$.

In discrete notation the above integral becomes

$$\sum_{j=9}^{1}\left\{\phi_j\hat{D}_j + \left\{\frac{\partial\phi}{\partial\eta}\right\}_j[\hat{D}]^{\eta_j}\right\}\Delta\eta_j = \phi_S\sum_{j=9}^{1}(\hat{D}_j\Delta\eta_j) \qquad \textbf{(4.18)}$$

For energy conservation, the vertical finite difference formulation of ϕ_k and $(\partial\phi/\partial\eta)_k$ applied to the remaining terms in equations **(4.16)** and **(4.17)** must be formulated in such a manner as to satisfy equation **(4.18)**.

Using $\left\{\frac{\partial\phi}{\partial\eta}\right\}_k = \frac{(\phi_{k-0.5} - \phi_{k+0.5})}{\Delta\eta_k}$, the LHS of equation **(4.18)** becomes

$$\sum_{j=9}^{1}\left\{\phi_j\hat{D}_j+\left\{\frac{\partial\phi}{\partial\eta}\right\}_j[\hat{D}]^{\eta_j}\right\}\Delta\eta_j$$

$$=\sum_{j=9}^{1}\phi_j\hat{D}_j\Delta\eta_j+\sum_{j=9}^{1}\left\{\frac{\phi_{j-0.5}-\phi_{j+0.5}}{\Delta\eta_j}\right\}[\hat{D}]^{\eta_j}\Delta\eta_j$$

$$=\sum_{j=9}^{1}\phi_j\hat{D}_j\Delta\eta_j+\sum_{j=9}^{1}\left(\phi_{j-0.5}-\phi_{j+0.5}\right)[\hat{D}]^{\eta_j}$$

$$=\sum_{j=9}^{1}\phi_j\hat{D}_j\Delta\eta_j+\left(\phi_{0.5}-\phi_{1.5}\right)[\hat{D}]^{\eta_1}+\left(\phi_{1.5}-\phi_{2.5}\right)[\hat{D}]^{\eta_2}+.....+\left(\phi_{8.5}-\phi_{9.5}\right)[\hat{D}]^{\eta_9}$$

$$=\sum_{j=9}^{1}\phi_j\hat{D}_j\Delta\eta_j+\phi_{0.5}[\hat{D}]^{\eta_1}-\phi_{1.5}\left([\hat{D}]^{\eta_1}-[\hat{D}]^{\eta_2}\right)-\phi_{2.5}\left([\hat{D}]^{\eta_2}-[\hat{D}]^{\eta_3}\right)-.....-\phi_{8.5}\left([\hat{D}]^{\eta_8}-[\hat{D}]^{\eta_9}\right)-\phi_{9.5}[\hat{D}]^{\eta_9}$$

Application of the principle that $[\hat{D}]^{\eta_k}=\int_0^{\eta_k}\hat{D}d\eta=\sum_{j=9}^{k+1}\hat{D}_j\Delta\eta_j+0.5\hat{D}_k\Delta\eta_k$ yields

$$=\sum_{j=9}^{1}\phi_j\hat{D}_j\Delta\eta_j+\phi_{0.5}\left\{\sum_{j=9}^{2}\hat{D}_j\Delta\eta_j+0.5\hat{D}_1\Delta\eta_1\right\}$$

$$-\phi_{1.5}\left\{\sum_{j=9}^{2}\hat{D}_j\Delta\eta_j+0.5\hat{D}_1\Delta\eta_1-\sum_{j=9}^{3}\hat{D}_j\Delta\eta_j-0.5\hat{D}_2\Delta\eta_2\right\}$$

$$-\phi_{2.5}\left\{\sum_{j=9}^{3}\hat{D}_j\Delta\eta_j+0.5\hat{D}_2\Delta\eta_2-\sum_{j=9}^{4}\hat{D}_j\Delta\eta_j-0.5\hat{D}_3\Delta\eta_3\right\}-.....$$

$$-\phi_{8.5}\left\{\sum_{j=9}^{9}\hat{D}_j\Delta\eta_j+0.5\hat{D}_8\Delta\eta_8-\sum_{j=9}^{10}\hat{D}_j\Delta\eta_j-0.5\hat{D}_9\Delta\eta_9\right\}-\phi_{9.5}\left\{\sum_{j=9}^{10}\hat{D}_j\Delta\eta_j+0.5\hat{D}_9\Delta\eta_9\right\}$$

But the summation $\left\{\sum_{j=9}^{k}\hat{D}_j\Delta\eta_j-\sum_{j=9}^{k+1}\hat{D}_j\Delta\eta_j\right\}=\hat{D}_k\Delta\eta_k$

$$=\sum_{j=9}^{1}\phi_j\hat{D}_j\Delta\eta_j+\phi_{0.5}\left\{\sum_{j=9}^{2}\hat{D}_j\Delta\eta_j+0.5\hat{D}_1\Delta\eta_1\right\}-0.5\phi_{1.5}\left\{\hat{D}_1\Delta\eta_1+\hat{D}_2\Delta\eta_2\right\}-0.5\phi_{2.5}\left\{\hat{D}_2\Delta\eta_2+\hat{D}_3\Delta\eta_3\right\}-.....$$

$$-0.5\phi_{8.5}\left\{\hat{D}_8\Delta\eta_8+\hat{D}_9\Delta\eta_9\right\}-0.5\phi_{9.5}\left\{\hat{D}_9\Delta\eta_9\right\}$$

$$= \phi_1 \hat{D}_1 \Delta\eta_1 + \phi_2 \hat{D}_2 \Delta\eta_2 + ... + \phi_8 \hat{D}_8 \Delta\eta_8 + \phi_9 \hat{D}_9 \Delta\eta_9$$

$$+ \phi_{0.5} \left\{ \sum_{j=9}^{2} \hat{D}_j \Delta\eta_j + 0.5 \hat{D}_1 \Delta\eta_1 \right\} - 0.5\phi_{1.5} \left\{ \hat{D}_1 \Delta\eta_1 + \hat{D}_2 \Delta\eta_2 \right\} - 0.5\phi_{2.5} \left\{ \hat{D}_2 \Delta\eta_2 + \hat{D}_3 \Delta\eta_3 \right\} - .....$$

$$- 0.5\phi_{8.5} \left\{ \hat{D}_8 \Delta\eta_8 + \hat{D}_9 \Delta\eta_9 \right\} - 0.5\phi_{9.5} \left\{ \hat{D}_9 \Delta\eta_9 \right\}$$

Let $\phi_k = 0.5(\phi_{k-0.5} + \phi_{k-0.5})$ and impose this notation to (ϕ_j ; j = 1 to 9) which appear in the first nine terms in the LHS of the previous equation.

$$= 0.5(\phi_{0.5} + \phi_{1.5}) \hat{D}_1 \Delta\eta_1 + 0.5(\phi_{1.5} + \phi_{2.5}) \hat{D}_2 \Delta\eta_2 + ... + 0.5(\phi_{7.5} + \phi_{8.5}) \hat{D}_8 \Delta\eta_8 + 0.5(\phi_{8.5} + \phi_{9.5}) \hat{D}_9 \Delta\eta_9$$

$$+ \phi_{0.5} \left\{ \sum_{j=9}^{2} \hat{D}_j \Delta\eta_j + 0.5 \hat{D}_1 \Delta\eta_1 \right\} - 0.5\phi_{1.5} \left\{ \hat{D}_1 \Delta\eta_1 + \hat{D}_2 \Delta\eta_2 \right\} - 0.5\phi_{2.5} \left\{ \hat{D}_2 \Delta\eta_2 + \hat{D}_3 \Delta\eta_3 \right\} - .....$$

$$- 0.5\phi_{8.5} \left\{ \hat{D}_8 \Delta\eta_8 + \hat{D}_9 \Delta\eta_9 \right\} - 0.5\phi_{9.5} \left\{ \hat{D}_9 \Delta\eta_9 \right\}$$

The cancellation of terms is possible only if $\phi_k = 0.5(\phi_{k-0.5} + \phi_{k-0.5})$.

$$= 0.5\phi_{0.5} \hat{D}_1 \Delta\eta_1 + \phi_{0.5} \left\{ \sum_{j=9}^{2} \hat{D}_j \Delta\eta_j + 0.5 \hat{D}_1 \Delta\eta_1 \right\} = \phi_{0.5} \hat{D}_1 \Delta\eta_1 + \phi_{0.5} \sum_{j=9}^{2} \hat{D}_j \Delta\eta_j$$

$$= \phi_S \sum_{j=9}^{1} \hat{D}_j \Delta\eta_j \qquad \text{since } \phi_S = \phi_{0.5}$$

This is equal to the RHS of equation **(4.18)**. This result leads to the following energy conservation requirement:

E6: When the vertical derivative $\left\{ \frac{\partial\phi}{\partial\eta} \right\}_k = \frac{(\phi_{k-0.5} - \phi_{k+0.5})}{\Delta\eta_k}$ is used, (ϕ_k) at any full-level (k), **must** be derived from $\phi_k = 0.5(\phi_{k-0.5} + \phi_{k-0.5})$.

4.5.4 Discrete requirements for temperature

The *flux internal energy* equation **(4.5)** is derived by multiplying the *flux* form of the *thermodynamic* equation **(4.10)** by (c_p), which yields the vertical derivative

$$\frac{\partial(c_p \hat{\omega} T')}{\partial \eta}$$

in the *total energy* equation (term (**c**) of equation **(4.6)**). For energy conservation the *vertical* integrated flux divergence of any quantity (with $\hat{\omega} = 0$ at $\eta = 0$ and 1) is zero. The vertical finite difference formulation of the temperature variable (T') is defined according to this energy conservation requirement. In this case the energy conservation requirement is

$$\int_0^1 \frac{c_p \partial(\hat{\omega} T')}{\partial \eta} d\eta = 0 \qquad \textbf{(4.19)}$$

For energy conservation the LHS of the discrete form of this equation **must** be equal to the RHS. In discrete notation the LHS becomes

$$\sum_{j=9}^{1} \left\{ c_p \frac{\partial(\hat{\omega} T')}{\partial \eta} \right\}_j \Delta\eta_j$$

When using $\left\{ \frac{\partial(\hat{\omega} T')}{\partial \eta} \right\}_k = \frac{(\hat{\omega}_{k-0.5} T'_{k-0.5} - \hat{\omega}_{k+0.5} T'_{k+0.5})}{\Delta\eta_k}$ becomes

$$\sum_{j=9}^{1} \left\{ c_p \frac{(\hat{\omega}_{j-0.5} T'_{j-0.5} - \hat{\omega}_{j+0.5} T'_{j+0.5})}{\Delta\eta_j} \right\} \Delta\eta_j$$

$$= c_p \{(\hat{\omega}_{0.5} T'_{0.5} - \hat{\omega}_{1.5} T'_{1.5}) + (\hat{\omega}_{1.5} T'_{1.5} - \hat{\omega}_{2.5} T'_{2.5}) + ... + (\hat{\omega}_{7.5} T'_{7.5} - \hat{\omega}_{8.5} T'_{8.5}) + (\hat{\omega}_{8.5} T'_{8.5} - \hat{\omega}_{9.5} T'_{9.5})\}$$
$$= c_p \{(\hat{\omega}_{0.5} T'_{0.5} - \hat{\omega}_{9.5} T'_{9.5})\} = 0$$

because $\hat{\omega} = 0$ at the bottom (η=1, k=0.5) and top (η=0, k=9.5) of the atmosphere. This is also equal to the RHS of equation **(4.19)**

E7: When using the vertical derivative $\left\{ \frac{\partial(\hat{\omega} T')}{\partial \eta} \right\}_k = \frac{(\hat{\omega}_{k-0.5} T'_{k-0.5} - \hat{\omega}_{k+0.5} T'_{k+0.5})}{\Delta\eta_k}$, **any** valid value for ($T'_{k-0.5}$ or $T'_{k+0.5}$) is suitable, because equation **(4.19)** will always integrate to zero in the vertical. In this study (T'), at any half-level, is derived from $T = a + b(\ln \eta)$ (APPENDIX C).

4.5.5 Discrete requirements for velocity

The *flux kinetic energy* equation **(4.4)** in this chapter is derived by multiplying the standard *momentum* equation **(4.1)** by $(\mu\underline{V})$, which yields the vertical derivative

$$\frac{\partial(\hat{\omega}E)}{\partial\eta}$$

in the *total energy* equation (term (**c**) in equation **(4.6)**). For energy conservation the *vertical* integrated flux divergence of any quantity (with $\hat{\omega} = 0$ at $\eta = 0$ and 1) is zero. The vertical finite difference formulation of the horizontal velocity $(\underline{V})$ is defined according to this energy conservation requirement. In this case the energy conservation requirement is

$$\int_0^1 \frac{\partial(\hat{\omega}E)}{\partial\eta}\,d\eta = 0 \qquad \textbf{(4.20)}$$

To obtain the *flux* formulation of the *kinetic energy* equation, one may also directly multiply the *flux* formulation of the *momentum* equation **(4.9)** by $\underline{V}$ (unlike the derivation in this chapter but using similar principles). This results in the vertical motion term

$$\underline{V}\cdot\frac{\partial(\hat{\omega}\underline{V})}{\partial\eta}$$

The terms involved in this vertical derivative are of particular importance. They involve half-level values of $\underline{V}$ which are multiplied by full-level values during the formation of the *kinetic energy* equation **(4.4)**. It is therefore important to ensure that these terms behave correctly in their discrete forms. It follows that

$$\underline{V}\cdot\frac{\partial(\hat{\omega}\underline{V})}{\partial\eta} = \underline{V}\cdot\left\{\underline{V}\frac{\partial\hat{\omega}}{\partial\eta} + \hat{\omega}\frac{\partial\underline{V}}{\partial\eta}\right\} = 2E\frac{\partial\hat{\omega}}{\partial\eta} + \hat{\omega}\frac{\partial\underline{E}}{\partial\eta} = 2E\frac{\partial\hat{\omega}}{\partial\eta} + \frac{\partial(\hat{\omega}E)}{\partial\eta} - E\frac{\partial\hat{\omega}}{\partial\eta} = E\frac{\partial\hat{\omega}}{\partial\eta} + \frac{\partial(\hat{\omega}E)}{\partial\eta}$$

To achieve the *energy* relation **(4.8)** it is necessary to take vertical integrals.

$$\int_0^1 \underline{V}\cdot\frac{\partial(\hat{\omega}\underline{V})}{\partial\eta}\,d\eta = \int_0^1 E\frac{\partial\hat{\omega}}{\partial\eta}\,d\eta + \int_0^1 \frac{\partial(\hat{\omega}E)}{\partial\eta}\,d\eta = \int_0^1 E\frac{\partial\hat{\omega}}{\partial\eta}\,d\eta \qquad \textbf{(4.21)}$$

since equation **(4.20)** is zero. For energy conservation the LHS of the discrete form of this equation **must** be equal to the RHS. In discrete notation the LHS of the integration **(4.21)** becomes

$$\sum_{j=9}^{1}\left\{\underline{V}\cdot\frac{\partial(\hat{\omega}\underline{V})}{\partial\eta}\right\}_j\Delta\eta_j$$

When using $\left\{\frac{\partial(\hat{\omega}\underline{V})}{\partial\eta}\right\}_k=\frac{(\hat{\omega}_{k-0.5}\underline{V}_{k-0.5}-\hat{\omega}_{k+0.5}\underline{V}_{k+0.5})}{\Delta\eta_k}$ we have

$$\sum_{j=9}^{1}\left\{\underline{V}_j\cdot\frac{(\hat{\omega}_{j-0.5}\underline{V}_{j-0.5}-\hat{\omega}_{j+0.5}\underline{V}_{j+0.5})}{\Delta\eta_j}\right\}\Delta\eta_j$$

$$=\underline{V}_1\cdot(\hat{\omega}_{0.5}\underline{V}_{0.5}-\hat{\omega}_{1.5}\underline{V}_{1.5})+\underline{V}_2\cdot(\hat{\omega}_{1.5}\underline{V}_{1.5}-\hat{\omega}_{2.5}\underline{V}_{2.5})+.....$$
$$+\underline{V}_8\cdot(\hat{\omega}_{7.5}\underline{V}_{7.5}-\hat{\omega}_{8.5}\underline{V}_{8.5})+\underline{V}_9\cdot(\hat{\omega}_{8.5}\underline{V}_{8.5}-\hat{\omega}_{9.5}\underline{V}_{9.5})$$

Let $\underline{V}_{k-0.5}=0.5(\underline{V}_{k-1}+\underline{V}_k)$ and $\underline{V}_{k+0.5}=0.5(\underline{V}_k+\underline{V}_{k+1})$

$$=0.5\underline{V}_1\cdot(\hat{\omega}_{0.5}(\underline{V}_0+\underline{V}_1)-\hat{\omega}_{1.5}(\underline{V}_1+\underline{V}_2))+0.5\underline{V}_2\cdot(\hat{\omega}_{1.5}(\underline{V}_1+\underline{V}_2)-\hat{\omega}_{2.5}(\underline{V}_2+\underline{V}_3))+.....$$
$$+0.5\underline{V}_8\cdot(\hat{\omega}_{7.5}(\underline{V}_7+\underline{V}_8)-\hat{\omega}_{8.5}(\underline{V}_8+\underline{V}_9))+0.5\underline{V}_9\cdot(\hat{\omega}_{8.5}(\underline{V}_8+\underline{V}_9)-\hat{\omega}_{9.5}(\underline{V}_9+\underline{V}_{10}))$$

$$=0.5(\hat{\omega}_{0.5}(\underline{V}_1\cdot\underline{V}_0+\underline{V}_1\cdot\underline{V}_1)-\hat{\omega}_{1.5}(\underline{V}_1\cdot\underline{V}_1+\underline{V}_1\cdot\underline{V}_2)+\hat{\omega}_{1.5}(\underline{V}_2\cdot\underline{V}_1+\underline{V}_2\cdot\underline{V}_2)-\hat{\omega}_{2.5}(\underline{V}_2\cdot\underline{V}_2+\underline{V}_2\cdot\underline{V}_3))+...$$
$$+\hat{\omega}_{7.5}(\underline{V}_8\cdot\underline{V}_7+\underline{V}_8\cdot\underline{V}_8)-\hat{\omega}_{8.5}(\underline{V}_8\cdot\underline{V}_8+\underline{V}_8\cdot\underline{V}_9)+\hat{\omega}_{8.5}(\underline{V}_9\cdot\underline{V}_8+\underline{V}_9\cdot\underline{V}_9)-\hat{\omega}_{9.5}(\underline{V}_9\cdot\underline{V}_9+\underline{V}_9\cdot\underline{V}_{10}))$$

Since $\underline{V}_{k-0.5}=0.5(\underline{V}_{k-1}+\underline{V}_k)$ and $\underline{V}_{k+0.5}=0.5(\underline{V}_k+\underline{V}_{k+1})$ was imposed, all the cross terms ($\underline{V}_k\underline{V}_{k-1}$ and $\underline{V}_k\underline{V}_{k+1}$) cancel to zero, or are zero because $\hat{\omega}_{0.5}=\hat{\omega}_{9.5}=0$.

$$=0.5(\hat{\omega}_{0.5}(\underline{V}_1\cdot\underline{V}_1)-\hat{\omega}_{1.5}(\underline{V}_1\cdot\underline{V}_1)+\hat{\omega}_{1.5}(\underline{V}_2\cdot\underline{V}_2)-\hat{\omega}_{2.5}(\underline{V}_2\cdot\underline{V}_2)+.....$$
$$+\hat{\omega}_{7.5}(\underline{V}_8\cdot\underline{V}_8)-\hat{\omega}_{8.5}(\underline{V}_8\cdot\underline{V}_8)+\hat{\omega}_{8.5}(\underline{V}_9\cdot\underline{V}_9)-\hat{\omega}_{9.5}(\underline{V}_9\cdot\underline{V}_9)$$

$$=0.5(\underline{V}_1\cdot\underline{V}_1)(\hat{\omega}_{0.5}-\hat{\omega}_{1.5})+0.5(\underline{V}_2\cdot\underline{V}_2)(\hat{\omega}_{1.5}-\hat{\omega}_{2.5})+.....$$
$$+0.5(\underline{V}_8\cdot\underline{V}_8)(\hat{\omega}_{7.5}-\hat{\omega}_{8.5})+0.5(\underline{V}_9\cdot\underline{V}_9)(\hat{\omega}_{8.5}-\hat{\omega}_{9.5})$$

But $E_k=0.5(\underline{V}_k\cdot\underline{V}_k)$

$$=E_1(\hat{\omega}_{0.5}-\hat{\omega}_{1.5})+E_2(\hat{\omega}_{1.5}-\hat{\omega}_{2.5})+.....+E_8(\hat{\omega}_{7.5}-\hat{\omega}_{8.5})+E_9(\hat{\omega}_{8.5}-\hat{\omega}_{9.5})$$

$$=\sum_{j=9}^{1}\left\{E_j\frac{(\hat{\omega}_{j-0.5}-\hat{\omega}_{j+0.5})}{\Delta\eta_j}\right\}\Delta\eta_j$$

This result is the discrete notation of $\int_0^1 E\frac{\partial\hat{\omega}}{\partial\eta}d\eta$ and equal to the RHS of equation **(4.21).**

E8: When using the vertical derivative, $\left\{\frac{\partial(\hat{\omega}\underline{V})}{\partial\eta}\right\}_k = \frac{(\hat{\omega}_{k-0.5}\underline{V}_{k-0.5} - \hat{\omega}_{k+0.5}\underline{V}_{k+0.5})}{\Delta\eta_k}$, $(\underline{V}_{k-0.5})$ and $(\underline{V}_{k+0.5})$ at any half-level (k-0.5) or (k+0.5) **must** be derived from $\underline{V}_{k-0.5} = 0.5(\underline{V}_{k-1} + \underline{V}_k)$ and $\underline{V}_{k+0.5} = 0.5(\underline{V}_k + \underline{V}_{k+1})$

CHAPTER 5

NUMERICAL SOLUTIONS AND THE SEMI-IMPLICIT TIME INTEGRATION

5.1 INTRODUCTION

Several numerical schemes used to solve the atmospheric equations in the CSIRO-9 Mark II AGCM are briefly outlined in the following chapter. Specific energy conservation requirements (***E1*** to ***E8*** in chapter 4) are necessary when constructing the vertical finite difference notation of terms in the atmospheric equations. Aspects concerning the horizontal treatment (spectral analyses and grid transforms) as well as the time integration (leapfrog method) are summarised below.

5.2 HYDROSTATIC EQUATION

In APPENDIX C a unique quantity ($\hat{\phi} \neq \mu\phi'$) is defined for the η-system in such a way that

$$\frac{\partial\hat{\phi}}{\partial(\ln\eta)} = -R(\mu T') = -R\hat{T} \quad \text{or} \quad \frac{\partial\hat{\phi}}{\partial\eta} = -\frac{R\hat{T}}{\eta} \qquad \textbf{(5.1)}$$

Vertical integration yields a vector-matrix $\underline{\hat{\phi}} = \underline{\underline{A}}\,\underline{\hat{T}}$.

The quantity $\hat{\phi}$ in the *hydrostatic* equation **(5.1)** may be solved at *half-levels* by using the finite difference notation

$$\frac{(\hat{\phi}_{k-0.5} - \hat{\phi}_{k+0.5})}{\Delta\eta_k} = -\frac{R\hat{T}_k}{\eta_k}$$

where $\hat{\phi}_{0.5} = \hat{\phi}_S$ is the surface value.

For energy conservation (requirement ***E3*** in chapter 4) *full-level* values must be derived from the half-level values.

$$\hat{\phi}_k = 0.5\left(\hat{\phi}_{k-0.5} + \hat{\phi}_{k-0.5}\right)$$

This method is used to solve $\hat{\phi}$ in the *flux momentum* equation **(3.8)**

5.3 STREAM FUNCTION AND VELOCITY POTENTIAL EQUATIONS

In the previous chapters all the main atmospheric equations have been derived. In this section the atmospheric equations are manipulated in a form which is suitable for spectral analyses. To achieve this, the horizontal velocity is written in terms of the stream function (ψ) and velocity potential (χ). Details on these functions are available in Holton (1992), Washington and Parkinson (1992) and Haltiner and Williams (1980), Haltiner (1971).

Vector components of the atmospheric equations are expressed in terms of spherical co-ordinates (λ, φ, r) where λ is longitude, φ is latitude and r is the radial distance from the centre of the Earth to any point in the atmosphere (figure 1). The formal derivation from rotating co-ordinates (x,y,z) to spherical co-ordinates may be achieved by using similar methods described in APPENDIX A. More details concerning vector operations in general curvilinear co-ordinate systems may be found in Spiegel, 1974.

From chapter 2 it follows that

$$\underline{V} = u\underline{i} + v\underline{j} \qquad \text{and} \qquad \underline{\nabla} = \frac{\partial}{\partial x}\underline{i} + \frac{\partial}{\partial y}\underline{j}$$

The horizontal velocity may be expressed in terms of the stream function (ψ) and velocity potential (χ). The standard (i) and μ-weighted (ii) forms are:

(i) $\underline{V} = \underline{k} \times \underline{\nabla}\psi + \underline{\nabla}\chi$ with $\xi = \nabla^2\psi$ and $D = \nabla^2\chi$

(ii) $\hat{\underline{V}} = \underline{k} \times \underline{\nabla}\hat{\psi} + \underline{\nabla}\hat{\chi}$ with $\hat{\xi} = \nabla^2\hat{\psi}$ and $\hat{D} = \nabla^2\hat{\chi}$

The components of the standard (left) and μ-weighted (right) velocities are

$$\underline{V} = -\frac{\partial\psi}{\partial y}\underline{i} + \frac{\partial\psi}{\partial x}\underline{j} + \frac{\partial\chi}{\partial x}\underline{i} + \frac{\partial\chi}{\partial y}\underline{j}$$
$$= \left\{\frac{\partial\chi}{\partial x} - \frac{\partial\psi}{\partial y}\right\}\underline{i} + \left\{\frac{\partial\psi}{\partial x} + \frac{\partial\chi}{\partial y}\right\}\underline{j}$$
$$= u\underline{i} + v\underline{j}$$

$$\hat{\underline{V}} = -\frac{\partial\hat{\psi}}{\partial y}\underline{i} + \frac{\partial\hat{\psi}}{\partial x}\underline{j} + \frac{\partial\hat{\chi}}{\partial x}\underline{i} + \frac{\partial\hat{\chi}}{\partial y}\underline{j}$$
$$= \left\{\frac{\partial\hat{\chi}}{\partial x} - \frac{\partial\hat{\psi}}{\partial y}\right\}\underline{i} + \left\{\frac{\partial\hat{\psi}}{\partial x} + \frac{\partial\hat{\chi}}{\partial y}\right\}\underline{j}$$
$$= \mu u\underline{i} + \mu v\underline{j}$$

which results in the following scalar component forms

$$u = \left\{\frac{\partial\chi}{\partial x} - \frac{\partial\psi}{\partial y}\right\} \; ; \; v = \left\{\frac{\partial\psi}{\partial x} + \frac{\partial\chi}{\partial y}\right\}$$

$$\mu u = \left\{\frac{\partial\hat{\chi}}{\partial x} - \frac{\partial\hat{\psi}}{\partial y}\right\} \; ; \; \mu v = \left\{\frac{\partial\hat{\psi}}{\partial x} + \frac{\partial\hat{\chi}}{\partial y}\right\}$$

In spherical co-ordinates this becomes

$$u = \frac{1}{r}\left\{\frac{\partial\chi}{\cos(\varphi)\partial\lambda} - \frac{\partial\psi}{\partial\varphi}\right\} \qquad \mu u = \frac{1}{r}\left\{\frac{\partial\hat{\chi}}{\cos(\varphi)\partial\lambda} - \frac{\partial\hat{\psi}}{\partial\varphi}\right\}$$

$$v = \frac{1}{r}\left\{\frac{\partial\psi}{\cos(\varphi)\partial\lambda} + \frac{\partial\chi}{\partial\varphi}\right\} \qquad \nu\mu = \frac{1}{r}\left\{\frac{\partial\hat{\psi}}{\cos(\varphi)\partial\lambda} + \frac{\partial\hat{\chi}}{\partial\varphi}\right\} \qquad \textbf{(5.2)}$$

Define $U = \cos(\varphi)u$, $V = \cos(\varphi)v$, $\hat{U} = \cos(\varphi)\mu u$ and $\hat{V} = \cos(\varphi)\mu v$

$$U = \frac{1}{r}\left\{\frac{\partial\chi}{\partial\lambda} - \cos(\varphi)\frac{\partial\psi}{\partial\varphi}\right\} \qquad \hat{U} = \frac{1}{r}\left\{\frac{\partial\hat{\chi}}{\partial\lambda} - \cos(\varphi)\frac{\partial\hat{\psi}}{\partial\varphi}\right\}$$

$$V = \frac{1}{r}\left\{\frac{\partial\psi}{\partial\lambda} + \cos(\varphi)\frac{\partial\chi}{\partial\varphi}\right\} \qquad \hat{V} = \frac{1}{r}\left\{\frac{\partial\hat{\psi}}{\partial\lambda} + \cos(\varphi)\frac{\partial\hat{\chi}}{\partial\varphi}\right\} \qquad \textbf{(5.3)}$$

Replacement of these components, $\mu f\underline{V} = f\underline{\hat{V}}$ and $\underline{\hat{C}} = (\hat{C}_\lambda \underline{i} + \hat{C}_\varphi \underline{j})$ in the *flux* formulation of the *vorticity* equation **(3.9),** and the application of some principal vector operators (*div* and *curl* operators) of general orthogonal co-ordinates (Spiegel, 1974; Haltiner, 1971) results in

$$\frac{\partial(\nabla^2\hat{\psi})}{\partial t} = -\frac{1}{r\cos^2(\varphi)}\left[\frac{\partial\left[(\hat{\xi} + \frac{\partial B}{\partial\eta}\delta_1)U\right]}{\partial\lambda} + \cos(\varphi)\frac{\partial\left[(\hat{\xi} + \frac{\partial B}{\partial\eta}\delta_1)V\right]}{\partial\varphi}\right] - 2\Omega\left[\sin(\varphi)\nabla^2\hat{\chi} + \frac{\hat{V}}{r}\right]$$

$$-\frac{1}{r\cos^2\varphi}\left[\frac{\partial\left[\cos(\varphi)C_\varphi\right]}{\partial\lambda} - \cos(\varphi)\frac{\partial\left[\cos(\varphi)C_\lambda\right]}{\partial\varphi}\right] \qquad \textbf{(5.4)}$$

where

$$C_\varphi = \frac{\partial(\hat{\omega}v)}{\partial\eta} + \left\{RT^* - (\phi' + \phi'_S + E')\frac{\partial B}{\partial\eta}\right\}\frac{1}{r}\frac{\partial P_S}{\partial\varphi} + \hat{D}v - \mu\hat{F}_\varphi$$

$$C_\lambda = \frac{\partial(\hat{\omega}u)}{\partial\eta} + \left\{RT^* - (\phi' + \phi'_S + E')\frac{\partial B}{\partial\eta}\right\}\frac{1}{r\cos(\varphi)}\frac{\partial P_S}{\partial\lambda} + \hat{D}u - \mu\hat{F}_\lambda$$

Let

$$\hat{A} = (\hat{\xi} + \frac{\partial B}{\partial\eta}\delta_1)U + \cos(\varphi)\hat{C}_\varphi \quad \text{and} \quad \hat{S} = \cos(\varphi)\hat{F}_\varphi$$

$$\hat{B} = (\hat{\xi} + \frac{\partial B}{\partial\eta}\delta_1)V - \cos(\varphi)\hat{C}_\lambda \quad \text{and} \quad \hat{R} = \cos(\varphi)\hat{F}_\lambda$$

After some further manipulation, the *vorticity* equation **(5.4)** becomes

$$\frac{\partial(\nabla^2\hat{\psi})}{\partial t} = -\frac{1}{r\cos^2(\varphi)}\left[\frac{\partial[\hat{A}]}{\partial\lambda} + \cos(\varphi)\frac{\partial[\hat{B}]}{\partial\varphi}\right] - 2\Omega\left[\sin(\varphi)\nabla^2\hat{\chi} + \frac{\hat{V}}{r}\right] \qquad \textbf{(5.5)}$$

Similarly, the *flux* formulation of the *divergence* equation **(3.10)** results in

$$\frac{\partial(\nabla^2\hat{\chi})}{\partial t} = -\frac{1}{r\cos^2(\varphi)}\left[\frac{\partial[\hat{B}]}{\partial\lambda} - \cos(\varphi)\frac{\partial[\hat{A}]}{\partial\varphi}\right] + 2\Omega\left[\sin(\varphi)\nabla^2\hat{\psi} + \frac{\hat{U}}{r}\right] - \nabla^2\hat{E} - RT_O\nabla^2 P_S - \nabla^2\hat{\phi} \qquad \textbf{(5.6)}$$

Note that $\hat{E} = (\mu E' + \mu\phi' + \mu\phi'_S - \hat{\phi})$ where $E' = E - E_O$ and $E = \frac{(U^2+V^2)}{2\cos^2(\varphi)}$

5.4 SPECTRAL FIELDS

The atmospheric equations are treated spectrally using spherical harmonics on the globe, namely

$$Y_n^m(\varphi,\lambda) = P_n^m \sin(\varphi) e^{im\lambda}$$

where P_n^m are Legendre polynomials of degree n. Fourier components are represented by $(e^{im\lambda})$. Here m and n-m represents the zonal and meridional planetary wave numbers respectively. Note that $|m| \le n$ and J=21 for a R21 spectral model. The atmospheric variables $\hat{\xi},\hat{D},\hat{T},P_S,\hat{\psi},\hat{\chi},\hat{U},\hat{V}$ may be expanded into a set of time-dependant spectral coefficients. For example $\hat{\xi}(t)_n^m$ being complex (containing an imaginary and real part) and spherical harmonics:

$$(\hat{\xi},\hat{D},\hat{T},P_S) = \sum_m \sum_n (\hat{\xi}(t),\hat{D}(t),\hat{T}(t),P_S(t))_n^m Y_n^m \qquad m=0,\ldots.J\ ;\ n=m,\ldots..m+J \qquad \textbf{(5.7)}$$

$$(\hat{\psi},\hat{\chi}) = r^2\sum_m \sum_n (\hat{\psi}(t),\hat{\chi}(t))_n^m Y_n^m \qquad m=0,\ldots.J\ ;\ n=m,\ldots..m+J \qquad \textbf{(5.8)}$$

$$(\hat{U},\hat{V}) = r\sum_m \sum_n (\hat{U}(t),\hat{V}(t))_n^m Y_n^m \qquad m=0,\ldots.J\ ;\ n=m,\ldots..m+J+1 \qquad \textbf{(5.9)}$$

The *main prognostic* equations may now be transformed to spectral form.

The non-linear terms of the *vorticity*, *divergence* and *thermodynamic* equations are evaluated through the grid transform method. This means that the atmospheric variables in these terms are required to be in a latitude/longitude grid format. These non-linear terms are:

$\hat{A}$: from equations **(5.5)** and **(5.6)**

$\hat{B}$: from equations **(5.5)** and **(5.6)**

$\hat{E}$: from equation **(5.6)**

$\underline{\nabla}\cdot(\hat{\underline{V}}T')$: from equation **(3.18)**

$$\left\{\frac{KT_o}{\eta}[\hat{D}]^{\eta}+\frac{1}{c_p}\frac{\partial\phi}{\partial\eta}[\hat{D}]^{\eta}+\frac{1}{c_p}RT\frac{\mu B}{p}(\underline{V}\cdot\underline{\nabla}P_s)+\hat{Q}-\frac{\partial(\hat{\omega}T')}{\partial\eta}\right\}$$: from equation **(3.18)**

The grid field variables required for these terms are $\hat{U}, \hat{V}, \hat{\xi}, \hat{D}, \hat{T}$ and P_s. Henderson-Sellers and McGuffie (1987) stated that the grid point values are calculated from the spectral equivalents (spectral to grid transform) by the application of the spectral expansions **(5.7)** and **(5.9)**. This is accomplished through additions over the (n) domain and then by use of a fast Fourier transform (FFT).

In the non-linear terms $\hat{A}$ and $\hat{B}$ the quantities δ_1 and δ_2 also need to be calculated:

$$\delta_1 = \underline{k}\cdot\underline{V}\times\underline{\nabla}P_s = \frac{1}{r\cos^2(\varphi)}\left[U\cos(\varphi)\frac{\partial P_s}{\partial\varphi}-V\frac{\partial P_s}{\partial\lambda}\right]$$

$$\delta_2 = \underline{V}\cdot\underline{\nabla}P_s = \frac{1}{r\cos^2(\varphi)}\left[V\cos(\varphi)\frac{\partial P_s}{\partial\varphi}+u\frac{\partial P_s}{\partial\lambda}\right]$$

where

$$\frac{\partial P_s}{\partial\lambda}=\sum_m\left\{\sum_n(P_s)_n^m P_n^m(\varphi)\right\}ime^{im\lambda} \quad \text{and} \quad \cos(\varphi)\frac{\partial P_s}{\partial\varphi}=\sum_m\left\{\sum_n(P_s)_n^m\cos(\varphi)\frac{\partial P_n^m(\varphi)}{\partial\varphi}\right\}e^{im\lambda}$$

which are readily derived, since $\cos(\varphi)\frac{\partial P_n^m(\varphi)}{\partial\varphi}$ can be derived from $P_n^m(\varphi)$

The non-linear terms, with a definition of equivalent Fourier harmonics ($\hat{A}_m, \hat{B}_m, \hat{E}_m, \hat{F}_m, \hat{G}_m$ and $\hat{H}_m$) are:

- $$r\sum_m \hat{A}_m e^{im\lambda} = (\hat{\xi} + \frac{\partial B}{\partial \eta}\delta_1)U + \frac{\partial(\hat{\omega}V)}{\partial \eta} + \left\{RT^* - (\phi' + \phi'_S + E')\frac{\partial B}{\partial \eta}\right\}\frac{\cos(\varphi)}{r}\frac{\partial P_S}{\partial \varphi} + \hat{D}V - \hat{S}$$
- $$r\sum_m \hat{B}_m e^{im\lambda} = (\hat{\xi} + \frac{\partial B}{\partial \eta}\delta_1)U - \frac{\partial(\hat{\omega}U)}{\partial \eta} - \left\{RT^* - (\phi' + \phi'_S + E')\frac{\partial B}{\partial \eta}\right\}\frac{1}{r}\frac{\partial P_S}{\partial \lambda} - \hat{D}U + \hat{R}$$
- $$r^2\sum_m \hat{E}_m e^{im\lambda} = (\mu E' + \mu\phi' + \mu\phi'_S - \hat{\phi})$$
- $$r\sum_m \hat{F}_m e^{im\lambda} = \hat{U}T'$$
- $$r\sum_m \hat{G}_m e^{im\lambda} = \hat{V}T'$$
- $$r\sum_m \hat{H}_m e^{im\lambda} = \frac{KT_O}{\eta}[\hat{D}]^\eta + \frac{1}{c_p}\frac{\partial \phi}{\partial \eta}[\hat{D}]^\eta + \frac{1}{c_p}RT\frac{\mu B}{p}(\underline{V}\cdot\underline{\nabla}P_S) + \hat{Q} - \frac{\partial(\hat{\omega}T')}{\partial \eta}$$

The next step is to construct the spectral atmospheric equations. From a given latitude/longitude grid field of an arbitrary atmospheric variable (κ), Fourier harmonics $(\kappa)_m$ may be derived from grid values along a specific Gaussian latitude (φ_g) by using FFTs (grid to spectral transform).

The spectral coefficients (κ_n^m) may be derived by using the following integral:

$$\kappa_n^m = \int_{-\frac{\pi}{2}}^{\frac{\pi}{2}} (\kappa)_m P_n^m \sin(\varphi) w(\varphi)$$

The integration is exact if Gaussian quadrature is used. This quadrature replaces the integral by a sum over Gaussian latitudes (φ_g), with Gaussian weights ($w(\varphi_g)$).

$$\kappa_n^m = \sum_{\varphi_g} \kappa_m(\varphi_g) P_n^m(\sin(\varphi_g)) w(\varphi_g)$$

The following is a useful feature of the spectral harmonics:

If $(\hat{\xi} = \nabla^2\hat{\psi})$ where $\hat{\xi} = \sum_m \sum_n \hat{\xi}_n^m Y_n^m$; $\hat{\psi} = a^2 \sum_m \sum_n \hat{\psi}_n^m Y_n^m$ then $\hat{\xi}_n^m = -n(n+1)\hat{\psi}_n^m$ meaning that ∇^2 has an immediate solution in spectral terms.

The grid to spectral transform of the prognostic atmospheric equations requires some manipulation, which is not provided in this document. Details are available in Holton (1992), Washington and Parkinson (1992), Haltiner and Williams (1980) and Haltiner (1971). The spectral atmospheric equations derived from **(5.5)**, **(5.6)**, **(3.18)** and **(3.15)** are:

- $$\frac{\partial\hat{\xi}_n^m}{\partial t} = \frac{\partial(\nabla^2\hat{\psi}_n^m)}{\partial t} = -\int_{-\frac{\pi}{2}}^{\frac{\pi}{2}} \frac{1}{\cos^2\varphi}\left\{ im(\hat{A}_m)P_n^m - (\hat{B}_m)\cos(\varphi)\frac{\partial P_n^m}{\partial\varphi}\right\}\cos\varphi d\varphi$$
$$+ 2\Omega\left\{n(n-1)\varepsilon_n^m\hat{\chi}_{n-1}^m + (n+1)(n+2)\varepsilon_{n+1}^m\hat{\chi}_{n+1}^m - \hat{V}_n^m\right\} \qquad \textbf{(5.10)}$$

- $$\frac{\partial\hat{D}_n^m}{\partial t} = \frac{\partial(\nabla^2\hat{\chi}_n^m)}{\partial t} = +\int_{-\frac{\pi}{2}}^{\frac{\pi}{2}} \frac{1}{\cos^2\varphi}\left\{ im(\hat{B}_m)P_n^m + (\hat{A}_m)\cos(\varphi)\frac{\partial P_n^m}{\partial\varphi}\right\}\cos\varphi d\varphi$$
$$- 2\Omega\left\{n(n-1)\varepsilon_n^m\hat{\psi}_{n-1}^m + (n+1)(n+2)\varepsilon_{n+1}^m\hat{\psi}_{n+1}^m + \hat{U}_n^m\right\}$$
$$+ n(n+1)\left\{\hat{E}_n^m + \boxed{\frac{RT_O P_{Sn}^m}{r^2} + \frac{\hat{\phi}_n^m}{r^2}}\right\} \text{ where } \varepsilon_n^m = \sqrt{(n^2-m^2)/(4n^2-1)} \qquad \textbf{(5.11)}$$

- $$\frac{\partial\hat{T}_n^m}{\partial t} = -\int_{-\frac{\pi}{2}}^{\frac{\pi}{2}} \frac{1}{\cos^2\varphi}\left\{ im(\hat{F}_m)P_n^m - (\hat{G}_m)\cos(\varphi)\frac{\partial P_n^m}{\partial\varphi}\right\}\cos\varphi d\varphi$$
$$+ \int_{-\frac{\pi}{2}}^{\frac{\pi}{2}} (\hat{H}_m)P_n^m\cos\varphi d\varphi - \boxed{\frac{KT_O}{\eta}\left[\hat{D}_n^m\right]^\eta} \qquad \textbf{(5.12)}$$

- $$\frac{\partial P_{Sn}^m}{\partial t} = -\left[\hat{D}_n^m\right]^1 = -\int_0^1 (\hat{D}_n^m)d\eta \qquad \textbf{(5.13)}$$

- $$\hat{E}_n^m = +\int_{-\frac{\pi}{2}}^{\frac{\pi}{2}} (\hat{E}_m)P_n^m\cos\varphi d\varphi \qquad \textbf{(5.14)}$$

$\boxed{\quad}$ = Gravity wave generating terms

Geopotential / temperature

The relationship between geopotential and temperature may be obtained by using the *hydrostatic* equation:

$$\frac{\partial\hat{\phi}}{\partial(\ln\eta)} = -R(\mu T') = -R\hat{T} \qquad \text{where} \qquad \hat{\phi} \neq \mu\phi'$$

Vertical integration will yield a vector-matrix $\underline{\hat{\phi}} = \underline{\underline{A}}\,\underline{\hat{T}}$, which relates $\hat{\phi}$ to $\hat{T}$. $\nabla^2\hat{\phi}$ is required in the *divergence* equation **(5.6)**, which becomes $n(n+1)\hat{\phi}_n^m / r^2$ in the equivalent spectral equation **(5.11)**. The vector-matrix $\underline{\hat{\phi}} = \underline{\underline{A}}\,\underline{\hat{T}}$ may be used to substitute the geopotentials with the appropriate functions of temperature when the time integration is performed.

Moisture

In the CSIRO-9 Mark II AGCM moisture is carried in grid form. When solving the *flux* formulation of the *moisture* equation **(3.20)**, the term $\underline{\nabla}\cdot(\underline{\hat{V}}q)$ is first evaluated as a spectral field, where after a spectral to grid transform is employed to obtain grid point values for

$$\frac{\partial\hat{q}}{\partial t} = \hat{S}_q - \underline{\nabla}\cdot(\underline{\hat{V}}q) - \frac{\partial(\hat{\omega}q)}{\partial\eta}$$

Note that the LHS of the equation becomes zero when $\hat{S}_q$ is removed, since the spectral evaluation of $\underline{\nabla}\cdot(\underline{\hat{V}}q)$ ensures a global mean of zero and the application of upper and lower boundary conditions of $\hat{\omega} = 0$ ensures that the vertical integral of the last term is also zero. However, in recent versions of the CSIRO models, the moisture is now treated by a Semi-Lagrangian Transport (SLT) grid point method (McGregor, 1993), rather than the original spectral/grid method.

5.5 TIME INTEGRATION

The leapfrog method is applied to perform the time integration of the spectral atmospheric equations. For any atmospheric variable κ the leapfrog assumption may be defined as

$$\frac{\partial\kappa^t}{\partial t} = \frac{\kappa^{t+1} - \kappa^{t-1}}{2\Delta t} \qquad \text{with } \Delta t \text{ being the time step}$$

5.5.1 Vorticity and moisture prognoses

Spectral prognoses of the vorticity **(5.10)** and moisture **(3.20)** equations are obtained by the application of a direct leapfrog method.

The spectral vorticity equation **(5.10)** in terms of the stream function is:

$$\frac{\partial(\hat{\xi}_n^m)}{\partial t} = \frac{\partial(\nabla^2\hat{\psi}_n^m)}{\partial t} = -n(n+1)\frac{\partial(\hat{\psi}_n^m)}{\partial t} = IP_n^m \qquad \textbf{(5.15)}$$

Here IP_n^m represents the RHS of equation **(5.10)**

The stream function equation is integrated over time by means of a direct leapfrog method.

5.5.2 Divergence, thermodynamic and surface pressure prognoses

Spectral prognoses of the divergence **(5.11)**, thermodynamic **(5.12)** and surface pressure **(5.13)** equations are integrated over time by the "semi-implicit" leapfrog method. In order to achieve longer time steps, these equations are coupled linearly by means of the gravity wave generating terms.

The spectral *divergence* equation **(5.11)** in terms of the velocity potential may be expressed as:

$$\frac{\partial(\hat{D}_n^m)}{\partial t} = \frac{\partial(\nabla^2\hat{\chi}_n^m)}{\partial t} = -n(n+1)\frac{\partial(\hat{\chi}_n^m)}{\partial t} = IX_n^m + \frac{n(n+1)}{r^2}\left\{RT_O P_{Sn}^m + \hat{\phi}_n^m\right\} - K_D(\hat{D}_n^m) \qquad \textbf{(5.16)}$$

where IX_n^m represents the spectral terms excluding the linear components of the gravity wave generated terms. These linear terms are contained in the second term on the RHS.

The term $K_D(\hat{D}_n^m)$ is included and represents any linear term arising from the vertical diffusion/mixing parameterization which may have to be evaluated *backward* in time for stability. The present CSIRO-9 Mark II AGCM evaluate such terms *backward* in time, which does not require the inclusion of the linearised part in the semi-implicit algorithm.

The spectral *thermodynamic* equation **(5.12)** is:

$$\frac{\partial\hat{T}_n^m}{\partial t} = IT_n^m - Fn(\hat{D}_n^m) - K_T(\hat{T}_n^m) \qquad \textbf{(5.17)}$$

where IT_n^m represents the spectral terms, excluding the linear components of the gravity wave generating terms, which are contained in the second term on the RHS.

$Fn(\hat{D}_n^m) = \frac{KT_O}{\eta}\left[\hat{D}_n^m\right]^{\eta} = \frac{KT_O}{\eta}\int_0^{\eta}(\hat{D}_n^m)d\eta = \frac{KT_O}{\eta}\sum_{j=0}^{\eta}(\hat{D}_n^m)_j\Delta\eta_j$ and $K_T(\hat{T}_n^m)$ is analogous to the $K_D(\hat{D}_n^m)$ term in equation **(5.16)**.

The spectral *surface pressure* equation **(5.12)** becomes:

$$\frac{\partial P_{Sn}^m}{\partial t} = -\left[\hat{D}_n^m\right]^1 = -\int_0^1(\hat{D}_n^m)d\eta = -\sum_{j=0}^{1}(\hat{D}_n^m)_j\Delta\eta_j \qquad \textbf{(5.18)}$$

Equations **(5.16)**, **(5.17)** and **(5.18)** are linked linearly, and may be converted to the following vector/matrix form:

$$\frac{\partial \underline{\hat{D}_n^m}}{\partial t} = \underline{IX_n^m} + \frac{n(n+1)}{r^2}\left\{R\underline{T_O}P_{Sn}^m + \underline{\underline{A}}\cdot\underline{\hat{T}_n^m}\right\} - \underline{\underline{K_D}}\cdot\underline{\hat{D}_n^m} \qquad \textbf{(5.19)}$$

$$\frac{\partial \underline{\hat{T}_n^m}}{\partial t} = \underline{IT_n^m} - \underline{\underline{G}}\cdot\underline{\hat{D}_n^m} - \underline{\underline{K_T}}\cdot\underline{\hat{T}_n^m} \qquad \textbf{(5.20)}$$

$$\frac{\partial P_{Sn}^m}{\partial t} = -\underline{\Delta\eta^T}\cdot\underline{\hat{D}_n^m} \qquad \textbf{(5.21)}$$

When applying the leapfrog method, the implicit algorithm becomes:

From equation **(5.21)**:

$$(P_{Sn}^m)^{t+1} = (P_{Sn}^m)^{t-1} - 2\Delta t\left\{\underline{\Delta\eta^T}\cdot(\underline{\hat{D}_n^m})^t\right\}$$

$$= (P_{Sn}^m)^{t-1} - 2\Delta t\left\{\underline{\Delta\eta^T}\cdot 0.5\left[(\underline{\hat{D}_n^m})^{t+1} + (\underline{\hat{D}_n^m})^{t-1}\right]\right\}$$

$$= (P_{Sn}^m)^{t-1} - \Delta t\,\underline{\Delta\eta^T}\cdot\left[(\underline{\hat{D}_n^m})^{t+1} + (\underline{\hat{D}_n^m})^{t-1}\right] \qquad \textbf{(5.22)}$$

From equation **(5.20)**:

$$(\underline{\hat{T}}_n^m)^{t+1} = (\underline{\hat{T}}_n^m)^{t-1} + 2\Delta t(\underline{IT}_n^m)^t - 2\Delta t\left\{\underline{\underline{G}} \cdot 0.5\left[(\underline{\hat{D}}_n^m)^{t+1} + (\underline{\hat{D}}_n^m)^{t-1}\right] - \underline{\underline{K_T}} \cdot (\underline{\hat{T}}_n^m)^{t+1}\right\}$$

$$(\underline{\underline{1}} + 2\Delta t\underline{\underline{K_T}}) \cdot (\underline{\hat{T}}_n^m)^{t+1} = (\underline{\hat{T}}_n^m)^{t-1} + 2\Delta t(\underline{IT}_n^m)^t - \Delta t\left\{\underline{\underline{G}} \cdot \left[(\underline{\hat{D}}_n^m)^{t+1} + (\underline{\hat{D}}_n^m)^{t-1}\right]\right\}$$

$$(\underline{\hat{T}}_n^m)^{t+1} = (\underline{\underline{1}} + 2\Delta t\underline{\underline{K_T}})^{-1} \cdot \left\{(\underline{\hat{T}}_n^m)^{t-1} + 2\Delta t(\underline{IT}_n^m)^t - \Delta t\underline{\underline{G}} \cdot \left[(\underline{\hat{D}}_n^m)^{t+1} + (\underline{\hat{D}}_n^m)^{t-1}\right]\right\} \qquad \textbf{(5.23)}$$

From equation **(5.19)**:

$$(\hat{D}_n^m)^{t+1} = (\hat{D}_n^m)^{t-1} + 2\Delta t(\underline{IX}_n^m)^t - 2\Delta t(\underline{\underline{K_D}}) \cdot (\underline{\hat{D}}_n^m)^{t+1}$$

$$+ 2\Delta t\frac{n(n+1)}{r^2}\left\{R\underline{T_O}0.5\left[(P_{Sn}^m)^{t+1} + (P_{Sn}^m)^{t-1}\right] + \underline{\underline{A}} \cdot 0.5\left[(\underline{\hat{T}}_n^m)^{t+1} + (\underline{\hat{T}}_n^m)^{t-1}\right]\right\}$$

$$= (\hat{D}_n^m)^{t-1} + 2\Delta t(\underline{IX}_n^m)^t - 2\Delta t(\underline{\underline{K_D}}) \cdot (\underline{\hat{D}}_n^m)^{t+1}$$

$$+ \Delta t\frac{n(n+1)}{r^2}\left\{R\underline{T_O}\left[(P_{Sn}^m)^{t+1} + (P_{Sn}^m)^{t-1}\right] + \underline{\underline{A}} \cdot \left[(\underline{\hat{T}}_n^m)^{t+1} + (\underline{\hat{T}}_n^m)^{t-1}\right]\right\}$$

Substitution of $(P_{Sn}^m)^{t+1}$ and $(\underline{\hat{T}}_n^m)^{t+1}$ from equations **(5.22)** and **(5.23)** yields

$$= (\hat{D}_n^m)^{t-1} + 2\Delta t(\underline{IX}_n^m)^t - 2\Delta t(\underline{\underline{K_D}}) \cdot (\underline{\hat{D}}_n^m)^{t+1}$$

$$+ \Delta t\frac{n(n+1)}{r^2}\left\{R\underline{T_O}2(P_{Sn}^m)^{t-1} - R\underline{T_O}\Delta t\underline{\Delta\eta^T} \cdot \left[(\underline{\hat{D}}_n^m)^{t+1} + (\underline{\hat{D}}_n^m)^{t-1}\right]\right\}$$

$$+ \Delta t\frac{n(n+1)}{r^2}\left\{\underline{\underline{A}} \cdot (\underline{\underline{1}} + 2\Delta t\underline{\underline{K_T}})^{-1} \cdot \left\{(\underline{\hat{T}}_n^m)^{t-1} + 2\Delta t(\underline{IT}_n^m)^t - \Delta t\underline{\underline{G}} \cdot \left[(\underline{\hat{D}}_n^m)^{t+1} + (\underline{\hat{D}}_n^m)^{t-1}\right]\right\} + \underline{\underline{A}} \cdot (\underline{\hat{T}}_n^m)^{t-1}\right\}$$

Rearrangement of terms leads to the expression

$$(\underline{\hat{D}}_n^m)^{t+1} + \Delta t \frac{n(n+1)}{r^2}\left\{R\underline{T}_O \Delta t \underline{\Delta\eta}^T \cdot (\underline{\hat{D}}_n^m)^{t+1} + \underline{\underline{A}} \cdot (\underline{\underline{1}} + 2\Delta t \underline{\underline{K}}_T)^{-1} \cdot \Delta t \underline{\underline{G}} \cdot (\underline{\hat{D}}_n^m)^{t+1}\right\} + 2\Delta t(\underline{\underline{K}}_D) \cdot (\underline{\hat{D}}_n^m)^{t+1}$$

$$= (\underline{\hat{D}}_n^m)^{t-1} + 2\Delta t(\underline{IX}_n^m)^t - \Delta t \frac{n(n+1)}{r^2}\left\{R\underline{T}_O \Delta t \underline{\Delta\eta}^T \cdot (\underline{\hat{D}}_n^m)^{t-1} + \underline{\underline{A}} \cdot (\underline{\underline{1}} + 2\Delta t \underline{\underline{K}}_T)^{-1} \cdot \Delta t \underline{\underline{G}} \cdot (\underline{\hat{D}}_n^m)^{t-1}\right\}$$

$$+ \Delta t \frac{n(n+1)}{r^2}\left\{2R\underline{T}_O (P_{Sn}^m)^{t-1} + \left[\underline{\underline{A}} \cdot (\underline{\underline{1}} + 2\Delta t \underline{\underline{K}}_T)^{-1} + \underline{\underline{A}}\right] \cdot (\underline{\hat{T}}_n^m)^{t-1} + \underline{\underline{A}} \cdot (\underline{\underline{1}} + 2\Delta t \underline{\underline{K}}_T)^{-1} 2\Delta t(\underline{IT}_n^m)^t\right\}$$

Let

$$\underline{\underline{AP}} = \underline{\underline{A}} \cdot (\underline{\underline{1}} + 2\Delta t \underline{\underline{K}}_T)^{-1},$$

$$\underline{\underline{AG}} = \Delta t \Delta t / r^2 \underline{\underline{A}} \cdot (\underline{\underline{1}} + 2\Delta t \underline{\underline{K}}_T)^{-1} \cdot \underline{\underline{G}}$$

$$\underline{\underline{J}} \cdot (\underline{\hat{D}}_I^m) = \Delta t \Delta t / r^2 R\underline{T}_O \underline{\Delta\eta}^T \cdot (\underline{\hat{D}}_n^m)$$

Therefore

$$\left\{\underline{\underline{1}} + n(n+1)\left[\underline{\underline{J}} + \underline{\underline{AG}}\right] + 2\Delta t(\underline{\underline{K}}_D)\right\} \cdot (\underline{\hat{D}}_n^m)^{t+1}$$

$$= \left\{\underline{\underline{1}} - n(n+1)\left[\underline{\underline{J}} + \underline{\underline{AG}}\right] \cdot (\underline{\hat{D}}_n^m)^{t-1}\right\} + 2\Delta t(\underline{IX}_n^m)^t + \frac{\Delta t}{r^2} n(n+1)\left\{2R\underline{T}_O (P_{Sn}^m)^{t-1} + (\underline{\underline{AP}}_n^m + \underline{\underline{A}}) \cdot (\underline{\hat{T}}_n^m)^{t-1} + 2\Delta t \underline{\underline{AP}}(\underline{IT}\right.$$

(5.24)

Al the quantities on the RHS of equation **(5.24)** are computed as a vector. The matrix vector equation may then be solved for $(\underline{\hat{D}}_n^m)^{t+1}$.

$(\underline{\hat{D}}_n^m)^{t+1}$ is then used in equation **(5.22)** and **(5.23)** to solve $(P_{Sn}^m)^{t+1}$ and $(\underline{\hat{T}}_n^m)^{t+1}$ respectively.

Finally, because of the leapfrog method, a weak time filter is applied to the main prognostic fields.

CHAPTER 6

VALIDATION OF THE MODEL SIMULATED CLIMATE OUTPUT

6.1 INTRODUCTION

Recent improvements in numerical techniques and computer technology substantially contributed to the challenges facing climate modellers in their effort to reproduce observed climatic patterns. Numerical climate simulations are accomplished by expressing the atmospheric system in terms of the laws of physics, including the laws of Newton. As a result of parameterisation and numerical assumptions, climate models still produce approximated results. It is therefore necessary to be cautious, and in particular to be aware of limitations arising from the chaotic (non-linear) nature of atmospheric propagation. It is, however, encouraging to note that the major observed climate patterns are adequately captured by modern climate AGCMs.

Since the development of the first models, AGCMs have been evaluated by means of comparisons with the best available observed climate fields.

In this chapter some of the major climate patterns produced by both the σ- and η-systems in the CSIRO-9 Mark II AGCM are compared with observed data. Vertical cross sections of the *zonal- and meridional wind speed* and *temperature* at the nine model levels (constant pressure levels in table 3) are expressed in terms of zonal means (figures 6(a),(b) to 13(a),(b) and figures 22(a),(b) to 24(a),(b)). Horizontal fields of these variables in the upper atmosphere (192.7 hPa or model level 7), as well as the *mean sea-level pressure* are also validated against observed climate fields (figures 14(a),(b), 15(a),(b), 18(a),(b) and 19(a),(b); 26(a),(b), 27(a),(b), 29(a),(b) and 30(a),(b); 36(a),(b), 37(a),(b), 39(a),(b) and 40(a),(b)). Comparisons for the *zonal* means of the *mean sea-level pressure* (figures 32 to 35) are also discussed.

In addition to the above comparisons, differences between the absolute magnitude of σ- and η-system deviations from the observed *zonal-* and *meridional winds*, *temperatures* and *sea-level pressures* have been calculated as follows:

$$\left| \left| (\sigma\text{-system simulations} - \text{observed}) \right| - \left| (\eta\text{-system simulations} - \text{observed}) \right| \right|$$

Graphical representations of these differences around the globe are depicted in figures 16, 17, 20, 21, 28, 31, 38 and 41. Positive results (shaded areas in the figures mentioned in the previous sentence) indicate regions where η-system simulations (relative to σ-system simulations) provided better approximations to the observed climatological fields.

Noticeable differences between σ- and η-system simulations are anticipated in the upper atmosphere over the Himalayas, the Andes mountains, the Rocky mountains, Mount Kilimanjaro, Greenland and Antarctica.

6.2 DATA (MODEL CLIMATE)

Model simulated climatologies have been compiled by performing two separate five-year control runs - firstly with a σ vertical co-ordinate model, and secondly with a model using a η vertical co-ordinate. Although both five-year control runs were started with identical initial fields, different initial fields were used to start the second, third, fourth and fifth years. This was accomplished by performing two continuous five-year seasonal cycle runs. Model simulated climate fields are normally provided in terms of monthly averages. Climate variables for the CSIRO-9 Mark II AGCM are available in 64 (east-west) by 56 (south-north) horizontal grid fields. Some variables are also available on nine pressure-levels (table 3).

Vertical output levels of the CSIRO-9 AGCM	Equivalent pressures
1	982.9 hPa
2	919.8 hPa
3	807.3 hPa
4	661.9 hPa
5	500.0 hPa
6	338.1 hPa
7	192.7 hPa
8	80.2 hPa
9	17.1 hPa

Table 3. Equivalent pressures for the 9 vertical model levels on which the model output are available. Model output from both the σ- and η-levels are interpolated to these pressure levels. Pressure levels are 1000 x (σ or η) level of model.

Model simulated climatologies for the *zonal- and meridional wind speed*, *temperature*, and *sea-level pressure* were obtained by calculating ensemble means using five ensemble members. Seasonal climatologies were calculated by using time averages over December, January, February (DJF) and June, July, August (JJA).

6.3 DATA (OBSERVED CLIMATE)

Global analyses of meteorological parameters available from the European Centre for Medium-Range Weather Forecasting (ECMWF) (Hoskins *et al*. 1989; ECMWF 1994) are generally accepted to be one of the best data sets available for validating present climate model simulations. In many aspects the ECMWF analysis provide a better climate than those compiled from observed data. ECMWF analyses have been archived at the CSIRO as 12 hourly analysis fields as well as monthly climatological fields (Watterson 1995). In this study climatologies for the seasons DJF and JJA were obtained from ECMWF analyses over the period 1985 to 1992. Non-weighted averages of the months DJF and JJA were used. ECMWF *zonal- and meridional wind* and *temperature* grid fields were linearly interpolated to fit the grid fields of the CSIRO-9 AGCM.

The Tropical Ocean and Global Atmosphere (TOGA) international program compiled a detailed data set of the ocean-atmosphere system valid for the period 1985 to 1994. An important output from this program was the compilation of a blended ECMWF/TOGA observed data set. The ECMWF/TOGA *sea level-pressure* fields were also interpolated to model grid and used for model evaluation.

6.4 ZONAL MEAN OF THE WIND SPEED

DJF *(Southern Hemisphere summer / Northern Hemisphere winter)*

The *zonal mean of the wind speed* for DJF as simulated by the CSIRO-9 for both the η- and σ-systems, as well as comparisons with the corresponding ECMWF analyses, are depicted in figures 6(a), 6(b), 7(a) and 7(b).

Sigma (σ) co-ordinates

The sub-tropical (200 hPa) jet stream (figure 6(a)), which peaks at $+35ms^{-1}$, is situated in the winter hemisphere at $30^{o}N$. The jet stream over the summer hemisphere is somewhat weaker and peaks at about $+30ms^{-1}$. As indicated by negative differences in figure 6(b), the core of the winter westerly jet appears to be slightly weaker than observed. The rapid deceleration of this jet near the tropopause is not simulated well by the σ-system. Easterly winds at the 100hPa

level over the equator are much weaker than observed (-16ms^{-1}), while stronger than observed flow is simulated at the same level above 30°N and 60°S. Westerly flow over the equatorial mid-atmosphere (400 hPa) is generally stronger than observed (+6ms^{-1}). The zonal mean flow over almost the entire depth of the atmosphere over latitudes greater than 50°N, is weaker than observed. Deviations between observed and model simulated fields in the vicinity of the surface are relatively small.

Hybrid (η) co-ordinates

Although weaker than observed (figure 7(b)), both the summer and winter sub-tropical upper atmospheric jet streams are simulated (figure 7(a)) quite well. Underestimation of the zonal wind speed applies for the summer jet stream as well as lower level winds at the same latitude. Westerly flow below the winter jet is generally stronger than observed. The η-system simulates the equatorial stratospheric and upper tropospheric easterlies somewhat better than the σ-system, but still tends to overestimate them.

Co-ordinate comparisons

Differences between model simulated and observed mean zonal flow in the upper atmosphere (0 to 200 hPa) are noticeable smaller in η-system simulations. This is indicative of a significant improvement by the η-system simulations. These improvements (smaller anomalies) are more significant over the summer hemisphere. η-system simulations also significantly improve on σ-system simulations over the equatorial mid-atmosphere (400 hPa).

JJA *(Southern Hemisphere winter / Northern Hemisphere summer)*

The *zonal mean of the wind speed* for JJA as simulated by the CSIRO-9 for both the η- and σ-systems, as well as comparisons with the corresponding ECMWF analyses, are depicted in figures 8(a), 8(b), 9(a) and 9(b).

Sigma (σ) co-ordinates

The winter upper atmospheric jet (polar winter jet at the top of the model atmosphere at 60°S) is noticeable stronger (65ms^{-1}) than the summer jet stream (15ms^{-1}) at 45°N. Zonal winds above the 200 hPa level, at 30°S, are significantly stronger than observed (+12ms^{-1}). This area of stronger than observed westerly flow extends northwards almost to the equator. Weaker than observed westerly flow is simulated over the tropics at the 100 and 900 hPa levels. An area of stronger than observed westerly flow also occurs in the troposphere and stratosphere at 60°N. The model simulates weaker than observed westerly flow above 200 hPa over the South Pole, but stronger westerly flow at lower levels

(between 200 and 600 hPa). No large anomalies are evident in the lower troposphere.

Hybrid (η) co-ordinates

The polar winter jet is also considerably stronger than the summer jet stream. The most obvious differences between model simulated and observed zonal mean flow occur at the 100 hPa level at 30^{O}S, as well as over the tropical mid-atmosphere. Zonal winds are also much stronger than observed ($8ms^{-1}$) over Antarctica.

Co-ordinate comparisons

The hybrid simulation is generally closer to the ECMWF analyses in the upper atmosphere (above 200 hPa). This is especially true for the summer hemisphere. At levels below 300 hPa the η-system simulates a much stronger than observed zonal flow over Antarctic and the tropical mid-troposphere.

6.5 MERIDIONAL MEAN OF THE WIND SPEED

DJF *(Southern Hemisphere summer / Northern Hemisphere winter)*

The *meridional mean* of the *wind speed* for DJF as simulated by the CSIRO-9 for both the η- and σ-systems, as well as comparisons with the corresponding ECMWF analyses, are depicted in figures 10(a), 10(b), 11(a) and 11(b).

Sigma (σ) co-ordinates

Tropical meridional flow at the surface of the earth (Hadley circulation), which includes the general north-south surface trade winds north of the equator and south-north surface trade winds south of the equator, are well captured (figure 10(a). Flow in the winter hemisphere is stronger than in the summer hemisphere. Similar cells (Ferrel and Polar cells) at higher latitudes are also well represented. The most noticeable differences between observed and model simulated surface mean meridional flow (figure 10(b) occur over higher latitudes (polewards of 60^{O}S and 60^{O}N). Large positive and negative anomalies also appear above the equator between the 200 and 300 hPa levels. At these levels the south-north flow in the Northern Hemisphere is generally weaker ($-1.75ms^{-1}$) than observed, while the concurrent simulated north-south flow in the Southern Hemisphere is stronger than observed. Model simulated upper atmospheric meridional flow in the winter hemisphere is substantially stronger than in the summer hemisphere. Over the rest of the atmosphere, the model simulated meridional flow provides an acceptable representation of observed patterns.

Hybrid (η) co-ordinates

Figures 11(a) and (b) depicts large differences between observed and model simulated meridional flow occur over higher latitudes, especially over Antarctica. Slightly north of the equator at the 200 hPa level, the simulated south-north meridional flow is significantly weaker (-1.75ms^{-1}) than observed. The correspondent opposite flow over the Southern Hemisphere is slightly stronger (0.25ms^{-1}) than observed. Except for Antarctica, meridional flow over the rest of the atmosphere is generally well simulated.

Co-ordinate comparisons

At surface levels, no significant differences occur between η- and σ-system simulations. In the tropical upper atmosphere (200 hPa) of the Southern Hemisphere, the η-system simulates the north-south flow of the Hadley circulation very well. However, both vertical co-ordinates enhance the Hadley circulation of the winter hemisphere.

JJA *(Southern Hemisphere winter / Northern Hemisphere summer)*

The *meridional mean of the wind speed* for JJA as simulated by the CSIRO-9 for both the η- and σ-systems, as well as comparisons with the corresponding ECMWF analyses, are depicted in figures 12(a), 12(b), 13(a) and 13(b).

Sigma (σ) co-ordinates

The tropical north-south meridional surface flow over the Southern Hemisphere is not only stronger than the south-north flow north of the equator, but also extends over the equator into the summer hemisphere (figure 12(a)). This may well be a simulation of the strong monsoon systems over India and Asia during the northern summer. Observations show that the model simulated surface south-north flow north of the equator is marginally stronger than observed (figure 12(b)). Large differences between model simulated and observed meridional flow occur over Antarctica. The north-south meridional flow over the equatorial upper troposphere above 400 hPa peaks at 1.25 ms^{-1}. The flow is too strong in the region just above, and too weak in the region just below this peak. This indicates that the model simulated core in meridional flow may be at a higher level than observed. The associated equatorial upper tropospheric south-north flow in the Northern Hemisphere is noticeably weaker than observed (0.25m s^{-1}).

Hybrid (η) co-ordinates

The η-system simulated meridional flow patterns are almost identical to the associated σ-system simulations (figures 13(a) and (b)). The strong south-north surface equatorial southerly flow is well modelled over the winter hemisphere.

The equatorial flow in the mid-troposphere peaks at 1.5ms^{-1} at an altitude of approximately 400 hPa, with stronger than observed north-south flow above the peak and weaker than observed north-south flow below the peak. This again indicates that the model simulated core in the upper tropospheric north-south tropical Hardley circulation may be at a greater altitude than observed. The strength of this core is also underestimated.

Co-ordinate comparisons

The η-system simulation shows small (0.25ms^{-1}) improvements below the 200 hPa level above 30 ^{O}N (summer hemisphere). Most differences between the two co-ordinate systems are, however, fairly small.

6.6 GLOBAL WIND DISTRIBUTION AT 192.7 hPa

DJF *(Southern Hemisphere summer / Northern Hemisphere winter)*

Section 6.5 show some evidence that the η-system simulations give a better approximation of the zonal mean flow near the 200 hPa level (figures 6(a) and (b)). Figures 6(a) and (b) do not provide information concerning mean spatial flow patterns. The *global wind velocity* for DJF at the 192.7 hPa level, as simulated by the CSIRO-9 for both the η- and σ-systems, as well as comparisons with the corresponding ECMWF analyses, are depicted by figures 14(a), 14(b), 15(a) and 15(b). Differences between the absolute deviation (σ-system deviations minus η-system deviations) from the observed fields are given in figures 16 and 17.

Sigma (σ) co-ordinates

In figure 14(a) the jet stream cores over the Asian and North American continents as well as the circumpolar Southern Hemisphere jet are well captured. A distinctive band of strong mid-latitude westerly flow is also depicted around the globe between 30^{o} and 60^{o}S in the Southern Hemisphere. Wind velocities are weaker than observed over Australia, Argentina, the northern parts of the Sahara and the north Atlantic Ocean off the coast of the USA. Stronger than observed wind velocities occur over the ocean to the south of Australia, east equatorial Africa, south western Africa and the adjacent ocean as well as the Amazon basin (figure 14(b)). Much of Antarctica has large anomalies.

Hybrid (η) co-ordinates

The mid-latitude westerly flow over the Southern Hemisphere is well presented (figure 15(a)), although wind velocities are lower than observed over the north Sahara, the northern parts of the Atlantic Ocean and the USA. Stronger than

observed easterlies are simulated over the Amazon basin (figure 15(b)). Some regions over Antarctica show noticeable differences between model simulated and observed flow.

Co-ordinate comparisons

Comparisons between figures 14(b) and 15(b) indicate that the η-system substantially contributes to improved model simulated wind velocities, especially over the summer hemisphere (Southern Hemisphere). These improvements (relative to the σ-system) are well illustrated in figure 16 (zonal wind components) and figure 17 (meridional wind components). In these figures shaded areas denote the magnitude of improvements as a result of η-system simulations. Substantial improvements in the zonal and meridional winds occur over most parts of Africa, in particular zonal wind improvements over the eastern equatorial Africa (Mount Kilimanjaro) and meridional wind improvements over south western Africa and the northern Sahara. The zonal wind also improved significantly over Australia where the split in the jet stream is suggested. Noticeable improvements are also present above the Andes mountains. In the winter hemisphere (Northern Hemisphere), some major improvements in zonal wind components also occur over the northern Atlantic Ocean and Himalayas. Significant improvements are also evident over China in the η-system simulated meridional flow. Improvements by η-system simulations appear to favour the summer hemisphere. White areas in figures 16 and 17 represent regions where σ-simulations performed better than η-simulations. They are in the minority especially as far as the zonal flow is concerned.

JJA *(Southern Hemisphere winter / Northern Hemisphere summer)*

The *global wind velocity* for JJA as simulated by the CSIRO-9 for both the η- and σ-systems, as well as comparisons with the corresponding ECMWF analyses, are depicted in figures 18(a), 18(b), 19(a) and 19(b). Differences between the absolute deviation (σ-system deviations minus η-system deviations) from the observed fields are given in figures 20 and 21.

Sigma (σ) co-ordinates

The strong band of mid-latitude westerly flow, which extends over a broader meridional band than during the DJF season (figure 15(a)), is well established over the Southern Hemisphere (figure 18(a)). This also applies to the easterly flow over the northern Indian Ocean. The westerly flow over northern South America is considerably stronger than observed (figure 18(b)). The westerlies are anomalously weaker over China.

Hybrid (η) co-ordinates

The predominantly westerly flow over most of the Southern Hemisphere is well captured. Differences between model simulated and observed wind velocity fields are particularly strong over northern South America extending eastwards to Africa. The easterly flow over the Indian Ocean corresponds well with observed patterns, while the large anomalies over China, as simulated by the σ-system, have been reduced considerably.

Co-ordinate comparisons

Wind simulations over high orography (Himalayas, Rocky mountains) in the summer hemisphere improves significantly in η-system simulations. The most significant improvements occur at the latitude 30^{o}N (Himalayas, northern Africa and the ocean to the south west of the United States of America (USA) (figures 20 and 21). In figure 20 the η-system also did better over Southern Africa, eastwards over Madagascar. The η-system did not produce better results over the central equatorial Atlantic Ocean, Peru, Brasilia as well as the east equatorial Pacific Ocean (figures 19(b) and 20).

6.7 ZONAL MEAN OF THE TEMPERATURE

DJF *(Southern Hemisphere summer / Northern Hemisphere winter)*

The *zonal mean of the temperature* for DJF as simulated by the CSIRO-9 for both the η- and σ-systems, as well as comparisons with the corresponding ECMWF analyses, are depicted in figures 22(a), 22(b), 23(a) and 23(b).

Sigma (σ) co-ordinates

The horizontal pole-to-equator increase in surface air temperatures, with the thermal equator slightly south of the equator (summer hemisphere), is well simulated. Both co-ordinate simulations show the stronger surface mid-latitude temperature gradients in the winter hemisphere. The simulated tropopause is also well represented. A general increase in temperature occurs throughout the lower stratosphere (figure 22(a)). Apart from stratospheric temperatures and lower tropospheric temperatures near Antarctica, model simulated temperatures throughout the depth of the troposphere are predominantly colder than observed (figure 22(b)). This negative anomaly maximises in the region above Antarctica (200 hPa) where temperatures are significantly colder than observed (-12K). These colder model simulated temperatures are indicative of an anomalously stronger vertical temperature gradient. Temperatures over the winter hemisphere above the north pole (200 hPa) are warmer (+5K) than observed. These positive anomalies also extend through most of the lower stratosphere.

Hybrid (η) co-ordinates

Model simulated isothems are almost identical in the σ- and η-system simulations. The positive temperature anomalies above the northern polar region (winter hemisphere at 200 hPa) and negative temperature anomalies above the southern polar region (summer hemisphere at 200 hPa) are still present in the η-system simulations. Apart from temperatures around Antarctica, most model simulated temperatures throughout the troposphere are colder than observed.

Co-ordinate comparisons

Surface temperatures from the surface of the Earth up to the 400 hPa level are almost identical in both vertical co-ordinate model simulations. The η-system simulations lead to significant improvements over the equatorial and sub-tropical upper atmosphere. Upper atmospheric temperatures above Antarctica (summer hemisphere) are generally similar in both model simulations. The η-system simulated temperatures near the 200 hPa level over the north pole are, however, much warmer than the associated observed and σ-system simulated temperatures.

JJA *(Southern Hemisphere winter / Northern Hemisphere summer)*

The *zonal mean of the temperature* for JJA as simulated by the CSIRO-9 for both the η- and σ-systems, as well as comparisons with the corresponding ECMWF analyses, are depicted in figures 24(a), 24(b), 25(a) and 25(b).

Sigma (σ) co-ordinates

The pole-to-equator temperature gradient, with the thermal equator in the Northern Hemisphere (approximately at 20^{o}N), is well captured in the σ-system simulations. At the surface of the Earth, differences between the simulated and observed temperatures increase from the equator towards the poles. Model simulated temperatures throughout the depth of the troposphere are predominantly colder than observed. Large differences (in the order of 6K) between model simulated and observed temperatures occur at the 200 hPa level. This includes warmer than observed (+6K) conditions above the south pole and colder than observed (-7K) conditions over the north pole as well as colder than observed (-6K) temperatures above the 50^{O}S latitude. Most stratospheric regions have warmer than observed temperatures. Figure 24(b) is in many respects a mirror of figure 22(b), expect for the large negative anomalies near the upper winter jet.

Hybrid (η) co-ordinates

The hybrid simulation satisfactory simulates the general global temperature gradients. At the surface, differences between model simulated and observed temperatures are larger over the polar regions. Noticeable differences include warmer than observed (+4K) upper troposphere temperatures above Antarctica and colder than observed (-5K) upper troposphere temperatures over the North Pole. Similar to the σ-system simulation, η-system simulations also produced colder than observed (-6K) temperatures above the 50^{O}S latitude at the 200hPa level. Curiously this feature was not observed in the winter hemisphere of the DJF simulations. The fact that both co-ordinate simulations simulated this feature seems to exclude orographic effects.

Co-ordinate comparisons

Temperature simulations above the Arctic and Antarctic regions near 200 hPa significantly improved with the η-system simulations. In contrast, the σ-system performed better in the upper atmosphere over equatorial regions.

6.8 GLOBAL TEMPERATURE DISTRIBUTION AT 192.7 hPa

DJF *(Southern Hemisphere summer / Northern Hemisphere winter)*

The *global temperature* for DJF at the 192.7 hPa level as simulated by the CSIRO-9 for both the η- and σ-systems, as well as comparisons with the corresponding ECMWF analyses, are depicted in figures 26(a), 26(b), 27(a) and 27(b). Differences between the absolute deviation (σ-system deviations minus η-system deviations) from the observed fields are given in figure 28.

Sigma (σ) co-ordinates

Large regions of significant warmer than observed temperatures are simulated to the west of the continents over the sub-tropics in the summer hemisphere (figure 26(a)). These temperatures are in the order of 6K above-normal (figure 26(b)). Temperatures over east and equatorial Africa, Brasilia and the South Pole region are generally colder than observed (approximately -3K). In the Northern Hemisphere, warmer than observed temperatures are simulated over most of the polar regions as well as over Siberia, the eastern and southern parts of Asia, while colder conditions occur over Europe, north America, north Atlantic- and Pacific Oceans.

Hybrid (η) co-ordinates

Unlike the σ-system simulations, noticeably smaller temperature anomalies occur over the subtropical regions of the summer hemisphere (figures 27(a),(b)). Large negative temperature anomalies occur over Antarctica. Warmer than observed temperatures (as high as +9K) have been simulated over most high latitude regions in the Northern Hemisphere. The North Pole region is remarkably warmer than observed.

Co-ordinate comparisons

Comparisons between figures 26(b) and 27(b) indicate that η-system simulations substantially improved model simulated temperatures, especially over the summer hemisphere (Southern Hemisphere). The magnitude of these improvements (relative to the σ-system) is illustrated by figure 28, where shaded areas denote improvements as a result of the η-system simulations. Substantial improvements (up to +4K) occur over sub-tropical latitudes in the summer hemisphere. The η-system simulations effectively filtered the large differences between simulated and observed temperatures over the summer hemisphere. Smaller improvements also occur over approximately the same latitudes in the Northern Hemisphere, while σ-system simulations perform better over the winter pole.

JJA *(Southern Hemisphere winter / Northern Hemisphere summer)*

The *global temperature* for JJA at the 192.7 hPa level as simulated by the CSIRO-9 for both the η- and σ-systems, as well as comparisons with the corresponding ECMWF analyses, are depicted in figures 29(a), 29(b), 30(a) and 30(b). Differences between the absolute deviation (σ-system deviations minus η-system deviations) from the observed fields are given in figure 31.

Sigma (σ) co-ordinates

Predominantly warmer conditions over the summer hemisphere (Northern Hemisphere) are well simulated (figure 29(a)). Here, temperatures are warmer than observed (+6^{O}K) over Africa, southern Europe, Atlantic Ocean and the USA extending to all of the areas above the oceans north of 30^{o}S. Negative temperature anomalies occur over the North Pole region. Colder conditions are simulated for the winter hemisphere over most of the upper mid-latitudes.

Hybrid (η) co-ordinates

Over the summer hemisphere warmer than observed temperatures are confined to north Africa, a small region over the Atlantic Ocean, Europe and a band spreading across the USA (figures 30(a),(b)). Colder than observed model

simulated temperatures prevailed over the North Pole region. Small positive temperature anomalies occur over most parts of Africa, northern South America and the adjacent oceans. Temperatures over the mid-latitude regions of the Southern Hemisphere are in general below-normal (-7 K).

Co-ordinate comparisons

There are significant improvements in the η-system simulated temperatures. Over the summer hemisphere, η-system simulations result in significant temperature improvements (figure 31). The temperature not only decreases over the mid-latitudes of the Northern Hemisphere, but also increases over the North Pole regions. An improvement of 5K occurs near the Mediterranean.

6.9 ZONAL MEAN OF THE MEAN SEA-LEVEL PRESSURE

DJF *(Southern Hemisphere summer / Northern Hemisphere winter)*

The *zonal mean of the mean sea-level pressure* for DJF as simulated by the CSIRO-9 for both the η- and σ-systems, as well as comparisons with the corresponding TOGA/ ECMWF analyses, are depicted in figures 32 and 33. Over continental regions the mean sea-level pressure is obtained by extrapolating the surface pressure down to sea level.

Sigma (σ) co-ordinates

Over the tropical, subtropical and mid-latitude areas, the simulated zonal mean of the mean-sea level pressure is almost identical to the observed field (figure 32).

Hybrid (η) co-ordinates

Apart from the southward displacement of the intersection point between the observed and model graphs, the hybrid simulation is virtually similar to the σ-system simulation (figure 33).

Co-ordinate comparisons

Both co-ordinate systems provide relative realistic zonal sea-level pressure simulations over the equatorial, subtropical and mid-latitude regions. η-system simulations did not improve on σ-system simulation over polar latitudes.

JJA *(Southern Hemisphere winter / Northern Hemisphere summer)*

The *zonal mean of the mean sea-level pressure* for JJA as simulated by the CSIRO-9 for both the η- and σ-systems, as well as comparisons with the corresponding TOGA/ ECMWF analyses, are depicted in figures 34 and 35.

Sigma (σ) co-ordinates

Higher observed zonal mean sea-level pressures over the subtropics (30° N and S) as well as lower pressures over the tropics are well simulated (figure 34). From 30 °N to the North Pole (summer hemisphere), larger differences occur between model simulated and observed mean sea-level pressures. Larger differences also occur in the Southern Hemisphere over higher latitudes(> 60°S).

Hybrid (η) co-ordinates

Apart from minor differences over Antarctica, η-system simulations of the zonal mean of sea-level pressures are almost identical to the corresponding σ-system simulations (figure 35).

Co-ordinate comparisons

A small improvement appears in η-system simulations around 30°S. In general, η-system simulations did not improve on σ-system simulation over polar latitudes.

6.10 GLOBAL MEAN SEA-LEVEL PRESSURE

DJF *(Southern Hemisphere summer / Northern Hemisphere winter)*

The *global mean sea-level pressure* for DJF as simulated by the CSIRO-9 for both the η- and σ-systems, as well as comparisons with the corresponding TOGA/ ECMWF analyses, are depicted in figures 36(a), 36(b), 37(a) and 37(b). Differences between the absolute deviation (σ-system deviations minus η-system deviations) from the observed fields are given in figure 38.

Sigma (σ) co-ordinates

As expected, pressures over the summer hemisphere is noticeable lower than over the winter hemisphere. The high / low mid-latitude pressure cells over oceans / continents in the summer hemisphere are well modeled (figure 36a). The Southern Hemisphere mid-latitude westerlies are well defined. The strong winter Asian continental high as well as winter hemisphere oceanic lows are well defined. The most significant differences between observed and model

simulated pressures in the Southern Hemisphere occur over regions of high orography (Andes and Antarctic ice cap) where lower than observed pressures are simulated. The large gradients in the anomaly field near the Himalayas may be attributed to the process of surface pressure extrapolation. Pressures over the Atlantic- and western Pacific Ocean are significantly lower than observed.

Hybrid (η) co-ordinates

Over the Southern Hemisphere, η-system simulations compare reasonably well with σ-system simulations. The spatial location of the major pressure patterns over the Northern Hemisphere is also quite similar (figures 37(a),(b)). The Southern Hemisphere mid-latitude westerlies are well simulated.
Co-ordinate comparisons

η-system simulations do not show obvious improvements in the Southern Hemisphere (summer hemisphere). Even though the formulation of the two co-ordinate systems is identical at the surface of the earth, significant improvements in sea-level pressure in the η-system simulations, appear over the north Atlantic Ocean. Areas showing improvement in η-system are also shaded in figure 38 where improvements higher than 4hPa occur over the north Atlantic Ocean, north America and south Indian Ocean.

JJA *(Southern Hemisphere winter / Northern Hemisphere summer)*

The *global mean sea level pressure* for JJA as simulated by the CSIRO-9 for both the η- and σ-systems, as well as comparisons with the corresponding TOGA/ ECMWF analyses, are depicted in figures 39(a), 39(b), 40(a) and 40(b). Differences between the absolute deviation (σ-system deviations minus η-system deviations) from the observed fields are given in figure 41.

Sigma (σ) co-ordinates

Over the Southern Hemisphere, a region of high pressure extends from South America eastwards over southern Africa and Australia. This is typical of winter circulation over the winter Southern Hemisphere (figure 39(a)). A strong meridional pressure gradient is simulated over the mid-latitudes (30^{o} to 60^{o} S). The alternation of high pressures (oceans) and low pressures (continents) are well simulated along the subtropical latitudes in the Northern Hemisphere. Large anomalies occur over Antarctica, the Andes and Himalayas (figure 39(b)). Smaller, but still noticeable differences between model simulated and observed pressures occur over the Rocky mountains, Greenland, and the mountains of north eastern Africa.

Hybrid (η) co-ordinates

The η-system simulations compare reasonably well with σ-system simulations (figures 40(a),(b)).

Co-ordinate comparisons

Figure 41 indicate considerable improvements by η-system simulations over and near Antarctica. Improvements of 6hPa also appear over the Himalayas. The η-system also contributes to improved simulations over the sub-tropical Pacific Ocean (30°S and 50°N) as well as over the northern parts of Asia.

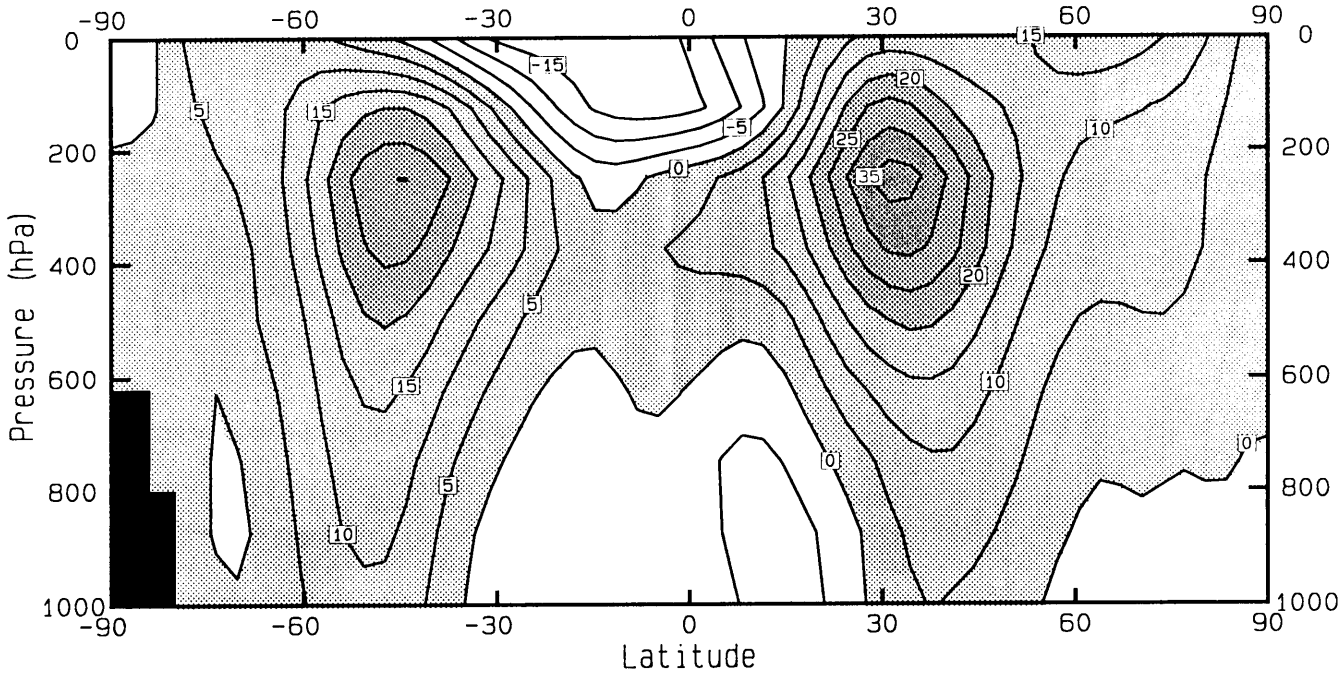

Figure 6(a): Zonal mean of the *zonal wind speed* (ms^{-1}) averaged over DJF as simulated by the CSIRO-9 AGCM using the **SIGMA** co-ordinate system.

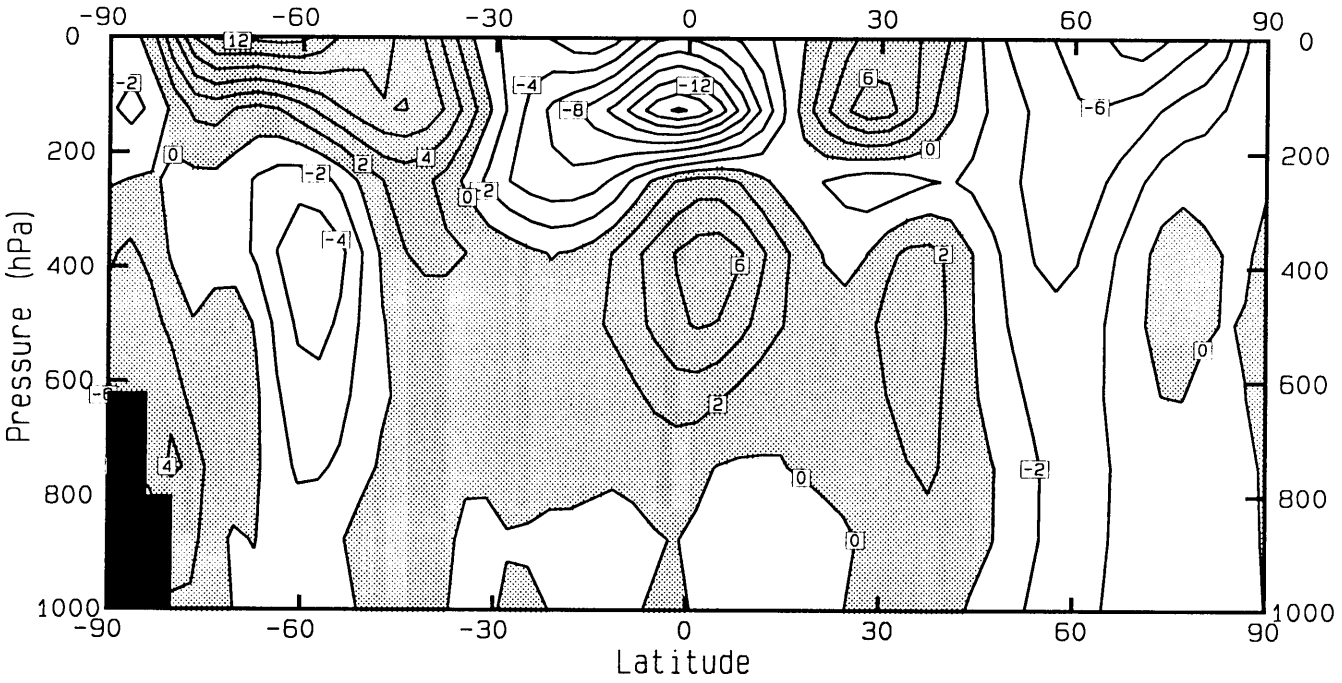

Figure 6(b): **SIGMA** simulations of figure 6(a) minus the corresponding **ECMWF** analysis.

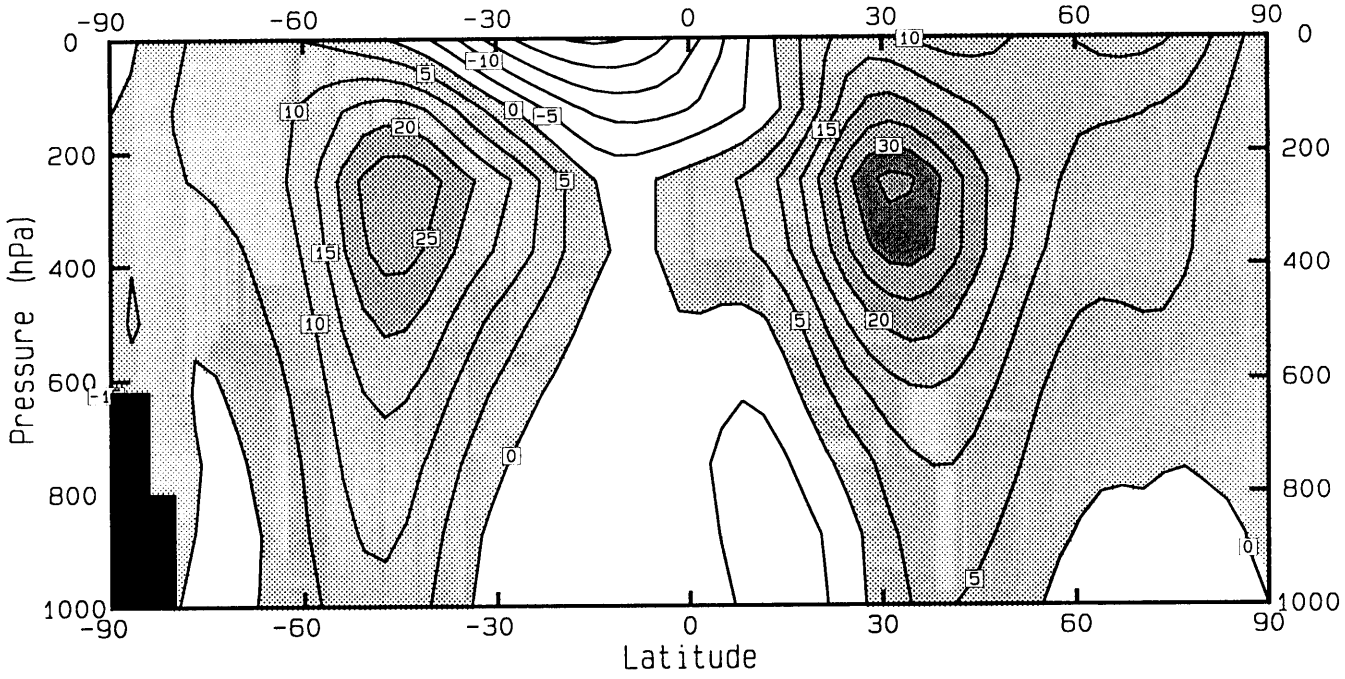

Figure 7(a): Zonal mean of the *zonal wind speed* (ms^{-1}) averaged over DJF as simulated by the CSIRO-9 AGCM using the **HYBRID** co-ordinate system.

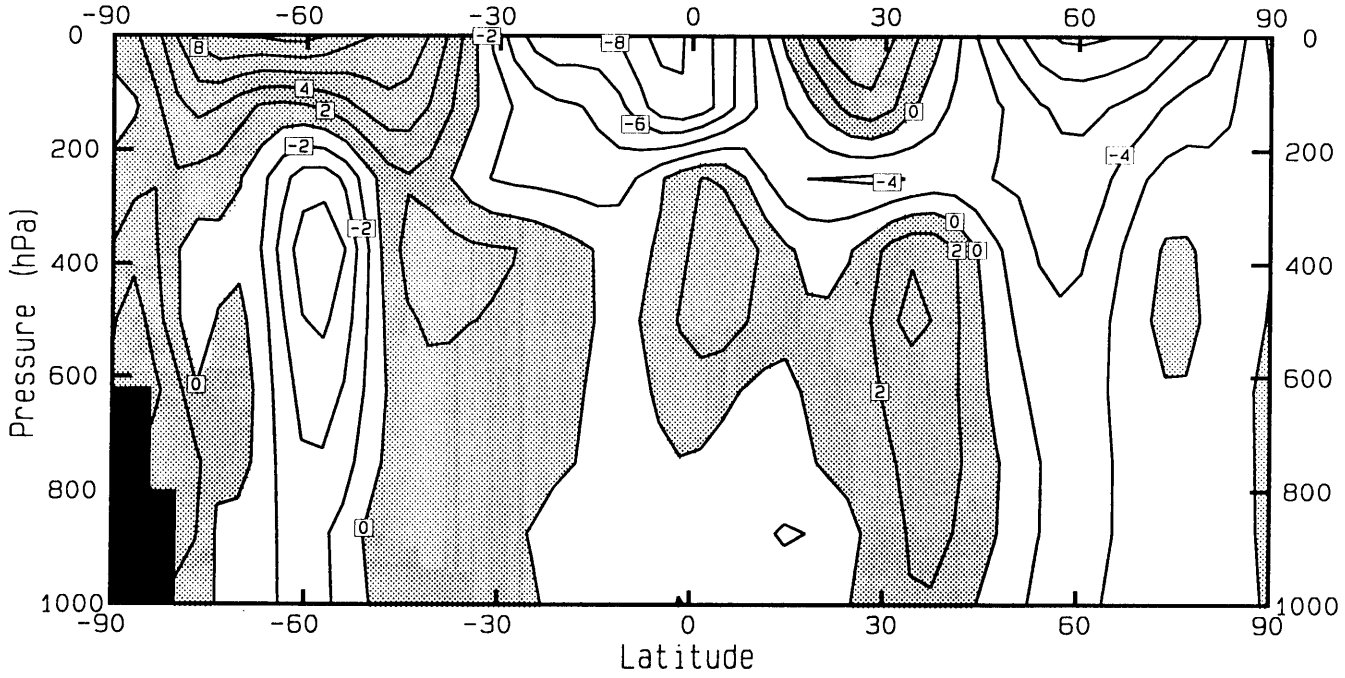

Figure 7(b): **HYBRID** simulations of figure 7(a) minus the corresponding **ECMWF** analysis.

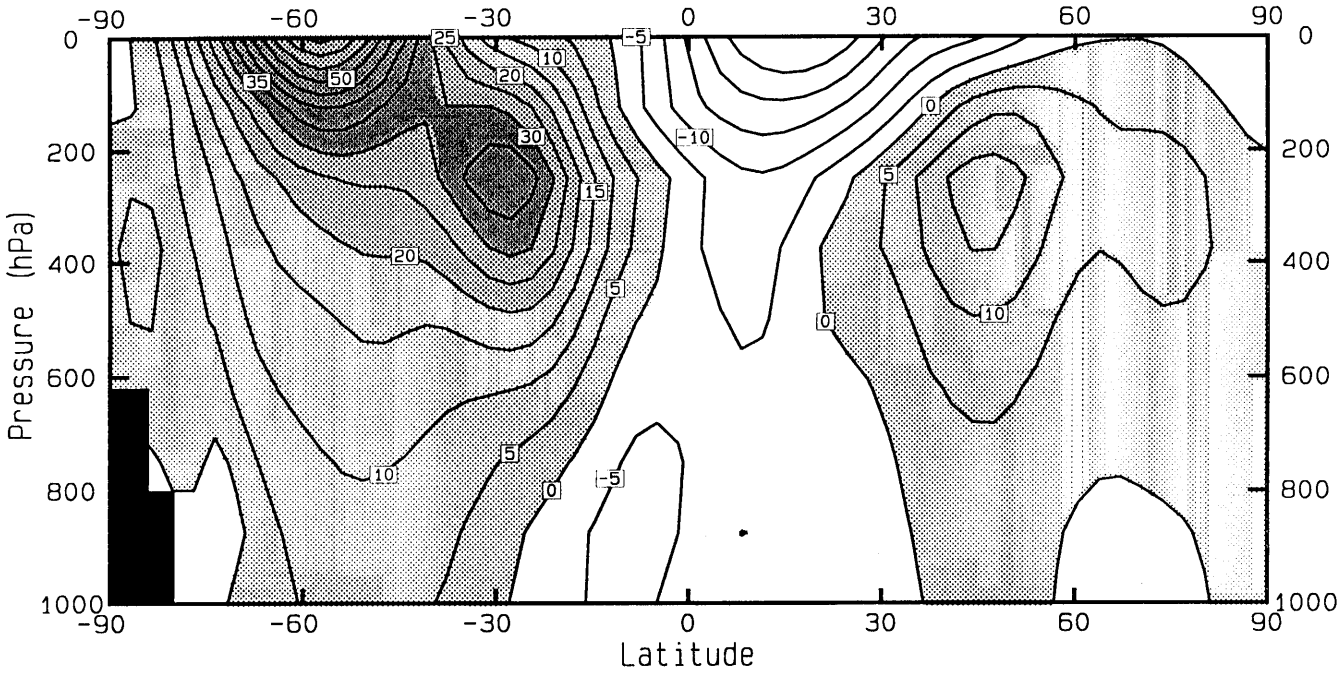

Figure 8(a): Zonal mean of the *zonal wind speed* (ms^{-1}) averaged over JJA as simulated by the CSIRO-9 AGCM using the **SIGMA** co-ordinate system.

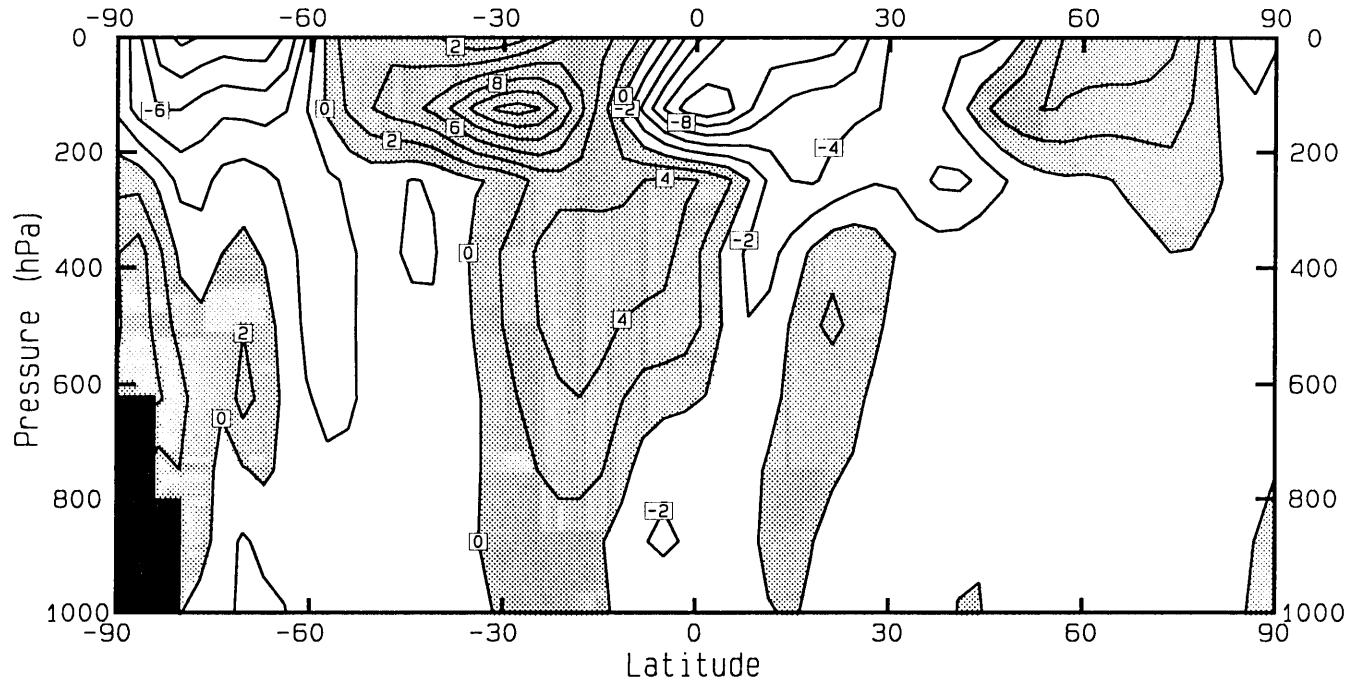

Figure 8(b): **SIGMA** simulations of figure 8(a) minus the corresponding **ECMWF** analysis.

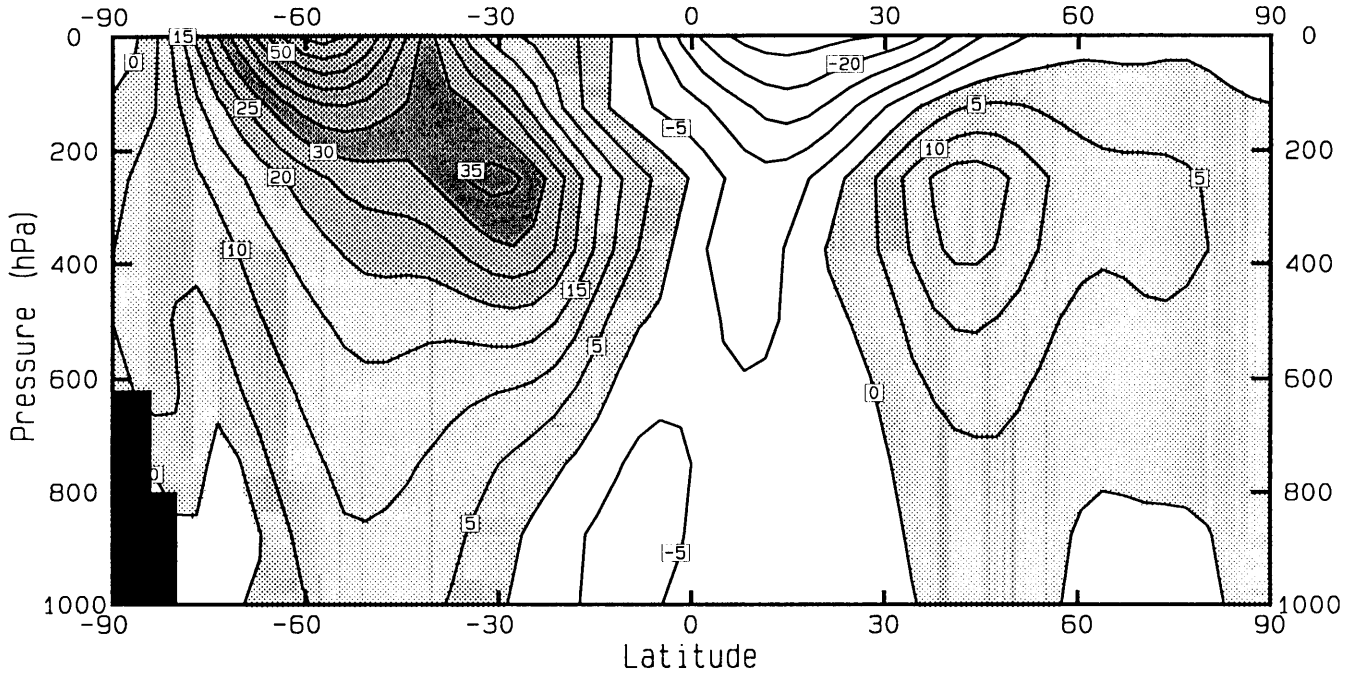

Figure 9(a): Zonal mean of the *zonal wind speed* (ms^{-1}) averaged over JJA as simulated by the CSIRO-9 AGCM using the **HYBRID** co-ordinate system.

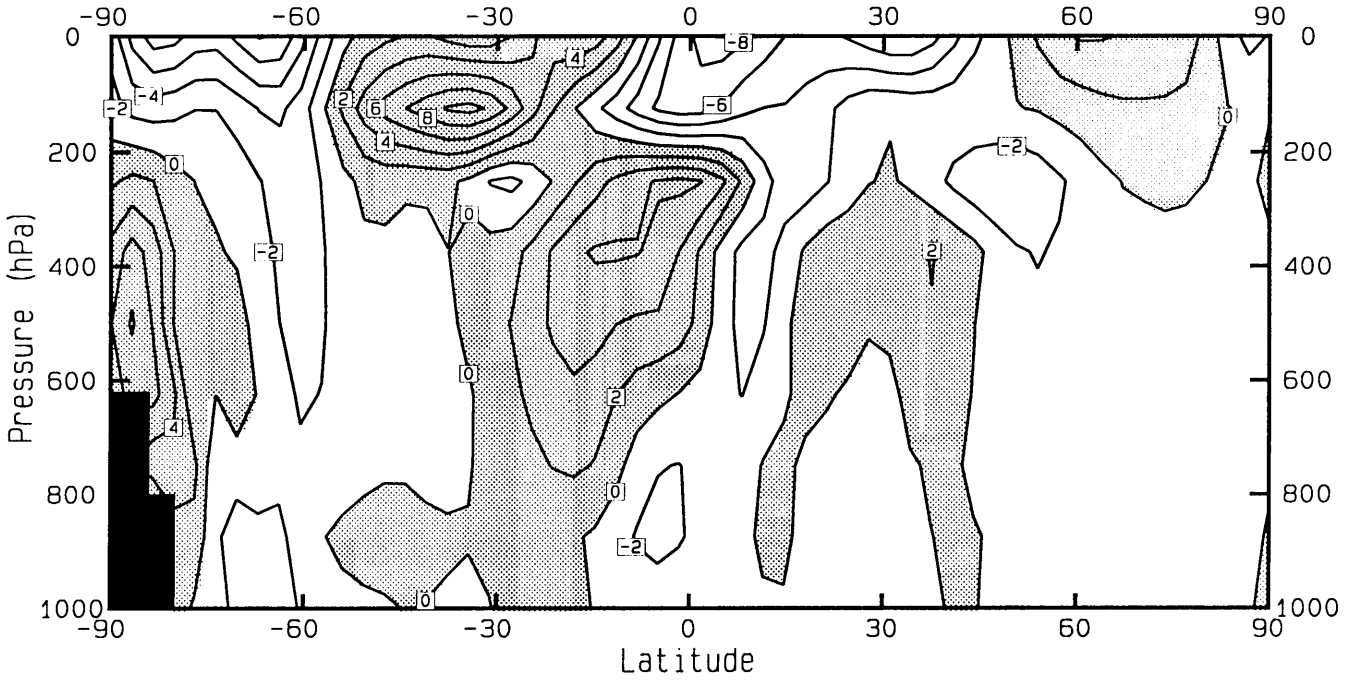

Figure 9(b): **HYBRID** simulations of figure 9(a) minus the corresponding **ECMWF** analysis.

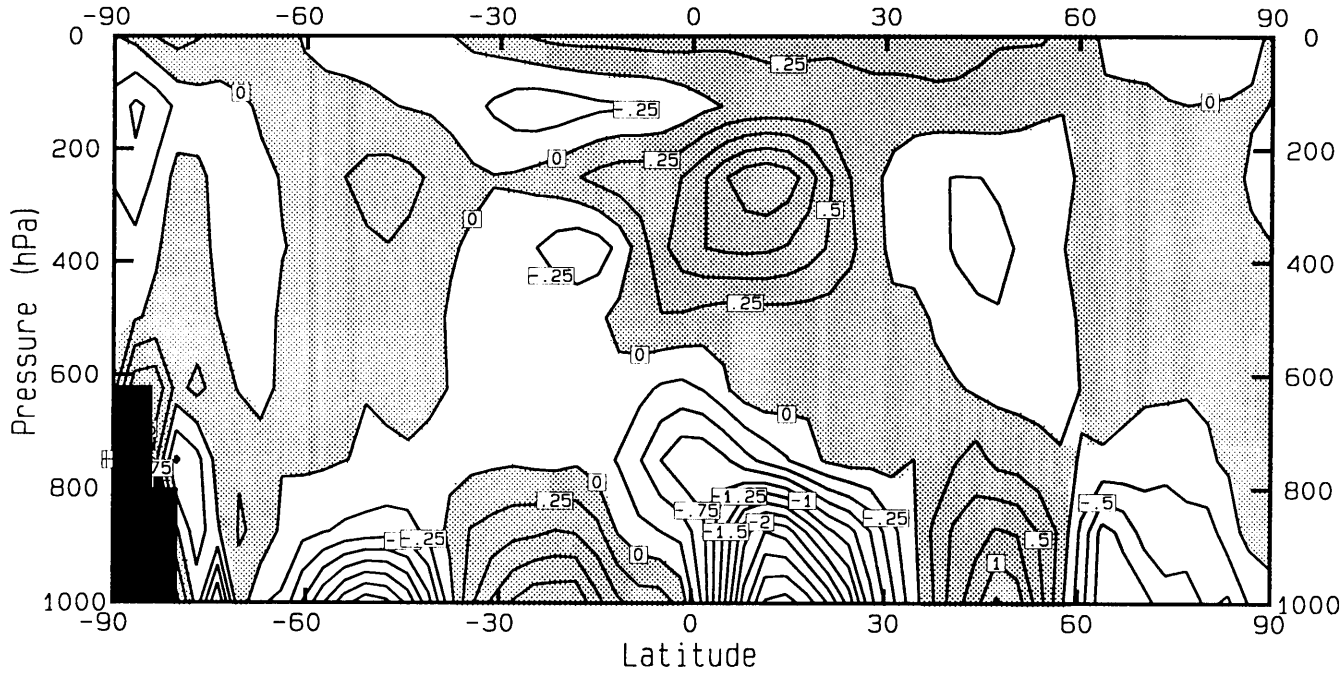

Figure 10(a): Zonal mean of the *meridional wind speed* (ms^{-1}) averaged over DJF as simulated by the CSIRO-9 AGCM using the **SIGMA** co-ordinate system.

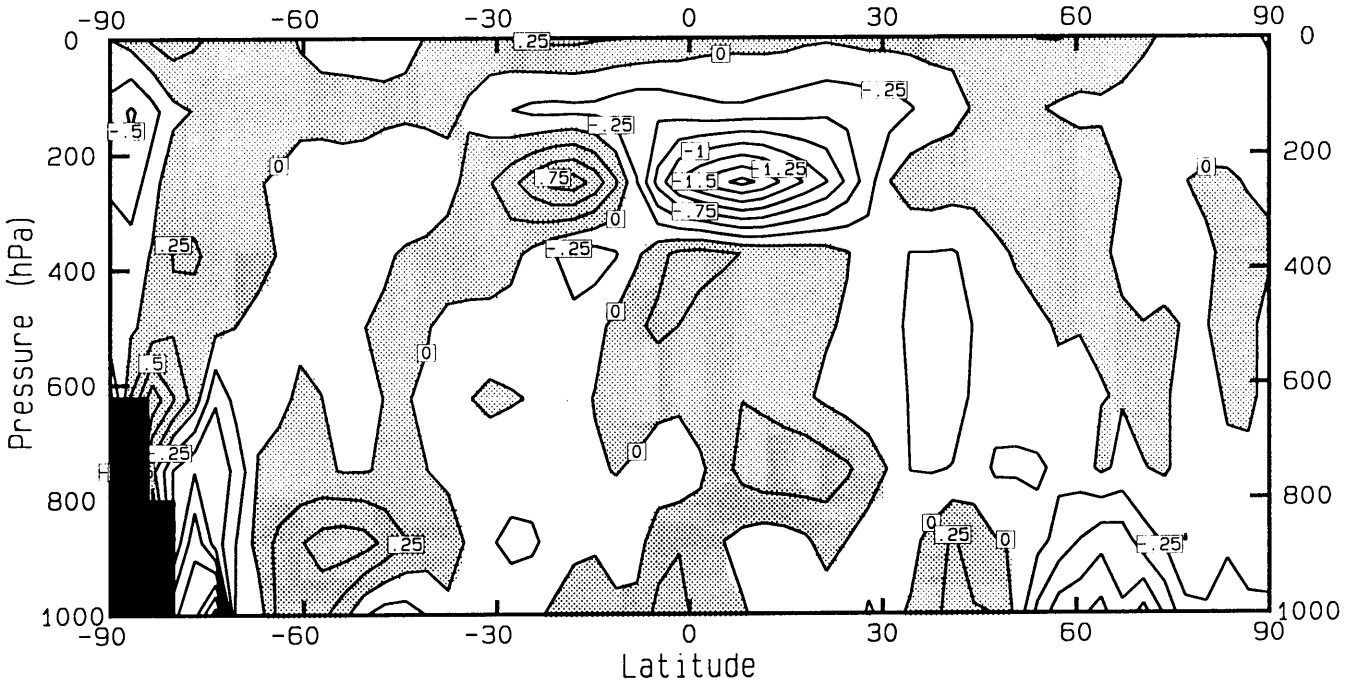

Figure 10(b): **SIGMA** simulations of figure 10(a) minus the corresponding **ECMWF** analysis.

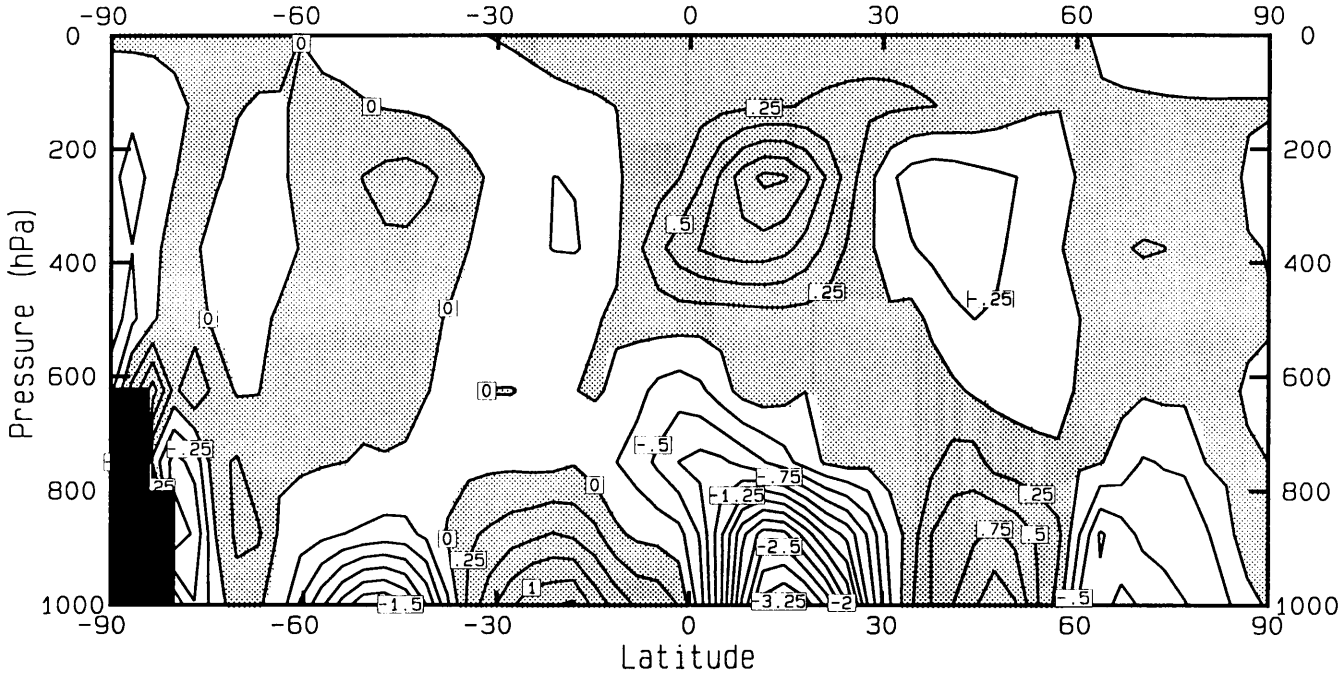

Figure 11(a): Zonal mean of the *meridional wind speed* (ms^{-1}) averaged over DJF as simulated by the CSIRO-9 AGCM using the **HYBRID** co-ordinate system.

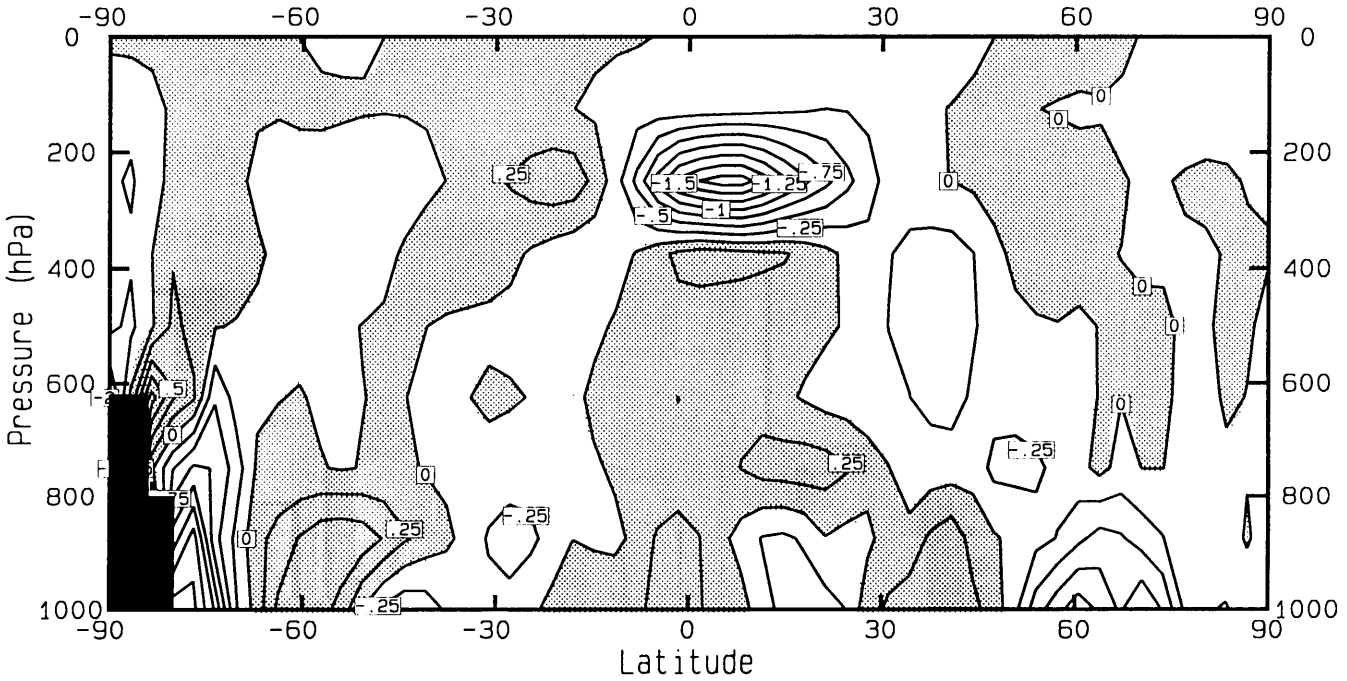

Figure 11(b): **HYBRID** simulations of figure 11(a) minus the corresponding **ECMWF** analysis.

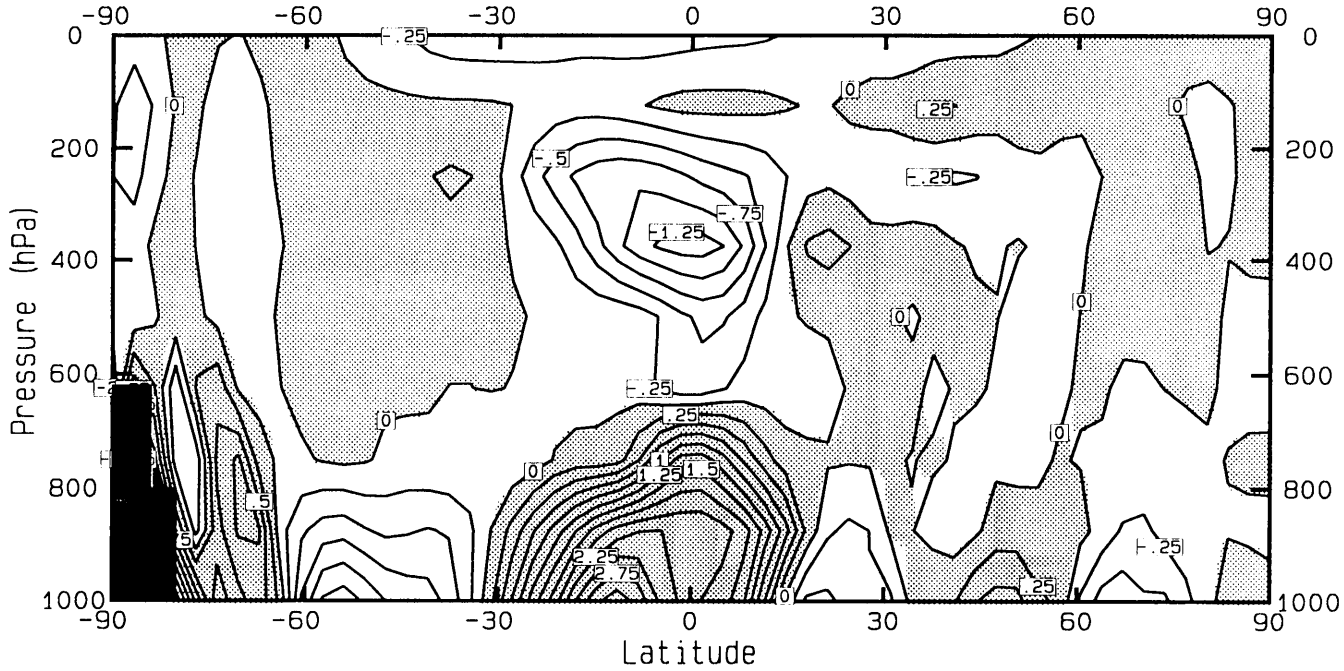

Figure 12(a): Zonal mean of the *meridional wind speed* (ms^{-1}) averaged over JJA as simulated by the CSIRO-9 AGCM using the **SIGMA** co-ordinate system.

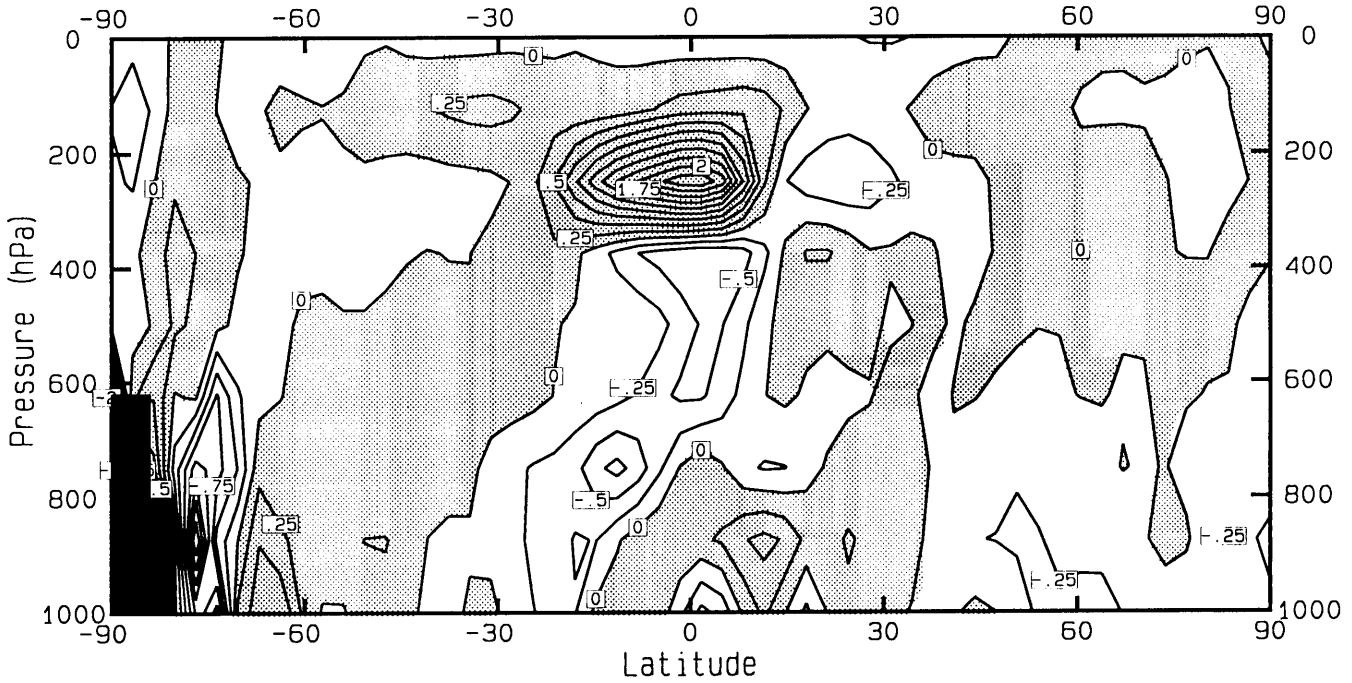

Figure 12(b): **SIGMA** simulations of figure 12(a) minus the corresponding **ECMWF** analysis.

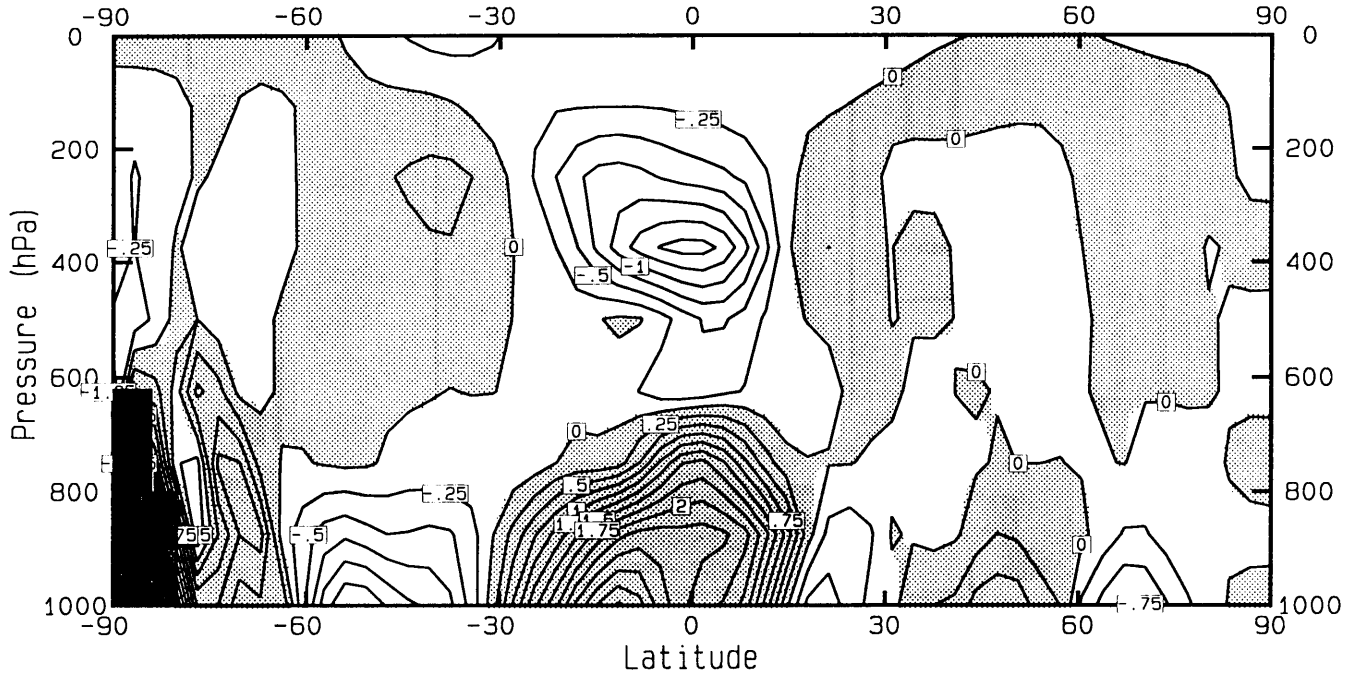

Figure 13(a): Zonal mean of the *meridional wind speed* (ms^{-1}) averaged over JJA as simulated by the CSIRO-9 AGCM using the **HYBRID** co-ordinate system.

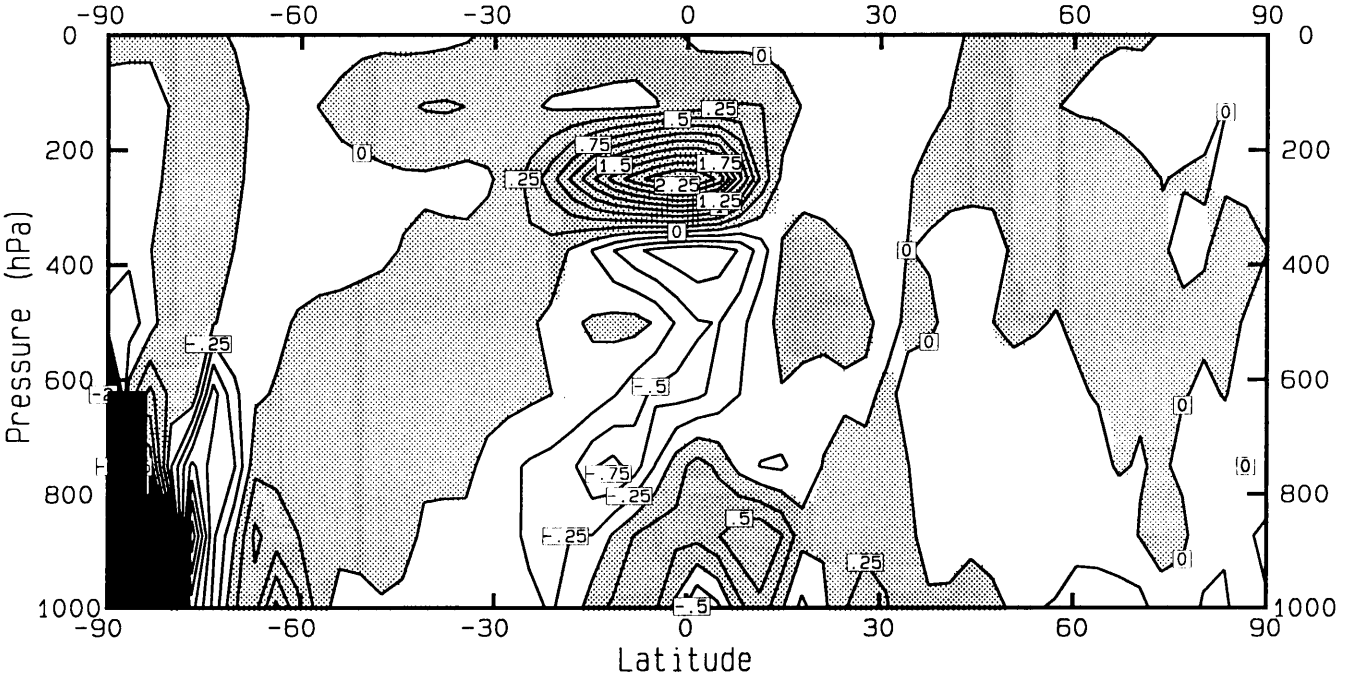

Figure 13(b): **HYBRID** simulations of figure 13(a) minus the corresponding **ECMWF** analysis.

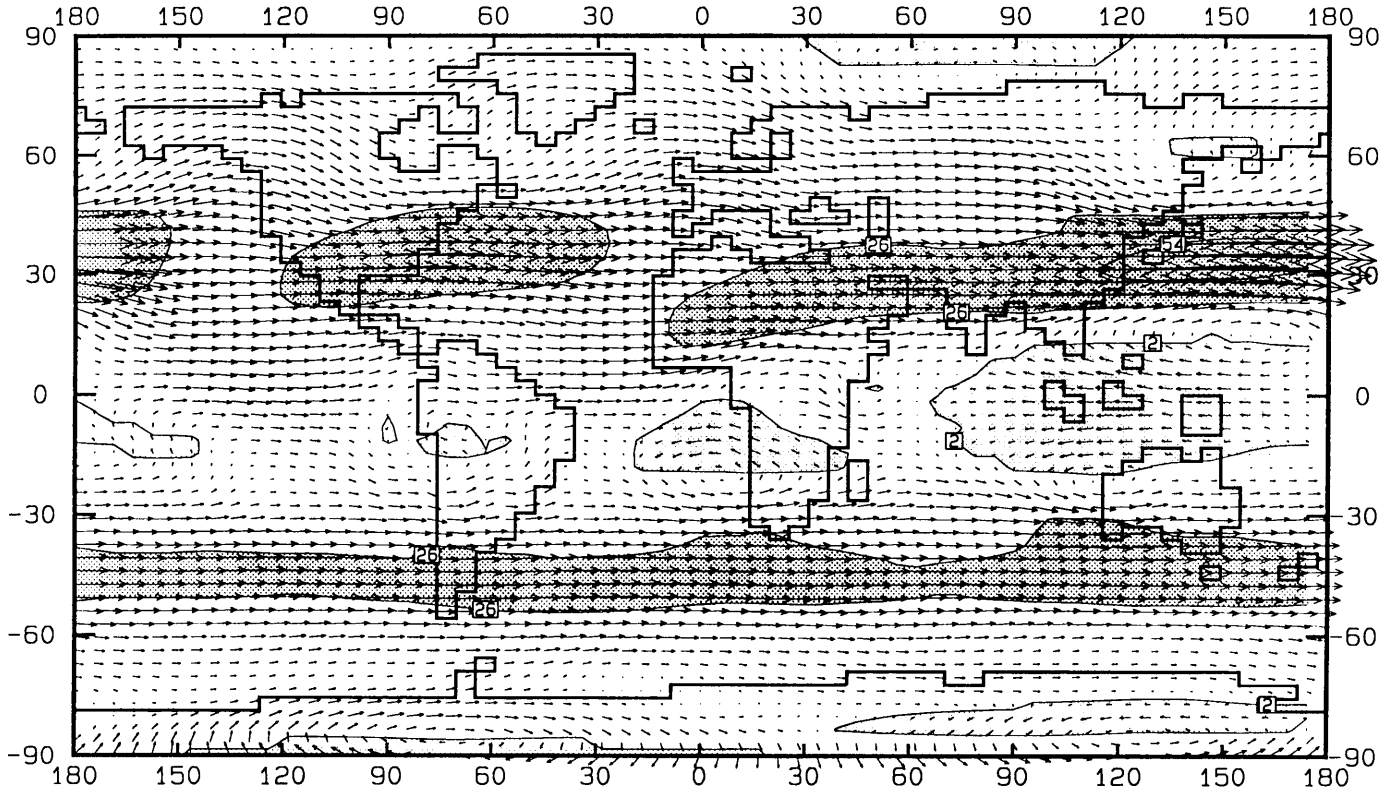

Figure 14(a): *Wind velocity* (ms^{-1}) averaged over DJF, as simulated by the CSIRO-9 AGCM using the **SIGMA** co-ordinate system, at the 192.7 hPa pressure level. Lighter and darker shaded areas represent wind velocities higher than 2 ms^{-1} (negative zonal components) and 26 ms^{-1} (positive zonal components) respectively.

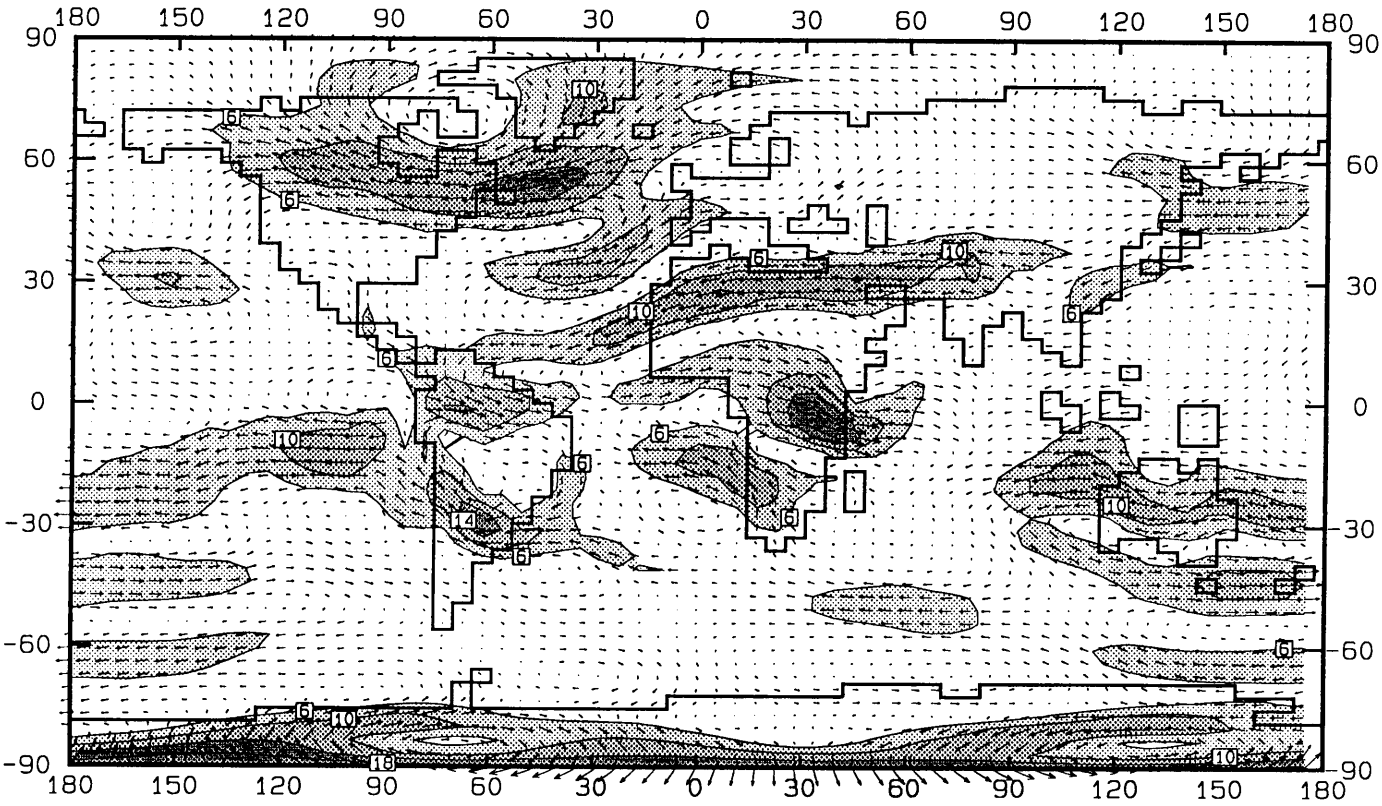

Figure 14(b): **SIGMA** simulations of figure 14(a) minus the corresponding **ECMWF** analysis. Anomalies larger than 6 ms^{-1} are shaded.

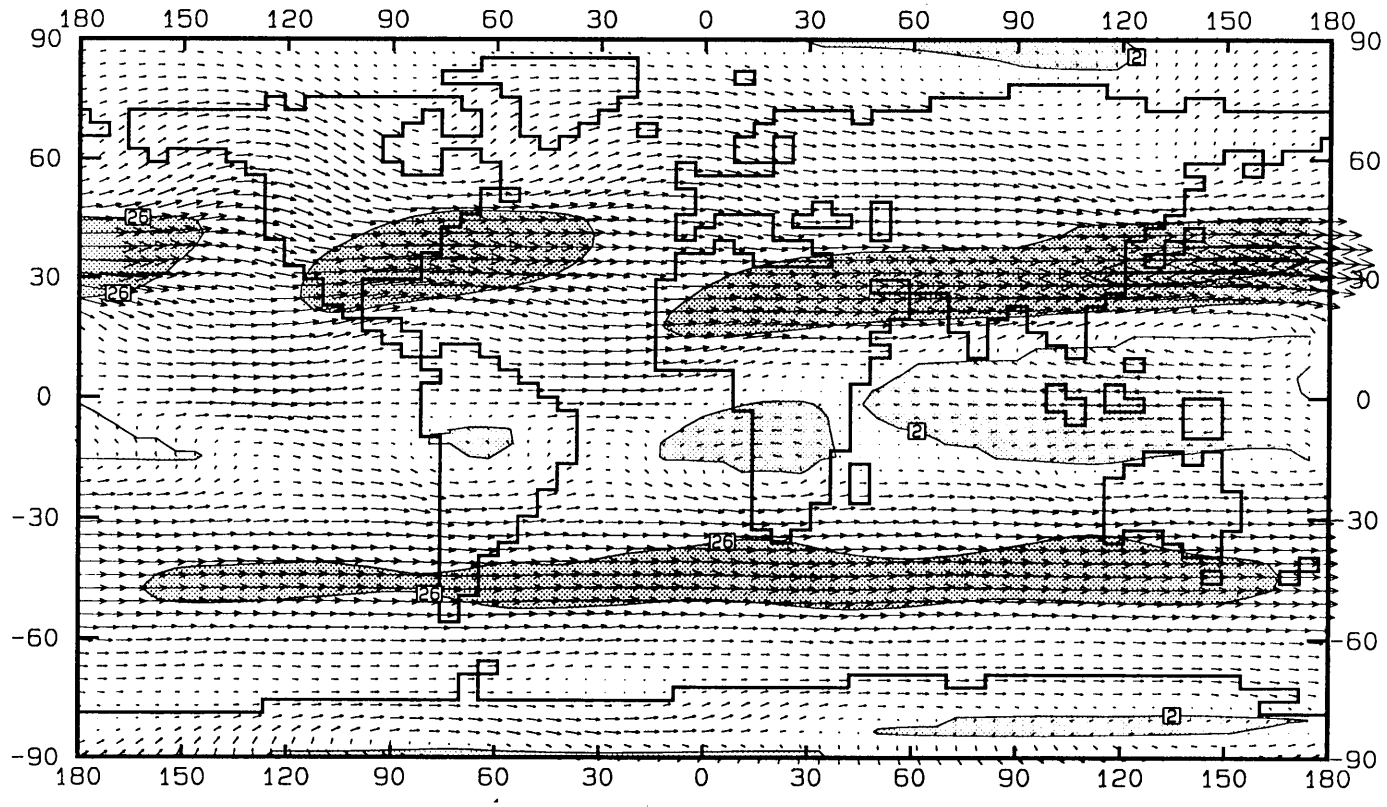

Figure 15(a): *Wind velocity* (ms^{-1}) averaged over DJF, as simulated by the CSIRO-9 AGCM using the **HYBRID** co-ordinate system, at the 192.7 hPa pressure level. Lighter and darker shaded areas represent wind velocities higher than 2 ms^{-1} (negative zonal components) and 26 ms^{-1} (positive zonal components) respectively.

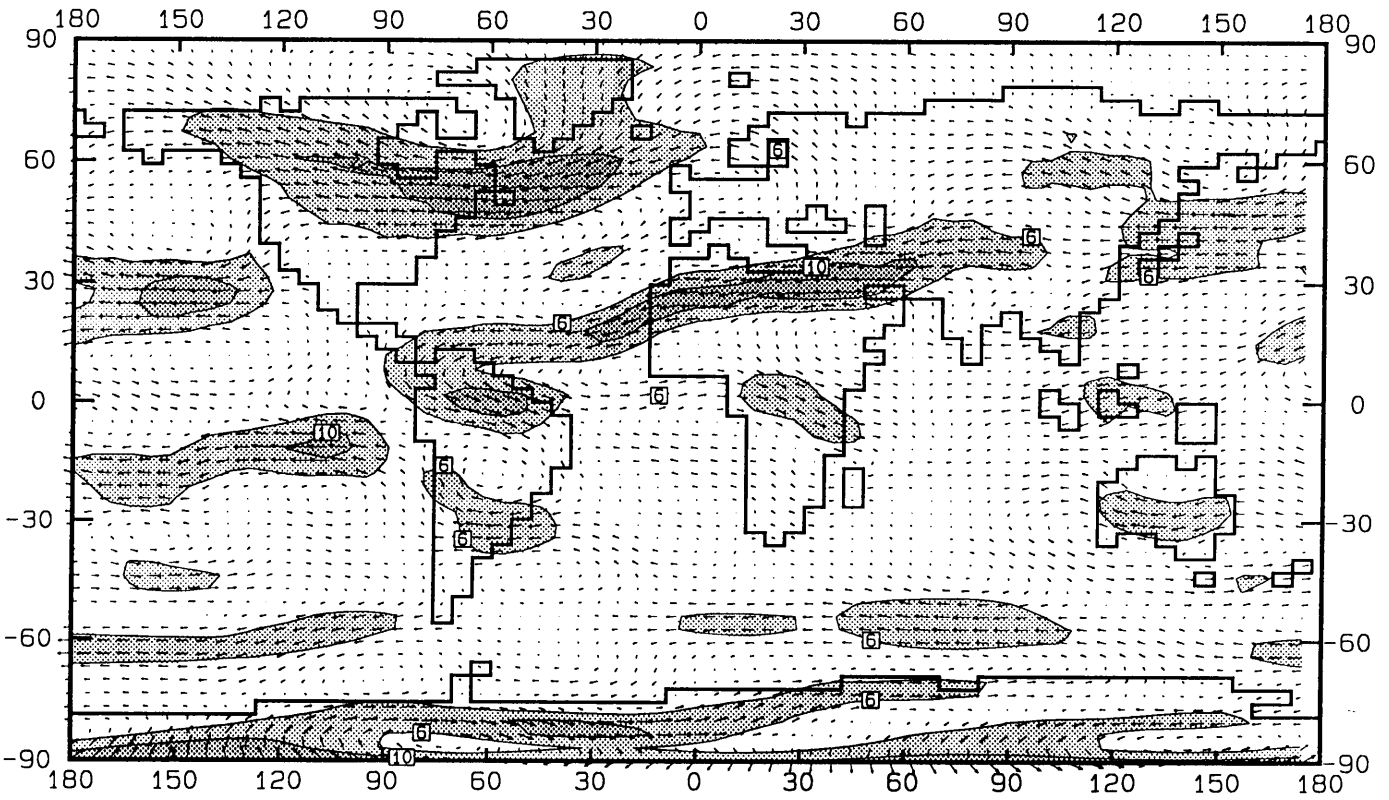

Figure 15(b): **HYBRID** simulations of figure 15(a) minus the corresponding **ECMWF** analysis. Anomalies larger than 6 ms^{-1} are shaded.

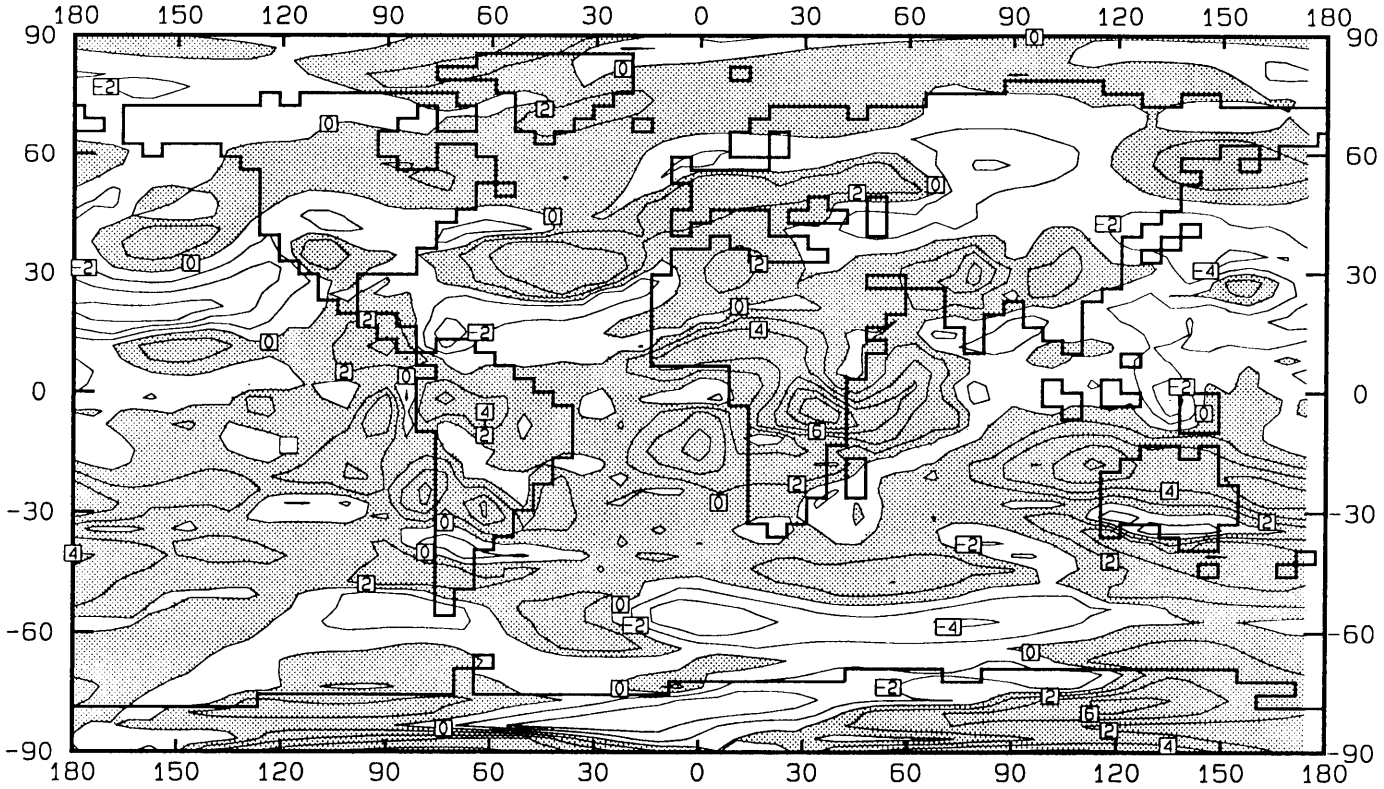

Figure 16: Differences between absolute deviations from the observed *zonal wind speed* (ms^{-1}) averaged over DJF at the 192.7 hPa pressure level (**SIGMA** co-ordinate system deviations minus **HYBRID** co-ordinate system deviations). Shaded areas denote improvements by **HYBRID** co-ordinate system simulations.

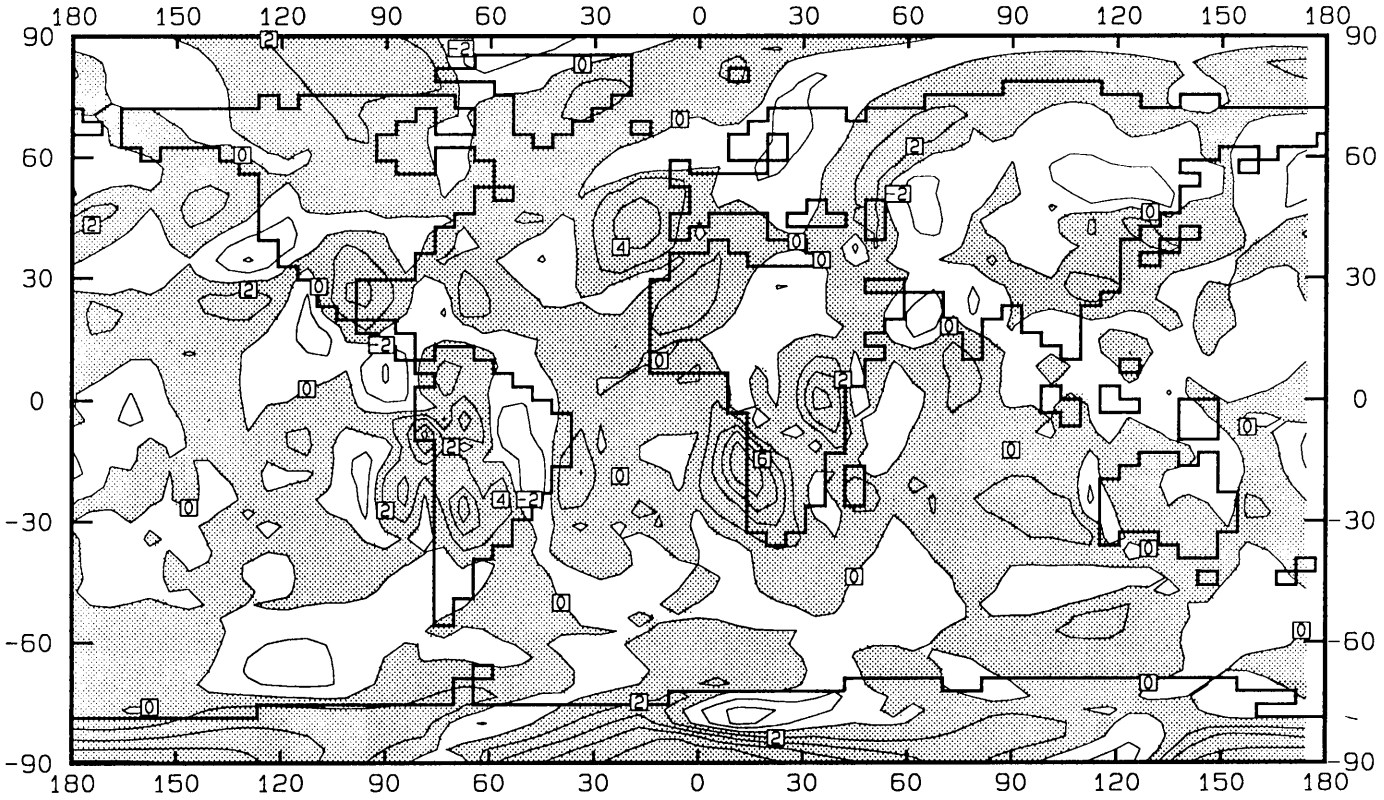

Figure 17: Differences between absolute deviations from the observed *meridional wind speed* (ms^{-1}) averaged over DJF at the 192.7 hPa pressure level (**SIGMA** co-ordinate system deviations minus **HYBRID** co-ordinate system deviations). Shaded areas denote improvements by **HYBRID** co-ordinate system simulations.

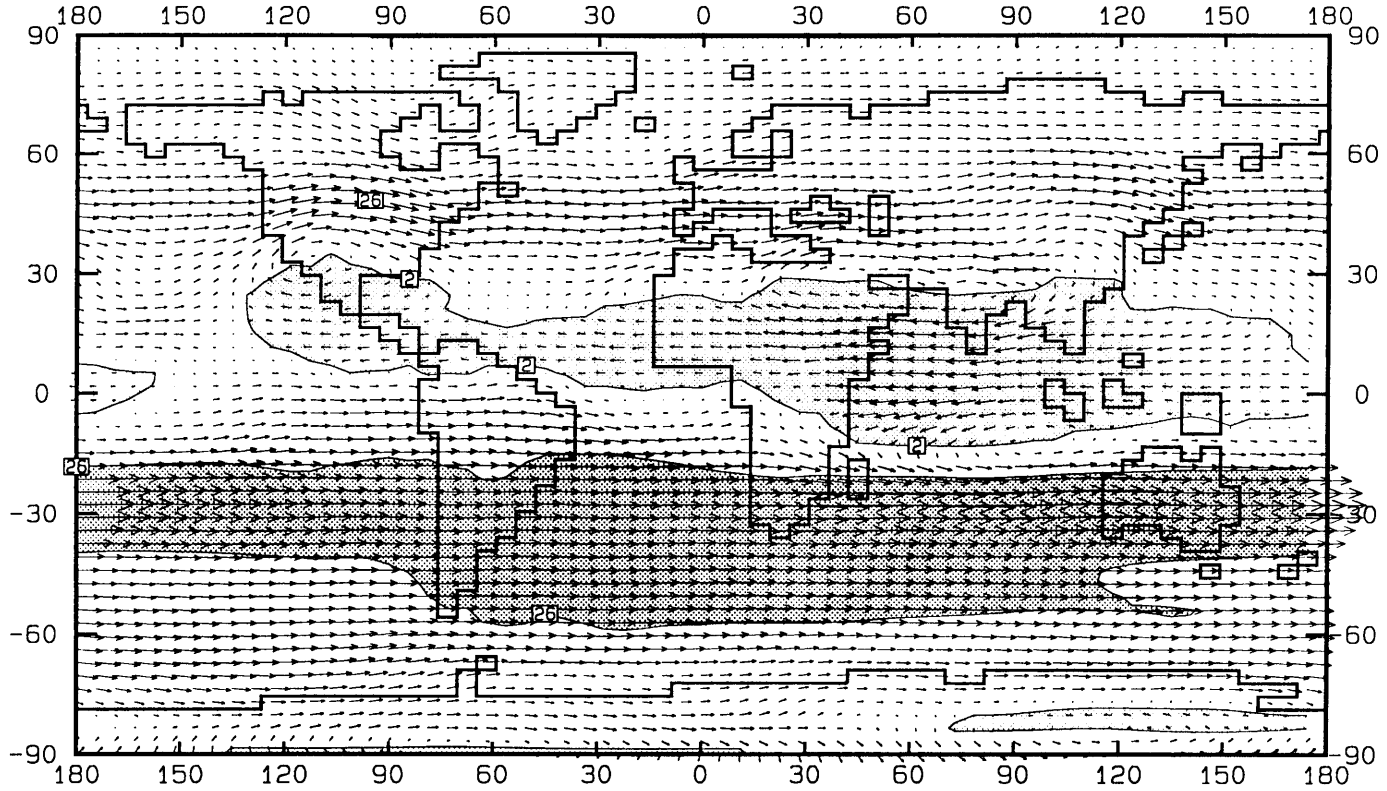

Figure 18(a): *Wind velocity* (ms^{-1}) averaged over JJA, as simulated by the CSIRO-9 AGCM using the **SIGMA** co-ordinate system, at the 192.7 hPa pressure level. Lighter and darker shaded areas represent wind velocities higher than 2 ms^{-1} (negative zonal components) and 26 ms^{-1} (positive zonal components) respectively.

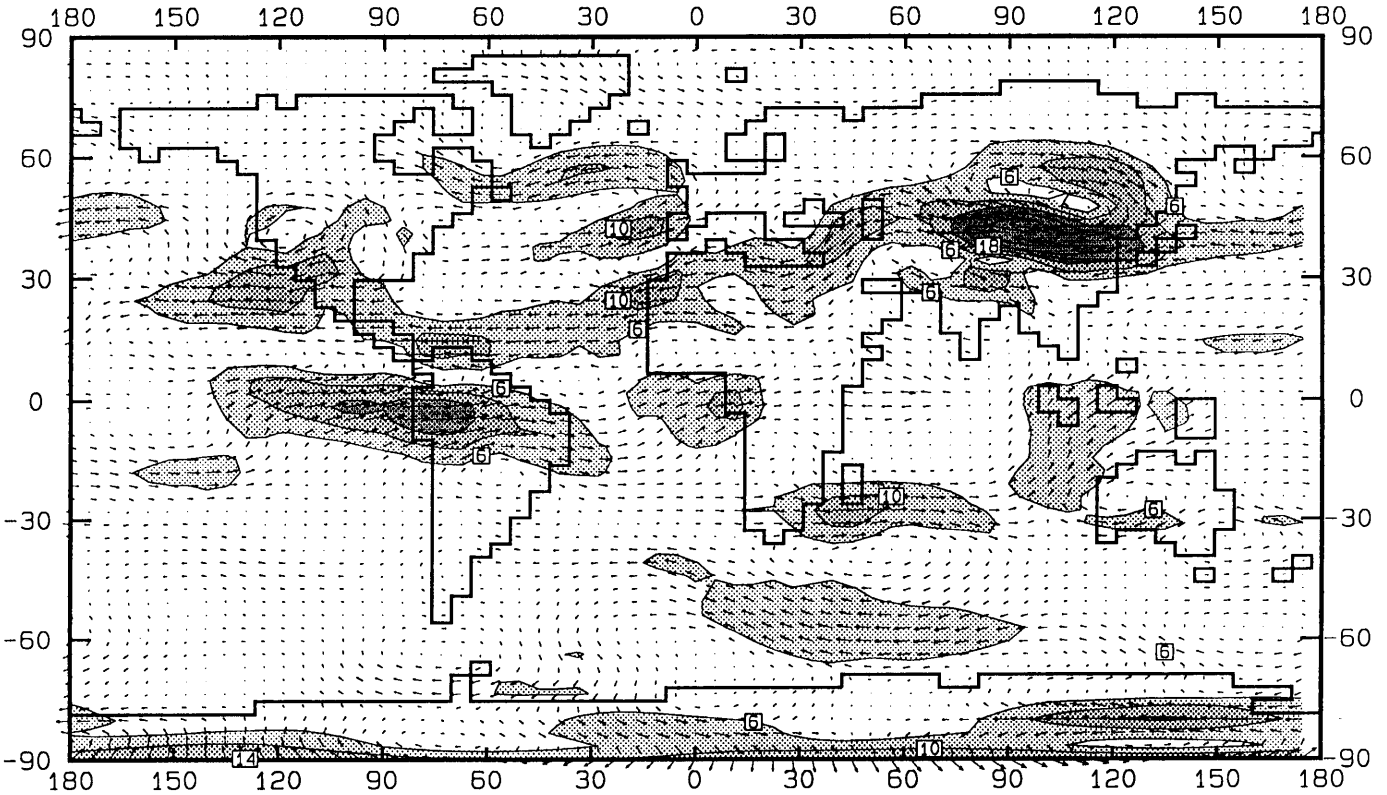

Figure 18(b): **SIGMA** simulations of figure 18(a) minus the corresponding **ECMWF** analysis. Anomalies larger than 6 ms^{-1} are shaded.

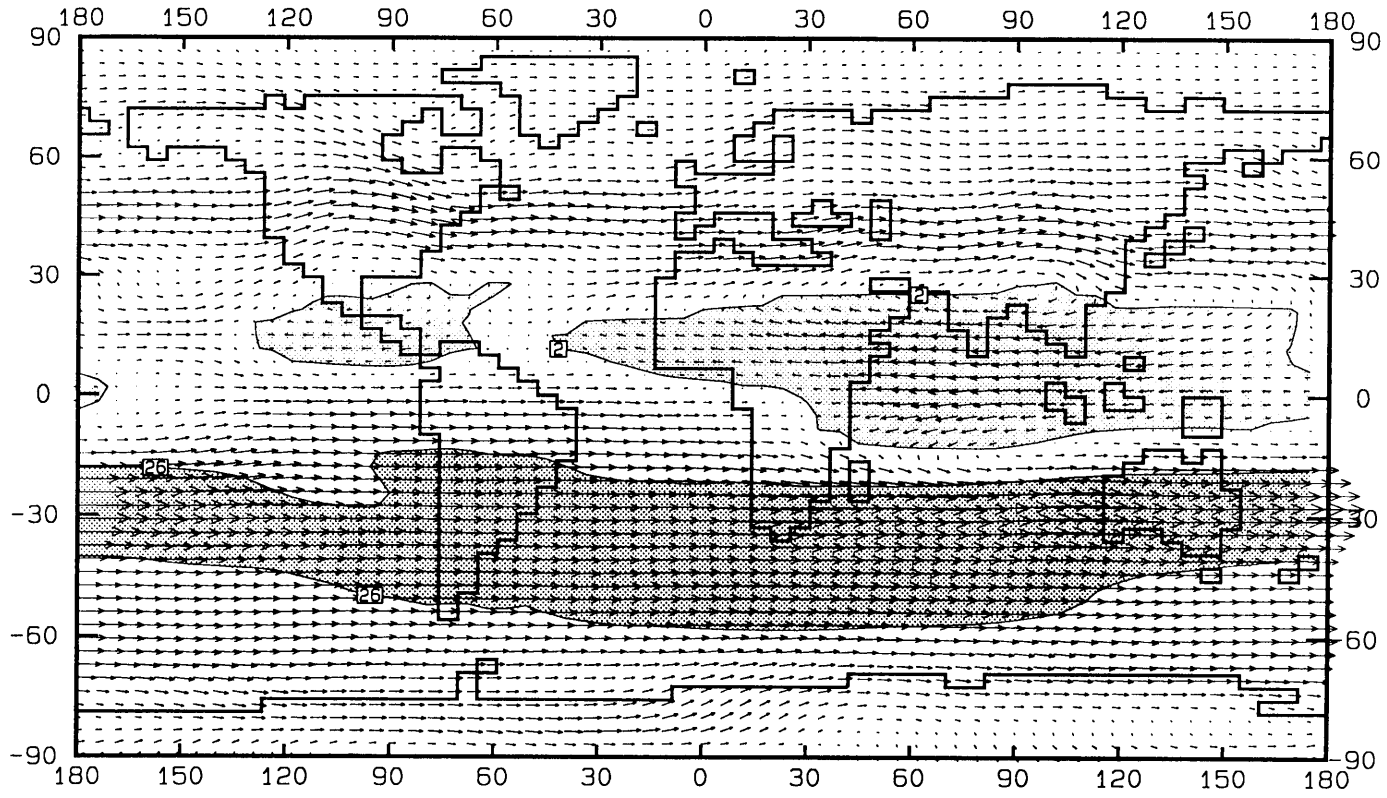

Figure 19(a): *Wind velocity* (ms^{-1}) averaged over JJA, as simulated by the CSIRO-9 AGCM using the **HYBRID** co-ordinate system, at the 192.7 hPa pressure level. The dark and light shaded areas represent wind velocities lower than -2 ms^{-1} and higher than +26 ms^{-1} respectively.

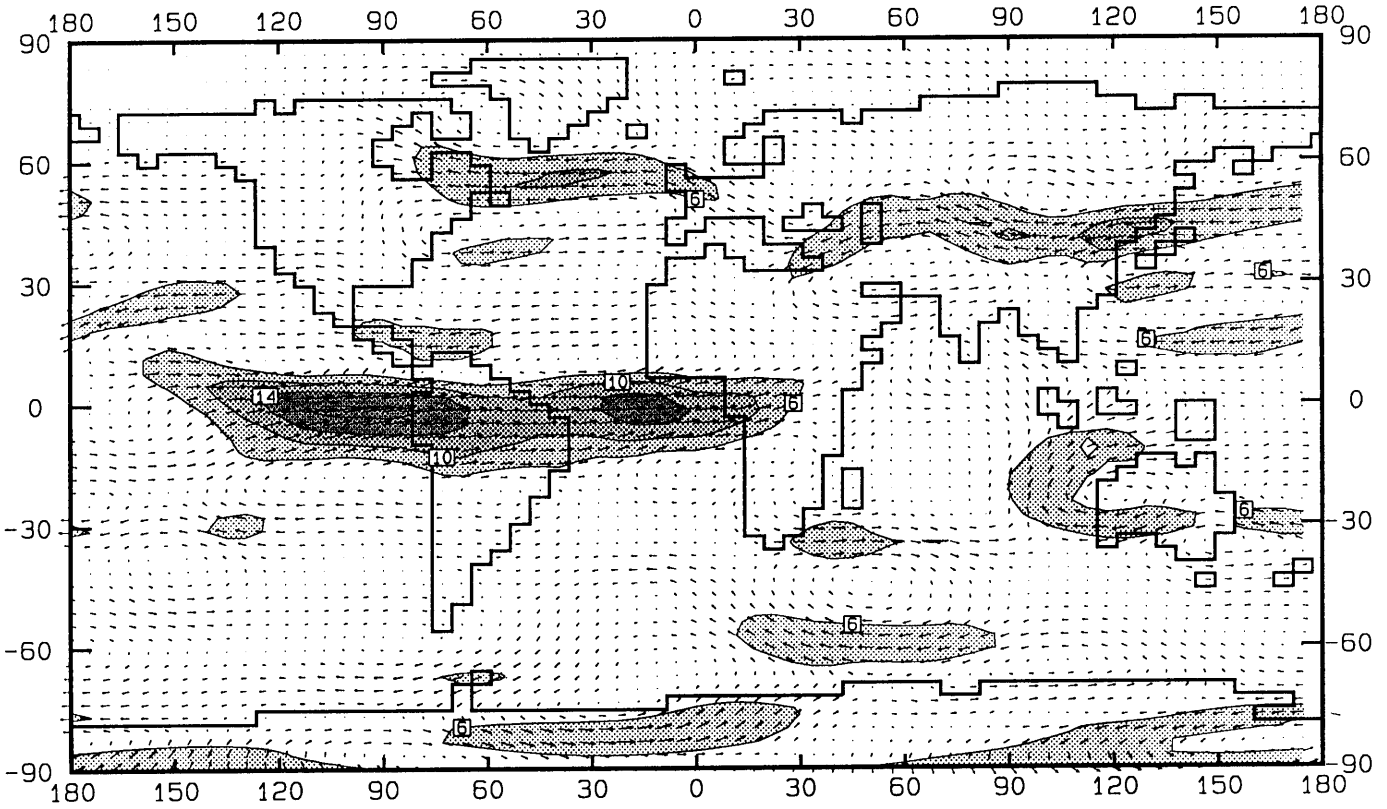

Figure 19(b): **HYBRID** simulations of figure 19(a) minus the corresponding **ECMWF** analysis. Anomalies larger than 6 ms^{-1} are shaded.

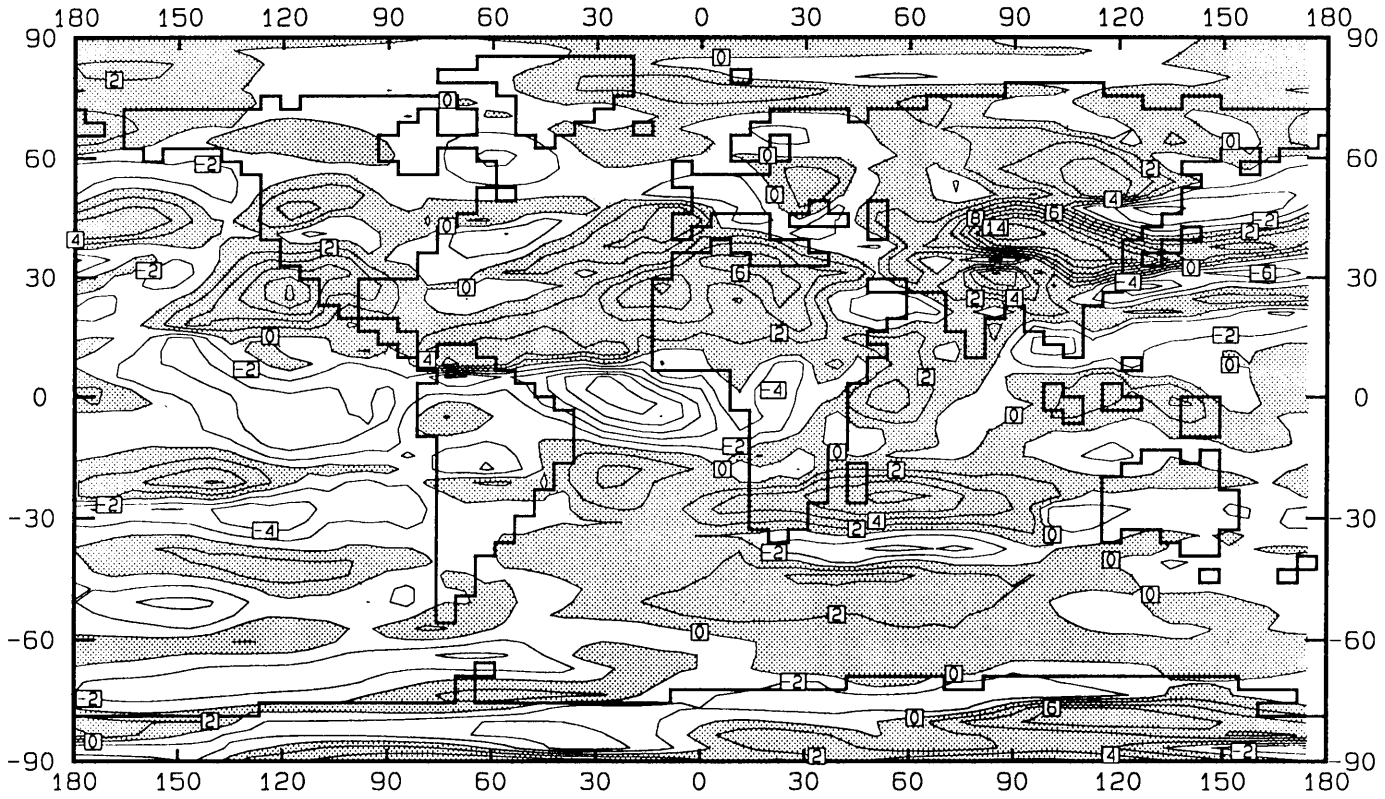

Figure 20: Differences between absolute deviations from the observed *zonal wind speed* (ms^{-1}) averaged over JJA at the 192.7 hPa pressure level (**SIGMA** co-ordinate system deviations minus **HYBRID** co-ordinate system deviations). Shaded areas denote improvements by **HYBRID** co-ordinate system simulations.

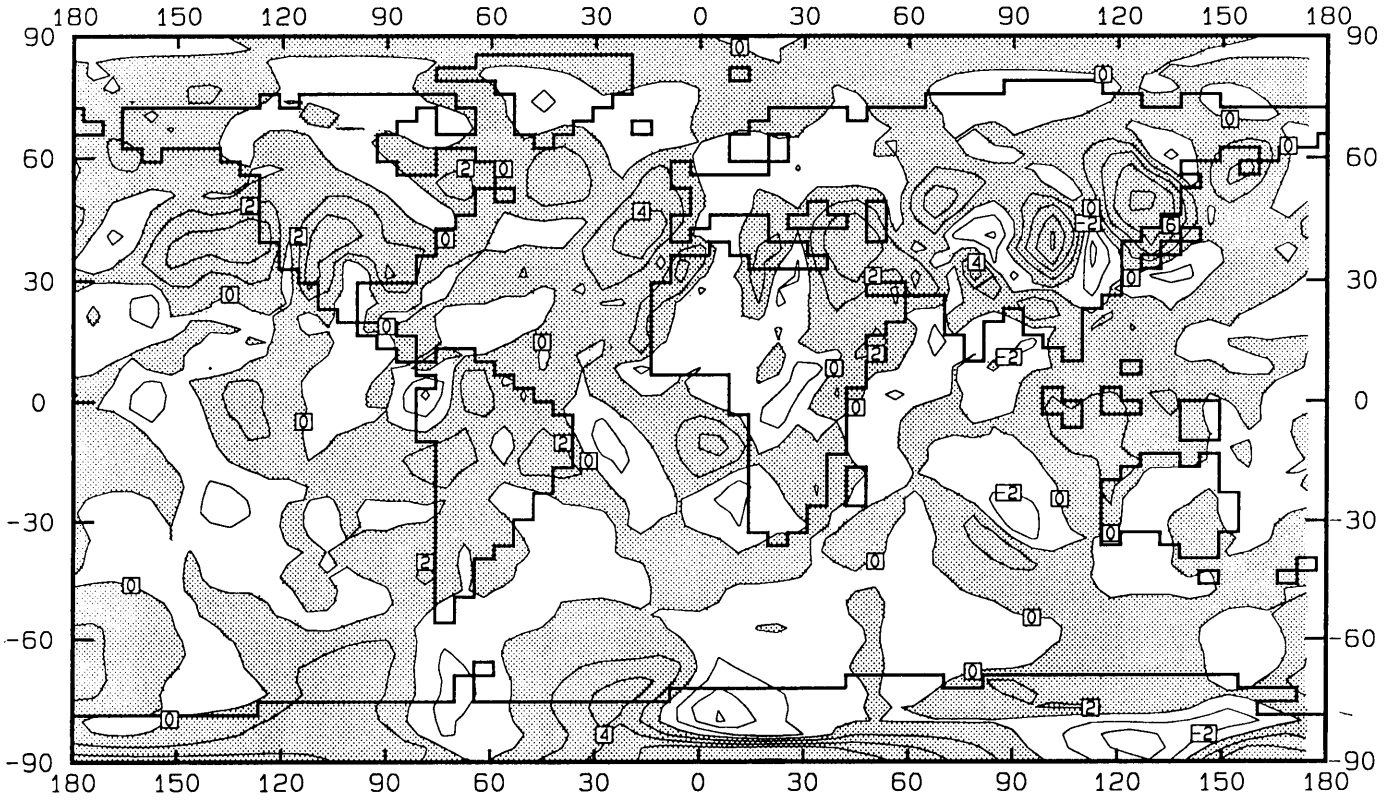

Figure 21: Differences between absolute deviations from the observed *meridional wind speed* (ms^{-1}) averaged over JJA at the 192.7 hPa pressure level (**SIGMA** co-ordinate system deviations minus **HYBRID** co-ordinate system deviations). Shaded areas denote improvements by **HYBRID** co-ordinate system simulations.

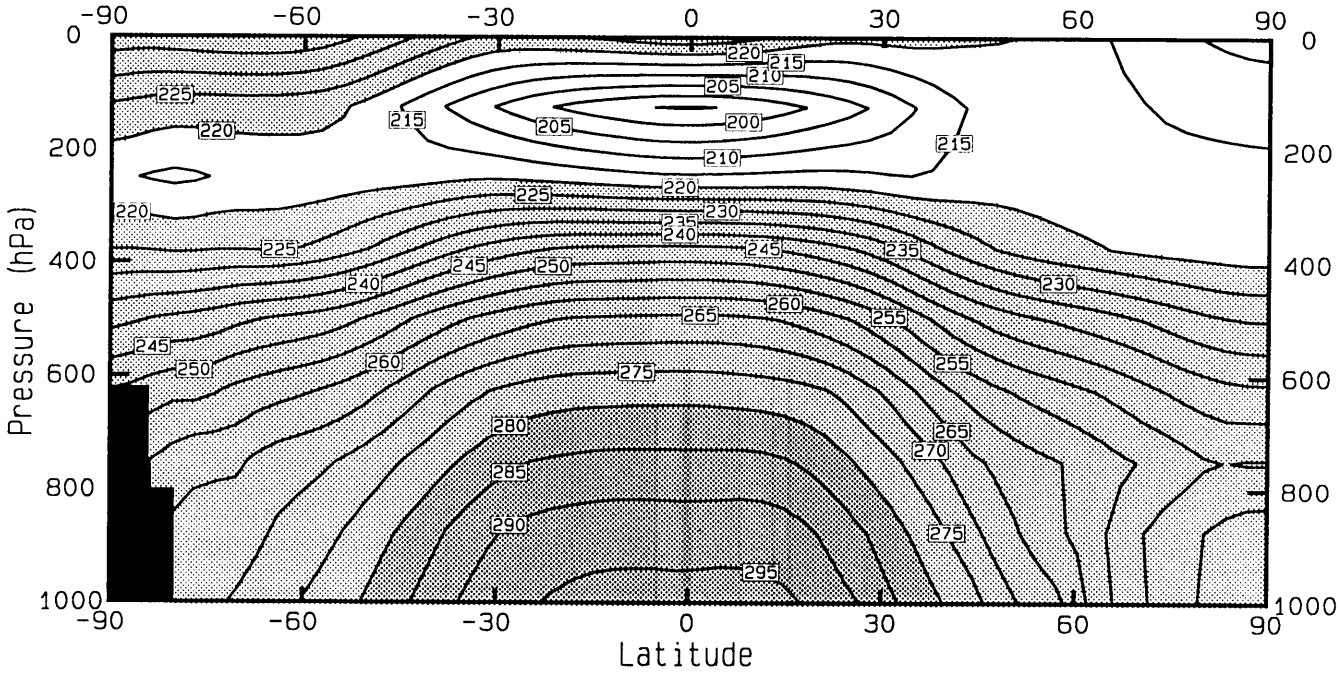

Figure 22(a): Zonal mean of the *temperature* (K) averaged over DJF as simulated by the CSIRO-9 AGCM using the **SIGMA** co-ordinate system.

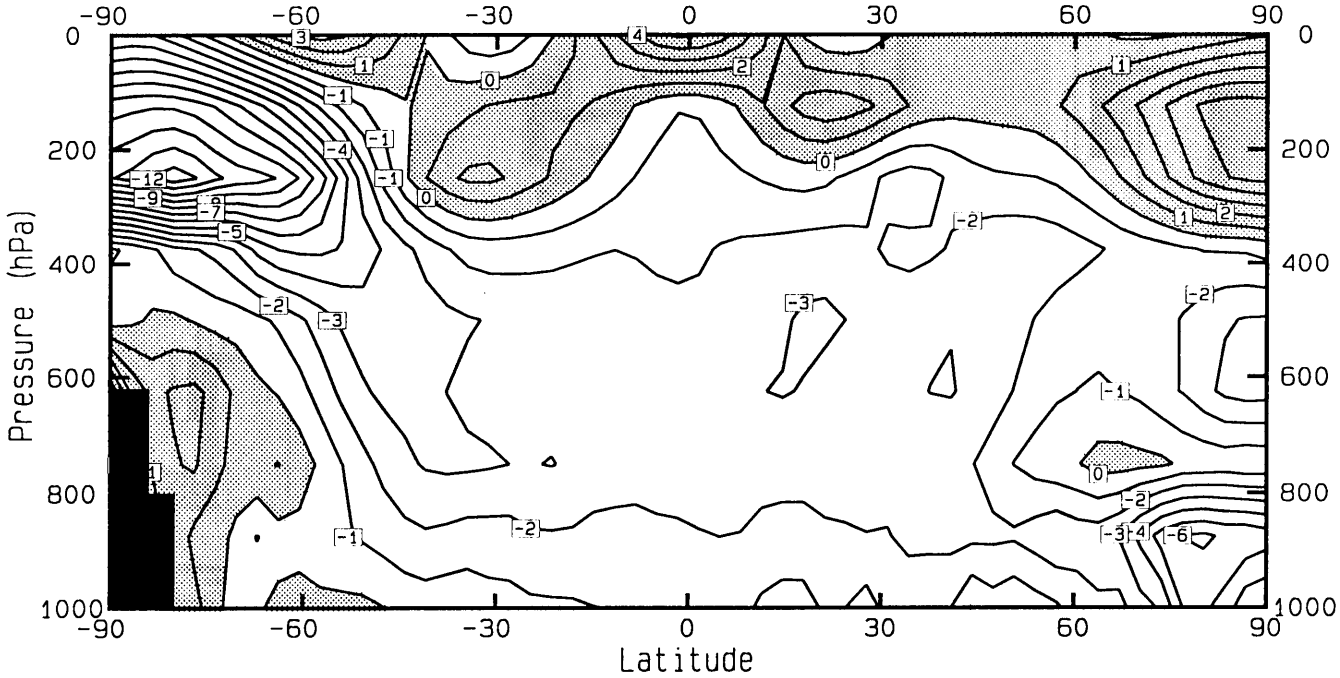

Figure 22(b): **SIGMA** simulations of figure 22(a) minus the corresponding **ECMWF** analysis.

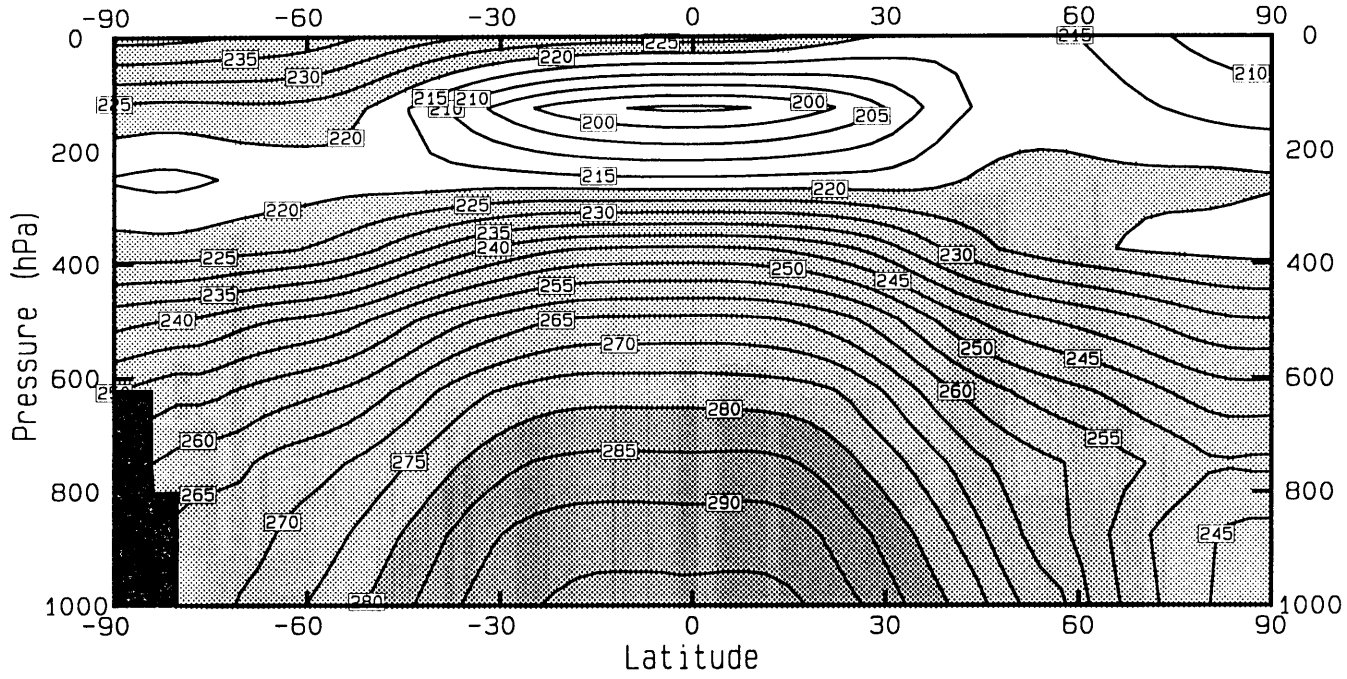

Figure 23(a): Zonal mean of the *temperature* (K) averaged over DJF as simulated by the CSIRO-9 AGCM using the **HYBRID** co-ordinate system.

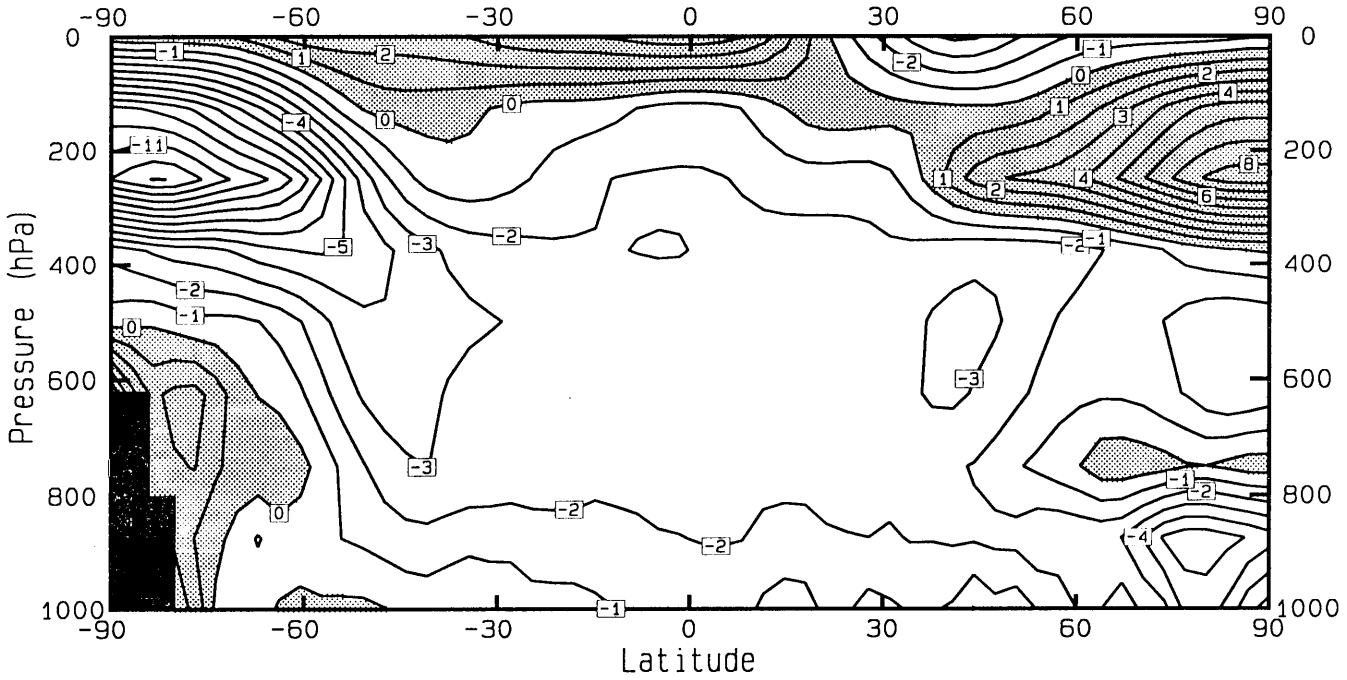

Figure 23(b): **HYBRID** simulations of figure 23(a) minus the corresponding **ECMWF** analysis.

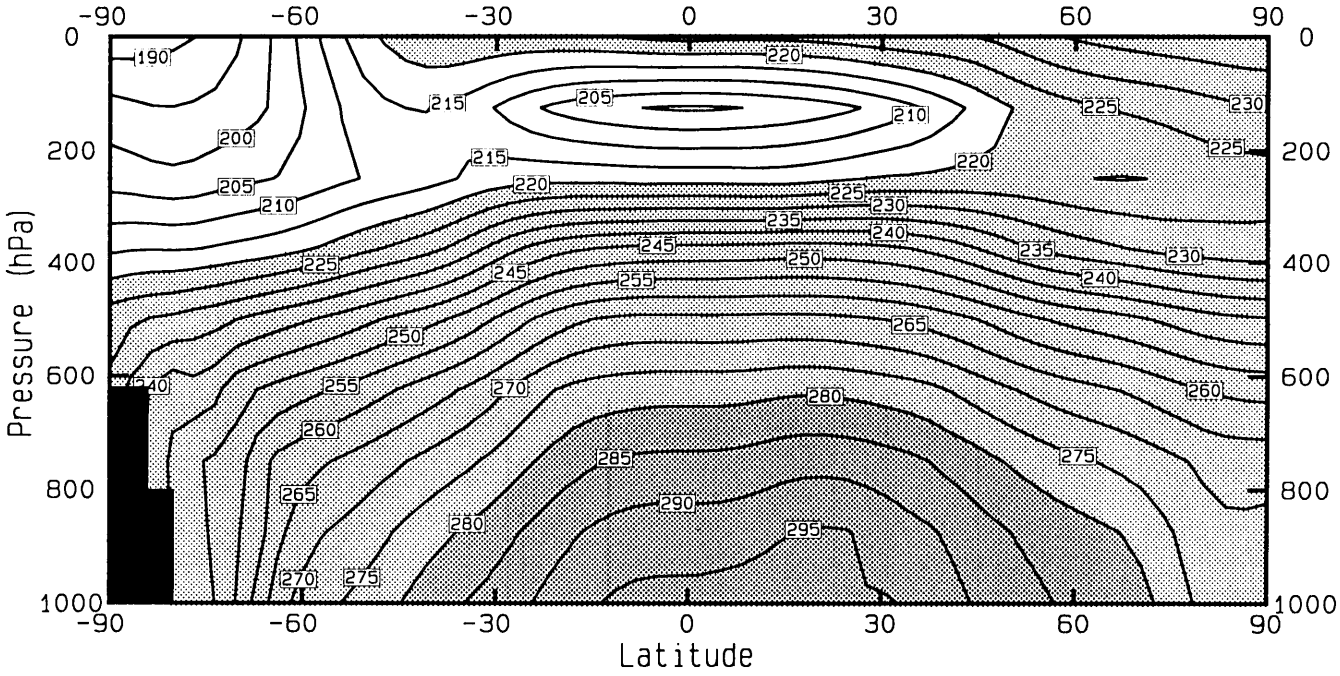

Figure 24(a): Zonal mean of the *temperature* (K) averaged over JJA as simulated by the CSIRO-9 AGCM using the **SIGMA** co-ordinate system.

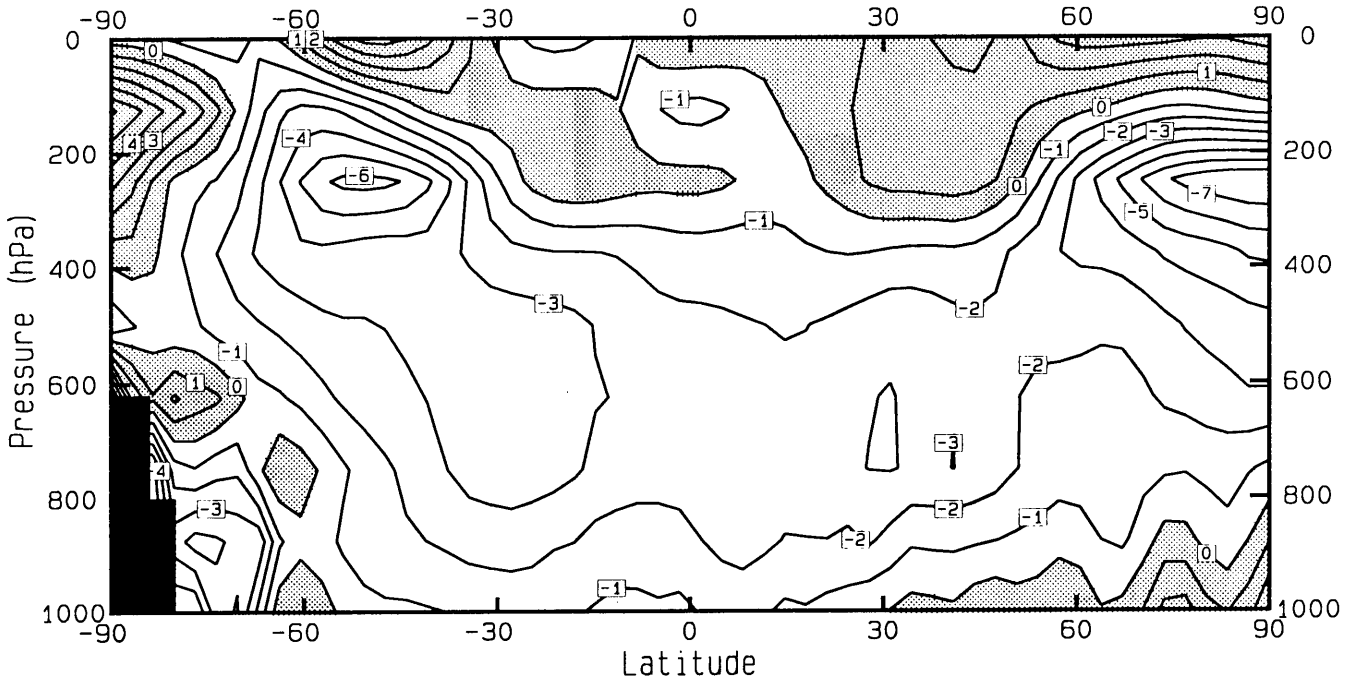

Figure 24(b): **SIGMA** simulations of figure 24(a) minus the corresponding **ECMWF** analysis.

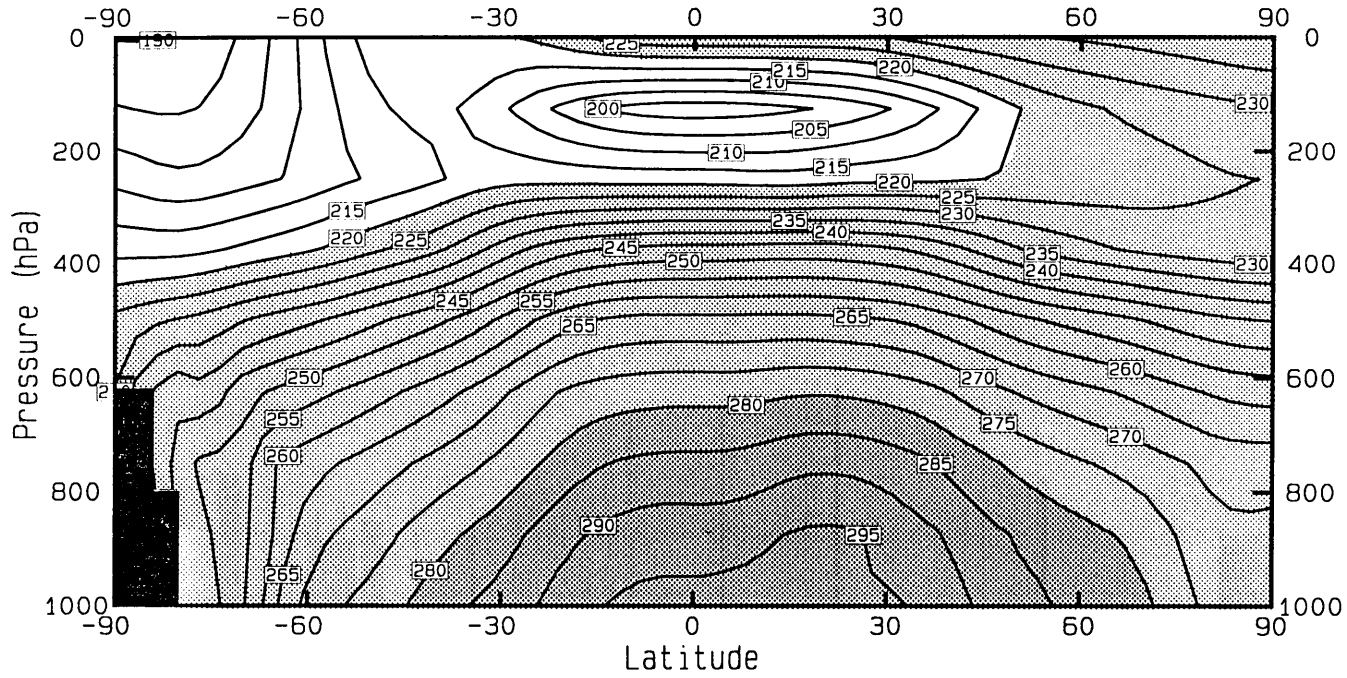

Figure 25(a): Zonal mean of the *temperature* (K) averaged over JJA as simulated by the CSIRO-9 AGCM using the **HYBRID** co-ordinate system.

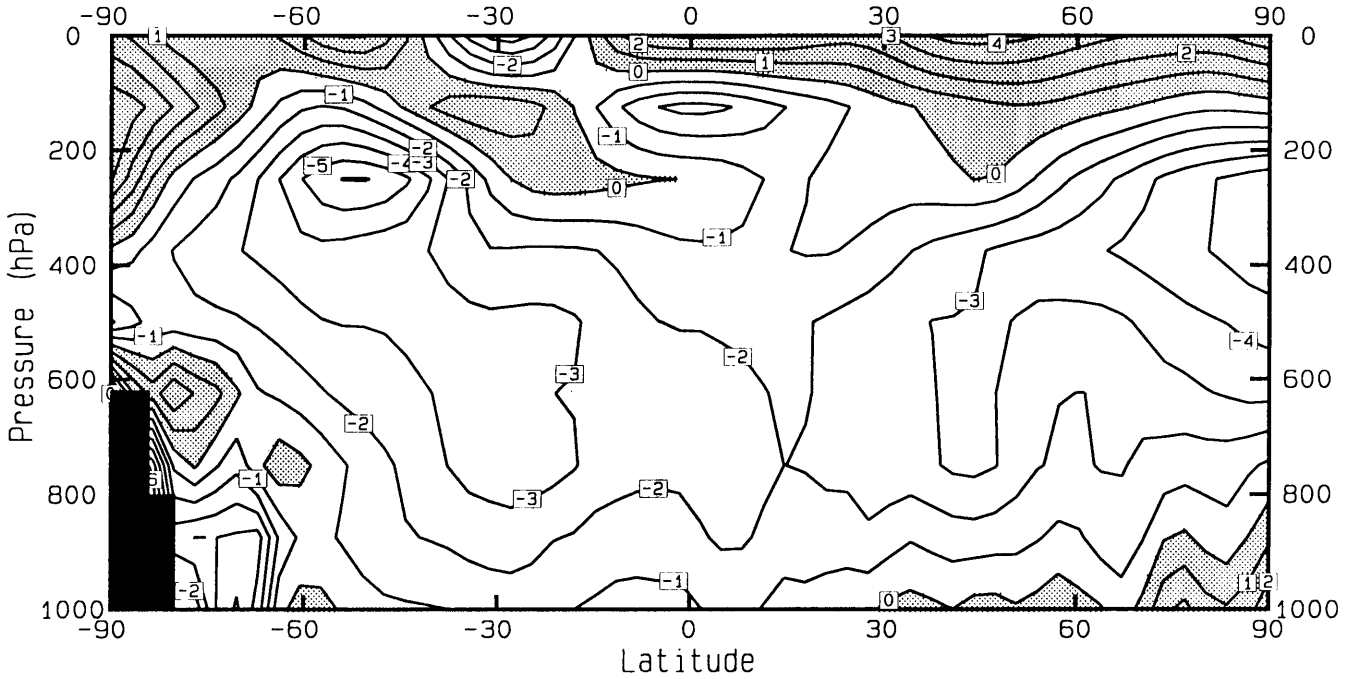

Figure 25(b): **HYBRID** simulations of figure 25(a) minus the corresponding **ECMWF** analysis.

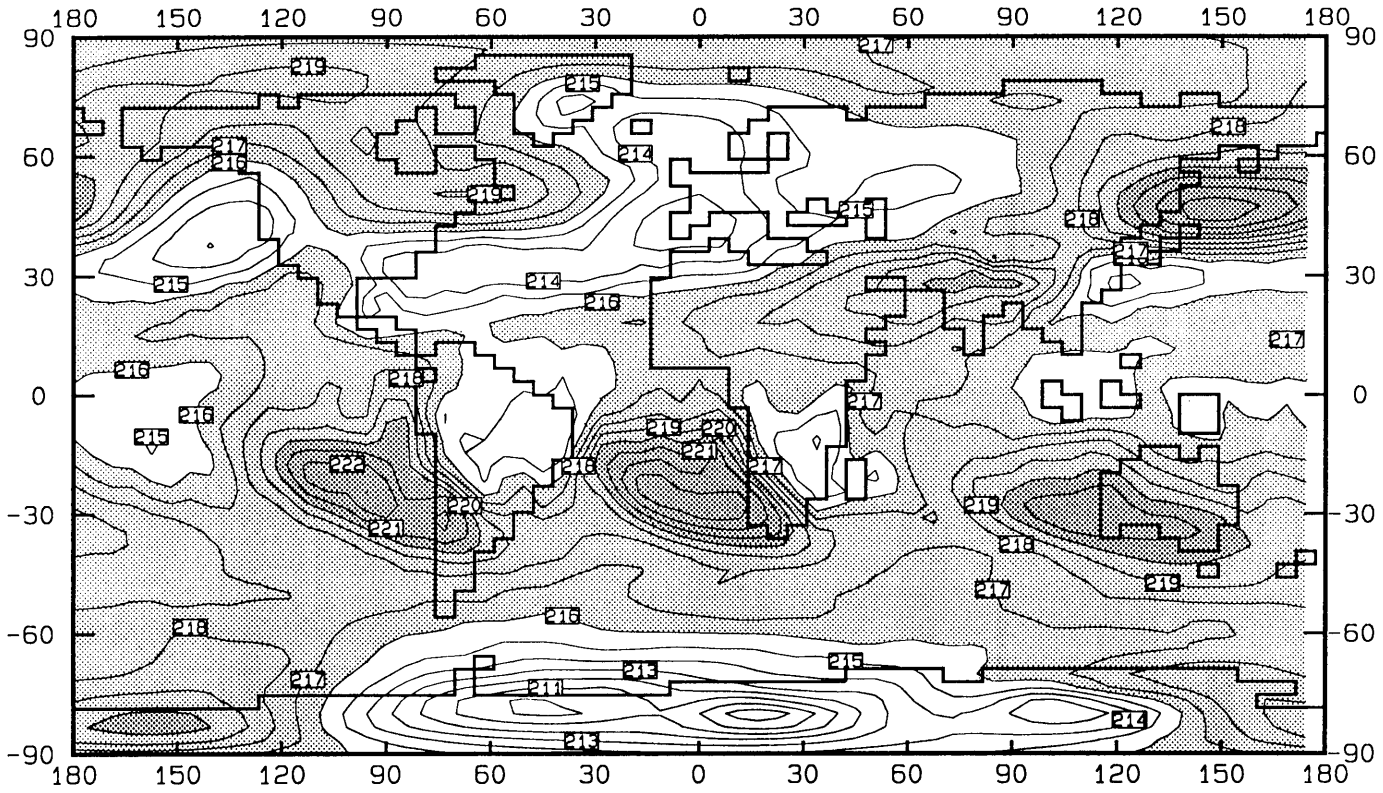

Figure 26(a): *Temperature* (K) averaged over DJF, as simulated by the CSIRO-9 AGCM using the **SIGMA** co-ordinate system, at the 192.7 hPa pressure level. Temperatures higher than 216 K are shaded.

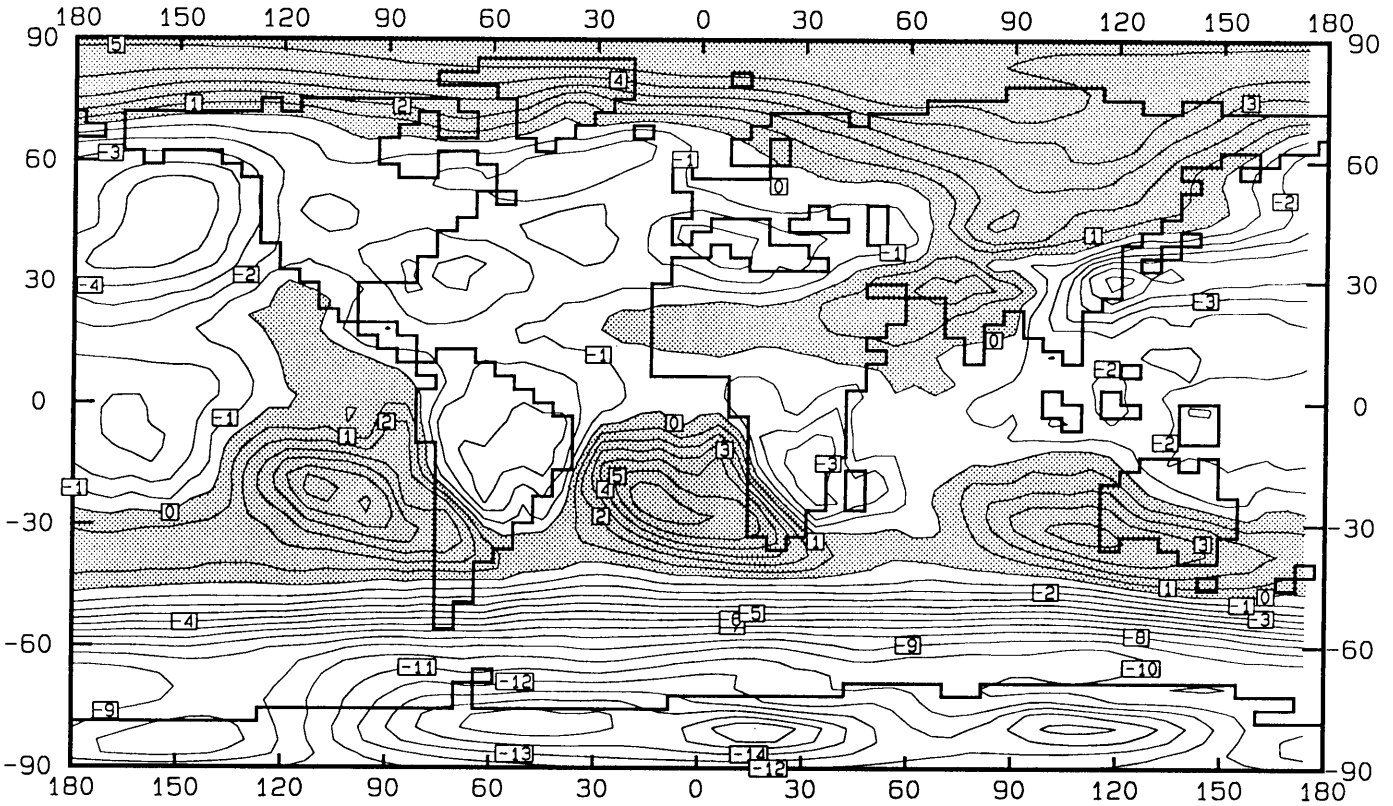

Figure 26(b): **SIGMA** simulations of figure 26(a) minus the corresponding **ECMWF** analysis. Positive anomalies are shaded.

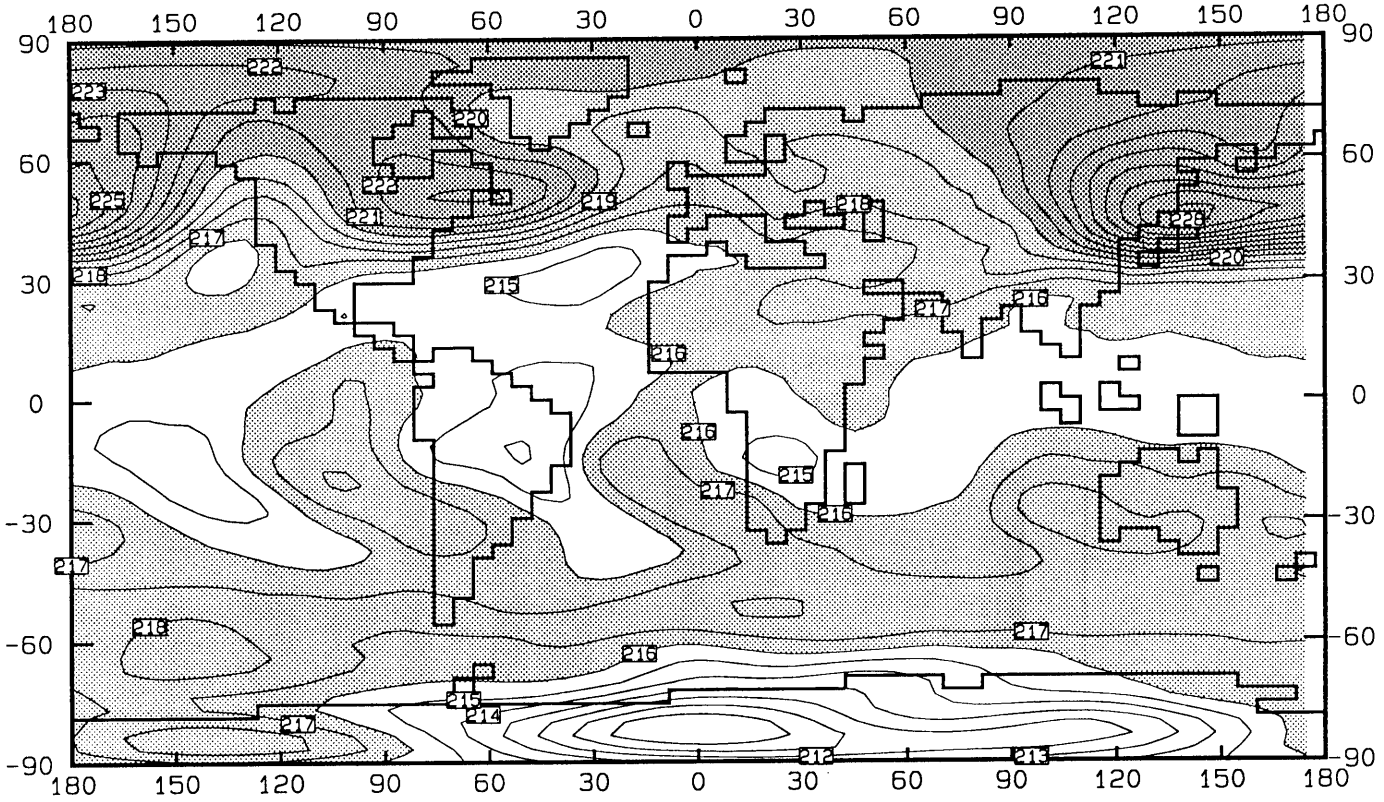

Figure 27(a): *Temperature* (K) averaged over DJF, as simulated by the CSIRO-9 AGCM using the **HYBRID** co-ordinate system, at the 192.7 hPa pressure level. Temperatures higher than 216 K are shaded.

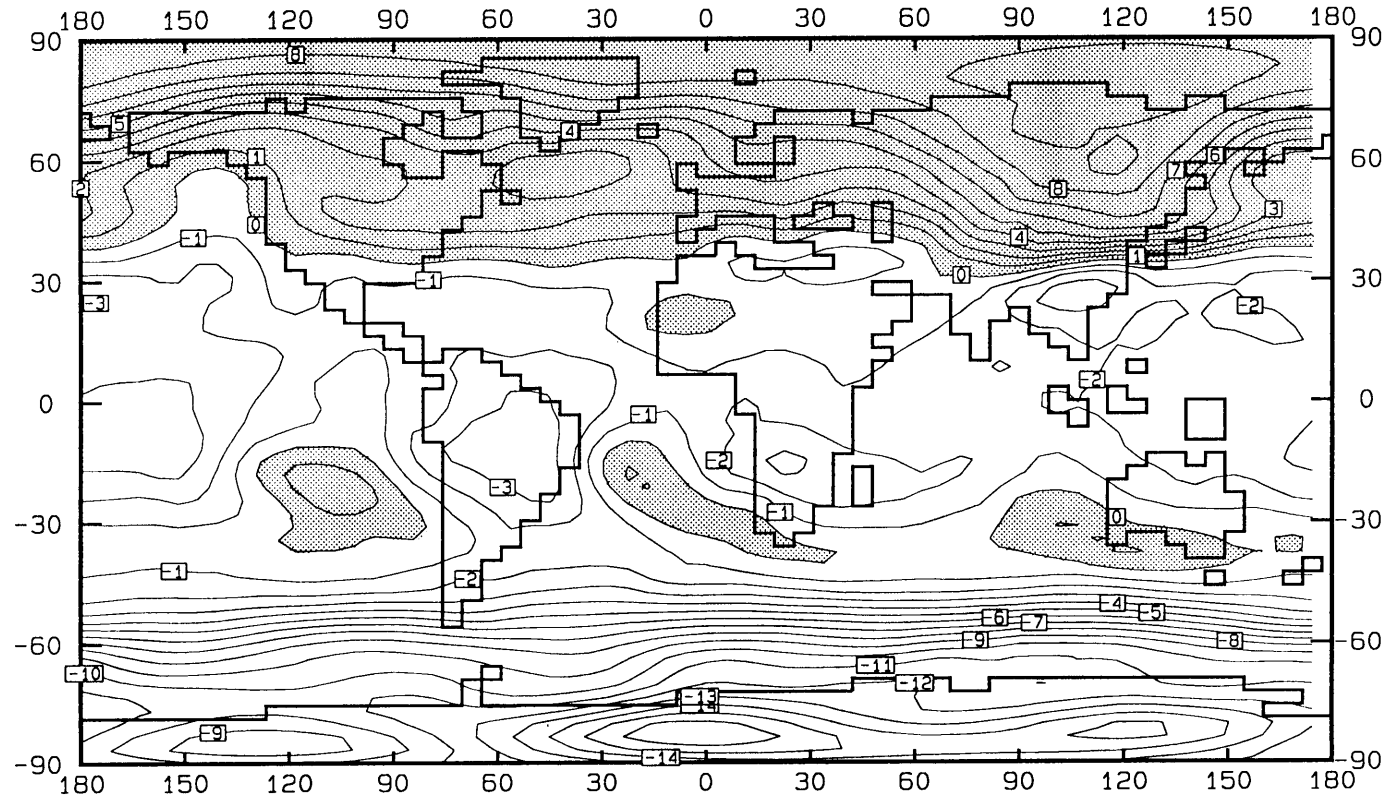

Figure 27(b): **HYBRID** simulations of figure 27(a) minus the corresponding **ECMWF** analysis. Positive anomalies are shaded.

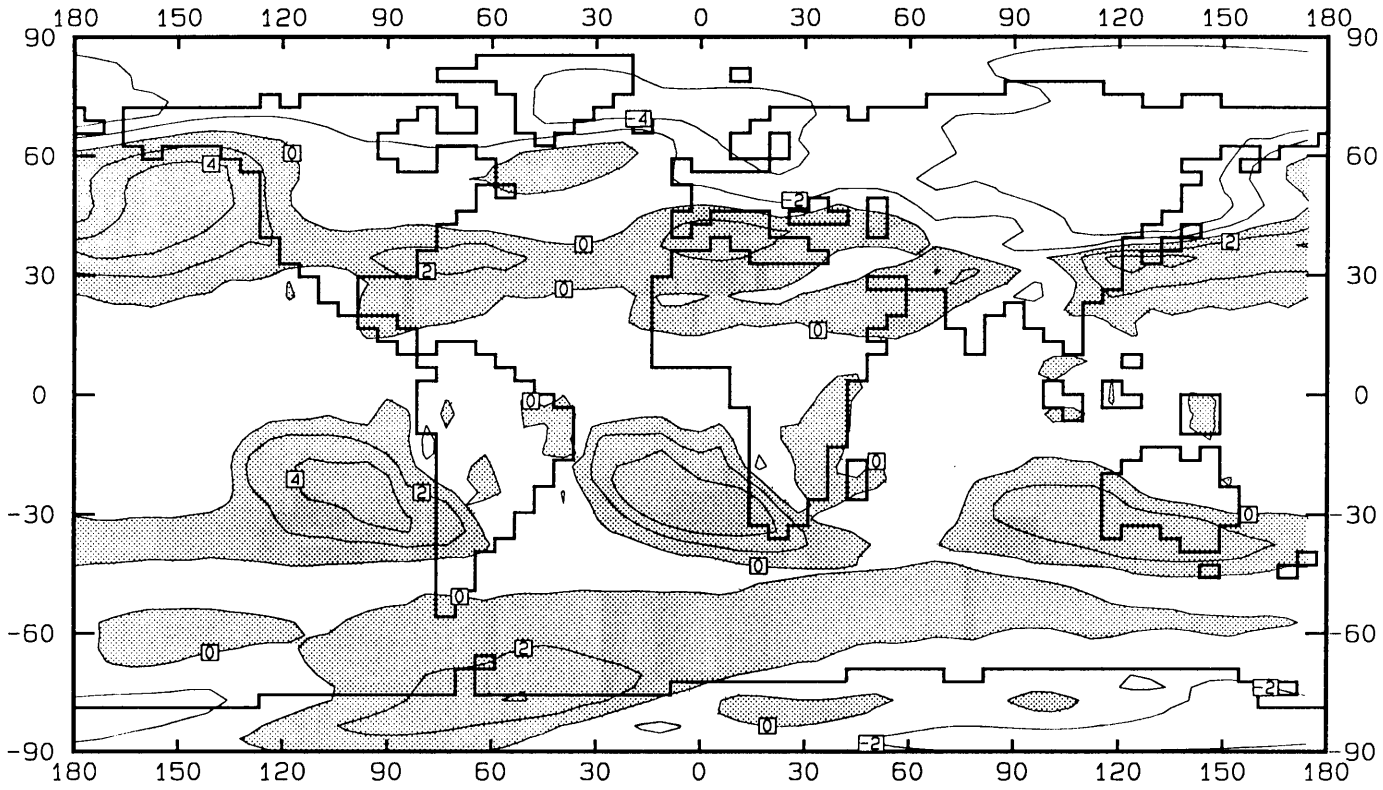

Figure 28: Differences between absolute deviations from the observed *temperature* (K) averaged over DJF at the 192.7 hPa pressure level (**SIGMA** co-ordinate system deviations minus **HYBRID** co-ordinate system deviations). Shaded areas denote improvements by **HYBRID** co-ordinate system simulations.

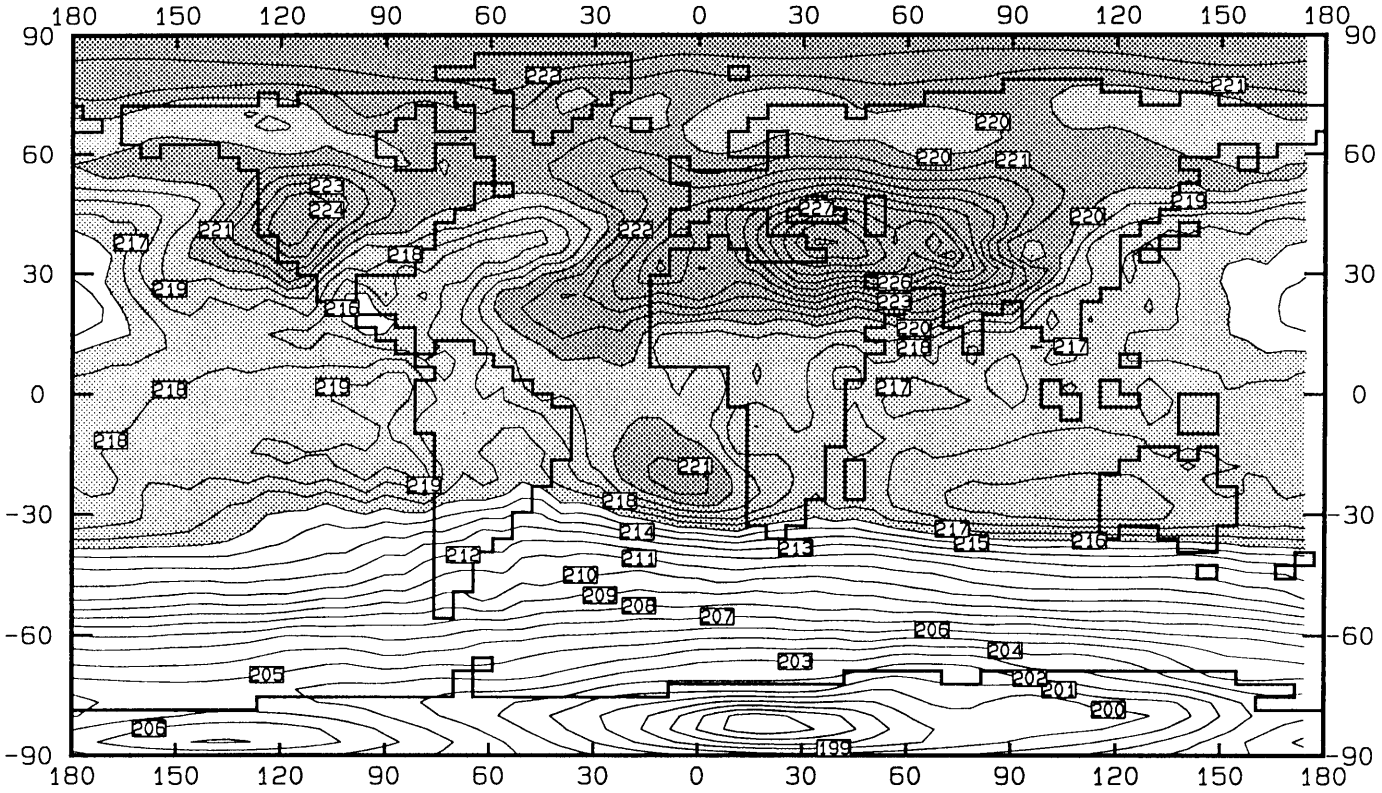

Figure 29(a): *Temperature* (K) averaged over JJA, as simulated by the CSIRO-9 AGCM using the **SIGMA** co-ordinate system, at the 192.7 hPa pressure level. Temperatures higher than 216 K are shaded.

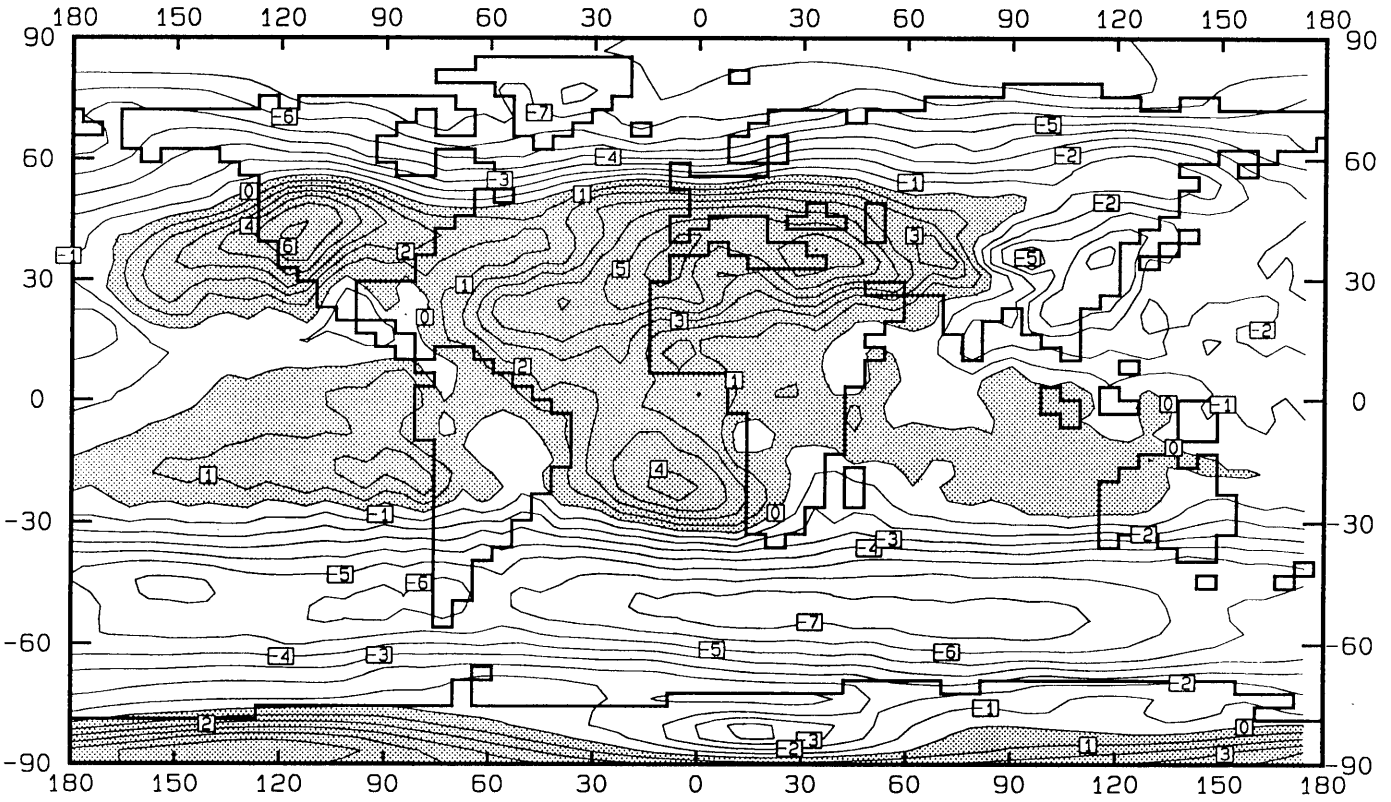

Figure 29(b): **SIGMA** simulations of figure 29(a) minus the corresponding **ECMWF** analysis. Positive anomalies are shaded.

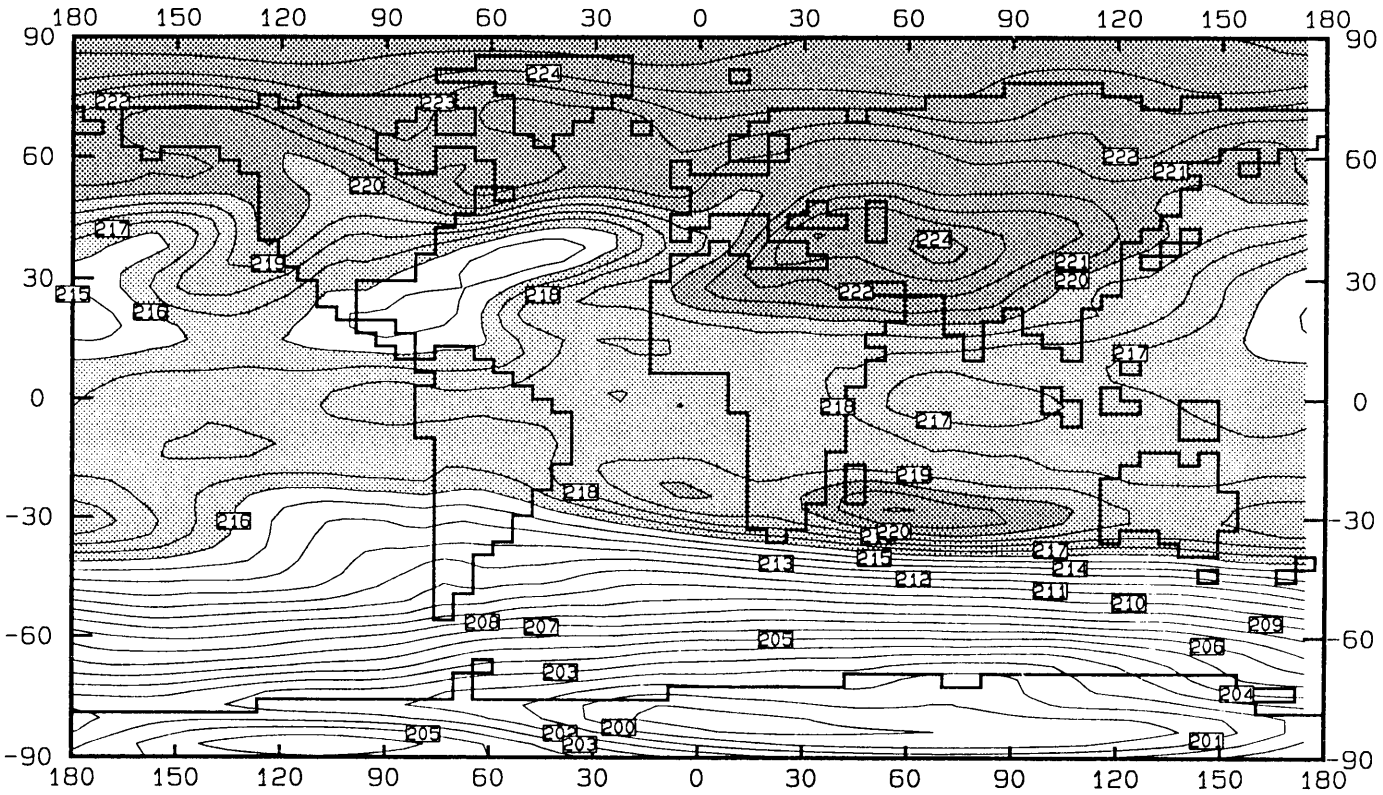

Figure 30(a): *Temperature* (K) averaged over JJA, as simulated by the CSIRO-9 AGCM using the **HYBRID** co-ordinate system, at the 192.7 hPa pressure level. Temperatures higher than 216 K are shaded.

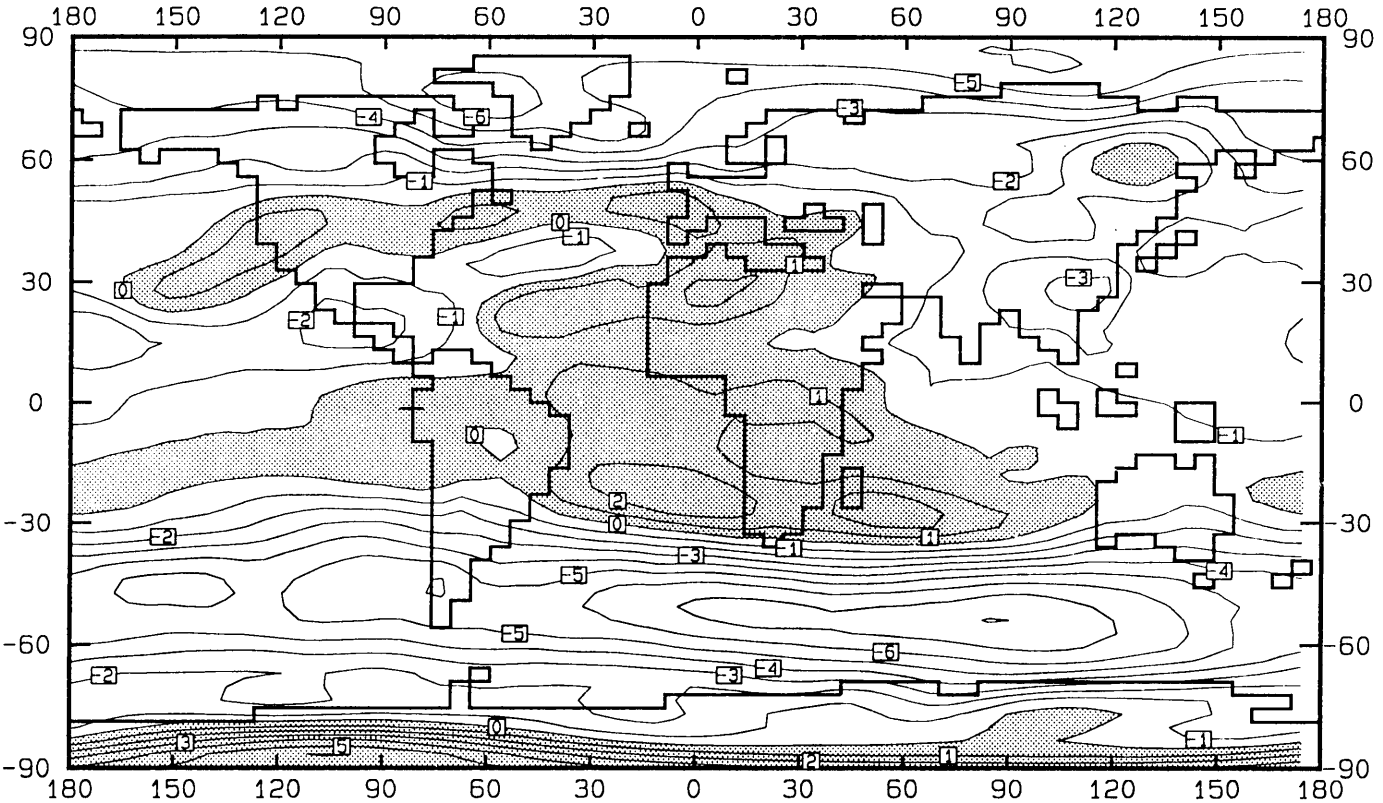

Figure 30(b): **HYBRID** simulations of figure 30(a) minus the corresponding **ECMWF** analysis. Positive anomalies are shaded.

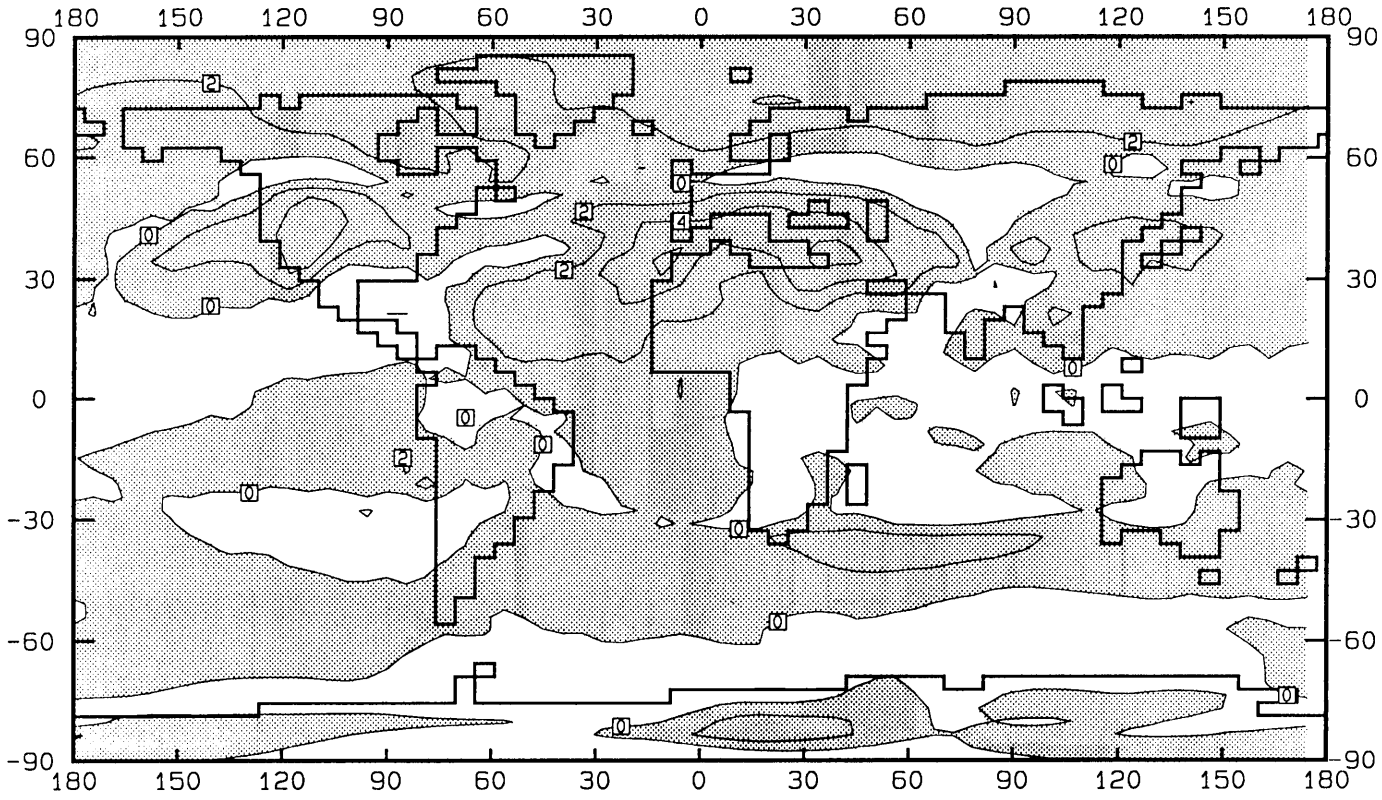

Figure 31: Differences between absolute deviations from the observed *temperature* (K) averaged over JJA at the 192.7 hPa pressure level (**SIGMA** co-ordinate system deviations minus **HYBRID** co-ordinate system deviations). Shaded areas denote improvements by **HYBRID** co-ordinate system simulations

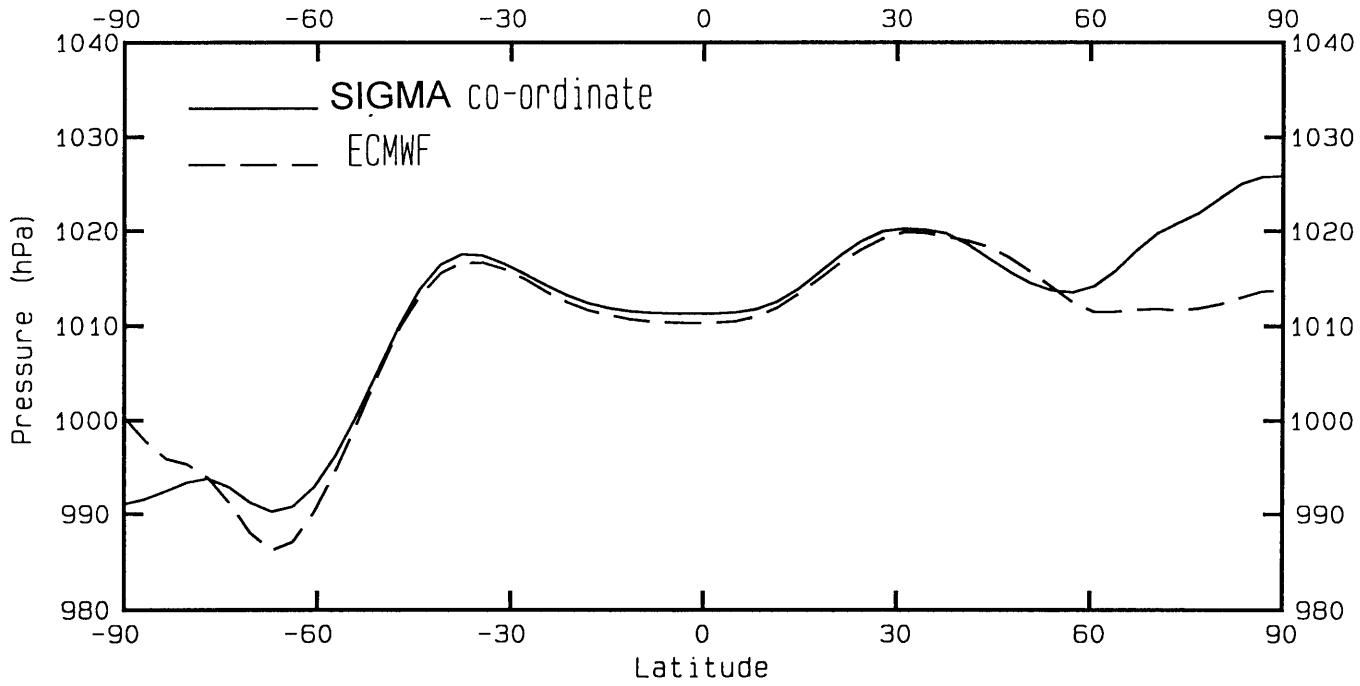

Figure 32: Zonal mean of the *mean sea level pressure* (hPa) averaged over DJF as simulated by the CSIRO-9 AGCM using the **SIGMA** co-ordinate system (solid lines) and **TOGA/ECMWF** analysis (dashed lines).

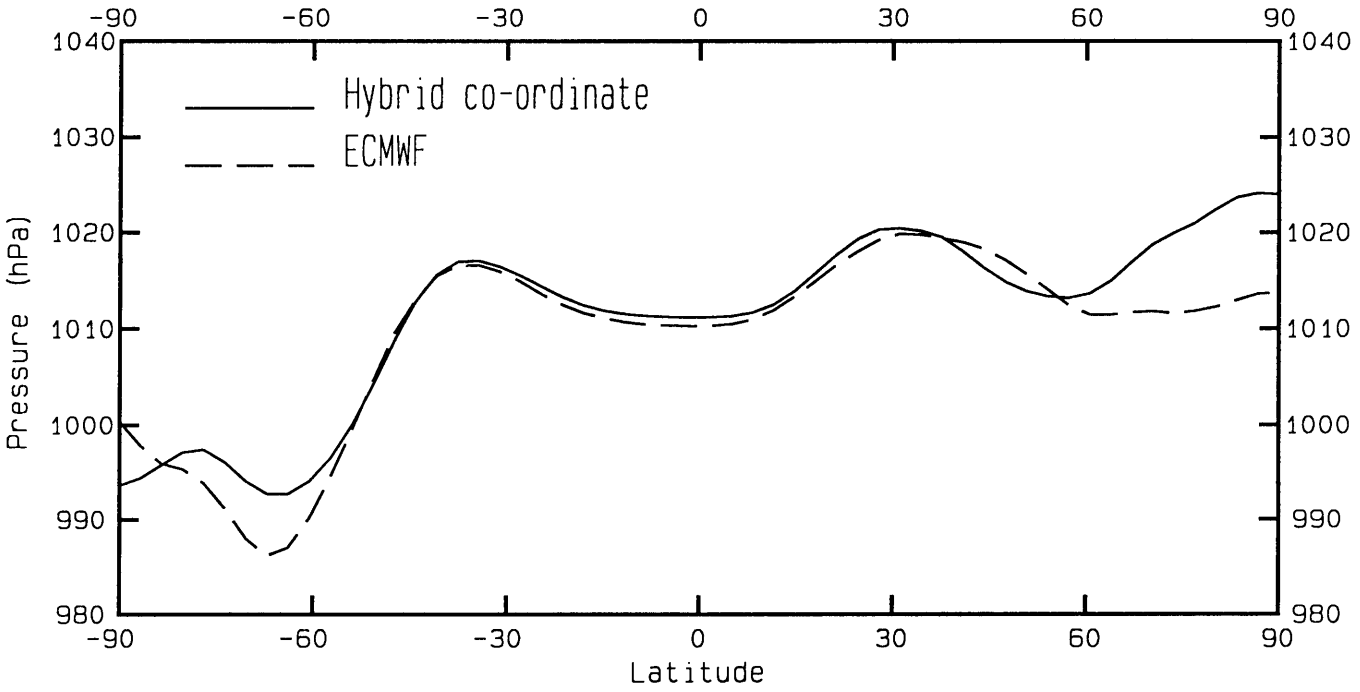

Figure 33: Zonal mean of the *mean sea level pressure* (hPa) averaged over DJF as simulated by the CSIRO-9 AGCM using the **HYBRID** co-ordinate system (solid lines) and **TOGA/ECMWF** analysis (dashed lines).

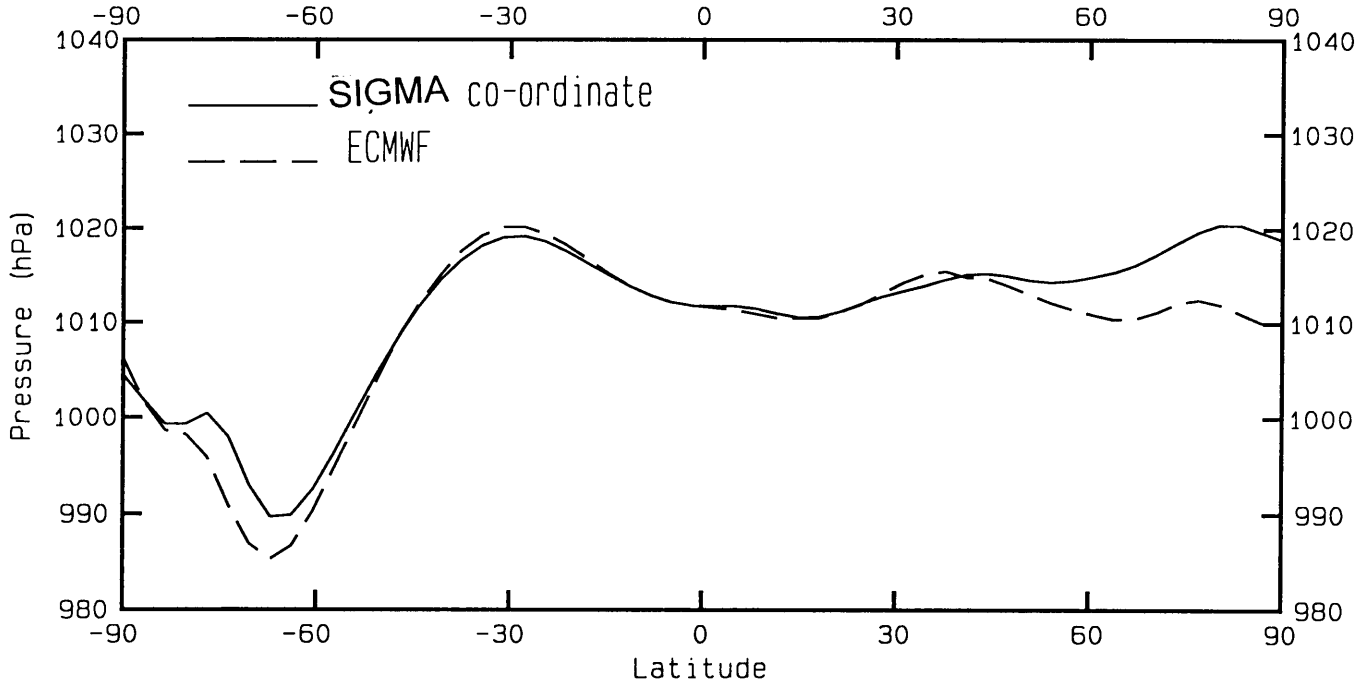

Figure 34: Zonal mean of the *mean sea level pressure* (hPa) averaged over JJA as simulated by the CSIRO-9 AGCM using the **SIGMA** co-ordinate system (solid lines) and **TOGA/ECMWF** analysis (dashed lines).

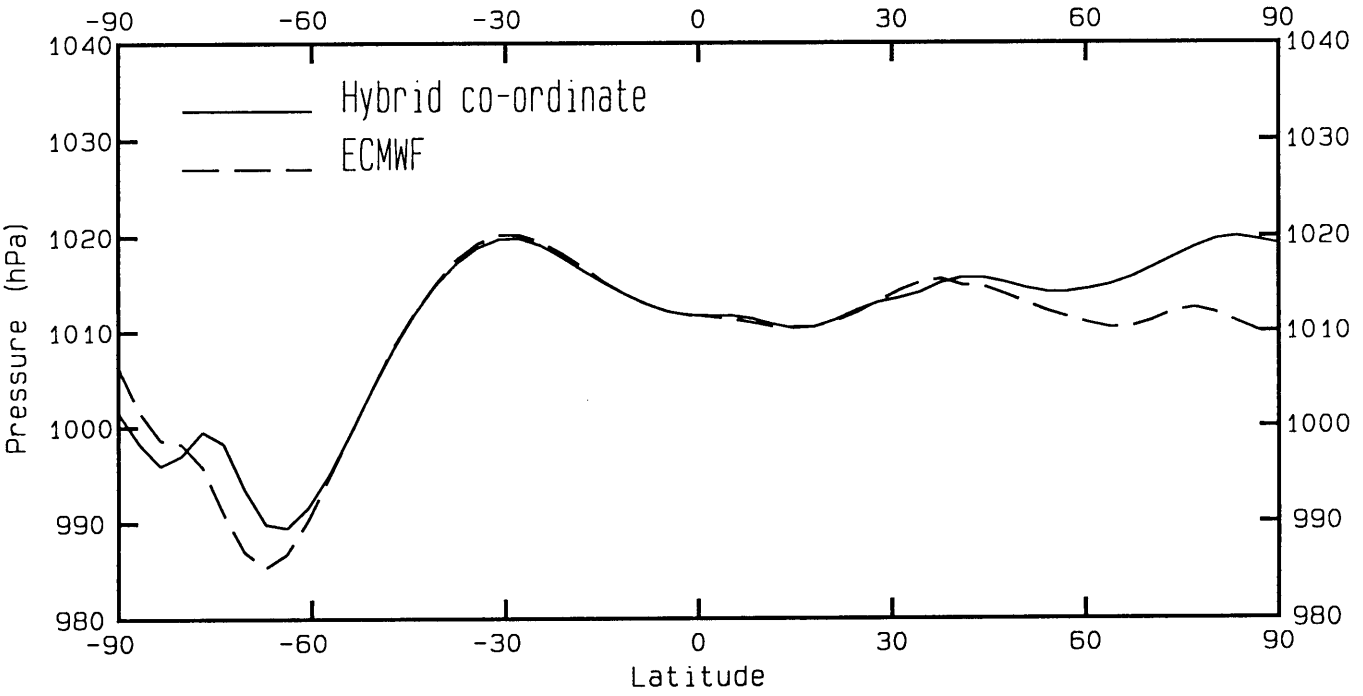

Figure 35: Zonal mean of the *mean sea level pressure* (hPa) averaged over JJA as simulated by the CSIRO-9 AGCM using the **HYBRID** co-ordinate system (solid lines) and **TOGA/ECMWF** analysis (dashed lines).

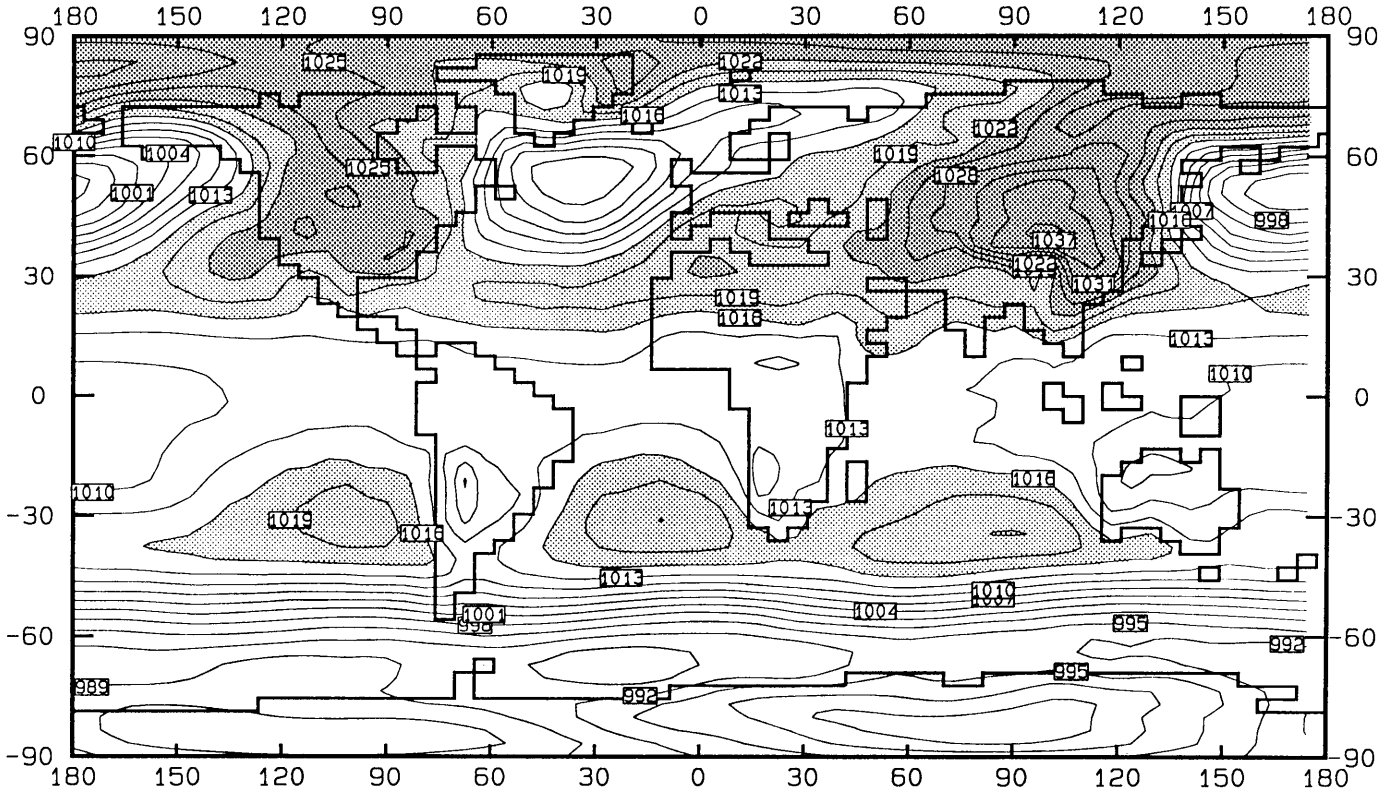

Figure 36(a): *Mean sea level pressure* (hPa) averaged over DJF as simulated by the CSIRO-9 AGCM using the **SIGMA** co-ordinate system. Pressure values higher than 1016 hPa are shaded.

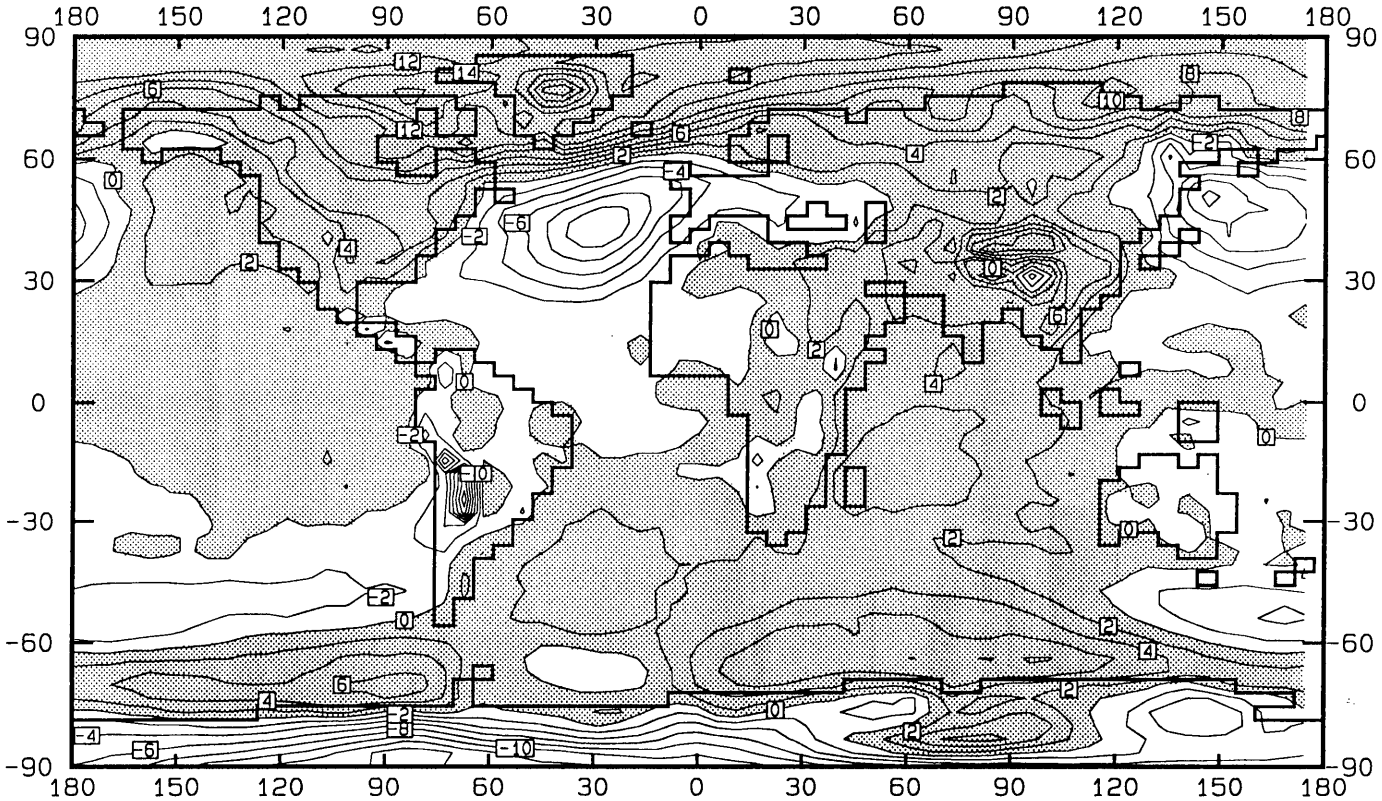

Figure 36(b): **SIGMA** simulations of figure 36(a) minus the corresponding **TOGA/ECMWF** analysis. Positive anomalies are shaded.

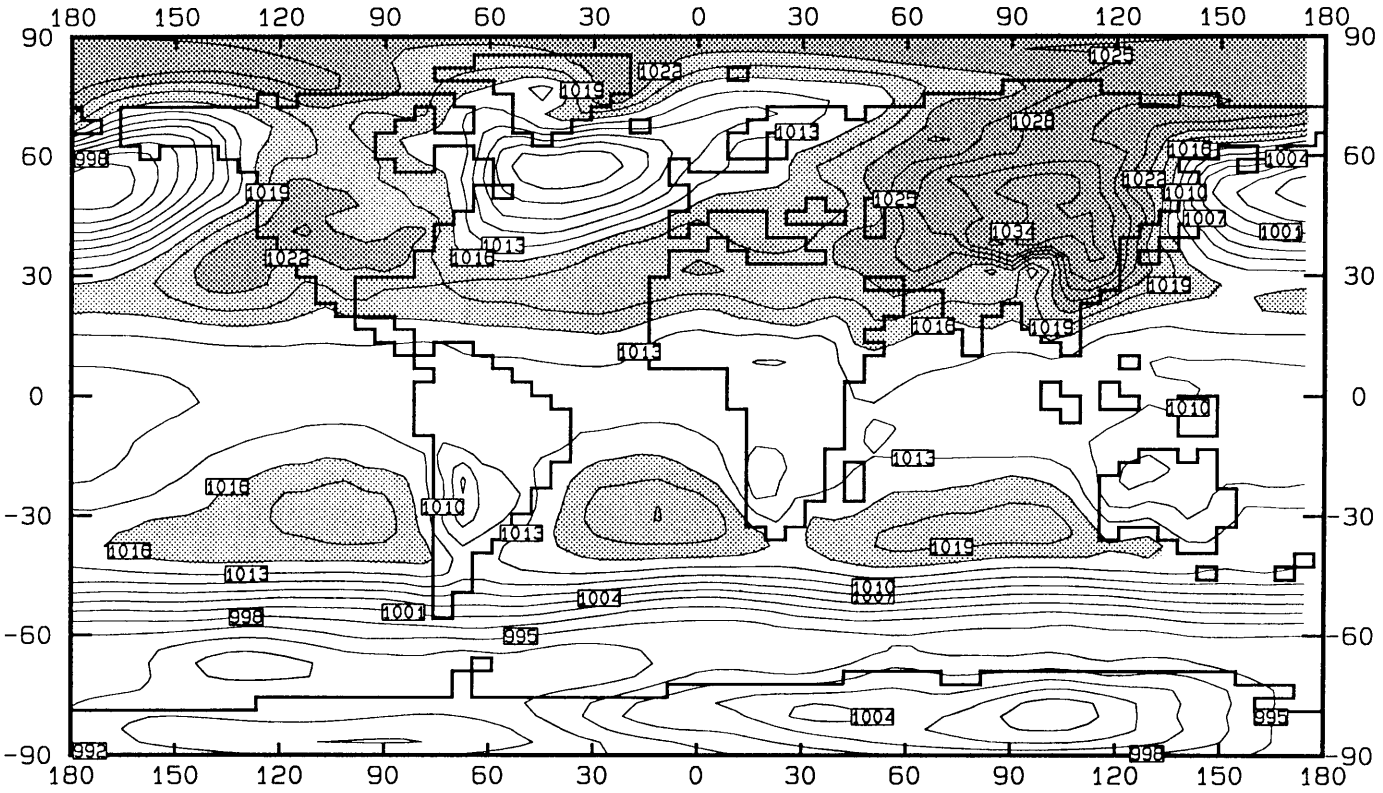

Figure 37(a): *Mean sea level pressure* (hPa) averaged over DJF as simulated by the CSIRO-9 AGCM using the **HYBRID** co-ordinate system. Pressure values higher than 1016 hPa are shaded.

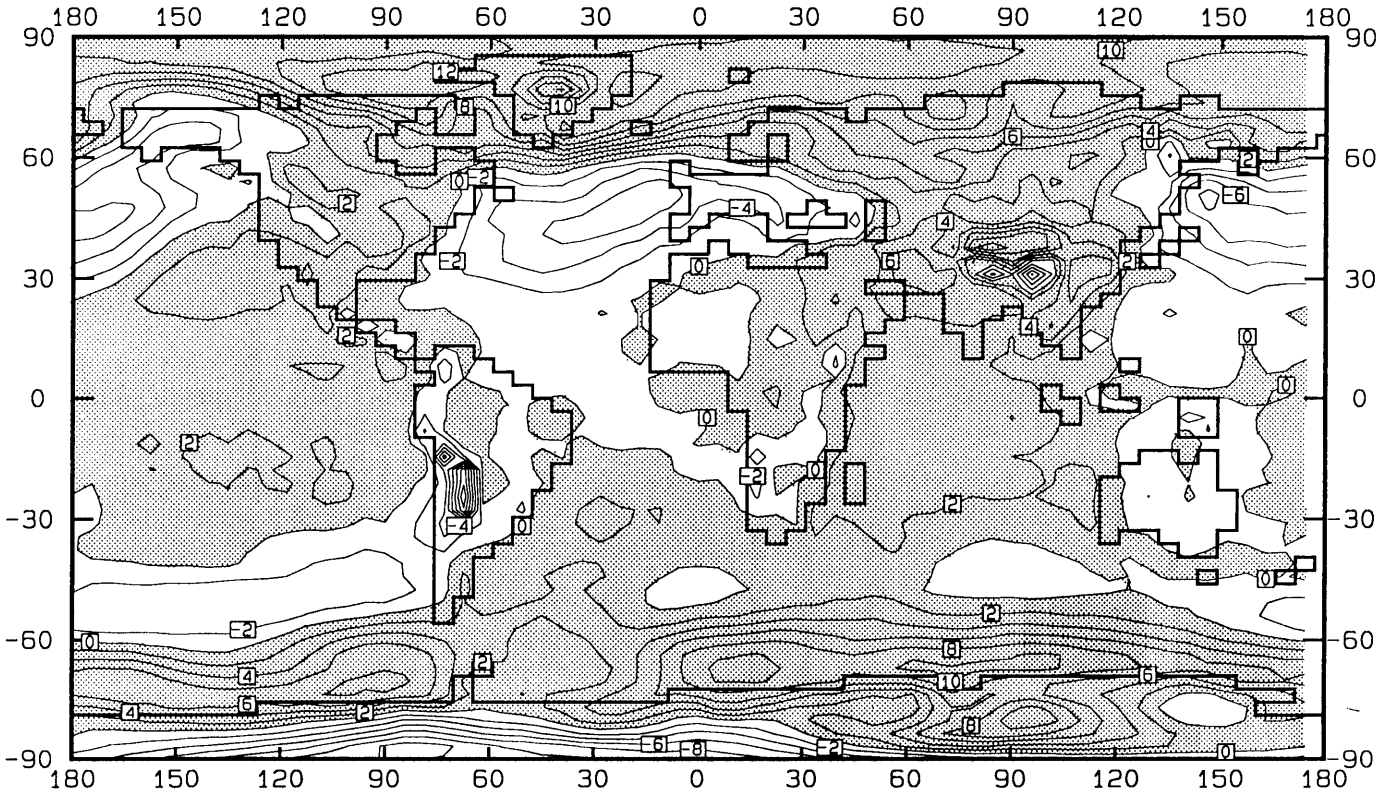

Figure 37(b): **HYBRID** simulations of figure 37(a) minus the corresponding **TOGA/ECMWF** analysis. Positive anomalies are shaded.

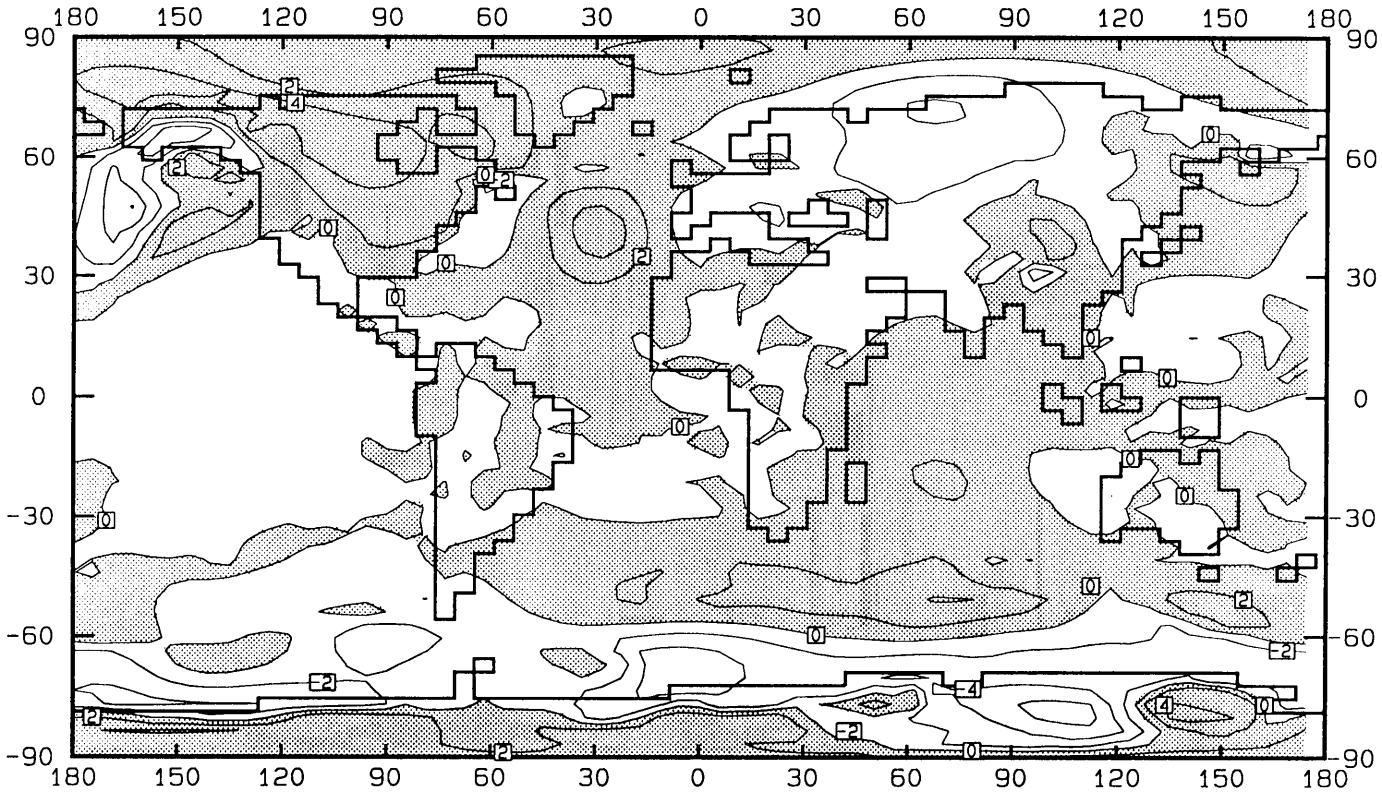

Figure 38: Differences between absolute deviations from the observed *sea-level pressure* (hPa) averaged over DJF. (**SIGMA** co-ordinate system deviations minus **HYBRID** co-ordinate system deviations). Shaded areas denote improvements by **HYBRID** co-ordinate system simulations.

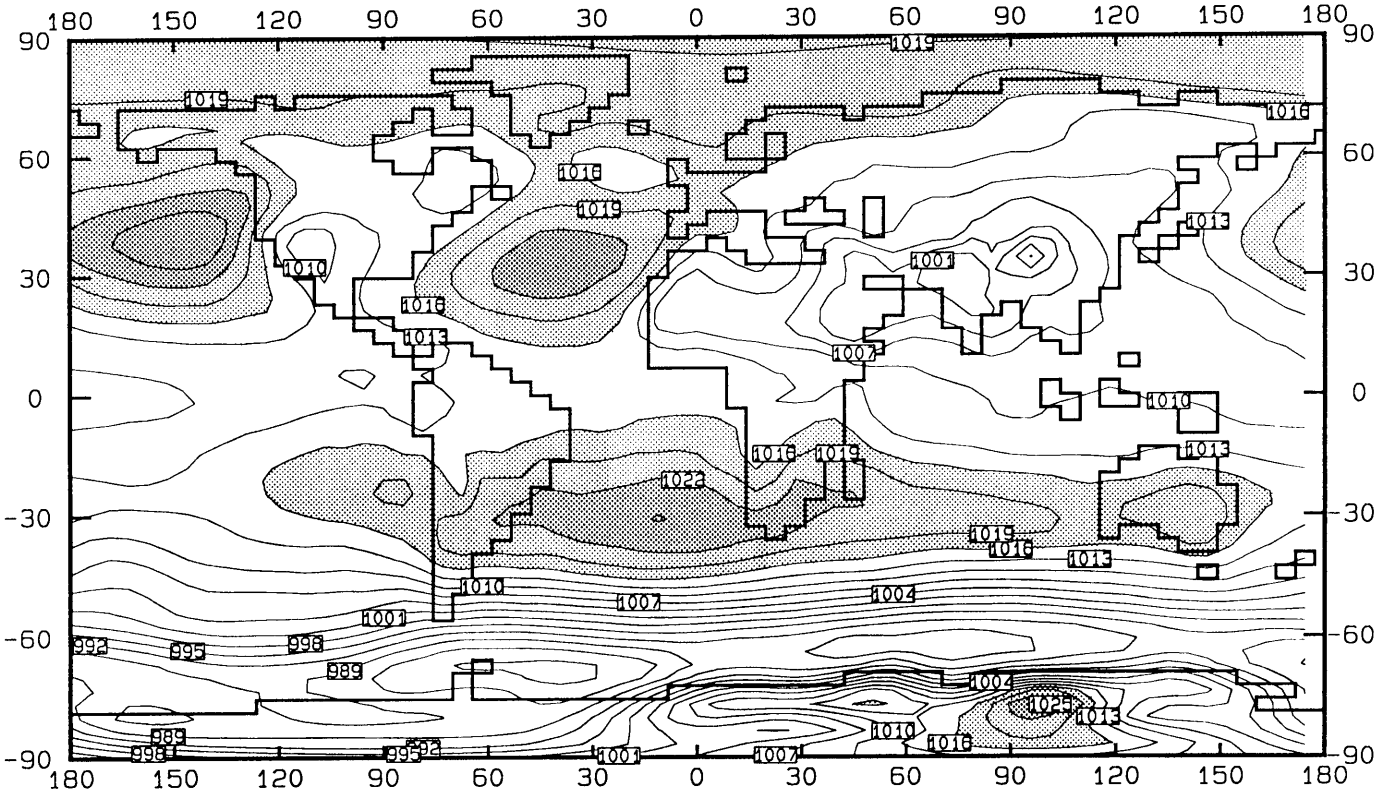

Figure 39(a): *Mean sea level pressure* (hPa) averaged over JJA as simulated by the CSIRO-9 AGCM using the **SIGMA** co-ordinate system. Pressure values higher than 1016 hPa are shaded.

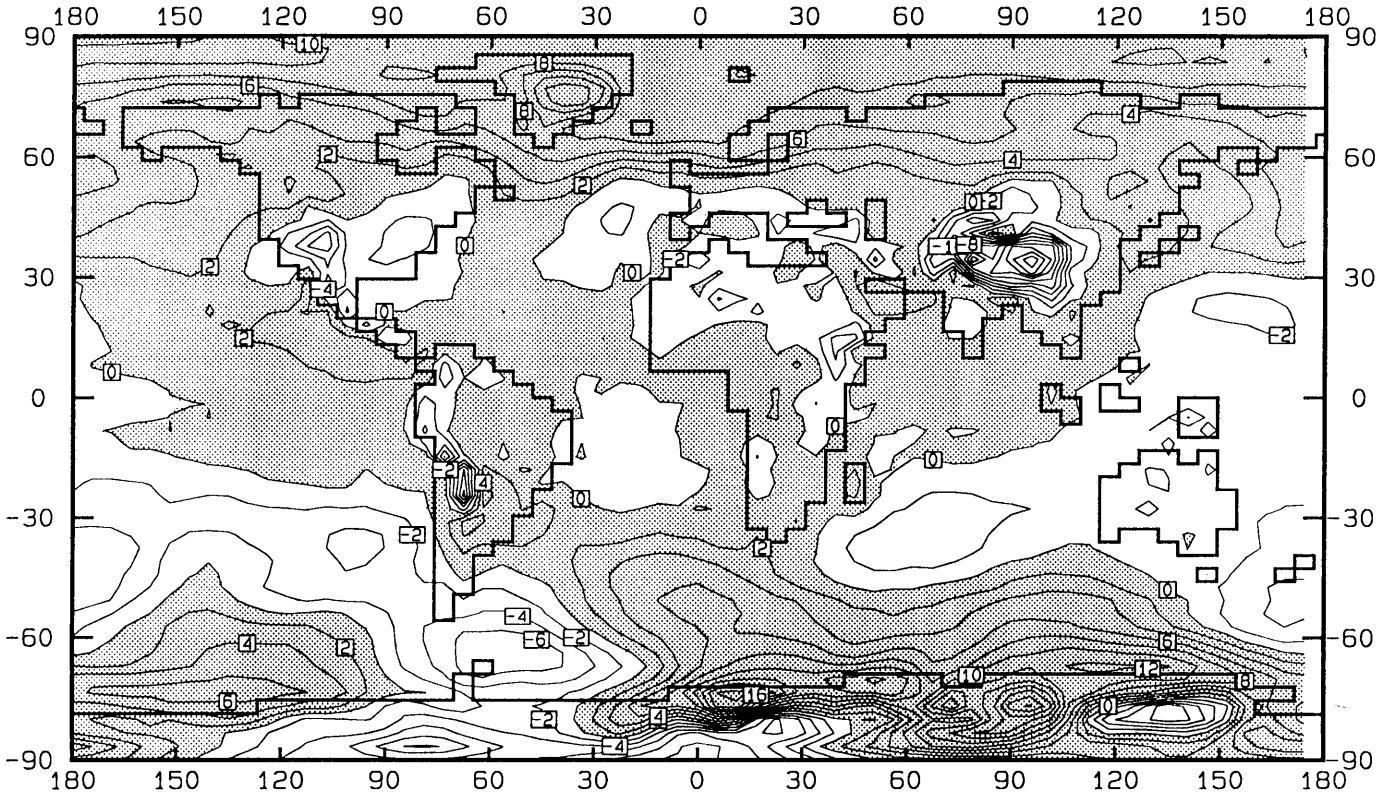

Figure 39(b): **SIGMA** simulations of figure 39(a) minus the corresponding **TOGA/ECMWF** analysis. Positive anomalies are shaded.

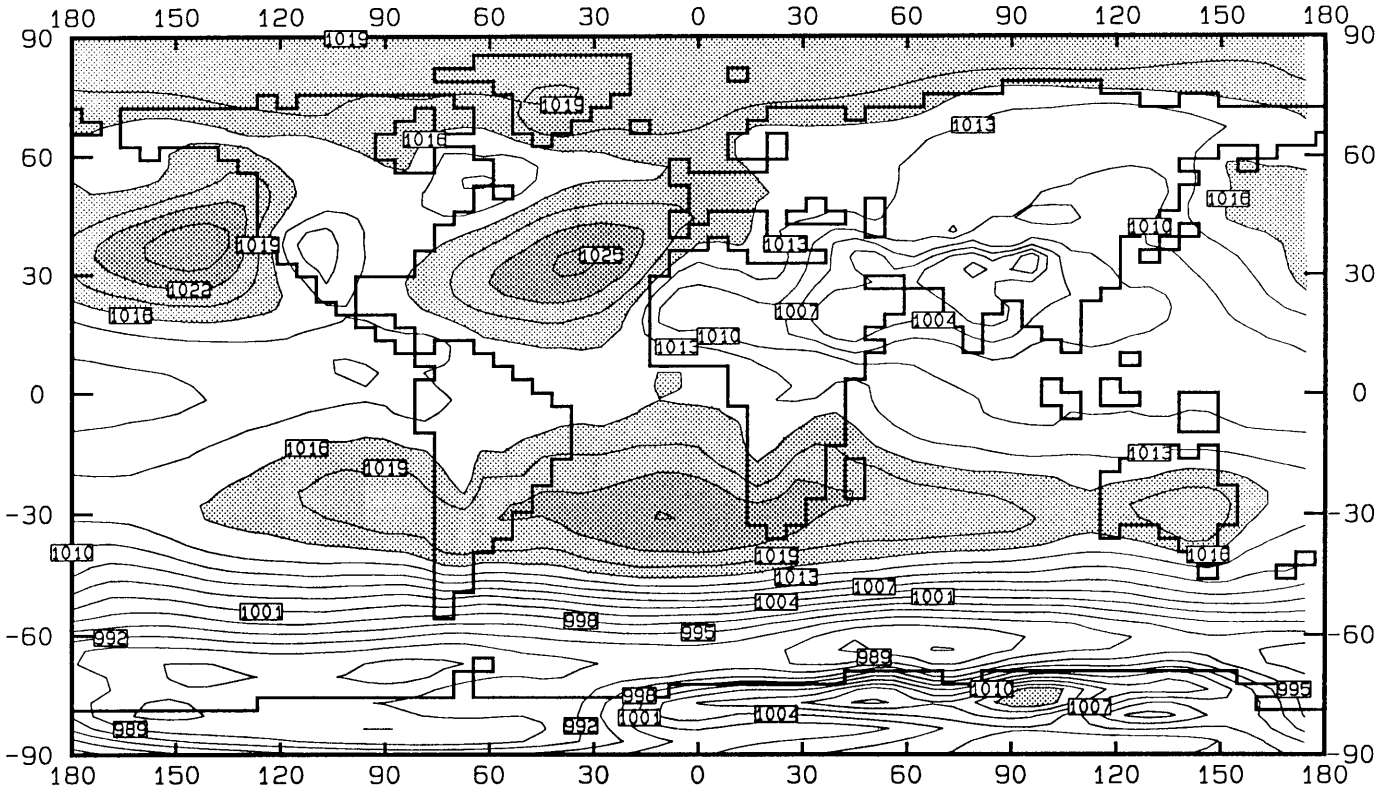

Figure 40(a): *Mean sea level pressure* (hPa) averaged over JJA as simulated by the CSIRO-9 AGCM using the **HYBRID** co-ordinate system. Pressure values higher than 1016 hPa are shaded.

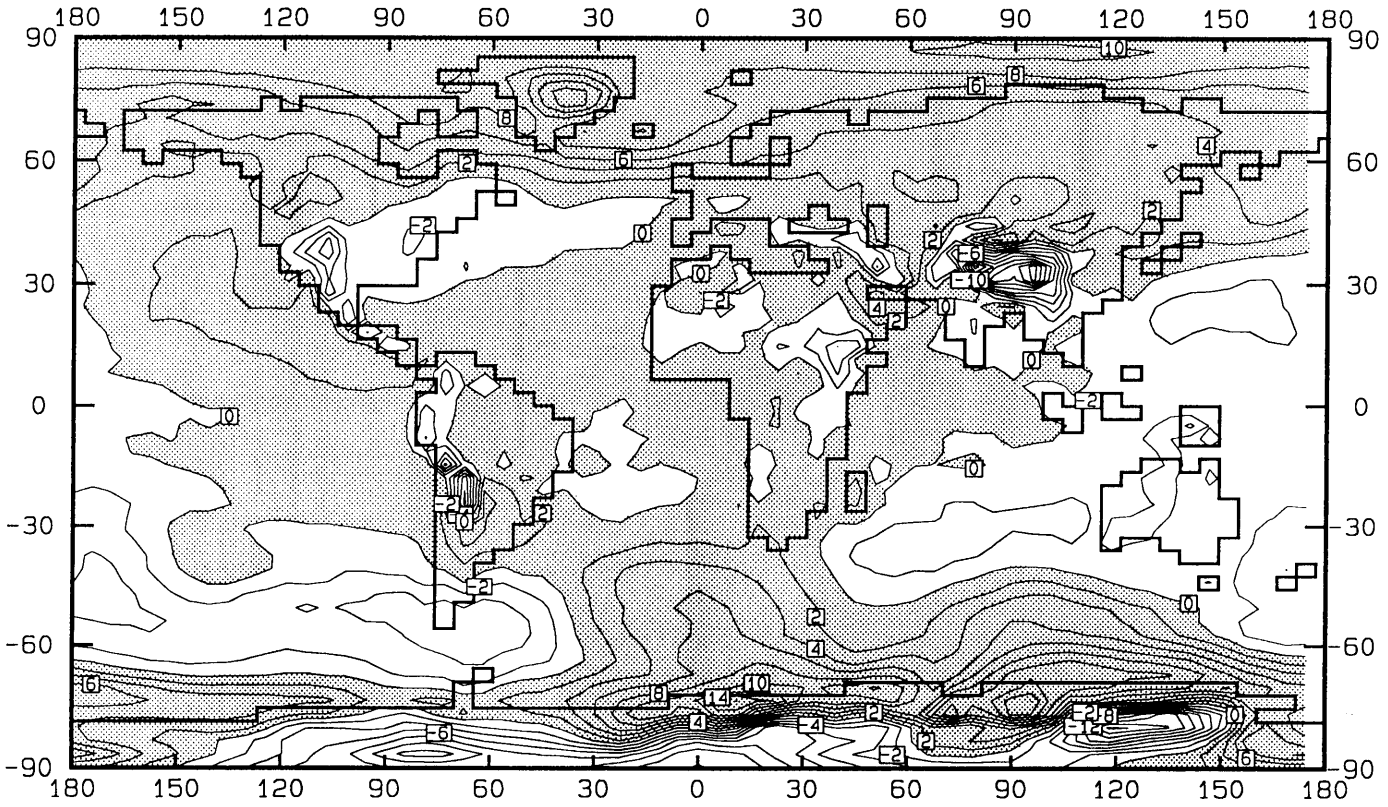

Figure 40(b): **HYBRID** simulations of figure 40(a) minus the corresponding **TOGA/ECMWF** analysis. Positive anomalies are shaded.

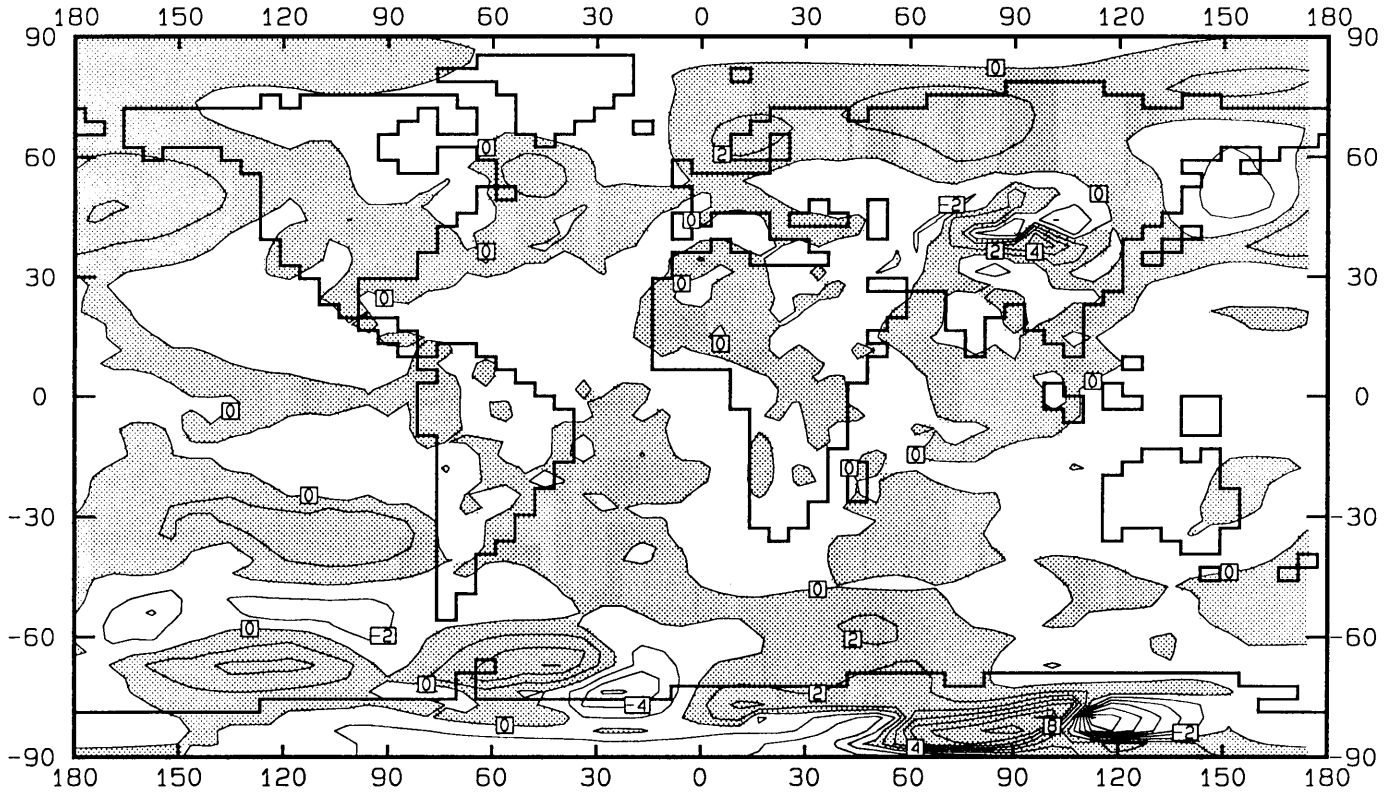

Figure 41: Differences between absolute deviations from the observed *sea-level pressure* (hPa) averaged over JJA. (**SIGMA** co-ordinate system deviations minus **HYBRID** co-ordinate system deviations). Shaded areas denote improvements by **HYBRID** co-ordinate system simulations.

CHAPTER 7

CONCLUSIONS

The primary objective of this study was to improve climate simulations generated by the CSIRO-9 (Mark II) AGCM at upper atmospheric model levels. To accomplish this, a hybrid vertical co-ordinate system (η-system) has been constructed in such a way that it converges to a sigma vertical co-ordinate system (or σ-system; $\sigma=p/P_S$) near the Earth's surface, while gradually changing to a pressure vertical co-ordinate system (or p- system) in the upper atmosphere. This involved the prescription of a number of co-ordinate conditions, which were solved by the use of matrix analysis, yielding a set of constant co-ordinate values at the ten model half-levels in the vertical.

The present model utilises a σ-system. The atmospheric equations, in flux formulation, have been converted to meet the requirements of a η-co-ordinate reference frame. During linearisation the linear components of the gravity wave generating terms have been expressed in a similar way to those used in the σ-system. For climate model simulations, it is vital that the total energy is conserved throughout the atmospheric system, especially when constructing the vertical discrete notation of the atmospheric equations. Specific energy conservation requirements applicable for the η-system were defined. The atmospheric equations in the η-system have been written in spectral form and were numerically solved (approximated) by using a semi-implicit leapfrog time integration.

Model simulated climatologies have been compiled by performing two five-year control runs - firstly with a σ-system model and secondly with a η-system model. Model simulated climatologies for the *zonal-* and *meridional winds*, *temperature* and *sea-level pressure* were obtained by calculating ensemble means using five ensemble members.

Both models adequately simulate the broader global climate patterns of the atmospheric variables considered. Model output fields generated by using the η-system showed significant improvements (relative to σ-system simulations) when compared with observed analyses (ECMWF, TOGA). This is particularly true for the upper troposphere and lower stratospheric levels contained in the model's atmosphere. Wind velocity improvements especially occur in the zonal wind components over high orography regions. These improvements are also, in general, more obvious over the summer hemisphere. η-system simulations have also improved model temperature fields in the upper troposphere and lower stratosphere. This is particularly true in the summer hemisphere where

significant improvements occur not only over high surface orography regions, but also over oceans. The formulation of the σ- and η-systems is identical at the surface of the earth, which results in small differences between the sea-level pressures simulated by the two co-ordinates. Large pressure anomalies over higher orography, which appear in both co-ordinate simulations, might be attributed to extrapolation from surface pressures to sea-level pressures.

The introduction of a hybrid vertical co-ordinate system undeniably contributed to improved climate model simulations in the upper levels of the atmosphere included in the CSIRO-9 AGCM. As part of this research, the computer code for the η-system has been incorporated as an option for use in present versions of the model.

APPENDIX A

Transformation of the dynamical atmospheric equations from a pressure- to a hybrid vertical co-ordinate system

A.1 INTRODUCTION

The *momentum, continuity* and *thermodynamic equations* are transformed from the conventional rotating *pressure* (or *isobaric*) *vertical co-ordinate system* (p-system as discussed in section 2.2) to the *hybrid vertical co-ordinate system* (η-system) as defined in Chapter 2. The derivation of the atmospheric equations for the η-system are similar to the *sigma vertical co-ordinate system* (σ-system ; $\sigma = p/P_S$) procedure followed by Holton (1992).

In the η-system the pressure value at each model half-level is defined as

$$p = A_O + P_S B \qquad \text{where} \qquad \mu = \frac{\partial p}{\partial \eta} = \frac{\partial A_O}{\partial \eta} + P_s \frac{\partial B}{\partial \eta}$$

Here $P_S = P_S(x,y,t)$. $A_O = A_O(\eta)$ and $B = B(\eta)$ are constants at each half-level.

Transformation from the p- to the η-system may be carried out by using the following diagram:

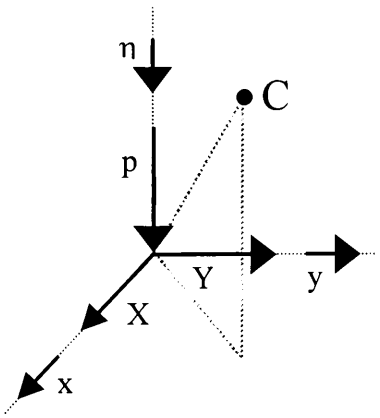

For any atmospheric variable A located at any point C in space the following applies:

$A = A\,(X, Y, p, \tau)$; p-system
$A = A\,(x, y, \eta, t)$; η-system

$x = X$
$y = Y$
$t = \tau$

Both the (X, Y, p, τ)- and (x, y, η, t) co-ordinate systems are orthogonal.

The partial x-derivative of variable A in the η-system may now be expressed as

$$\frac{\partial A}{\partial x} = \frac{\partial A}{\partial X}\frac{\partial X}{\partial x} + \frac{\partial A}{\partial Y}\frac{\partial Y}{\partial x} + \frac{\partial A}{\partial p}\frac{\partial p}{\partial x} + \frac{\partial A}{\partial \tau}\frac{\partial \tau}{\partial x} \qquad \text{replace } x = X \;;\; Y = y \;;\; \tau = t$$

$$= \frac{\partial A}{\partial X}\frac{\overbrace{\partial x}^{1}}{\partial x} + \frac{\partial A}{\partial Y}\frac{\overbrace{\partial y}^{0}}{\partial x} + \frac{\partial A}{\partial p}\frac{\partial p}{\partial x} + \frac{\partial A}{\partial \tau}\frac{\overbrace{\partial t}^{0}}{\partial x}$$

$$= \frac{\partial A}{\partial X} + \frac{\partial A}{\partial p}\frac{\partial p}{\partial x}$$

replace the relation

$$\frac{\partial A}{\partial p} = \frac{\partial A}{\partial \eta}\frac{\partial \eta}{\partial p} = \frac{\partial A}{\partial \eta}\frac{1}{\mu} = \frac{1}{\mu}\frac{\partial A}{\partial \eta} \qquad \textbf{(A.1)}$$

$$= \frac{\partial A}{\partial X} + \frac{1}{\mu}\frac{\partial A}{\partial \eta}\frac{\partial p}{\partial x}$$

which finally yields

$$\frac{\partial A}{\partial X} = \frac{\partial A}{\partial x} - \frac{1}{\mu}\frac{\partial A}{\partial \eta}\frac{\partial p}{\partial x} \qquad \textbf{(A.2)}$$

Similar follows for the partial y- and t-derivatives of A in the η-system that

$$\frac{\partial A}{\partial Y} = \frac{\partial A}{\partial y} - \frac{1}{\mu}\frac{\partial A}{\partial \eta}\frac{\partial p}{\partial y} \qquad \textbf{(A.3)}$$

$$\frac{\partial A}{\partial \tau} = \frac{\partial A}{\partial t} - \frac{1}{\mu}\frac{\partial A}{\partial \eta}\frac{\partial p}{\partial t} \qquad \textbf{(A.4)}$$

The partial X-, Y- and τ -derivatives of A in the p-system have been expressed in terms of the corresponding partial derivatives in the η-system. Equations **(A.2)** and **(A.3)** may be combined in the following vector expression

$$\underline{\nabla}_p = \underline{\nabla}_\eta - \frac{1}{\mu}\underline{\nabla}_\eta p\frac{\partial}{\partial \eta} \qquad \textbf{(A.5)}$$

where $\underline{\nabla}_p = \frac{\partial}{\partial X}\underline{i} + \frac{\partial}{\partial Y}\underline{j}$ and $\underline{\nabla}_\eta = \frac{\partial}{\partial x}\underline{i} + \frac{\partial}{\partial y}\underline{j}$ denotes the horizontal partial derivatives applied with the vertical components (p or η) held constant. The vectors $\underline{i}$ and $\underline{j}$ are unit vectors in the $X = x$ and $Y = y$ directions respectively.

The momentum equation is transformed from the p- to η-system by evaluating each one of the terms (**a**),(**b**),(**c**) and (**d**) individually.

(**a**) :

As indicated by equation **(A.6)** the *total* time (τ) derivative of velocity ($\underline{V}$) in the p-system ($\frac{d\underline{V}}{d\tau}$) may be replaced by the correspondent time (t) derivative in the η-system ($\frac{d\underline{V}}{dt}$) where $\underline{V} = \underline{V}(X, Y, p, \tau) = \underline{V}(x, y, \eta, t)$.

From equation **(A.6)** follows that

$$\frac{d\underline{V}}{d\tau} = \frac{d\underline{V}}{dt} = \frac{\partial \underline{V}}{\partial t} + \underline{V} \cdot \underline{\nabla}_\eta \underline{V} + \dot{\eta}\frac{\partial \underline{V}}{\partial \eta}$$

(**b**) :

Apply equation **(A.5)** to the *pressure gradient force* (**b**) :

$$\underline{\nabla}_p \Phi = \underline{\nabla}_\eta \Phi - \frac{1}{\mu}\underline{\nabla}_\eta p \frac{\partial \Phi}{\partial \eta}$$

By using the *hydrostatic approximation* ($\partial p = -\rho \partial \Phi$) as well as the *equation of state* ($p = \rho RT$) the second term on the right becomes

$$-\frac{1}{\mu}\underline{\nabla}_\eta p \frac{\partial \Phi}{\partial \eta} = -\frac{\partial \eta}{\partial p}\frac{\partial \Phi}{\partial \eta}\underline{\nabla}_\eta p = -\frac{\partial \Phi}{\partial p}\underline{\nabla}_\eta p = -\left\{-\frac{1}{\rho}\right\}\underline{\nabla}_\eta p = \frac{RT}{p}\underline{\nabla}_\eta p$$

Substituting this into (**b**) yields

$$\underline{\nabla}_p \Phi = \underline{\nabla}_\eta \Phi + \frac{RT}{p}\underline{\nabla}_\eta p$$

Replace $p = A_O + P_S B$ in the second term on the right

$$\frac{RT}{p}\underline{\nabla}_\eta p = \frac{RT}{(A_O + BP_S)}\underline{\nabla}_\eta (A_O + BP_S) = \frac{RTB}{(A_O + BP_S)}\underline{\nabla}_\eta P_S = \frac{RTB}{p}\underline{\nabla}_\eta P_S$$

which results in

$$\underline{\nabla}_p \Phi = \underline{\nabla}_\eta \Phi + \frac{RTB}{p}\underline{\nabla}_\eta P_S$$

(**c**) :

The unit vector $\underline{k}$ in the p-system is equivalent to the unit vector $\underline{k}$ in the η-system and therefore

$$f\underline{k}\times\underline{V} = (f\underline{k}\times\underline{V})_p = (f\underline{k}\times\underline{V})_\eta$$

The footnotes p and η refer to the co-ordinate system in which the term is evaluated.

(**d**) :

For the *friction forces* (**d**) apply

$$\underline{F} = \underline{F}_p = \underline{F}_\eta$$

The *momentum equation* in the η-system may therefore finally be expressed as:

$$\frac{\partial \underline{V}}{\partial t} + (\underline{V}\cdot\underline{\nabla}_\eta)\underline{V} + \dot{\eta}\frac{\partial \underline{V}}{\partial \eta} + \underline{\nabla}_\eta\Phi + \frac{RTB}{p}\underline{\nabla}_\eta P_S + f\underline{k}\times\underline{V} = \underline{F} \qquad \textbf{(A.8)}$$

A.3 Continuity Equation

The *continuity equation* in the p-system (Holton, 1992) is:

$$\underline{\nabla}_p\cdot\underline{V} + \frac{\partial\omega}{\partial p} = 0$$

(**a**) (**b**)

The *continuity equation* may also be transformed from the p- to η-system by evaluating each term individually.

(**a**) :

Apply equation **(A.5)** and replace $p = A_O + P_S B$; $A_O = A_O(\eta)$ and $B = B(\eta)$

$$\underline{\nabla}_p\cdot\underline{V} = \underline{\nabla}_\eta\cdot\underline{V} - \frac{1}{\mu}\underline{\nabla}_\eta\cdot p\frac{\partial \underline{V}}{\partial\eta} = \underline{\nabla}_\eta\cdot\underline{V} - \frac{1}{\mu}\underline{\nabla}_\eta\cdot(A_O + P_S B)\frac{\partial \underline{V}}{\partial\eta} = \underline{\nabla}_\eta\cdot\underline{V} - \frac{B}{\mu}\underline{\nabla}_\eta\cdot P_S\frac{\partial \underline{V}}{\partial\eta}$$

(**b**) :

From equation **(A.6)** and $p = A_O + P_S B$ follows that the *vertical velocity* in the p-system can be expressed as

$$\omega = \frac{dp}{dt} = \frac{d}{dt}(A_O + BP_S) = \frac{dA_O}{dt} + \frac{d(BP_S)}{dt} = \frac{dA_O}{dt} + B\frac{dP_S}{dt} + P_S\frac{dB}{dt}$$

Replace ω in term (**b**)

$$\frac{\partial\omega}{\partial p} = \frac{\partial}{\partial p}\left\{\frac{dA_O}{dt} + B\frac{dP_S}{dt} + P_S\frac{dB}{dt}\right\}$$

The combination of (**a**) and (**b**) results in the following formulation of *the continuity equation* in the η-system

$$\underline{\nabla}_\eta \cdot \underline{V} - \frac{B}{\mu}\underline{\nabla}_\eta \cdot P_S\frac{\partial \underline{V}}{\partial\eta} + \frac{\partial}{\partial p}\left\{\frac{dA_O}{dt} + B\frac{dP_S}{dt} + P_S\frac{dB}{dt}\right\} = 0$$

Replacement of $\frac{dA_O}{dt}$ and $\frac{dB}{dt}$ as defined in equation **(A.7)** give

$$\underline{\nabla}_\eta \cdot \underline{V} - \frac{B}{\mu}\underline{\nabla}_\eta \cdot P_S\frac{\partial \underline{V}}{\partial\eta} + \frac{\partial}{\partial p}\left\{\dot\eta\frac{\partial A_O}{\partial\eta} + B\frac{dP_S}{dt} + P_S\dot\eta\frac{\partial B}{\partial\eta}\right\} = 0$$

Using the relation $\frac{\partial}{\partial p} = \frac{\partial\eta}{\partial p}\frac{\partial}{\partial\eta} = \frac{1}{\mu}\frac{\partial}{\partial\eta}$ yields

$$\underline{\nabla}_\eta \cdot \underline{V} - \frac{B}{\mu}\underline{\nabla}_\eta \cdot P_S\frac{\partial \underline{V}}{\partial\eta} + \frac{1}{\mu}\frac{\partial}{\partial\eta}\left\{\dot\eta\frac{\partial A_O}{\partial\eta} + B\frac{dP_S}{dt} + P_S\dot\eta\frac{\partial B}{\partial\eta}\right\} = 0$$

The surface pressure (P_S) is not a function of η and therefore

$$\underline{\nabla}_\eta \cdot \underline{V} - \frac{B}{\mu}\frac{\partial}{\partial\eta}(\underline{\nabla}_\eta \cdot P_S\underline{V}) + \frac{1}{\mu}\frac{\partial}{\partial\eta}\left\{\dot\eta\frac{\partial A_O}{\partial\eta} + B\frac{dP_S}{dt} + P_S\dot\eta\frac{\partial B}{\partial\eta}\right\} = 0$$

$$\underline{\nabla}_\eta \cdot \underline{V} - \frac{B}{\mu}\frac{\partial}{\partial\eta}(\underline{\nabla}_\eta \cdot P_S\underline{V}) + \frac{1}{\mu}\frac{\partial}{\partial\eta}\left\{\dot\eta\frac{\partial A_O}{\partial\eta}\right\} + \frac{B}{\mu}\frac{\partial}{\partial\eta}\left\{\frac{dP_S}{dt}\right\} + \frac{1}{\mu}\frac{dP_S}{dt}\frac{\partial B}{\partial\eta} + \frac{1}{\mu}\frac{\partial}{\partial\eta}\left\{P_S\dot\eta\frac{\partial B}{\partial\eta}\right\} = 0$$

(a) **(b)**

(A.9)

Applying equation **(A.6)** and $P_S = P_S(x,y,t)$ the *total* time (t) derivative of surface pressure may be expressed as $\frac{dP_S}{dt} = \frac{\partial P_S}{\partial t} + \underline{V} \cdot \underline{\nabla}_\eta P_S$

Term (**b**) in equation **(A.9)** therefore becomes

$$\frac{B}{\mu}\frac{\partial}{\partial \eta}\left\{\frac{dP_S}{dt}\right\} = \frac{B}{\mu}\frac{\partial}{\partial \eta}\frac{\partial P_S}{\partial t} + \frac{B}{\mu}\frac{\partial}{\partial \eta}(\underline{V} \cdot \underline{\nabla}_\eta P_S)$$

$$= \frac{B}{\mu}\frac{\partial}{\partial t}\frac{\partial P_S}{\partial \eta} + \frac{B}{\mu}\frac{\partial}{\partial \eta}(\underline{V} \cdot \underline{\nabla}_\eta P_S) \qquad \text{where} \quad \frac{\partial P_S}{\partial \eta} = 0$$

$$= \frac{B}{\mu}\frac{\partial}{\partial \eta}(\underline{\nabla}_\eta P_S \cdot \underline{V})$$

This is an expression equal to term (**a**) in equation **(A.9)** but of opposite in sign. After rearranging the remaining terms equation **(A.9)** becomes

$$\underline{\nabla}_\eta \cdot \underline{V} + \frac{1}{\mu}\frac{dP_S}{dt}\frac{\partial B}{\partial \eta} + \left[\frac{1}{\mu}\frac{\partial}{\partial \eta}\left\{\dot{\eta}\frac{\partial A_O}{\partial \eta}\right\} + \frac{1}{\mu}\frac{\partial}{\partial \eta}\left\{P_S\dot{\eta}\frac{\partial B}{\partial \eta}\right\}\right] = 0$$

Multiply each term by μ

$$\mu\underline{\nabla}_\eta \cdot \underline{V} + \frac{dP_S}{dt}\frac{\partial B}{\partial \eta} + \left[\frac{\partial}{\partial \eta}\left\{\dot{\eta}\frac{\partial A_O}{\partial \eta}\right\} + \frac{\partial}{\partial \eta}\left\{P_S\dot{\eta}\frac{\partial B}{\partial \eta}\right\}\right] = 0 \qquad \textbf{(A.10)}$$

(**a**) (**b**) (**c**)

The two terms in (**c**) of equation **(A.10)** may be simplified

$$\frac{\partial}{\partial \eta}\left\{\dot{\eta}\frac{\partial A_O}{\partial \eta}\right\} + \frac{\partial}{\partial \eta}\left\{P_S\dot{\eta}\frac{\partial B}{\partial \eta}\right\}$$

$$= \frac{\partial}{\partial \eta}\left[\dot{\eta}\left\{\frac{\partial A_O}{\partial \eta} + P_S\frac{\partial B}{\partial \eta}\right\}\right] \qquad \text{but } \mu = \left\{\frac{\partial A_O}{\partial \eta} + P_S\frac{\partial B}{\partial \eta}\right\}$$

$$= \frac{\partial}{\partial \eta}(\dot{\eta}\mu)$$

Terms (**a**) and (**b**) in equation **(A.10)** are

$$\mu\underline{\nabla}_\eta\cdot\underline{V}+\frac{dP_s}{dt}\frac{\partial B}{\partial\eta}$$

Apply equation **(A.6)** with $P_s = P_s(x,y,t)$

$$=\mu\underline{\nabla}_\eta\cdot\underline{V}+\left\{\frac{\partial P_s}{\partial t}+\underline{V}\cdot\underline{\nabla}_\eta P_s\right\}\frac{\partial B}{\partial\eta}$$

$$=\mu\underline{\nabla}_\eta\cdot\underline{V}+\frac{\partial B}{\partial\eta}\frac{\partial P_s}{\partial t}+\frac{\partial B}{\partial\eta}\underline{V}\cdot\underline{\nabla}_\eta P_s$$

$$=\mu\underline{\nabla}_\eta\cdot\underline{V}+\frac{\partial}{\partial t}\left\{P_s\frac{\partial B}{\partial\eta}\right\}-P_s\frac{\partial}{\partial t}\left\{\frac{\partial B}{\partial\eta}\right\}+\underline{V}\cdot\underline{\nabla}_\eta\left\{P_s\frac{\partial B}{\partial\eta}\right\}-\underline{V}\cdot P_s\underline{\nabla}_\eta\left\{\frac{\partial B}{\partial\eta}\right\}$$

Since $B = B(\eta)$ we have $P_s\dfrac{\partial}{\partial t}\left\{\dfrac{\partial B}{\partial\eta}\right\}=0$ and $\underline{V}\cdot P_s\underline{\nabla}_\eta\left\{\dfrac{\partial B}{\partial\eta}\right\}=0$.

Terms (**a**) and (**b**) in equation **(A.10)** may therefore be simplified to

$$=\mu\underline{\nabla}_\eta\cdot\underline{V}+\frac{\partial}{\partial t}\left\{P_s\frac{\partial B}{\partial\eta}\right\}+\underline{V}\cdot\underline{\nabla}_\eta\left\{P_s\frac{\partial B}{\partial\eta}\right\}$$

noting that $A_O = A_O(\eta)$

$$=\mu\underline{\nabla}_\eta\cdot\underline{V}+\frac{\partial}{\partial t}\left\{\frac{\partial A_O}{\partial\eta}+P_s\frac{\partial B}{\partial\eta}\right\}+\underline{V}\cdot\underline{\nabla}_\eta\left\{\frac{\partial A_O}{\partial\eta}+P_s\frac{\partial B}{\partial\eta}\right\}$$

where $\mu=\dfrac{\partial A_O}{\partial\eta}+P_s\dfrac{\partial B}{\partial\eta}$

$$=\mu\underline{\nabla}_\eta\cdot\underline{V}+\frac{\partial\mu}{\partial t}+\underline{V}\cdot\underline{\nabla}_\eta\mu$$

$$=\frac{\partial\mu}{\partial t}+\underline{\nabla}_\eta\cdot\{\mu\underline{V}\}$$

Substitution into terms (**a**), (**b**) and (**c**) from equation **(A.10)** provides the *continuity* equation in the η-system.

$$\boxed{\frac{\partial\mu}{\partial t}+\underline{\nabla}_\eta\cdot(\mu\underline{V})+\frac{\partial}{\partial\eta}(\mu\dot{\eta})=0}\qquad\textbf{(A.11)}$$

A.4 Thermodynamic Energy Equation

From the *thermodynamic energy* equation in the p-system (Holton, 1992) follows

$$\frac{dT}{dt} = \frac{1}{\rho}\frac{\omega}{c_P} + \frac{Q}{c_P}$$

Substitute the *equation of state* ($\frac{1}{\rho} = \frac{RT}{p}$) and replace ($K = \frac{R}{c_P}$)

$$\frac{dT}{dt} = K\frac{T\omega}{p} + \frac{Q}{c_P}$$

(**a**)

The *thermodynamic energy* equation is transformed from the p- to η-system by evaluating term (**a**). The remaining terms are identical for both systems.

(**a**) :

The *total* time (τ) derivative in the p-system ($\frac{dT}{d\tau}$) may be replaced by the *total* time (t) derivative in the η-system where $T = T(x,y,\eta,t)$.

From equation **(A.6)** it follows that

$$\frac{dT}{d\tau} = \frac{dT}{dt} = \frac{\partial T}{\partial t} + \underline{V}\cdot\underline{\nabla}_\eta T + \dot{\eta}\frac{\partial T}{\partial \eta}$$

The *thermodynamic energy* equation (subsequently also refer to as the *thermodynamic* equation) in the η-system becomes

$$\boxed{\frac{\partial T}{\partial t} + \underline{V}\cdot\underline{\nabla}_\eta T + \dot{\eta}\frac{\partial T}{\partial \eta} = \frac{KT\omega}{p} + \frac{Q}{c_P}} \qquad \text{with} \quad p = A_O + P_S B \qquad \textbf{(A.12)}$$

A.5 Moisture Equation

The prognostic equation for humidity (q) may be written as

$$\frac{dq}{dt} = S_q$$

Here (S_q) is the source / sink term of water vapour, and includes horizontal and vertical mixing terms.

For the η–system equation **(A.6)** yields

$$\frac{dT}{d\tau} = \frac{dT}{dt} = \frac{\partial T}{\partial t} + \underline{V} \cdot \underline{\nabla}_\eta T + \dot{\eta}\frac{\partial T}{\partial \eta}$$

and the *moisture* equation in the η-system becomes

$$\frac{\partial q}{\partial t} + \underline{V} \cdot \underline{\nabla}_\eta q + \dot{\eta}\frac{\partial q}{\partial \eta} = S_q \qquad \textbf{(A.13)}$$

APPENDIX B

Fortran code for solving the co-ordinate condition matrix

The code of a *Fortran* program developed to solve the functions $A_O(\eta)$ and $B(\eta)$ for each hybrid HALF-level is listed below. The subroutine (*gaussj)* from Press *et.al* (1992) was used to solve the *co-ordinate condition matrix* from section 2.7.

For consisentcy, and energy conservation, the derivatives

$$\frac{\partial A_O}{\partial \eta} \text{ and } \frac{\partial B}{\partial \eta}$$

at FULL-levels must be computed from HALF-level values of $A_O(\eta)$ and $B(\eta)$.

```
      programme vertc

c**** neq = number of conditions or matrix equations.
c**** nl  = number of full-levels, nlp = nl+1 = number of half-levels.
      parameter (neq=10,neq2=neq/2,nlp=10,nl=9)
      real c(neq,1),mat(neq,neq)
      real anh(nlp),bnh(nlp),anf(nl),bnf(nl)
      real dadnf(nl),dbdnf(nl)
      real hybh(nlp),hyb(nl)
      real alpha,alpha0,alpha1
      real Poo,ptm2,suma,sumb
      real dapbdn

c*************************************************************
c**** This program compute hybrid vertical co-ordinate functions A(n), B(n)  ****
c**** and dA/dn, dB/dn derivatives for CSIRO-9 (Mark II) AGCM level          ****
c**** spacing (9 levels):                                                   ****
c**** A(n),B(n) - at half levels and dA/dn,dB/dn,B(n) - at full levels.      ****
c**** ------------------------------------------------------------------     ****
c**** The pressure at level n is defined by                                 ****
c**** p(n,Ps) = Ao(n) + Ps x B(n);                                          ****
c**** Ps=surface pressure,Poo=MSLP=1013.2                                   ****
c*************************************************************
```

```
c**** General Smagorinsky formula for hybrid half-levels
      do k=1,nlp
      hybh(k)=(nl+1-k)**2*(nl-2+2.*k)/nl**3
      enddo
c**** Average hybrid half-levels to obtain hybrid full-levels
      do k=1,nl
      hyb(k)=0.5*(hybh(k)+hybh(k+1))
      enddo

c**** Global mean sea-level pressure (MSLP)
      Poo=1013.2

c**** Thickness of half-level (nlp-2) which is constant pressure
      ptm2=Poo*hybh(nlp-2)

c**** Ratio between thickness over highest orography and thickness over lowest orography
c**** (Atmospheric thickness above 500mb) = alpha*(Atmospheric thickness above
c****1013.2mb)
      alpha=(500.0-ptm2)/(Poo-ptm2)

c**** Constants with alpha  (for improved level thicknesses: alpha * 0.5 is used)
      alpha=alpha*0.5
      alpha1=alpha*Poo-500.0
      alpha0=(1.0-alpha)

c**** Set matrics =0
      do 10 j=1,neq
     do 10 l=1,neq
10    mat(i,j)=0.0

c**** PRE-DEFINED CONDITIONS FOR HYBRID CO-ORDINATES

c**** CONDITION 1 (hybh=1 on surface)
      do 12 j=1,neq2
12    mat(1,j)=hybh(1)**j
      c(1,1)=0.0

c**** CONDITION 2
      do 14 j=1,neq2
14    mat(2,j+neq2)=hybh(1)**j
      c(2,1)=1.0

c**** CONDITION 3
      do 16 j=1,neq2
```

```
16      mat(3,j+neq2)=hybh(nlp-1)**j
        c(3,1)=0.0
c**** CONDITION 4
        do 18 j=1,neq2
18      mat(4,j+neq2)=hybh(nlp-2)**j
        c(4,1)=0.0

c**** CONDITION 5
        do 22 j=1,neq2
22      mat(5,j)=hybh(nlp-1)**j
        c(5,1)=Poo*hybh(nlp-1)

c**** CONDITION 6
        do 24 j=1,neq2
24      mat(6,j) =hybh(nlp-2)**j
        c(6,1)=Poo*hybh(nlp-2)

c**** CONDITION 7
        do 26 j=1,neq2
        mat(7,j)=-alpha0*(hybh(2)**j)
26      mat(7,j+neq2)=alpha1*(hybh(2)**j)
        c(7,1)=alpha1

c**** CONDITION 8
        do 28 j=1,neq2
        mat(8,j)=alpha0*(hybh(2)**j-hybh(3)**j)
28      mat(8,j+neq2)=-alpha1*(hybh(2)**j-hybh(3)**j)
        c(8,1)=0.0

c**** CONDITIONS 9 and 10
        if(nl.eq.9)i=5
        if(nl.eq.18)i=9
        do 30 j=1,neq2
        mat(9,j)=hybh(i)**j
30      mat(9,j+neq2)=Poo*(hybh(i)**j)
        c(9,1)=Poo*hybh(i)

        if(nl.eq.9)i=7
        if(nl.eq.18)i=13
        do 32 j=1,neq2
        mat(10,j)=hybh(i)**j
32      mat(10,j+neq2)=Poo*(hybh(i)**j)
        c(10,1)=Poo*hybh(i)
```

```
c**** CO-ORDINATE CONDITION MATRIX SOLUTION: mat(i,j)*xx(i,1) = c(i,1)
      call gaussj(mat,neq,neq,c,1,1)

c**** MATRIX c(i,1) ARE REPLACED BY THE SOLUTION xx(i,1)

c**** A=anh(k) and B=bnh(k) at each hybrid half-level
      do 34 k=1,nlp
      suma=0.0
      sumb=0.0
      do 36 j=1,neq2
      suma=suma+c(j,1)*(hybh(k)**j)
36    sumb=sumb+c(j+neq2,1)*(hybh(k)**j)
      anh(k)=suma
      bnh(k)=sumb
      apb=suma+sumb
34    continue

c**** Set A(half-level 1) = 0.0, B(half-level 1) = 1.0,
c**** B(half-levels 8,9) = 0.0 as defined in conditions 1,3,4
      anh(1)=0.000000000000E+00
      bnh(1)=1.000000000000E+00
      bnh(nlp-1)=0.000000000000E+00
      bnh(nlp-2)=0.000000000000E+00

c**** For consisentcy, and energy conservation, the values
c**** at FULL-levels must be computed from HALF-level values
      do 38 k=1,nl
      anf(k)=0.5*(anh(k)+anh(k+1))
      bnf(k)=0.5*(bnh(k)+bnh(k+1))
      dadnf(k)=(anh(k)-anh(k+1))/(hybh(k)-hybh(k+1))
      dbdnf(k)=(bnh(k)-bnh(k+1))/(hybh(k)-hybh(k+1))
c**** dapbdn must be close to Poo
      dapbdn=dadnf(k)+dbdnf(k)
38    continue

c**** Print the results
      do k=1,nlp
      print*,hybh(k),anh(k),bnh(k),(dapbdn)
      enddo
      end
```

```
      subroutine gaussj(a,n,np,b,m,mp)

c**** Subroutine was obtained from Press et.al (1992)

      integer m,mp,n,np,nmax
      real a(np,np),b(np,mp)
      parameter (nmax=50)
      integer i,icol,irow,j,k,l,ll,indxc(nmax),indxr(nmax),ipiv(nmax)
      real big,dum,pivinv
      do 11 j=1,n
      ipiv(j)=0
11    continue
      do 22 i=1,n
      big=0.
      do 13 j=1,n
      if(ipiv(j).ne.1)then
      do 12 k=1,n
      if (ipiv(k).eq.0) then
      if (abs(a(j,k)).ge.big)then
      big=abs(a(j,k))
      irow=j
      icol=k
      endif
      else if (ipiv(k).gt.1) then
      pause 'singular matrix in gaussj'
      endif
12    continue
      endif
13    continue
      ipiv(icol)=ipiv(icol)+1
      if (irow.ne.icol) then
      do 14 l=1,n
      dum=a(irow,l)
      a(irow,l)=a(icol,l)
      a(icol,l)=dum
14    continue
      do 15 l=1,m
      dum=b(irow,l)
      b(irow,l)=b(icol,l)
      b(icol,l)=dum
15    continue
      endif
```

```
      indxr(i)=irow
      indxc(i)=icol
      if (a(icol,icol).eq.0.) pause 'singular matrix in gaussj'
      pivinv=1./a(icol,icol)
      a(icol,icol)=1.

      do 16 l=1,n
      a(icol,l)=a(icol,l)*pivinv
16    continue
      do 17 l=1,m
      b(icol,l)=b(icol,l)*pivinv
17    continue
      do 21 ll=1,n
      if(ll.ne.icol)then
      dum=a(ll,icol)
      a(ll,icol)=0.
      do 18 l=1,n
      a(ll,l)=a(ll,l)-a(icol,l)*dum
18    continue
      do 19 l=1,m
      b(ll,l)=b(ll,l)-b(icol,l)*dum
19    continue
      endif
21    continue
22    continue
      do 24 l=n,1,-1
      if(indxr(l).ne.indxc(l))then
      do 23 k=1,n
      dum=a(k,indxr(l))
      a(k,indxr(l))=a(k,indxc(l))
      a(k,indxc(l))=dum
23    continue
      endif
24    continue
      return
      end
```

APPENDIX C

Geopotential as a function of the vertical profile of temperature

C.1 INTRODUCTION

By using the *hydrostatic approximation*, each one of the *geopotential* variables (ϕ, ϕ' and ϕ_O as defined in section 3.3) can be expressed as a function of the vertical profile of *temperature*. In this appendix the functions, which relate geopotentials to temperatures, are derived for the σ- as well as the η-system.

Brief details are outlined to show why it is necessary to have a modified semi-implicit treatment in the η-system (relative to the σ-system) of the geopotential term ($\hat{\phi}$) as appearing in the *divergence* equation **(3.10)**.

The semi-implicit time integration of the atmospheric equations requires that the gravity wave generating terms linking the *thermodynamic* **(3.18)**, *divergence* **(3.10)** and *surface-pressure tendency* **(3.15)** equations be treated implicitly (Gordon; 1981).

The *divergence* equation **(3.10)** is

$$\frac{\partial \hat{D}}{\partial t} = NL_D - RT_O \underline{\nabla}^2 P_S - \underline{\nabla}^2 \hat{\phi}$$

The *thermodynamic* equation **(3.18)** is

$$\frac{\partial \hat{T}}{\partial t} = NL_T - \frac{KT_O}{i}[\hat{D}]^i \qquad \text{for} \quad i = \sigma \text{ or } \eta$$

NL_D and NL_T denote some non-linear terms in the *divergence*- and *thermodynamic* equations respectively. Unlike the linear gravity wave generating components, these non-linear terms are treated explicitly through the usual grid transform method.

The *surface-pressure tendency* equation **(3.15)** is given by

$$\frac{\partial P_s}{\partial t} = -[\hat{D}]^1$$

The *divergence* equation is linked to the *thermodynamic* equation through $\hat{\phi}$, since it is required that $\hat{\phi}$ is directly related to $\hat{T}$ through the *hydrostatic* equation **(C.1)**. For an implicit method it is necessary that $\hat{\phi}$ is related, in the vertical sense, to $\hat{T}$ by means of a vector-matrix in the form $\underline{\hat{\phi}} = \underline{\underline{A}}\,\underline{\hat{T}}$, where the vectors $\underline{\hat{\phi}}$ and $\underline{\hat{T}}$ represents the vertical levels per horizontal spectral element. Details of this method may be found in Gordon (1981).

This method turns out to be straightforward in the σ-system since the *hydrostatic* equation (see equation **(C.5)**) gives $\frac{\partial \phi'}{\partial(\ln\sigma)} = -RT'$ from which $\frac{\partial(P_S\phi')}{\partial(\ln\sigma)} = -RP_ST'$ because $\frac{\partial P_S}{\partial\sigma} = 0$. By defining $\hat{\phi} = (P_S\phi')$ in the σ-system gives $\frac{\partial(\hat{\phi})}{\partial(\ln\sigma)} = -R\hat{T}$. This is integrated vertically to yield a vector-matrix relationship $\underline{\hat{\phi}} = \underline{\underline{A}}\,\underline{\hat{T}}$, which is equal to equation **(C.6)**, where $\underline{\underline{A}}$ is a matrix depending upon R and σ only and is thus constant.

In the η-system, however, it is found that an equivalent expression cannot be derived from the *hydrostatic* equation to link $\frac{\partial(\mu\phi')}{\partial(\ln\eta)}$ directly to $-R\mu T'$ in a similar way than achieved in the σ-system as shown in equation **(C.6)**. However, for the sake of applying a semi-implicit treatment in the η-system, using the insight gained from the σ-system, a unique quantity $\hat{\phi}$ is defined such that $\frac{\partial(\hat{\phi})}{\partial(\ln\eta)} = -R\mu T' = -R\hat{T}$. This will then yield the vector-matrix $\underline{\hat{\phi}} = \underline{\underline{A}}\,\underline{\hat{T}}$. **Note that $\hat{\phi}$ defined for the η-system is NOT equal to $\mu\phi'$**, but it is a close approximation. By treating this quantity implicitly in the η-system, the gravity wave generated terms are addressed in the same way as in the σ-system. Also note that the equations still require that $\hat{\phi}$ be derived from the *hydrostatic* equation for use in equation **(3.9)** and **(3.10)** via $\hat{C}$.

C.2 HYDROSTATIC APPROXIMATION

In Holton (1992) the *hydrostatic approximation* is defined as

$\frac{\partial p}{\partial z} = -\rho g$ from $\partial\phi = g\partial z$ follows that $\partial p = -\rho g dz = -\rho\partial\phi$

Thus

$\frac{\partial\phi}{\partial p} = -\frac{1}{\rho}$ replace ρ by using the equation of state ($p=\rho RT$)

$\frac{\partial\phi}{\partial p} = -\frac{RT}{p}$ equation (2.1) gives $\mu = \frac{\partial p}{\partial\eta}$ and therefore

$$\frac{\partial\phi}{\partial p} = \frac{\partial\phi}{\partial\eta}\frac{\partial\eta}{\partial p} = \frac{\partial\phi}{\partial\eta}\frac{1}{\mu} = -\frac{RT}{p}$$

The *hydrostatic approximation* in the η-system may be written as

$$\boxed{\frac{\partial\phi}{\partial\eta} = -RT\frac{\mu}{p}} \qquad \textbf{(C.1)}$$

The hydrostatic approximation in the σ-system may be derived in a similar manner. The vertical co-ordinate in the σ-system is $\sigma = p/P_S$.

To highlight essential differences between the σ- and η-systems, the functions relating the geopotential variables (ϕ_O, ϕ and ϕ') to temperature are separately derived for both the η- and σ-system.

C.3 GEOPOTENTIAL AS A FUNCTION OF TEMPERATURE

Geopotential in the η-**system**	Corresponded σ-**system** formulation
From the *hydrostatic approximation*, equation **(C.1)**, follows that	From the *hydrostatic approximation* (Holton, 1992) follows that
$\frac{\partial\phi}{\partial\eta} = -RT\frac{\mu}{p}$	$\frac{\partial\phi}{\partial\sigma} = -RT\frac{P_s}{p} = -RT\frac{1}{\sigma}$
and therefore	and therefore
$\eta\frac{\partial\phi}{\partial\eta} = -RT\frac{\eta\mu}{p} = -RTf \quad \text{where } f = \frac{\eta\mu}{p}$	$\sigma\frac{\partial\phi}{\partial\sigma} = -RT$
which results in	which results in
$\boxed{\frac{\partial\phi}{\partial(\ln\eta)} = -RTf}$	$\boxed{\frac{\partial\phi}{\partial(\ln\sigma)} = -RT}$ **(C.2)**
(ϕ) is solved by integrating equation **(C.2)** in the vertical	(ϕ) is solved by integrating equation **(C.2)** in the vertical
$\int_{\phi}^{\phi[\eta=1]}\partial\phi = -R\int_{\eta}^{1}Tf\partial(\ln\eta)$	$\int_{\phi}^{\phi[\sigma=1]}\partial\phi = -R\int_{\sigma}^{1}T\partial(\ln\sigma)$
The integral is numerically solved by vertical summation	The integral is numerically solved by vertical summation
$\phi_{[\eta=1]} - \phi = -R\sum_{i=\eta}^{1}Tf\Delta(\ln i)$	$\phi_{[\sigma=1]} - \phi = -R\sum_{i=\sigma}^{1}T\Delta(\ln i)$
which finally yields	which finally yields
$\phi = R\sum_{i=\eta}^{1}Tf\Delta(\ln i) + \phi_{[\eta=1]}$	$\phi = R\sum_{i=\sigma}^{1}T\Delta(\ln i) + \phi_{[\sigma=1]}$
where ($\phi_{[\eta=1]} = \phi_S$) is the surface contribution as introduced in section 3.3.	where ($\phi_{[\sigma=1]} = \phi_S$) is the surface contribution.

Geopotential in the η-**system**	Corresponded σ-**system** formulation
Assuming that $T = a + b\ln(\eta)$, a matrix is derived which relates ϕ to T. This matrix will, however, differ from matrix $\underline{\underline{A}}$ in equation **(C.3)** for the σ-system.	Assuming that $T = a + b\ln(\sigma)$, a matrix $\underline{\underline{A}}$ is derived which relates ϕ to T: $$\underline{\phi} = \underline{\underline{A}}\,\underline{T} \qquad \textbf{(C.3)}$$
From section (3.3) follows that $\phi = \phi_O + \phi'$ and $T = T_O + T'$ where (ϕ_O) has a different constant value for each model half-level and (T_O) is isothermal in the vertical (= 290° K).	From section (3.3) follows that $\phi = \phi_O + \phi'$ and $T = T_O + T'$ where (ϕ_O) has a different constant value for each model half-level and (T_O) is isothermal in the vertical (= 290° K).
Geopotential mean (ϕ_O)	**Geopotential mean (ϕ_O)**
In accordance with equation **(C.2)** the vertical change of (ϕ_O) is **set** to be $$\frac{\partial\phi_O}{\partial(\ln\eta)} = -RT_O$$	In accordance with equation **(C.2)** the vertical change of (ϕ_O) is **set** to be $$\frac{\partial\phi_O}{\partial(\ln\sigma)} = -RT_O \qquad \textbf{(C.4)}$$

The two equations in **(C.4)** are identical since (η) and (σ) have the same value for each model half-level, and $RT_O = R.(290)$ is a global isothermal constant.

(ϕ_O) is solved by integrating equation **(C.4)** in the vertical $$\int_{\phi_O}^{\phi_O[\eta=1]} \partial\phi_O = -RT_O \int_{\eta}^{1} \partial(\ln\eta)$$ The integral is numerically solved by vertical summation $$\phi_{O[\eta=1]} - \phi_O = -RT_O \sum_{i=\eta}^{1} \Delta(\ln i)$$ which finally yields	(ϕ_O) is solved by integrating equation **(C.4)** in the vertical $$\int_{\phi_O}^{\phi_O[\sigma=1]} \partial\phi_O = -RT_O \int_{\sigma}^{1} \partial(\ln\sigma)$$ The integral is numerically solved by vertical summation $$\phi_{O[\sigma=1]} - \phi_O = -RT_O \sum_{i=\sigma}^{1} \Delta(\ln i)$$ which finally yields

Geopotential in the η-**system**	Corresponded σ-**system** formulation
$\phi_O = RT_O \sum_{i=\eta}^{1} \Delta(\ln i) + \phi_{O[\eta=1]}$	$\phi_O = RT_O \sum_{i=\sigma}^{1} \Delta(\ln i) + \phi_{O[\sigma=1]}$
where ($\phi_{O[\eta=1]} = \phi_{SO}$) is the surface mean contribution as introduced in section 3.3.	where ($\phi_{O[\sigma=1]} = \phi_{SO}$) is the surface mean contribution.
Assuming that $T = a + b\ln(\eta)$, the same matrix $\underline{\underline{A}}$ in equation **(C.3)** may be used to relates (ϕ_O) to (T_O): $\underline{\phi_O} = \underline{\underline{A}}\,\underline{T_O}$	Assuming that $T = a + b\ln(\sigma)$, the same matrix $\underline{\underline{A}}$ in equation **(C.3)** may be used to relates (ϕ_O) to (T_O): $\underline{\phi_O} = \underline{\underline{A}}\,\underline{T_O}$

It was shown that the mean geopotential (ϕ_O) is solved in exactly the same way for both the η- and σ-systems. The geopotential perturbation (ϕ') still needs to be solved. This is achieved by replacing $\phi = \phi_O + \phi'$ into equation **(C.2)**:

Geopotential perturbation (ϕ')

$$\frac{\partial\phi}{\partial(\ln\eta)} = \frac{\partial(\phi_O + \phi')}{\partial(\ln\eta)} = \frac{\partial\phi_O}{\partial(\ln\eta)} + \frac{\partial\phi'}{\partial(\ln\eta)}$$

and therefore

$$\frac{\partial\phi'}{\partial(\ln\eta)} = \frac{\partial\phi}{\partial(\ln\eta)} - \frac{\partial\phi_O}{\partial(\ln\eta)}$$

Apply equations **(C.2)** and **(C.4)**

$$= (-RTf) - (-RT_O)$$

$$= -R(Tf - T_O)$$

which results in

$$\frac{\partial\phi'}{\partial(\ln\eta)} = -R(Tf - T_O)$$

Geopotential perturbation (ϕ')

$$\frac{\partial\phi}{\partial(\ln\sigma)} = \frac{\partial(\phi_O + \phi')}{\partial(\ln\sigma)} = \frac{\partial\phi_O}{\partial(\ln\sigma)} + \frac{\partial\phi'}{\partial(\ln\sigma)}$$

and therefore

$$\frac{\partial\phi'}{\partial(\ln\sigma)} = \frac{\partial\phi}{\partial(\ln\sigma)} - \frac{\partial\phi_O}{\partial(\ln\sigma)}$$

Apply equations **(C.2)** and **(C.4)**

$$= (-RT) - (-RT_O)$$

$$= -R(T - T_O)$$

which results in

$$\frac{\partial\phi'}{\partial(\ln\sigma)} = -RT' \qquad \textbf{(C.5)}$$

Geopotential in the η-**system**	Corresponded σ-**system** formulation

Note that for the η-system the geopotential perturbation (ϕ') is expressed in terms of $(Tf - T_O)$, which is very close to but not a real temperature perturbation.

(ϕ') is solved by vertically integrating equation **(C.5)**

$$\int_{\phi'}^{\phi'[\eta=1]} \partial\phi' = -R \int_{\eta}^{1} (Tf - T_O)\partial(\ln\eta)$$

Since (f) is close to unity, this integral is nearly identical to the corresponding σ-integral. By using equation **(2.1)** the function (f) may be written as

$$f = \frac{\eta\mu}{p} = \frac{\eta}{A_O + P_S B}\left[\frac{\partial A_O}{\partial\eta} + P_S\frac{\partial B}{\partial\eta}\right]$$

This integral is numerically solved by vertical summation

$$\phi'_{[\eta=1]} - \phi' = -R\sum_{i=\eta}^{1}(Tf - T_O)\Delta(\ln i)$$

which finally yields

$$\phi' = R\sum_{i=\eta}^{1}(Tf - T_O)\Delta(\ln i) + \phi'_{[\eta=1]}$$

where $(\phi'_{[\eta=1]} = \phi'_S)$ is the surface perturbation contribution as introduced in section 3.3.

Assuming that $T = a + b\ln(\eta)$, a matrix can be derived which relates ϕ to $(Tf - T_O)$. This matrix will, however, differ from matrix $\underline{\underline{A}}$ in equation **(C.3)**.

(ϕ') is solved by vertically integrating equation **(C.5)**

$$\int_{\phi'}^{\phi'[\sigma=1]} \partial\phi' = -R \int_{\sigma}^{1} T'\partial(\ln\sigma)$$

The integral is numerically solved by adding in the vertical

$$\phi'_{[\sigma=1]} - \phi' = -R\sum_{i=\sigma}^{1} T'\Delta(\ln i)$$

which finally yields

$$\phi' = R\sum_{i=\sigma}^{1} T'\Delta(\ln i) + \phi'_{[\sigma=1]}$$

where $(\phi'_{[\sigma=1]} = \phi'_S)$ is the surface perturbation contribution.

Assuming that $T = a + b\ln(\sigma)$, the same matrix $\underline{\underline{A}}$ in equation **(C.3)** may be used to relate (ϕ') to (T'):

$$\underline{\phi'} = \underline{\underline{A}}\,\underline{T'}$$

It is important to note that, unlike the σ-system, where $\underline{\phi'} = \underline{\underline{A}}\,\underline{T'}$, the geopotential perturbation in the η-system (ϕ') **cannot be related directly** to the temperature perturbation T' by using matrix $\underline{\underline{A}}$.

In a similar way it can be shown that for the P_s-weighted geopotential perturbation in the σ-system the following relation applies:

$$(P_s\underline{\phi'}) = \underline{\underline{A}}(P_s\underline{T'}) \qquad \textbf{(C.6)}$$

In this case, for the η-system, the corresponding weighting factor $\mu\phi'$ **cannot be related directly** to the corresponding μ-weighed temperature $\mu T'$ by using matrix $\underline{\underline{A}}$.

REFERENCES

Baer, F. 1964. Integration of the Spectral Vorticity Equation. *J. Atm. Sci.*, **21**, 260 - 276.

Bourke, W. 1974. A multi-level spectral model. I. Formulation and hemispheric integrations. *Mon. Wea. Rev.*, **102**, 687-701.

Bourke, W., McAvaney, B., Puri, K. and Thurling, R. 1977. Global modelling of atmospheric flow by spectral methods, *Methods in Computational Physics,* Vol. **17**, J. Chang, Ed., Academic Press, 173-265.

Burger, A.P and Riphagen, H.A. 1990. The Basic Equations in Meteorological Dynamics - a Reexamination of Unsimplified Forms for a General Vertical Coordinate. *Beitr. Phys. Atmosph.,* Vol. **63,** No. **3/4**, 151-164.

Burger, A.P and Riphagen, H.A. 1999. Energy Conservation for a General Vertical Coordinate - A Reexamination of Unsimplified Forms. *Contr. Amos. Phys..,* Vol. **72,** No. **1**, 25-50.

Chouinard, C. and Bèland, M. 1986. A Simple Gravity Wave Drag Parameterization for Use in Medium-Range Weather Forcast Models. *Atmosphere-Ocean*, **24** (**2**), 91-110.

Eliassen, A. 1949. The quasi-static equations of motion with pressure as independent variable. *Geofysiske Publikasjoner,* **17**, no. **3**, 43pp

Ellsaesser, H.W 1966. Evaluation of Spectral Versus Grid Methods of Hemispheric Numerical Weather Prediction. *J.Appl.Met.* **5**, 246-262.

ECMWF 1994. *The description of the ECMWF/WCRP level III-A globakl atmospheric data archive - technical Attachment.* Director, ECMWF, Shinfield Park, Reading/Berks. RG2 9AX, UK.

Godart, O. 1984. Meteorological equations in isobaric co-ordinates. *Annales de la Societe Scientifique de Bruxelles,* T. **97, IV**, 173-227.

Gordon, H.B. 1981. A flux formulation of the spectral atmospheric equations suitable for use in long-term climate modeling. *Mon. Wea. Rev.*, **109**, 56-64.

Gordon, H.B. 1983. Synoptic cloud variations in a low resolution spectral atmospheric model. *J. Geophys. Res.* **88**, 6563-6575.

Gordon, H.B. and Hunt, B.G. 1987. Interanual variability of the simulated hydrology in a climate model - implications for drought. *Climate Dynamics*, **1**, 113-130.

Gordon, H.B. and Hunt, B. G. 1991. Droughts, floods and sea surface temperature anomalies: a modelling approach. *Int. J. Climatol.*, **11**, 347-365.

Hack, J.J, Boville, B.A., Briegleb, B.P., Kiehl, J.T., Rasch, P.J. and Williamson, D.L. 1993. *Description of the NCAR Community Climate Model (CCM2).* NCAR Technical Note, Climate and Global Dynamics Division, National Centre for Atmospheric Research, Boulder, Colorado, USA, 43pp.

Haltiner, G.J. (1971). *Numerical weather prediction.* John Wiley & Sons, Inc. ISBN: 0 471 34580 6, 317pp.

Haltiner, J.H. and Williams, R.T. 1980. *Numerical Prediction and Dynamic Meteorology.* 2nd ed. John Wiley & Sons, Inc., New York, ISBN 0-471-05971-4, 477pp.

Henderson-Sellers, A. and McGuffie, K. 1987. *A Climate Modelling Primer.* John Wiley & Sons Ltd. Inc., New York, ISBN 0 471 91462 2, 217pp.

Hess,S.L. (1959) *Introduction to theoretical Meteorology.* Henry Holt and Company, New York, 362pp.

Holton, J.R. 1992. *An Introduction to Dynamic Meteorology*. 3rd ed. Academic Press, Inc. 1250 Sixth Avenue, San Diego, California 92101, 511pp.

Hoskins, B,J and Simmons, A.J. 1975. A multi-layer spectral model and the semi-implicit method. *Quart. J.R.Met.Soc.*, **101**, 637-655.

Hoskins, B.J, Hsu, H.H, James, I.N., Matsutani, M., Sardeshmukh, P.D. and White, G.H. 1989. *Diagnostics of the global atmospheric circulation based on ECMWF analyses 1979-1989.* WCRP-27, WMO/TD No. **326**.

Hunt, B.G. and Gordon, H.B. 1988. The problem of "naturally" occurring drought. *Climate Dynamics*, **3**, 19-33.

Hunt, B.G. and Gordon, H.B. 1989. Diurally varying regional climatic simulations. *Int. J. Climatol.*, **9**, 331-356.

Hunt, B.G. and Gordon, H.B. 1991. Simulations of the 1988 US drought. *Int. J. Climatol.*, **11**, 629-644.

Hunt, B.G., Zebiak, S.E and Cane, M.A. 1994. Experimental predictions of climatic variability for lead times of twelfe months. *Int. J. Climatol.*, **14**, 507-526.

Jury, M.R., Pathack, B., Rautenbach, C.J.deW. and van Heerden,J. 1996. Drought over South Africa and Indian Ocean SST: Statistical and GCM results. *The Global Atmosphere and Ocean System*, **4**, 47-63.

Kasahara, A. 1966. The dynamical influence of orography on the large-scale motion of the atmosphere. *J. Atmos. Sci.,* **23**, 259-271.

Kasahara, A. 1974. Various Vertical Coordinate Systems Used for Numerical Weather Prediction. *Mon. Wea. Rev.,* **102**, 509-523.

Kasahara, A. 1978. Further Sudies on a Spectral Model of the Global Barotropic Primitive Equations with Hough Harmonic Expansions. *J. Atm. Sci.*, Vol. **35**, No **11**, 2043-2051.

Mason, S.J., Lindesay, J.A. and Tyson, P.D. 1994. Simulating drought in Southern Africa using sea surface temperature variations. *Water SA (South Africa)*, Vol **20** No **1**, 15-21.

Mechoso, C.R., Suarez, M.J., Yamazaki, K., Spahr, J.A. and Arakawa,A. 1982. A study of the sensitivity of numerical forecasts to an upper boundary in the lower stratosphere. *Mon. Wea. Rev.,* **110**, 1984-1993.

McGregor, J.L. 1993. Economical determination of departure points for semi-Lagrangian models. *Mon. Wea. Rev.,* **121**, 221-230.

McGregor, J.L., Gordon, H.B., Watterson, I.G., Dix, M.R. and Rotstayn, L.D. 1993. *The CSIRO 9-level Atmospheric General Circulation Model.* CSIRO Division of Atmospheric Research Technical Paper No. **26**, Aspendale, Vic, Australia. 89pp.

Nakamura, H. 1978. Dynamical Effects of Mountains on the General Circulation of the Atmosphere: I. Development of Finite-Difference Schemes Suitable for Incorporating Mountains. *J. Met. Soc.Japan*, Vol. **44**, No **5**, 237-244

Phillips, N.A. 1957. A Coordinate System having some Special Advantages for Numerical Forecasting. *J. Meteorology*, Vol **56,** no **5**, 317-339.

Platzman, G.W. 1960. The Spectral form of the Vorticity Equation. *J. Meteorology*, **17**, 635-644.

Press, W.H., Teukolsky, S.A., Vetterling, W.T. and Flannery, B.P. 1992. *Numerical recipes in Fortran, the art of scientific computing.* Cambridge University Press, The Pitt Building, Trumpington Street, Cambridge CB2 1RP, 40 West 20th Street, New York, NY 10011-4211, USA, pp 963.

Rautenbach, C.J.deW. 1995. *The Implementation of a Hybrid Vertical Coordinate System on the Non-Linear Dynamics of the CSIRO-9 AGCM.* Presentation during the 12th Annual Conference of the South African Society for Atmospheric Sciences, Pretoria, South Africa.

Rautenbach, C.J.deW. and van Heerden, J. 1995. *Modelling Climate using the CSIRO-9 AGCM.* Presentation during the 12th Annual Conference of the South African Society for Atmospheric Sciences, Pretoria, South Africa.

Rautenbach, C.J.deW. and van Heerden, J. 1996. *The characteristics of the anomalous Rainfall and Sea Surface Temperature fields which occurred over the South African region during the 1995/96 summer season.* Presentation during the 13th Annual Conference of the South African Society for Atmospheric Sciences, Cape Town, South Africa.

Rautenbach, C.J.deW. 1997. *A GCM Study Describing Teleconnections between Global SST Anomalies and the Copious Summer Rainfall over South Africa (1995/96).* Presentation during the 5th International Conference on Southern Hemisphere Meteorology and Oceanography, Pretoria, South Africa.

Read, H.H. and Watson, J. 1970. *Introduction to Geology*. Second edition,Macmillan and Co LTD. London and Basingstoke. 693pp.

Richardson, L.F. 1922. *Weather Prediction by Numerical Process*. Cambridge University Press, reprinted Dover, New York, 1965, 410pp.

Robert, A.J. 1966. The Integration of a Low Order Spectral Form of the Primitive Meteorological Equations. *J. Met. Soc.Japan*, Vol. **44**, No **5**, 237-244.

Sangster, W.E. 1960. A method of representing the horizontal pressure force witout reduction of station pressures to sea level. *J. Meteorology*, Vol **17,** 166-176.

Silberman, I. 1954. Planetary Waves in the Atmosphere. *J. Meteorology*, **11**, 27- 34.

Simmons, A.J and Hoskins, B.J. 1978. Stability of the Semi-Implicit Method of Time Integration. *Mon. Wea. Rev.*, **106**, 405-412.

Simmons, A.J. and Burridge, D.M. 1981. An Energy and Angular-Momentum Conserving Vertical Finite-Difference Scheme and Hybrid Vertical Coordinates. *Mon. Wea. Rev.*, **109**, 758-766.

Simmons, A.J. and Strüfing, R. 1981. *An Energy and Angular Momentum Conserving Finite-difference scheme, Hybrid Coordinates and medium-range weather prediction.* ECMWF Technical Report No. 28, Shinfield Park, Reading, Berkshire, UK, 68pp.

Simmons, A.J. and Strüfing, R. 1983. Numerical forecasts of stratospheric warming events using a model with a hybrid vertical coordinate. *Quart.J.R.Met.Soc*, **109**, 81-111.

Smagorinsky, J, Mnaabe, S. and Holloway, L. 1965. Numerical results from a nine-level general circulation model of the atmosphere. *Mon. Wea. Rev.,* **93**, 727-768.

Smith, I.N. 1995. A GCM Simulation of Global Climate Interannual Variability: 1950-1988. *J. Climate*, **0**, 1-10.

Smith, I.N. and Gordon, H.B. 1992. General circulation model simulations of precipitation and atmospheric circulation changes associated with equatorial Pacific warm sea surface temperature anomalies - results from an ensemble of long term integrations. *Climate Dynamics*, **7**, 141-154.

Spiegel, M.R. 1974. *Schaum's Outline Series: Theory and Problems of Vector Analyses and an Introduction to Tensor Analysis.* McGraw-Hill International Book Company, New York, ISBN 07 084378 3, 225pp.

Taljaart, J.J. 1985. *Cut-off lows in the South African region.* South African Weather Bureau Technical Paper. no. 14, 153pp.

Tennant, W.J and van Heerden J. 1994. The influence of orography and local sea-surface temperature anomalies on the development of the 1987 Natal floods: a general circulation model study. *South African J. Science*, **90**, 45-49.

Triegaardt, D.O., Van Heerden, J. and Steyn, P.C.L. 1988. Anomalous Precipitation and floods during February 1988*, Tech.Pap.South African Weather Bureau* , **23**, 25pp.

Truter, M.M and Rautenbach, C.J.deW. 1994. *Ocean-Atmosphere coupled experiments with the CSIRO 4-level Climate Model.* Presentation during the Eleventh Annual Conference of the South African Society for Atmospheric Sciences, Pretoria, South Africa.

Van Heerden, J. and Hurry, L. 1987. *Southern Africa's Weather Patterns*. 2nd ed. Via Africa Limited, Acacia books, Reg. No. 70/03235/06, 501 Merino Building, 140 Pretorius Street, Pretoria, South Africa. ISBN 0 86817 045 3, 95pp.

Van Heerden, J., Rautenbach, C.J.deW. and Truter, M.M. 1995. Techniques for seasonal and longer term rainfall prediction in South Africa. *Water Research Commission Report No* **373/1/92**, 1-51.

Van Heerden, J. and Rautenbach, C.J.deW. 1997. *A GCM Simulation of the Impact on the Atmospheric Circulation over Africa by Boundary Forcing due to Sea Surface Temperature Anomalies in the Central Indian Ocean.* Presentation during the 5th International Conference on Southern Hemisphere Meteorology and Oceanography, Pretoria, South Africa.

Washington, A.J. 1965. *Basic Technical Mathematics with Calculus.* Addison-Wesley Publishing Company INC, Reading, UK, 595pp.

Washington, W.M. and Parkinson, C.L. 1992. *An Introduction to Three-Dimensional Climate Modeling*. University Science Books, 20 Edgehill Road, Mill Valley, California, 422pp.

Watterson, I.G. (1995). *Interpolated CSIRO-9 resolution observed climate obtained from ECMWF, TOGA and Legates & Willmott rainfall data fields.* CSIRO(DAR), Aspendale, Victoria, Australia.